Alteration assemblage in the lower units of the Uitkomst Complex, Mpumalanga Province, South Africa.

by

NICOLAAS CASPER STEENKAMP

A thesis submitted in partial fulfilment of the requirements for the degree of

DOCTOR PHILOSOPHIA

In the

DEPARTMENT GEOLOGY

FACULTY OF NATURAL & AGRICULTURAL SCIENCES

UNIVERSITY OF PRETORIA

August 2012

DECLARATION

I, **Nicolaas Casper Steenkamp**, hereby declare that this thesis that I hereby submit for the Degree DOCTOR PHILOSOPHIA (PhD) at the University of Pretoria is my own work has not previously been submitted by me for a degree at this or any other university.

Signature: _____   **Date:** _____

Abstract

The Uitkomst Complex is located within the Great Escarpment area close to the town of Badplaas, approximately 300 km due east of Pretoria, in the Mpumalanga Province, South Africa. This complex is believed to represent a layered conduit system related to the 2.06 Ga Bushveld Complex. The succession from the bottom up comprises the Basal Gabbro- (BGAB), Lower Harzburgite- (LHZBG) and Chromitiferous Harzburgite (PCR) Units, collectively referred to as the Basal Units, followed by the Main Harzburgite- (MHZBG), Upper Pyroxenite-(PXT) and Gabbronorite (GN) Units, collectively referred to as the Main Units. The Basal Unit is largely hosted by the Malmani Dolomite Formation, in the Pretoria Group of the Transvaal Supergroup sediments. The Lower Harzburgite Unit contains numerous calc-silicate xenoliths derived from the Malmani Dolomite.

The Basal Units host the economically important nickel-bearing sulphide and chromite deposits exploited by the Nkomati Mine. An area of extensive localized talc-chlorite alteration is found in the area delineated for large scale open cast mining. This phenomenon has bearing on the nature and distribution of the sulphide minerals in the Chromitiferous Harzburgite and to a lesser extent the Lower Harzburgite Units.

The Basal Unit is comprised of both near pristine areas of mafic minerals and areas of extensive secondary replacement minerals. Of the olivine minerals, only fosterite of magmatic origin is found, the fosterite suffered hydrothermal alteration resulting in replacement of it by serpentine and secondary magnetite. Three different types of diopside are found, the first is a primary magamatic phase, the second is a hybrid "transitional" phase and the third, a skarn phase. Hydrothermal alteration of the matrix diopside led to the formation of actinolite-tremolite pseudomorphs. This secondary tremolite is intergrown with the nickeliferous sulphide grains. Chromite grains are rimmed or replaced by secondary magnetite. Pyrrhotite grains is also rimmed or replaced by secondary magnetite. Talc and chlorite is concentrated in the highly altered rocks, dominating the PCR unit. Primary plagioclase and calcite do not appear to have suffered

alteration to the same extent as the other precursor mafic magmatic and hydrothermal minerals.

It is suggested that the PCR was the first unit to be emplaced near the contact of the dolomite and shale host rock. The more primitive mafic mineral composition and presence of chromitite attest to this interpretation. The LHZBG and MHZBG units may have been emplaced simultaneously, the LHZBG below and the MHZBG above. Interaction and partial assimilation of the dolomitic country rock led to a disruption of the primary mafic mineralogy, resulting in the preferential formation of diopside at the expense of orthopyroxene and plagioclase. Addition of country rock sulphur resulted in sulphur saturation of the magma and resulted in the observed mineralization. The downward stoping of the LHZBG magma, in a more "passive" pulse-like manner led to the formation of the calc-silicate xenolith lower third of this unit.

It is proposed that the interaction with, and assimilation of the dolomitic host rock by the intruding ultramafic magmas of the Basal Units are responsible, firstly, for the segregation of the nickeliferous sulphides from the magma, and secondly for the formation of a carbonate-rich deuteric fluid that affected the primary magmatic mineralogy of the Basal Unit rocks.

The fluids released during the assimilation and recrystallization of the dolomites also led to the serpentinization of the xenoliths themselves and probably the surrounding hybrid and mafic- ultramafic host rocks. The CO_2-rich fluids migrated up and outward, while the H_2O-rich fluids remained confined to the area around the xenoliths and LHZBG unit. The H_2O-rich fluid is thought to be responsible for the retrograde metamorphism of the precursor magmatic and metamorphic minerals in the Lower Harzburgite Unit. The formation of an exoscarn within the dolomitic country rocks and a selvage of endoskarn on the contact form an effective solidification front that prevented further contamination of the magma. It is also suggested that these solidification fronts constrained the lateral extent of the conduit.

The CO_2-enriched deutric fluid was able to migrate up to the PCR unit. Here the fluid was not removed as effectively as in the underlying parts of the developing conduit. This resulted in higher CO_2-partial pressures in the PCR unit, and the stabilization of talc-carbonate assemblages that extensively replaced the precursor magmatic mineralogy.

Intrusion of the magma into the shales, which may have been more susceptible to assimilation and greater stoping, led to a broadening in the lateral extent of the Complex, in the Main units above the trough-like feature occupied by the Basal Units.

Late-stage, hydrous dominated fluid migration is inferred to have been constrained to the central part of the conduit. This is demonstrated by the dominance of chlorite in the central part of the Uitkomst Complex in the study area. The Uitkomst Complex was further deformed by later intrusions of dolerite dykes. Weathering of the escarpment led to exposure of the conduit as a valley and oxidation of the surficial exposed rocks.

[810 words].

TABLE OF CONTENTS

CHAPTER 1 INTRODUCTION, PURPOSE AND METHODOLOGY

CHAPTER 2 THE GEOLOGY OF THE UITKOMST COMPLEX AND ITS SURROUNDINGS

CHAPTER 3: METHODOLOGY

CHAPTER 4 PETROGRAPHY AND MINERAL GEOCHEMISTRY

4.1 – PRIMARY MAFIC MINERALS

CHAPTER 5 – SECONDARY MINERALS IN THE LHZBG AND PCR UNITS

CHAPTER 6 - REACTION OF THE INTRUSIVE ROCKS WITH THE COUNTRY ROCKS AND WITH XENOLITHS

CHAPTER 7 GEOCHEMISTRY OF THE TALC-RICH PART OF THE UITKOMST COMPLEX

CHAPTER 8: CONSTRAINING THE EFFECT OF HYDROTHERMAL ALTERATION

LIST OF FIGURES

LIST OF TABLES

CHAPTER 1 INTRODUCTION, PURPOSE AND METHODOLOGY

1.1 Introduction

The Uitkomst Complex is considered to represent a satellite body of the Bushveld Complex (de Waal and Gauert, 1997; Marsch, 2003; de Waal, Graham and Armstrong, 2006). It is located between the towns of Machadodorp and Barberton in the Great Escarpment area in the Mpumalanga Province of South Africa. The Complex consists of a layered suite of ultramafic and mafic rock types that formed within a magma conduit (Gauert, 1998), intruded at 2044 ± 8 Ma. Preferential weathering of the mafic rocks has led to the formation of a valley, in which erosion has led to the exposure of the lowermost units of the complex on the farm Vaalkop 608JT, with successively higher parts of the stratigraphy being exposed westwards on the farms Uitkomst 541JT and Slaaihoek 540JT (Theart, 2000). Disseminated and massive sulphide and chromite ore bodies have been delineated within the lower units of the Complex.

The shallower economically mineralized parts of the Main Mineralized Zone of the Complex are targeted by the Nkomati Mine's expansion programme, and during the period July-December 2005 this zone was responsible for 23% of the general mine output and increasing steadily. This production was from the underground area overlying the Massive Sulphide Body. The Massive Sulphide Body (MSB) was exhausted in the first quarter of 2008. Mining is expected to continue utilizing the underground infrastructure, and production will be supplemented by three open cast pits, giving an expected life of mine of approximately 16 years. The first two pits were exhausted by 2010 and the focus is on the development of Pit 3 and is the focus of this investigation. The upper northwestern area contains high levels (>15 %) of altered mineralization that has a detrimental effect on the beneficiation of the ore by means of froth floatation to produce the concentrates. The location of Nkomati Mine is shown in Figure 1.1

1.2 Nkomati Mine

The sulphide ores of the Uitkomst Complex is being mined by the Nkomati Mine, owned by African Rainbow Minerals (ARM) and Norilsk Nickel in a 50:50 joint venture. This follows the take-over of LionOre by Norilsk Nickel.

ECT, an Anglovaal subsidiary, purchased the initial mineral rights to mine gold on the farms Mamre and Slaaihoek 540 - JT in 1939 (Company Report, 2007). During the early 1970's an INCO/AngloAmerican Prospecting Services joint venture began exploring the Uitkomst Intrusion for nickel (Anonymous, 2007). In 1992 Anglo American Corporation (AAC) conducted a feasibility study to exploit the disseminated sulphides on the farm Uitkomst as part of an open pit operation, but it was deemed not sufficiently economical (ARM Annual report, 2007).

During the early 1990's Slaaihoek was re-explored by Anglovaal and this was followed by a major drilling program commencing in 1993 (Theart, 2000). This and earlier programmes delineated three disseminated sulphide mineralized zones, namely the Basal Mineralized Zone (BMZ), Main Mineralized Zone (MMZ) and the Chromititic Pyroxenite Mineralized Zone (PCMZ). A Massive Sulphide Body (MSB) located at the base of the Uitkomst Complex was also identified (Theart, 2000). In the period 1993-94 a vertical shaft was sunk to a depth of 450 meters below surface to obtain a bulk sample for metallurgical test work (Theart, 2000). In 1995 the Anglovaal/AAC joint venture was formed to investigate the viability of the combined resources on Slaaihoek 540 – JT and Uitkomst 541 - JT. The pilot plant was constructed and commissioned towards the end of 1995 (Theart, 2000). The results of a feasibility study in 1996 showed that mining of the MSB of the Uitkomst Complex would be viable, and prompted the construction of the MSB concentrator plant and other infrastructure (Theart, 2000). In 1997, Nkomati Mine became South Africa's first primary nickel producer (Theart, 2000). In 2004, Anglovaal Minerals Ltd (later to be renamed African Rainbow Minerals Ltd) acquired AAC's share in the mine (Anonymous, 2007). The current joint venture was formed on 2 February 2005, African Rainbow Minerals Ltd announced the creation of a 50:50 non-incorporated business with LionOre Mining International Limited with regards to the Nkomati Mine.

At present mining of disseminated sulphides takes place via underground and open pit mining. The oxidized chromite reserve is being mined as part of the pre-strip operations to expose the LHZBG for open pit operations (Anonymous, 2010). The MSB (Massive

Sulphide Body) that was the initial target of mining was exhausted by February 2008 (Anonymous, 2010). The expansion projects, Phase 2a and b, aim to mine the MMZ ores from two areas, namely the current underground infrastructure and from surface mining which would also incorporate mining of the PCMZ and near surface chromite ores (Anonymous, 2010). The ore obtained from the PCMZ (Peridotic Chromitite Mineralised Zone, after mine nomenclature) is being processed separately by the PCMZ concentrator plant.

The MMZ was mined out in Pit 1 during 2009 and Pit 2 during 2010 (Smith and Kotze, 2010). Pit 3 was being developed at the time this thesis was written and has a life expectancy of 16 years. As part of the Phase 2a expansion project, the MMZ plant capacity was increased to 375 000 tpm during 2010. The Phase 2b expansion aims to develop the current MMZ plant into a 250 000 tpm PCMZ plant (Anonymous, 2010).

During 2006 Nkomati mined and produced approximately 300 000 tonnes of lumpy chromite ore from open pit 3 after successful testing of the product (Anonymous, 2007). The chromite resource overlies the disseminated sulphide resource of the MMZ in the open pit 3 area and is mined as part of the pre-strip for this open pit (Anonymous, 2007). The PCMZ material is being stockpiled for later extraction of the chromite (Anonymous, 2010).

An aerial view of the infrastructure and surroundings at Nkomati Mine is provided in Figure 1.1 and 1.2.
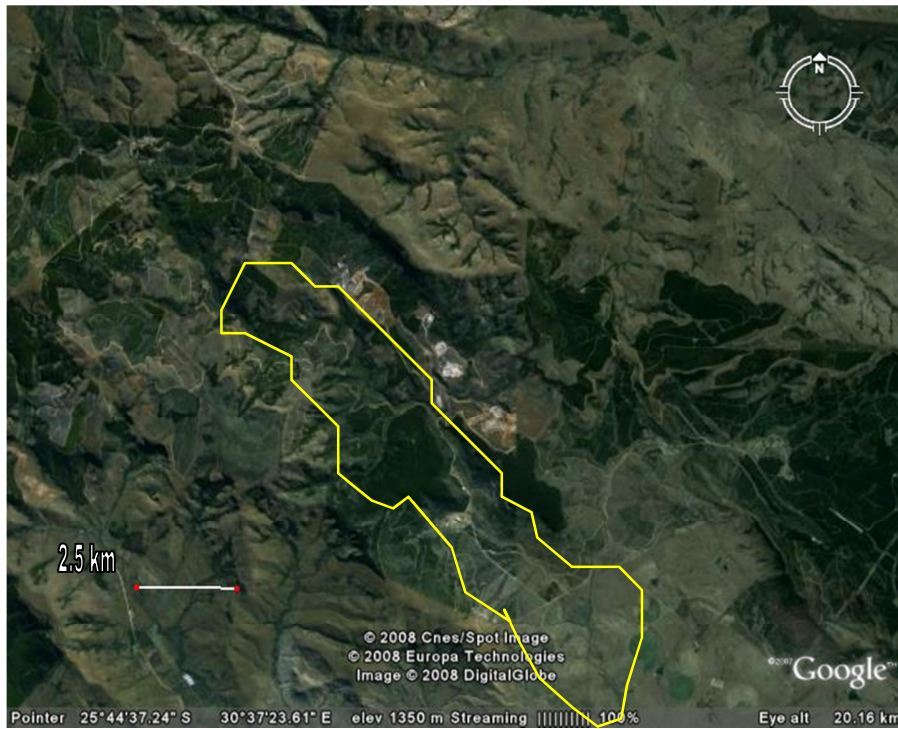
Figure 1.1. Aerial view of Nkomati Mine and surroundings. The surface exposure of the Uikomst is indicated by the yellow line. The white bar represents 2.5 kilometers (image from Google Earth, 2008).

Figure 1.2. Aerial view of the infrastructure at Nkomati Mine. The white bar represents 250 meters (image from Google Earth, 2007).

1.3 Comparison with other intrusions

To understand the processes involved in the interaction between carbonate country rock and intruding magma in the Uitkomst Complex, as well as the possible assimilation of the carbonate rocks by the intrusion, the available literature on several other intrusions has been considered. Of these, the Platreef is considered the most significant as both deposits were probably formed in response to the interaction between the Bushveld Complex magma and interaction with the Malmani dolomite of the Transvaal Supergroup. The Platreef and the interaction between the Bushveld magma and the Transvaal Supergroup sediments have been investigated by various authers, e.g. Kinnard et al., (2005), MacDonald et al., (2005), Armitage et al., (2002), Harris and Chaumba, (2001) and Gain and Mostert, (1982). Similarities and differences between the Platreef and Uitkomst Complex will be discussed in subsequent sections. Other examples where pervasive assimilation examples were described include intrusions in the Kola Belt in Siberia (Li, et al., 2003; Barnes et al., 2001; Dokuchaeva and Yakovlev, 1994), Ioko-Dovyren (Wenzel, et al., 2001; Wenzel, et al., 2002) in Russia and the Horavaer intrusion (Barnes et al., 2005) in Norway.

The effect of partial assimilation e.g. along the contact of other intrusions into carbonate country rock was also considered. These examples include the contact reactions at Gebel Yelleq in Egypt (Abu El-Enen et al., 2004), at Werfen in Italy (Povoden et al., 2002), Adamello in Italy (Bucher-Nurminen, 1982), Tokatoka in New Zealand (Baker and Black, 1980) and Scawt Hill in Northern Ireland (Tilley and Harwood, 1931).

The Uitkomst Complex is also compared to other conduit systems such as the Kabanga intrusion,Tanzania (Deblonde and Tack, 1999; Evans et al., 1999; Evans et al., 2000), and the Pants Lake and Voisey's Bay in North America (Li, Ripley and Naldrett, 2001) intrusions. Reference is also made to xenoliths from the Eastern Bushveld (Wallmach, Hatton and Droop, 1989) and from the Kiglapait Intrusion, Labrador (Owen, 2000).

1.4 Aims of the study

The purpose of the research project is to investigate the cause and effects of the extensive talc-chlorite alteration found in the Lower Harzburgite and Chromiferous Harzburgite Units of the Uitkomst Complex, localized in the upper north-western portion of the intrusion. This phenomenon has bearing on the nature and distribution of the sulphide minerals in the Chromatiferous Harzburgite Mineralized Zone (PCMZ) and to a lesser extent the Main Mineralized Zone (MMZ) ore bodies. These affected orebodies are currently being exploited in the underground operation and in the area delineated for a large scale open cast mine, referred to as Pit 3.

The possible effects of the interaction between the intruding magma source of the mineralized lower units and the dolomite country rocks are currently unknown. In order to quantify these effects the nature and abundance of the xenoliths in the lower units will be considered. The origin and nature of the alteration fluids responsible for the composition and distribution of the alterations zones will be determined. The formation of the hybrid rocks and the other effects of the assimilation processes on the composition and physical properties of the magma will be considered. The interaction between the magma and the country rocks will further be used to determine its influence on the shape of the intrusion and the effects of carbonate-rich and other late-stage fluids on primary magmatic and hybrid minerals must be investigated.

The methodology employed in this investigation consists of a systematic review of the available data, using the borehole logs made available for this study by ARM and a comparative literature study. The analytical component is comprised of petrographical descriptions of thin sections made from selected pieces of quartered core, obtained from the Moody's estate core-yard, and geochemical data obtained from whole rock analyses of these pieces of core, using x-ray diffraction (XRD), x-ray fluorescence (XRF) will be used. The geochemistry of the minerals present has been established by means of electron microprobe (EMP) analyses.

1.5 Study area

The study area is located in the shallow part of the Uitkomst Complex, where the basal units of the Complex outcrop on the farm Uitkomst 541JT. The area has been indicated in Figure 1.3 as the "study area" and largely coincides with that of the deeper part of Pit 3 in this figure. The area falls slightly outside the north-western border of the designated open pit area. The "narrower" part of the intrusion, referred to later in the dissertation, falls in the upper left part of the study area block. The "wider" part of the intrusion referred to in the dissertation falls in the central and lower right part of the study area.
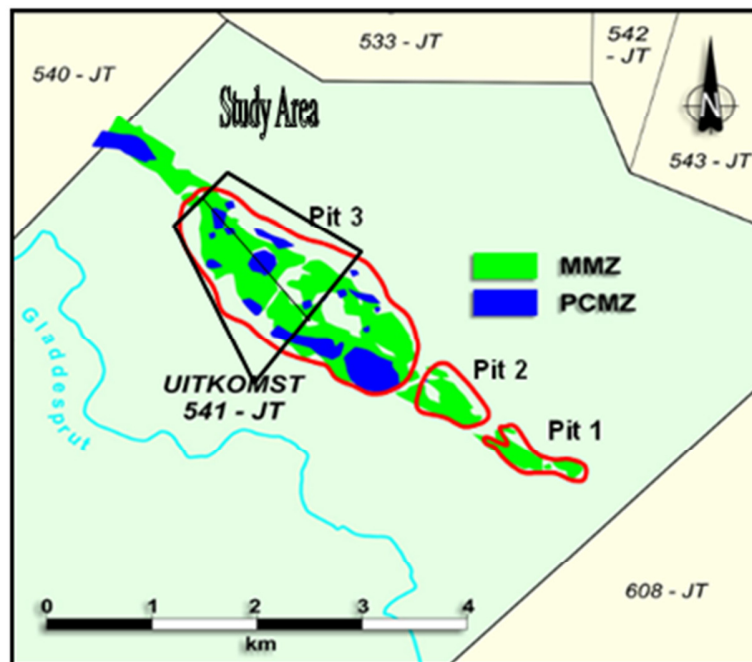
Figure 1.3. A Surface projection of the distribution of the mineralized zones in the area indicated for the large scale open pit operation. The study area falls in "Pit 3" (red line) where indicated by the box (black line). The cross-section is along the thin black solid line in the study area box. (Adapted after: Nkomati Mine Geological Staff, pers. Comm. 2005).

A section through the orebody in the study area is given in Figure 1.5 and is indicated by the arrow lines. The locality of the boreholes selected for sampling and analyses are shown in a plan view, which also indicates the approximate margins of the complex in this area in Figure 1.6. The thick black line represents the inferred boundary of the Uitkomst Complex and the dashed line represents the inferred area that may contain relative proportions talc in excess of 15 %. This area has been deemed a "talc rich zone" from composite metallurgical test samples taken in the area identified for the large scale open pit operation (Bradford, Internal company report, 1996).

Figure 1.4. Section of the area indicated for the development of a large scale open pit operation. The study area is located in the upper northwestern to central part of Pit 3. The study area extents further to the North West than indicated on the diagram. Adapted after Theart (1996). Next page.

Figure 1.5. Positions of the boreholes sampled during this investigation. The dashed line indicate the inferred "talc rich zone" as determined from composite samples (After L. Bradford, pers. Comm. ,2005). Subsequent page.

Figure 1.4

Figure 1.5

CHAPTER 2 THE GEOLOGY OF THE UITKOMST COMPLEX AND ITS SURROUNDINGS

2.1 Regional geology and host stratigraphy

The Uitkomst Complex intruded the lower parts of the Transvaal Supergroup (Kenyon et al. 1986 Gauert et al. 1995; Theart, 2000; Theart and de Nooy, 2001 and Li et al, 2002). The regional geology of the area into which the Uitkomst Complex intruded is given in Table 2.1 and a simplified geological map is presented in Figure 2.1.

Table 2.1. The stratigraphy of the lower part of the Transvaal Supergroup around the Uitkomst Complex.

Supergroup	Group	Formation	Lithology
Transvaal Supergroup	Pretoria	Timeball Hill	Shale and quartzite
		Rooihoogte	Conglomerate/breccia, quartzite
	Chuniespoort	Monte Christo	Light coloured dolomite and chert
		Oaktree	Dolomite and quartzite
	Wolkberg	Black Reef Quartzite	Conglomerate, grit, quartzite
Basement	Nelshoogte Granite		

In the area of the Uitkomst Complex the basement is composed of the Archean Nelshoogte Granites (Li et al., 2002; Maier et al., 2004). U-Pb dating of zircon from the biotite-rich trondhjemite gneiss indicate an age of 3320 ± 40 Ma for the Kaap Valley and Nelshoogte Plutons (Anhaeusser, 2001). These plutons also host younger Archean syenite intrusions (Anhaeusser, 2001). The Nelshoogte Pluton extents from the southwest of the Barberton Greenstone Belt for a distance of approximately 20 kilometers before it disappears beneath the Proterozoic cover rocks of the Escarpment, approximately 10 kilometers north of Badplaas (Anhaeusser, 2001). The basement is overlain in paleovalleys by basaltic lavas, immature polymictic quartzites and shales and tuffs of the Godwan Formation, a possible correlate of the Ventersdorp Supergroup (Li et al., 2002; Maier et al., 2004), but elsewhere

in this area the basement rocks are directly overlain by the sedimentary rocks of the Transvaal Supergroup (Maier et al., 2004).

The lower units of the Uitkomst Complex intrude directly above the basement contact on rare occasions (Kenyon et al., 1986), but more often above the Black Reef Quartzite and quartzites belonging to the Oaktree Formation of the Malmani Subgroup (Gauert et al, 1995; Li et al, 2002; Maier et al., 2004) into the dolomitic counry rock. The Black Reef Quartzites is overlain by 145-300 meters of Malmani subgroup dolomites and minor sandstones which have a maximum age of 2549 ± 2.6 Ma (Pb-Pb single zircon) (de Waal et al., 2001; Maier et al., 2004). The dolomites of the Malmani subgroup have minor intercalations of sulfidic shale (Maier et al., 2004). A 5-10 meter thick transgressive chert- rich conglomerate layer known as the Bevets Conglomerate Member of the Rooihoogte Formation in the area (Maier et al., 2004) lies directly on the Malmani dolomites, representing a regional transgressive erosion plain. Erosion during the deposition of the Brevets conglomerate has completely removed the upper parts of the Malmani Subgroup. This conglomerate is in turn overlain by 1 200 m of graphitic shale with minor quartzites and ironstones (Timeball Hill Formation; Li et al., 2002; Maier et al., 2004). A laterally non-persistent quartzite, the Klapperkop Quartzite is developed several hundred meters above the shale formation's lower contact (Maier et al., 2004).

According to Snyman (1998), corundum in the form of dark, translucent sapphire has been found on the farm Uitkomst 541 JT, but the host rock is not specified. However, corundum-bearing contact metamorphosed shales are exposed on a small hill to the southwest of the Complex on the farm Uitkomst near its northeastern boundary (pers. comm. H.F.J. Theart, 2007).
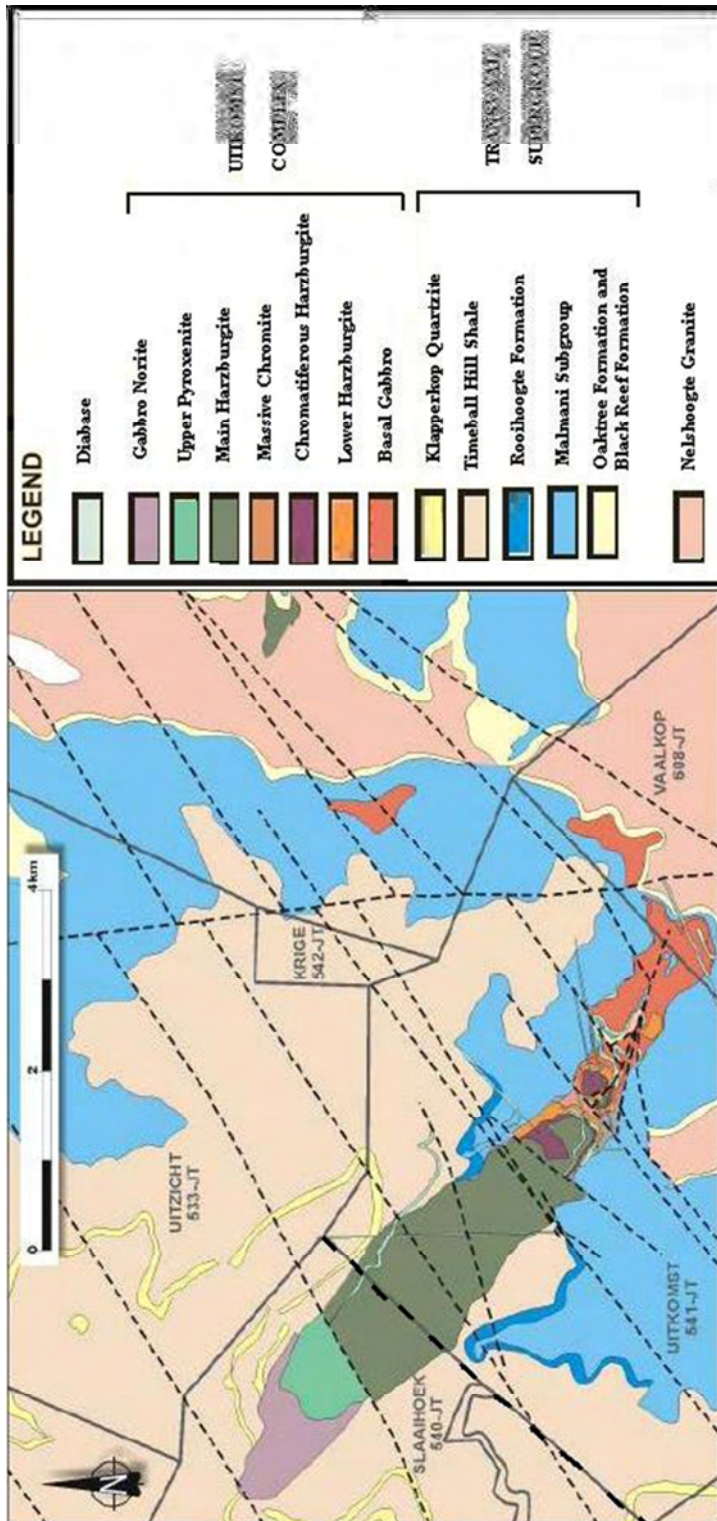
Figure 2.1. Simplified geological map indicating the surface outcrop of both country rock and Uitkomst Complex. The dashed line indicates the Slaaihoek-Uitkomst boundary. (Adapted after pers. comm. Nkomati Mine Geological Staff, 2005).

13

2.2 Bushveld igneous complex

The Uitkomst Complex is hosted by the 2500 Ma Transvaal Supergroup sediments overlying the Archean granite basement rock of the Kaapvaal craton. The country rocks around the Uitkomst Complex are discussed in more detail in Chapter 2. The Uitkomst Complex has been suggested to be genetically related to the 2060 Ma, Bushveld Igneous Complex (BIC; de Waal and Gauert, 1997), also hosted within the Kaapvaal craton by Transvaal Supergroup sediments (Figure 2.2). The Bushveld Igneous Complex is comprised of a Western-, Eastern-, Northern- and Southern limb. The mafic/ultramafic component of the BIC is subdivided into several zones, arranged form the bottom up: Marginal-, Lower-, Critical-, Main- and Upper Zones and referred to as the Rustenburg Layered Suite (RLS). The stratigraphic classification of the Eastern-, Western- and Northern Limb is given in Table 2.2. The Southern Limb is omitted as it is obscured by later Karoo sediments.

The Northern limb of the BIC contains units closest in composition to the Uitkomst Complex in the mineralized zone referred to as the Platreef. The Platreef is considered to represent a zone of interaction between the Bushveld magma of the Critical Zone and the Pretoria Group sediments that host the Northern limb. The Platreef and the product "parapyroxenite" are discussed in more detail in Chapter two.

The intrusion of magmas of differing composition has been suggested to have resulted in the formation of the BIC and its mineralized horizons (Robb, 2005). The different magmas are referred to as:

- B1 magma, a boninitic magma that formed the Lower Zone
- B2 and B3 magma that gave rise to the Lower- and Upper Critical Zone
- B4 magma is inferred to have been part of the Main Zone due to elevated Sr-isotope ratios, although a pristine example of this magma has not been encountered yet (de Waal and Gauert, 1997).

Table 2.2 Stratigraphic classification of the R.L.S. (Adapted after SACS, 1980)

Zone			Eastern Limb		Western Limb		Northern Limb	
Main	Subzone C	Roossenekal Subunit	Luiperdshoek Olivine Diorite			Bierkraal Magnetite Gabbro		Molendraai Magnetite Gabbro
	Subzone B		Ironstone Magnetite Gabbro					
	Subzone C		Magnet Heights Gabbronorite					
Main	Upper Subzone	Dsjate Subsuite	Mapoch Gabbronorite			Pyramid Gabbronorite		Mapela Gabbronorite
	Lower subzone		Leolo Mountain Gabbronorite					
			Winnaarshoek Norite-Anorthosite					
Critical	Upper Subzone	River subsuite	Winterveld Norite-Anorthosite	Schilpadnest subsuite	Mathlagame Norite-Anorthosit			Grassvalley Norite-Anorthosite
	Lower Subzone	Dwars subsuite	Mooihoek Pyroxenite		Ruighoek Bronzitite			
Lower	Upper pyroxenite subzone	Croydon Subsuite	Serokolo Bronzitite	Vlakfontein Subsuite	Tweelaagte Bronzitite		Zoetveld Subsutie	Moorddrift Harzburgite-Pyroxenite
			Jaglust Harzburgite		Groenfontein Harzburgite			Drummondlea Harzburgite
	Harzburgite subzone		Rostock Bronzitite		Makgope Bronzitite			Volspruit Pyroxenite
	Lower Pyroxenite subzone		Clapham Bronzitite		Eerlyk Bronzitite			
Marginal			Shelter Norite		Kroondal Norite			
					Kolobeng Norite			
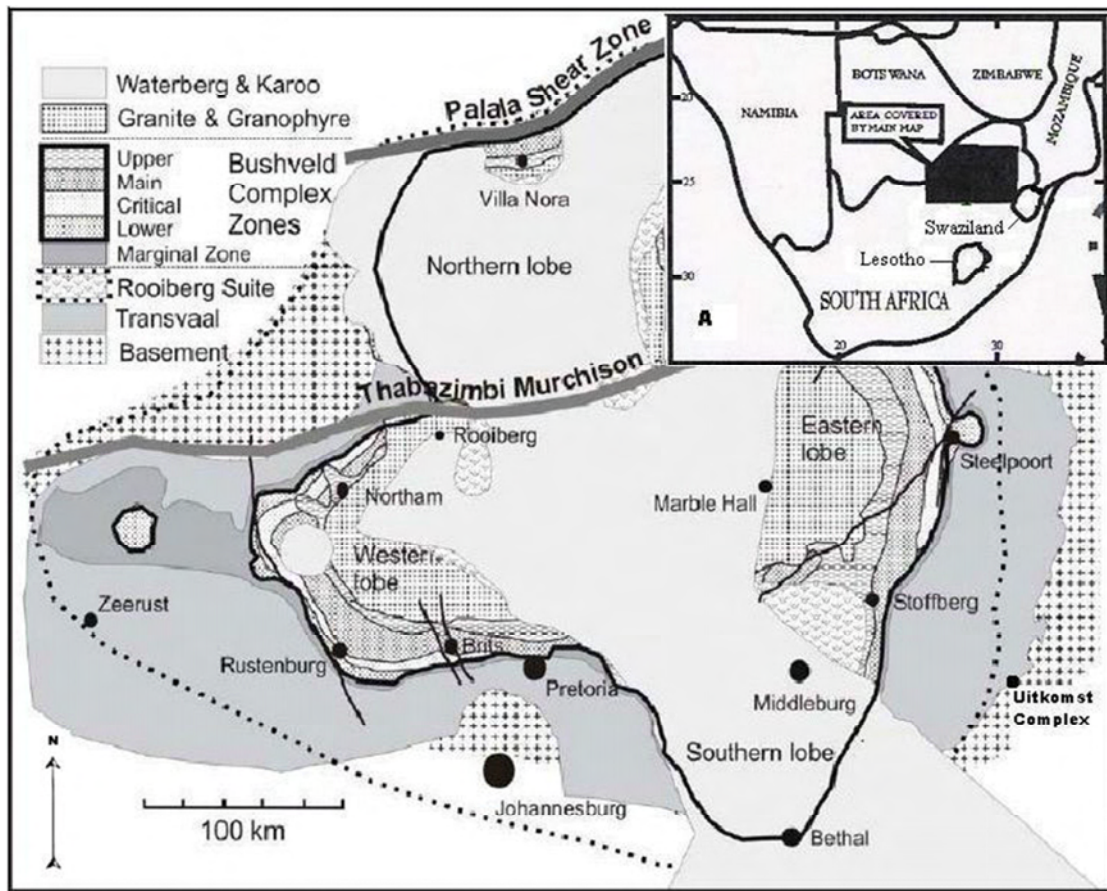
Figure 2.2 The position of the Uitkomst Complex. Insert A. The location of the Bushveld Igneous Complex, South Africa. Insert B. The position of the Uitkomst Complex relative to the Bushveld Complex is indicated by the cross (Adapted after: F.J. Kruger, 2005).

The main mineralized zones in the BIC that are of economic importance are the UG2 and Merensky Reef, containing the world's largest resource of Platinum Group Minerals (PGM's) and chromite. Both these units are hosted in the Critical Zone. The BIC is also host to the world's largest vanadium deposit, associated with the Main Magnetite Layer, found in the Upper Zone.

2.3 Previous gold mining in the area

Gold was mined on Marme 535 JT and Slaaihoek 541 JT and yielded over 10 tons during the life of mine (Ward and Wilson, 1998). The gold mineralization forms part of the Transvaal Drakensberg gold field (Ward and Wilson, 1998). The gold mineralization occurs

16

associated with Cu- and Bi-sulphides within a flat-reef Au-quartz-carbonate-sulphide vein (Ward and Wilson, 1998). The thickness of the vein is between zero and seven meters and the gold is distributed erratically (Ward and Wilson, 1998). The vein is situated in the Timeball Hill shales that form part of the Pretoria Group and immediately overlies the Uitkomst Complex (Ward and Wilson, 1998). The flat reefs or bedding-parallel veins have been linked to "water-sills" that resulted from high fluid pressures of a deep seated magmatic source (Ward and Wilson, 1998). The mineralization is indicated to have taken place at pressures of between 2.2 and 2.5 kilobar, which may represent a possible crustal depth of between 7 and 8 kilometers and at a temperature of 320 ˚C (Ward and Wilson 1998).

2.4 The Uitkomst Complex

The age of the Uitkomst Complex is inferred to be 2044±8 Ma (U-Pb zircon) and that would make it coeval with the Bushveld Complex (Theart and de Nooy, 2001; Li et al., 2001; Maier et al., 2004). In terms of age and composition, the complex may be considered to be a satellite body of the Bushveld Complex (Theart and de Nooy, 2001; Li et al., 2001; Maier et al., 2004). Other complexes and intrusions that are considered to be satellite intrusions to the Bushveld Complex are the Roodekraal Complex, Lindques Drift Intrusion, Rietfontein Complex, Heidelberg Intrusion and the Kaffirskraal Complex (Marsh, 2003; de Waal, Graham, Armstrong, 2006). These intrusions are considered to be syn-Bushveld high-Ti igneous suites and are referred to as HITIS (de Waal et al., 2006).

The shape of the Uitkomst Complex in cross section has been described as either trough- or anvil- shaped (Figure 2.2) (van Zyl, 1996; Gauert et al., 1996; de Waal and Gauert, 1997; de Waal, Maier, Armstrong and Gauert, 2001; Li, et al. , 2002; Maier, et al., 2004). The intrusion plunges at an angle of –4.5˚ (Theart and de Nooy, 2001) and is intruded between the quartzite of the Oaktree Formation of the Malmani Subgroup, forming the floor, and the Klapperkop Quartzite Member of the Timeball Hill Formation, Pretoria Group, forming the roof (Gauert et al., 1996; de Waal and Gauert, 1997; Li et al., 2002). Indications are that the Complex intruded from the NW to the SE (van Zyl, 1996; Hornsey, 1999; de Waal and Gauert, 1997). It has also been determined by means of geophysical methods and drilling

that the intrusion extends to the northwest, under the escarpment (Gauert et al., 1996; Theart and de Nooy, 2001, Li et al., 2002). The complex is inferred to have intruded at a depth of 6 - 8 kilometers below the sedimentary cover (Gauert et al., 1996; Gauert, 1998; Ward and Wilson, 1998). The individual units of the complex along the centre of the trough show very consistent thicknesses in the part intersected by drilling over a plunge distance of 12 kilometers (Theart and de Nooy, 2001). The intrusion has an average true thickness along the centre of 670 meters (Theart and de Nooy, 2001), but vertical dilation owing to the intrusion of post-consolidation diabase sills, resulted in a modified thickness of 850 meters (de Waal et al., 2001).

The original field terminology for the stratigraphy was introduced by INCO geologists in the 1980's and was reported by Kenyon et al. (1986). These terms are given along with the lithological subdivision as suggested by Gauert et al. (1995) indicated next to it, with the abbreviation in brackets. The relative thickness of each unit is also given as well as an indication of being part of the conduit or closed stage. The subdivision of the different units of the Uitkomst Complex into a Basal Group and a Main Group (Theart and de Nooy, 2001) is also included in Table 2.2.

Table 2.3. Lithological Subdivision of the Uitkomst Complex.

Lithological Name (Gauert et al., 1995)	Field Terminology (Kenyon, 1986)	Thickness (Woolfe, 1996)	Stage (Gauert)	Group (Theart and de Nooy, 2001)
Gabbronorite (GN)	Upper Gabbro (UGB)	10-20 meters	Closed	Main
	Norite (NU)	250-300 meters		
Upper Pyroxenite (PXT)	Upper Pyroxenite (PXT)	60-80 meters		
Main Harzburgite (MHZBG)	Peridotite (Prdt)	200-300 meters	Conduit	
	Massive Chromite (MCR)	0-5 meters		
Chromatiferous Harzburgite (PCR)	Chromitic Pyroxenite (PCR)	30-56 meters		Basal
Lower Harzburgite (LHZBG)	Lower Pyroxenite (LrPXT)	20-40 meters		
Basal Gabbro (BGAB)	Basal Gabbro (BGAB)	0-7 meters		

The ore bodies of the Uitkomst Complex are confined to the lower units of the Uitkomst Complex (Basal Group). The unit terminology as recommended by Gauert (1998) will be used in this study. However, the field terminology as originally proposed by INCO geologist and reported by Kenyon et al., (1986) and subsequently modified by Anglovaal geologists are used in the borehole logs (Appendix 1).

An idealized cross-section of the Uitkomst Complex is given in Figure 2.3. The terminology has been adapted to Gauert's classification.
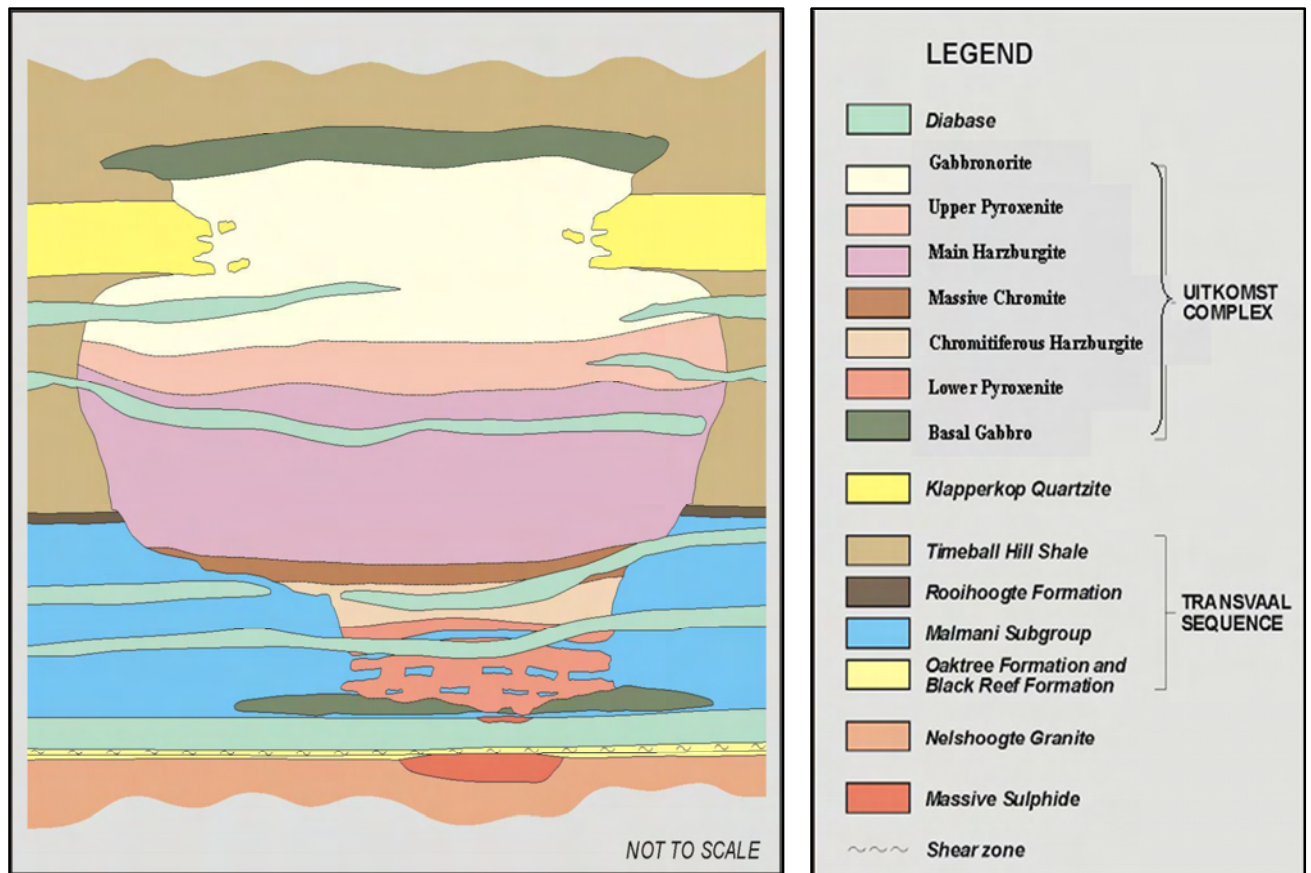
Figure 2.3. Idealized cross-section of the Uitkomst Complex. (Figure adapted after pers. comm. Nkomati Mine Geological Staff and legend adjusted to Gauert classification).

The lower three units are confined to a narrow trough-like keel, following the NW-SE trend of the sub-vertical fracture zones observed in the area (de Waal and Gauert, 1997; Hornsey, 1999).

There are two prominent thrust zones found in and near to the Uitkomst Complex. The first is the Basal Shear Zone and is found in the lower most dolomitic unit of the Oaktree Formation of the Malmani Subgroup (Hornsey, 1999; Theart, 2000). The dominant mineral in the Basal Shear Zone is calcite followed by quartz and minor iron and manganese oxides (Hornsey, 1999). The alteration minerals found in the Basal Shear Zone is tremolite and minor chlorite and biotite (Hornsey, 1999). The second thrust zone is found in the highly

altered parts of the PCR and is characterized by chlorite-talc schist zones (Theart, 2000) resulting in duplication of the LHZBG and the PCR in the vicinity of the old MSB mine section (Theart, 2000). In addition to these there are sub-horizontal schistose zones present in both the MHZBG and the PXT Units, consisting mainly of talc, dolomite, magnesite and chlorite and talc-chlorite schist zones respectively, but related duplication of lithological units could not be demonstrated in these cases (Theart, 2000).

A literature review of the tectonic history of the BIC and surrounding areas suggest that post-intrusive was present in the area, e.g. Hattingh (1980), Sharp and Chadwick (19781) and Perritt and Roberts (2007). However, the structures preserved in the intrusion and surrounding country rock does not reflect these events. The shear zones in the intrusion are typical of synchronous or immediately post-intrusive deformation, during solidification of the intrusion (pers. comm. Bumby, 2010).

2.4.1. Basal Gabbro Unit (BGAB)
The average thickness of the BGAB Unit is 6 meters (van Zyl, 1996; Gauert et al., 1996; Gomwe 2000; de Waal et al., 2001) with a maximum thickness of 15 meters (Strauss, 1995; Gauert et al., 1996; Hornsey, 1999; Gomwe, 2002). This zone can also be completely absent (Gomwe, 2002). The base of the unit is marked by a chill margin of between 0.2 and 1.5 meters (Strauss, 1995; van Zyl, 1996; Hornsey, 1999). The gradational contact of the BGAB Unit (Strauss, 1995) with the LHZBG Unit is usually obscured by pegmatitic phases and by the presence of sedimentary xenoliths. The BGAB Unit is laterally more extensive than the overlying LHZBG Unit, with sill-like extensions roughly parallel to the Basal Shear Zone extending up to 400 meters into the country rocks (de Waal and Gauert, 1997; Hornsey, 1999; Gomwe, 2002; Li et al., 2002; Maier et al., 2004). The contact with the Black Reef is sometimes defined by a strongly sheared talc-chlorite-carbonate alteration product (van Zyl, 1996), but the unit is usually developed 2 meters above the Basal Shear Zone in the dolomitic host rock (de Waal and Gauert, 1997). The BGAB is better developed towards the northeastern part of the complex opposed to the uneven development in the rest of the intrusion (de Waal and Gauert, 1997). This unit is unevenly developed due to the

undulating nature of the Black Reef Quartzites, and may be in places completely absent (Gauert et al., 1996).

In the vicinity of the Massive Sulphide Body, the Unit appears to have been cross-cut and possibly ingested by the overlying LHZBG Unit magma (Hornsey, 1999). Field observations indicate that the direction of intrusion was from the northwest to the southeast (de Waal and Gauert, 1997; Hornsey, 1999). A sub-ophitic igneous texture is still visible in this unit (van Zyl, 1996), despite the subsequent alteration that affected the unit. de Waal and Gauert (1997) suggest that the magma giving rise to this unit resulted from a mixing of B1- and B2-type magma, which led to the formation of Bu-type magma that chilled against the country-rock. The BGAB thus represents the super-cooled chill zone of the intrusion (Strauss, 1995; Gauert et al., 1996; de Waal et al., 2001; Li et al., 2002).

2.4.2 Marginal Gabbro Unit (MG)

The MG Unit is found close to or forms the northeastern contact of the Uitkomst Complex with the host rock and along this contact of the intrusion on the farm Uitkomst 541JT (de Waal and Gauert, 1997; Gauert, 1998). It is mineralogically similar to the BGAB Unit, but occurs at the same elevation (up to 200 meters above the base of the intrusion) as the LHZBG and MHZBG Units and grades into the cumulate rocks of these units (de Waal et al., 2001; de Waal and Gauert, 1997). The medium to coarse grained MG Unit is generally feldspar- rich and partly mineralized with sulphide minerals. The unit contains traces of graphite (de Waal and Gauert, 1997). It has been implied that the presence of this unit indicates that the chamber was probably filled with gabbroic magma before the formation of the layered sequence (de Waal et al., 2001). The implication of this phenomenon is that the magma of the BGAB had a larger vertical extent in the position of the current central trough. This gabbroic magma may have been completely removed by emplacement of the later magma pulses of the LHZBG and PCR/MHZBG units. The MG is suggested here to represent a relict of the first conduit magmatic emplacement.

2.4.3 Lower Harzburgite Unit (LHZBG)

The LHZBG Unit has an average thickness of 50 meters (van Zyl, 1996; Gauert et al., 1996; de Waal et al., 2001) but a maximum thickness of up to 90 meters (Gomwe, 2002) on the farm Uitkomst 541JT. The contact with the BGAB Unit is gradational, as discussed above (Gauert et al., 1996; Theart, 2000; de Waal et al., 2001). In places the LHZBG Unit thermally eroded the BGAB Unit and now forms the base of the intrusion (Li et al., 2002; Gomwe, 2002). There is also evidence that the BGAB Unit was removed physically in places by thrusting at the base of the Complex (pers. comm., H.F.J. Theart, 2006). The LHZBG Unit occurs in what is known as the central trough (Gomwe, 2002), and consists of a variety of rock types, including poikilitic harzburgite, lherzolite, wehrlite and websterite (de Waal et al., 2001; Li et al., 2002; Maier et al., 2004; Steenkamp, 2004).

This unit contains numerous quartzitic and carbonaceous xenoliths, derived mainly from the Malmani Dolomites (Gauert et al., 1996; Hornsey, 1999; Theart, 2000; de Waal et al., 2001). These xenoliths are flattened in the direction of the original layering and form rafts that are oriented parallel to the igneous layers (van Zyl, 1996; Hornsey, 1999). The preservation of flat-lying sedimentary rafts, at the appropriate elevation relative to the stratigraphy in the sedimentary wall rocks of the Complex, may indicate a passive style of intrusion (Theart, 2000). A "passive style" of intrusion suggests that the magma was emplaced in an infiltrative manner rather than through direct magmatic flow. The metamorphosed dolomites, now preserved as calc-silicate rocks, make up as much as a third of the volume of the unit (Gauert, 1996; Maier et al., 2004). In some cases massive sulphides accumulate around the dolomite xenoliths, possibly filling voids that were generated during devolatization (Maier et al, 2004). Additionally large concentrations of coarse disseminated sulphide grains seem to be associated with the xenoliths (Li et al., 2002). Disseminated sulphides are also more concentrated in the olivine wehrlite layers, where the disseminated sulphides frequently grade into massive sulphides surrounding the dolomite xenoliths (Li et al., 2002). In contrast, the hybrid rock, which may represent the magma-dolomite interaction product, is sometimes less mineralized or completely barren (Hornsey, 1999). In the vicinity of the country rock a pegmatiodal pyroxenite is developed

(van Zyl, 1996). The mafic phases within the LRHZB Unit consist dominantly of poikilitic harzburgite, with local variations to feldspar-bearing lherzolite and grading into sulphide-rich feldspathic olivine-wehrlite and into amphibolite (van Zyl, 1996; Gomwe, 2000).

2.4.4 The presence of "Parapyroxenite" in the LHZBG

"Parapyroxenite" is a term for altered pyroxenite, defined by the geologists of Sandsloot Mine (operated by Potgietersrus Platinum Ltd., a subsidiary of Anglo Platinum) as "a highly altered rock of varying thickness which is possibly a mechanical mixture of calcsilicate material (metamorphosed and metasomatised dolomite), pyroxene-rich igneous rocks and minor serpentinites" (Harris and Chaumba, 2001). In the Northern limb of the Bushveld Complex, where the Platreef is in contact with dolomite, parapyroxenite is an important rock type. "Parapyroxenite" has also been defined by MacDonald et al., (2005) as a massive diopside-clinopyroxenite that is locally enriched in metamorphic olivine that suffered variable degrees of serpentinization.

The hybrid rock encountered in the LHZBG Unit in the study area may also be called a parapyroxenite, using the Sandsloot definition. The dominance of diopsidic-clinopyroxene with triple junctions and the presence of fassaite indicate a thermal metamorphic origin for parts of the LHZBG Unit. In addition, the presence of primary orthopyroxene, clinopyroxene and olivine in close proximity to metamorphic clinopyroxene indicates a magmatic component in such rocks.

The large range in texture and mineral assemblages from pristine to mineral assemblages indicative of complete retrograde metamorphism also indicate the important role of hydrothermal fluids that interacted with the rocks of the LHZBG Unit to form more hydrous mineral assemblages.

2.4.5 Chromitiferous Harzburgite Unit (PCR)

The PCR Unit has an average thickness of 60 meters (van Zyl, 1996; Hornsey, 1999; Gomwe, 2002). This unit is confined to the upper portion of the deep central trough, but also drapes onto the sidewalls (Hornsey, 1999; Theart, 2000; Gomwe, 2002). It is hosted by the Malmani dolomite, Bevets Conglomerate and the base of the Timeball Hill Formation (Maier et al., 2004). In comparison with the LHZBG Unit, xenoliths are uncommon to absent in this unit (Gauert et al., 1996; Gauert, 1998; Hornsey, 1999). The contact with the LHZBG Unit is gradational, with the contact being obscured in places by a talc-schist zone interpreted to be a ductile shear zone (van Zyl, 1996; Gomwe, 2000; Theart, 2000). The unit consists of abundant lenses, layers and schlieren of massive chromite in a highly altered harzburgitic matrix (van Zyl, 1996; Hornsey, 1999; Gomwe, 2002). The harzburgite has been almost completely replaced by talc, carbonate, mica (phlogopite), chlorite and serpentine, obscuring the nature of the primary precursor (van Zyl, 1996; Hornsey, 1999; Gomwe, 2002). The unit may contain up to 5 vol% of sulphides, consisting of disseminated sulphides (pyrrhotite with lesser chalcopyrite and pentlandite) (Maier et al., 2004). The sulphides are particularly concentrated in clinopyroxene-bearing lithologies (de Waal et al., 2001).

The stratigraphy appears inverted with a harzburgite (PCR Unit) with a more primitive composition, overlying a pyroxenite (LHZBG Unit) with a less primitive composition. This phenomenon has been attributed to decreasing assimilation of country rock dolomite with stratigraphic height (Dodd, 2004), and not reversed differentiation as suggested by Kenyon, Attridge and Coetzee, (1986).

2.4.6 Massive Chromitite Unit (MCR)

The chromite content increases towards the top of the PCR Unit (van Zyl, 2000), where several massive chromite layers occur, reaching thicknesses of up to 15 meters, probably due to tectonic duplication (Maier et al., 2004). The top of the PCR Unit is marked by a massive chromite layer with a thickness of between 0-15 meters (van Zyl, 1996; Gomwe, 2000). Where the massive chromite layer is present its contacts are marked by schistose,

ductile shear zones (Theart, 2000). The massive chromite layers comprise one or more layers of chromite intercalated with highly altered silicate laminations. The thickest part of the Massive Chromite layer occurs in the southeastern part of the Uitkomst Complex and outcrops as three chromite hills on the farm Uitkomst (Gauert, 1998), and pinches out towards the northwest (Li et al., 2002).

Gauert (1998) suggested that the sulphur segregation triggered by the degassing of the dolomite xenoliths and wall rocks caused an increase in volatiles in the magma and this culminated with the precipitation of the Massive Chromite unit. However, the Cr/Fe ratio of chromite grains in the Massive Chromite varies between 1.4 and 1.86. This argues against high oxygen fugacity during its formation and indicates that the Massive Chromite layers formed under low oxygen fugacity conditions (Gauert, 1998).

2.4.7 Main Harzburgite Unit (MHZBG)

The average thickness of this unit is 330 meters (van Zyl, 1996; Gauert et al., 1996; Hornsey, 1999; Gomwe, 2000; Li et al., 2002). It caps the central trough (Gomwe, 2002). The contact with the underlying MCR is sharp, except where the contact is obscured by a talc-chlorite schist zone (Theart, 2000). This unit consists mainly of harzburgite which locally grades into dunite (van Zyl, 1996; Hornsey, 1999; Gomwe, 2000). A number of thin chromite seams with thicknesses not exceeding 30 centimetres, intercalated with harzburgite layers, are found near the base of the unit (Theart, 2000). Towards the top of the unit, the harzburgite contains intercalated pyroxenite layers that have gradational contacts. Small sulphide grains, dominated by pyrrhotite, are present throughout the unit, but are more abundant in irregular patches. These patches are more abundant in the lower 10 meters (van Zyl, 1996; Gomwe, 2000) and again in thin horizons in the upper portions (50-90 meters below top of the unit) of the Complex (Gomwe, 2002; Li et al., 2002). Minor dunite and numerous thin chromite layers become more common towards the northwest (Hornsey, 1999; Li et al., 2002).

The cumulus minerals in the unit are olivine (65-70 vol%) increasing upwards from the base (Gomwe, 2002). The rounded olivine grains are poikilitically enclosed in coarse grained orthopyroxene oikocrysts (40-80%) and less commonly (10-20%) in clinopyroxene (Theart, 2000). Chromite (1-5 vol. %) and oikocrystic orthopyroxene (20-15 vol. %) decreasing from the base upwards (Gomwe, 2002) are also present. The chromite becomes more Fe-rich near the top of the unit, with Mg/(Mg+Fe)=0.4 and Cr/(Cr+Fe+Al) = 0.5 (de Waal et al., 2001). The intercumulus minerals are plagioclase, clinopyroxene and amphibole (5-10 vol%; Gomwe, 2002).

Serpenitinization is the main alteration type that affected this unit (van Zyl, 1996). The extent of serpenitinization decreases from the base of the unit upwards (Gomwe, 2002). Magnetite and magnesite is common in the serpenitinized zone along with lizardite, chrysotile, chrysotile and talc (Gomwe, 2002). Talc-carbonate alteration is rare in this unit (van Zyl, 1996). A sub-horizontal schistose zone, up to 15 meters wide and believed to represent a ductile shear zone. This schistose zone may possibly be related to more than one phase of thrust deformation. The schistose zone consists of talc, dolomite, magnetite and chlorite (Gauert, 1998). Crosscutting and concordant pegmatoidal rocks consisting of pyroxenes and feldspar with minor carbonates and quartz are found in the MHZBG Unit. This pegmatite phase however contain no sulphide mineralization in contrast to the LHZBG. This may be explained by the fact that the oxygen fugacity in this unit is controlled by the quartz-magnetite-fayalite buffer (Gauert et al., 1996), preventing the formation of sulphides. The pegmatoidal rocks have sharp contacts and are intrusive into the surrounding rocks (Theart, 2000).

2.4.8 Lower Peridotite Subunit (LrPRD)

The LrPRD subunit is found within the MHZBG Unit where the underlying MCR Unit is not developed (Theart, 2000). This unit is characterized by numerous lenses and thin layers of semi-massive chromites within the harzburgitic rocks. The subunit also hosts disseminated sulphide mineralization (Theart, 2000). It consists mainly of chromatic-harzburgite with lesser chromite rich pyroxenite and pyroxenite (Theart, 2000). This

subunit is not as intensely altered as the underlying PCR Unit, and is developed in the deeper parts of the complex on Slaaihoek 540 - JT (Theart, 2000).

2.4.9. Pyroxenite Unit (PXT)

The PXT Unit has a transitional contact with the MHZBG Unit. It has an average thickness of 60 meters (van Zyl, 1996; Gomwe, 2000). The basal contact is gradational over 1-2 meters (Gomwe, 2002) with appreciable amount of olivine present. The unit consists of a medium-grained pyroxnite intercalated with thinner peridotite layers towards its base (Theart, 2000). A sub-horizontal talc-chlorite schist zone is also present in parts of this unit (Theart, 2000).

The PXT Unit has been interpreted as a transitional interval where the unit may be subdivided into three parts:

i)   The lower olivine-orthopyroxenite

ii)   The central orthopyroxenite with minor chromite and sulphides

iii) The upper norite to gabbronorite, showing an increase in the amount of plagioclase, clinopyroxene and minor quartz with height (Gauert 1998; van Zyl, 1996; Hornsey, 1999; Gomwe, 2000: Li et al., 2002). This upper part of the unit grades into the overlying Gabbronorite unit (GN).

This unit is markedly unaffected by secondary alteration when compared to the underlying units (van Zyl, 1996). However, in places the orthopyroxene is rimmed by an alteration halo of tremolite, phlogopite and fuchsite which provides evidence of interaction with a late-stage fluid (Gomwe, 2002). This unit is intruded by concordant and discordant pegmatoidal rocks consisting of feldspar, pyroxene and calcite (Theart, 2000).

The cumulus minerals in the unit are orthopyroxene (>80 vol%) and olivine (decreasing form the base to the top where it is completely absent), chromite and clinopyroxene being locally present (± 5 vol%) (Gomwe, 2002). The post-cumulus phases are plagioclase (increasing from the bottom upward 10-50 vol %), clinopyroxene, phlogopite, amphibole

and quartz, decreasing from the top of the unit to the base (Gomwe, 2002). Disseminated sulphides up to 1wt% occur in the upper portion of the unit (Li et al., 2002).

2.4.10 Gabbronorite Unit (GN)

The GN Unit has an average thickness of 250 m and a gradational lower contact with the PXT Unit (van Zyl, 1996; Gomwe, 2000). The GN Unit has a sill-like lateral extension of ±1.4 kilometers (Gomwe, 2002), and displays vertical compositional layering, varying from melanocratic at the base of the unit to leucocratic at the top contact (Gomwe, 2002; Li et al., 2002). The top contact of this unit is formed by a chilled margin (van Zyl, 1996) showing a sharp contact with the Timeball Hill Formation (which is thermally altered to hornfels). The gabbroic rocks near the contact are marked by the presence of "feather amphiboles" (Theart, 2000). This unit also contains xenoliths of quartzite and argillaceous rocks derived from the Timeball Hill shale (van Zyl, 1996; Theart, 2000; Li et al., 2002). A thin cumulus magnetite layer occurs near the base of the unit, while magnetite of uncertain paragenesis is observed within the sedimentary rocks above the contact (Theart, 2000).

The upper part of the GN Unit is noticeably more primitive than the underlying diorites. This is shown by a sharp reversal towards higher MgO, Mg#, Ni and Cr values (Maier et al., 2004). It has been proposed that the upper GN Unit represents crystallization of the initial magma pulses against the roof (Maier et al., 2004). The mineralogy of the lower part consists of 50-60 vol. % plagioclase, whereas the clinopyroxene content increases with height from the base while orthopyroxene decreases (Gomwe, 2002).

The principal alteration mineral in the GN Unit is amphibole (hornblende) which increases in abundance from the bottom of the unit and constitutes approximately 10 vol. % (Gomwe, 2002). Chlorite has been found to dominate the centres of some pseudomorphed primary mineral grains (Gomwe, 2002). In the upper part of the GN Unit, the cumulus minerals consist of 40-60 vol. % plagioclase, 20-40 vol. % orthopyroxene and 5-10 vol. % clinopyroxene (Gomwe, 2002). The intercumulus minerals consist of quartz, increasing from 5-10 vol. % from the bottom of the unit, biotite, apatite and zircon (Gomwe, 2002).

This unit contains <1 vol. % disseminated sulphides (Gomwe, 2002). Alteration of the upper part of the GN Unit is more pervasive, where the alteration mineral assemblage comprises amphibole (hornblende and actinolite-tremolite), alkali-feldspars, chlorite and epidote (Gomwe, 2002).

2.5 Previous models of the intrusion of the Uitkomst Complex

A simplified sequence of intrusion for the Uitkomst Complex may be given as:

- A series of NW-SE trending fractures existed in the area of the intrusion according to de Waal et al. (2001).

- **Stage 1**: An initial pulse of magma, represented by the BGAB Unit intruded close to the contact between the Archean granite and the overlying Transvaal sediments. This created and filled the initial conduit, as indicated by the presence of the MG Unit forming a marginal contact higher up in the stratigraphy.

- **Stage 2**: Shortly after emplacement of the BGAB Unit, the magma pulses responsible for the formation of the LHZBG Unit, started flowing through the conduit. These pulses assimilated some of the gabbroic magma and dolomites. The most primitive pulses are represented by the wehrlitic layers. The assimilation of carbonates led to the precipitation of sulphides and the creation of hybrid rocks, such as the parapyroxenite. The passive nature of intrusion of these pulses is demonstrated by the preservation of calc-silicate xenoliths with the preserved layering oriented parallel to the layering in the country rocks. According to Hornsey (1999), the intrusion of these pulses would have led to the creation of a radial tensile fracture pattern in the overlying sediments. The volume of magma increased over time, as indicated by the decrease of xenoliths in the upper part of the LHZBG Unit, the intrusion likely propagated upward rapidly before creating lateral space.

- **Stage 3**: It is inferred that further pulses, creating the PCR Unit, intruded after the LHZBG Unit without a significant hiatus. These more voluminous pulses probably flushed the conduit of xenoliths.
- **Stage 4**: The formation of the MCR Unit layer on top of the PCR Unit probably represents the mixing event of an influx of new, Cr-rich reducing magma. Intrusive pulses of the MHZBG Unit magma followed, until the system eventually evolved to a closed system.

De Waal and Gauert, (1997) and Gauert (1998) found that the magma mixture that constitutes the Uitkomst Complex is dominated by B1 magma towards the NW, while the SE is dominated by B2 magma. This is observed in more abundant sulphide mineralization towards the NW and chromite mineralization towards the SE. The size of the intrusion has also been found to increase towards the SE (Hornsey, 1999; de Waal et al., 2001). The LHZBG and PCR Units are inferred to have been formed by crystal settling from a contaminated basic magma (van Zyl, 1996).

Several genetic relationship models have been proposed. Blom (1988), suggested that the inferred Mooiland Complex, in Mpumalanga, close to the Uitkomst Complex, indicated on the locality map (Figure 2.3) could have acted as a feeder to the Uitkomst Complex. The presence of the Mooiland Complex is inferred from an aeromagnetic and gravity anomaly that was believed to be caused by a magnetized, sill-like body, 1 400 m deep with a thickness of approximately 500 m. The gravity model predicts a 2 500 m thick sill-like body, dipping to the south, which has a density contrast of 410 kg/m^3 with respect to the Archean granites. The high susceptibility used in the two dimensional modelling process is indicative of a high percentage of magnetite present in the body, similar to that of the upper zone of the Rustensburg Layered Suite. Another similarity found between the Mooiland bodies and the Rustenburg Layered Suite is the fact that only the upper unit of the gravitational model is magnetic. From a colour coded aeromagnetic map and Bouguer anomaly map it was found that the Mooiland bodies are not linked to the main Bushveld Complex body, but should rather be seen as an intrusive complex on its own. It should be

noted that the Uitkomst Complex is more ultramafic in nature with significant chromite cumulates and no confirmed magnetite cumulates relative to the Mooiland bodies.

Mafic-ultramafic sills that are considered to be analogous to the Uitkomst Complex have been described by Maier et al. (2001). These sills are found near the contact of the sedimentary and volcanic rocks of the Silverton Formation (Transvaal Supergroup), on the farms Blaawboschkraal, Swartkopje and Waterval. The location of these three farms, the inferred location of the Mooiland intrusion and the farms Slaaihoek 540 - JT and Uitkomst 541 - JT is shown in Figure 2.4.

Kruger (2004) suggested that, (referred to by the author as the Nkomati conduit intrusion) the conduit might have served as an upper zone magma conduit of a more extensive southern lobe of the Bushveld Complex. Alternatively the conduit could have fed into a volcanic- or peripheral sill phase that eroded away.
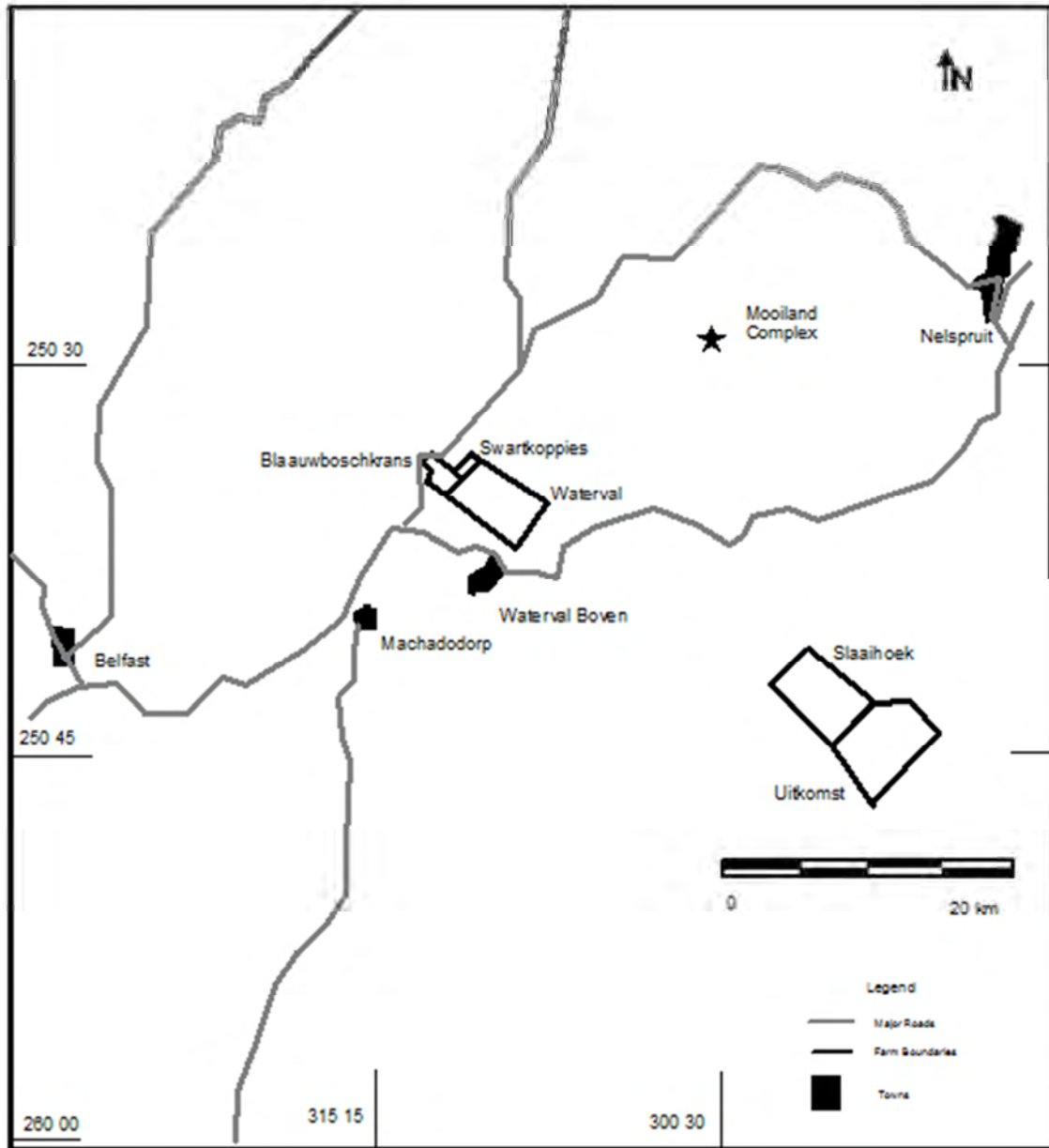
Figure 2.4. Locality Map indicating the position of the mafic-ultramafic intrusions related to the Bushveld Complex on or near the escarpment in Mpumalanga. Image adapted after Maier et al., (2001) with the Mooiland intrusion's position inferred from Blom (1988).

2.6. The Pit 3 open cast operation

The exploitation of the shallow chromite resource, located in the exposed shallow part of the Uitkomst Complex on the farm Uitkomtst 541 JT, will form part of the large scale open pit three operation (Theart, 1997; Anonymous, 2007). The shallow oxidized chromite resource will be mined first as part of the pre-strip (Figure 2.6) to expose the underlying disseminated sulphide ore bodies of the PCMZ and MMZ (Theart, 2000; Anonymous, 2007).   The sulphide minerals in this material above the groundwater table is oxidized and rendered unextractable. However in the deeper parts of the orebodies the sulphide minerals may have to be extracted first before the chromite may be utilized. The extent of the pre-strip is indicated in Figure 2.5.

Figure 2.5 Pre-strip in the Pit 3 area, November 2008 (Image, Google Earth, 2008).

CHAPTER 3: METHODOLOGY

3.1 Delimitations

The original focus of the investigation was to determine the alteration characteristics of the lithological units hosting the economic mineralization in the Uitkomst complex. For this purpose the study concentrated on those (or adjacent) boreholes that returned poor metallurgical recoveries during the feasibility test work conducted by Anglovaal Minerals (Ltd.) (L.Bradford, internal company report, 1996).

This project does not attempt to describe the entire succession of the Uitkomst Complex. Only representative samples from those affected lithological units encountered along a broadly defined profile and cross-section through the area of interest were sampled and analysed.

This thesis does not attempt to describe the metamorphic aureole surrounding the intrusion. Only a brief overview of the calc-silicate xenoliths is given as it is suggested that these inclusions may have a bearing on the mineralization in the complex. The metamorphic aureole is the subject of a project undertaken by Jens Kriste under the supervision of Dr. C.D.K. Gauert (University of the Free State).

It is assumed that all of the borehole descriptions by various company geologists contained in the logs are complete and correct.

3.2 Description of Methods

3.2.1 Sample selection

A map indicating the so-called talc-rich area on Uitkomst was used to select boreholes for this investigation (pers. comm. L. Bradford, 2005). The range of boreholes was chosen in such a way that it provides an approximate cross section through the lithlogies in the area designated for the future open cast mine. The boreholes selected are; UK3, UK12, UK20,

UK32, UK44, UK48, UK57, UK61 and UK68. Most of the boreholes are situated near the inferred edge of the Uitkomst Complex in the study area (Figure 1.6).

Representative samples of quartered core were taken at two to three meter intervals, where the Basal Gabbro, Lower Harzburgite and Chromatitic Harzburgite Units were intersected. Each sample was approximately twenty centimeters in length. Of these samples a selected few were broken into three pieces, as indicated in Appendix 1. The first of these was used to make thin sections and later polished thin sections, the second was crushed for whole rock analyses and the third kept for control purposes, should a duplicate be required.

3.2.2 Utilization of borehole logs

Borehole logs of the selected boreholes were obtained from African Rainbow Minerals Ltd. The borehole logs were utilized in part to aid in the selection of samples. The logs were also used in calculations, including the determination of the ratio of xenolith content to igneous rock mass, unit thickness, and thickness of the underlying host rock and in determining the proximity of samples to shear zones and diabase sills.

3.2.3 Thin sections

Thin sections for microscopic investigation were made at the Sectioning Laboratory of the Geology Department, University of Pretoria. The initial thin sections were used to describe the petrography, determine the mineral assemblages and establish the degree of alteration. This information was used to select samples for which polished thin sections were prepared for microprobe analyses. Samples that contained large amounts of minerals that may expand during normal polishing procedures were identified and submitted to the De Beers GeoScience Centre for making polished thin sections, using the paraffin method.

3.2.4 Sample preparation for X-Ray Diffraction (XRD) and X-Ray Florescence (XRF) analyses

In an effort to minimize contamination, the quartered core piece selected for analyses by XRD and XRF were wrapped in sample bags and broken into pea-sized fragments. The fragments were then milled in a carbon steel pot in the refurbished Dickie and Stockler

swing mill to the consistency of baby powder (<70 µm). A more comprehensive discussion of the sample preparation is given in Appendix 3. XRD and XRF analyses were preformed on 5 samples from the BGAB Unit, 23 from the LHZBG Unit, 6 xenoliths from the LHZBG Unit, 21 from the PCR Unit and 3 from the LrPRD Unit.

3.2.5 XRD Analyses

Samples were prepared according to the standard method applied in the XRD laboratory of the University of Pretoria. The samples were analysed in a PANalytical X'Pert PRO X-Ray Powder Diffractometer fitted with X'Celerator detector. Semi-quantitative mineral phase analyses of the samples were obtained with the aid of the Rietveld method and by using Autoquant software. The minerals analysed for are: actinolite, amesite, calcite, chlorite, chalcopyrite, goethite, quartz, muscovite, plagioclase, talc, biotite, chromite, diopside, dolomite, fosterite, hornblende, lizarite, pyrite, pyrrhotite, phlogopite, enstatite, cordierite, epidote and grossular.

Samples were crushed before being milled in a carbon steel mill pot. The mill pot was cleaned by milling pure quartz sand and washing with acetone and drying. The pot was then pre-contaminated with a small piece of the sample material to be milled. The milled material was then hand-pressed into the holder, using the in house back-fill method. The sample material is heaped on the holder, held in place by a spring loaded support holder. The material is then distributed evenly in the opening of the holder. Using a stainless steel, solid cylinder the material is manually compressed into the back opening of the holder. The excess material is then cleared of around the cylinder before the back support is placed on the holder (Loubser and Verryn, 2008; Steenkamp, 2009). X-Ray Diffraction (XRD) was used to determine the phases (minerals) present in the sample. Quantitative determination is done using the Rietveld method.

3.2.6 XRF Analyses

Samples were prepared according to the standard procedures of the XRF laboratory of the University of Pretoria. This is described in Appendix 3. The samples were analysed in an

ARL9400XP+ X-Ray Fluorescence Spectrometer. The instrument uses a sequential wavelength dispersive spectrometer to perform quantitative major and trace element analysis. The instrument uses UniQuant software to produce results. The elements analysed for consisted of the major oxides, SiO_2, TiO_2, Al_2O_3, Fe_2O_3, MnO, MgO, CaO, Na_2O, K_2O, P_2O_5, Cr_2O_3, NiO and SO_3. The trace elements analysed for consisted of As, Cu, Ga, Mo, Nb, Ni, Pb, Rb, Sr, Th, U, W, Y, Zn, Zr, Cl, Co, Cr, F, S, Sc, V, Cs, Ba, La and Ce.

Sample material was crushed in preparation for milling in a carbon-steel mill pot. In order to minimize cross-contamination the mill is cleaned after every sample by milling quartz sand and washing with acetone. A small sample was then milled to pre-contaminate the mill.

Major and Trace element analysis were executed on a pressed powder briquette using the ARL9400XP+ spectrometer. Elements are analysed, using an adaptation of the method described by Watson (1996) using a saturated Mowiol 40-88 solution as binder. The milled sample material was placed in aluminium cups to increase stability and strength before being pressed at $\pm$ 7 tons/in^2 (Loubser and Verryn, 2008; Steenkamp, 2009).

The XRF Spectrometer is calibrated with certified reference materials. The NBSGSC fundamental parameter program was used for Cl, Co, Cr, V, Ba and Sc. The Compton peak ratio method was used for the other trace elements. W, Cl, F and S should be considered semi-quantitative. Only pressed powder briquettes were used as most of the samples contained significantly large amounts of sulphides. Loss on ignition (LOI) is determined by weighing three (3) grams of powdered material into a pre-weighted aluminum-silicate crucible. The material is dried overnight at 100 °C and weighed again before being roasted overnight at 1000 °C and weighed (Loubser and Verryn; 2008). The method for determining LOI is described by Loubser and Verryn (2008).

The CIPW (Cross, Iddings, Pirrson, Washington) normative mineral calculation was applied to the XRF results, using *MinPet* software. The CIPW norm values are presented at the bottom of the tables.

3.2.7 Electron Microprobe (EMP) Analyses

Polished thin sections were made of the samples that were selected for mineral analyses. The grains of interest were identified with the aid of an optical microscope using both transmitted and reflected light. The minerals were photographed with a Leica microscope fitted with digital imaging equipment and connected to a computer for capturing and saving images for subsequent orientation in the microprobe.

The points selected for analyses were marked using a diamond-scribe fitted optical microscope. This microscope is connected to a computer that uses *Cotrans* software for logging the points that could subsequently be located in the electron microprobe. The polished thin sections were then cleaned and carbon coated in an EMITECH K950X turbo pump driven Carbon Coater.

The Geology Department, University of Pretoria operates a CAMECA SX 100 Electron Probe Micro Analyser. This instrument is fitted with four wavelength dispersive spectrometers as well as the latest energy dispersive system from Röntec. This allows the determination of the mineral composition of individual grains at microscopic scale. This instrument was used for the analyses of the silicate-, oxide-, sulphide and platinum group minerals. The silicate and oxide minerals were analysed on the basis of the following elements: SiO_2, TiO_2, Al_2O_3, FeO, MnO, MgO, CaO, Na_2O, K_2O, F, Cl, Cr_2O_3 and NiO. The sulphides were analysed on the basis of the following elements: S, Fe, Co, Ni, Cu and As.

The counting times on peak positions are 20 seconds and 10 seconds on background positions. A ZAF corrections procedure is applied throughout (Pers. Comm. Gräser, 2005).

Certified standards are used for silicate analyses, using the following standards for each element:

1. A Wollastonite Standard is used for Si and Ca.
2. Pure Oxide Standards are used for Mg, Al, Mn, Cr, Ti, Ni and Fe.
3. An Orthoclase Standard is used for K.
4. An Albite Standard is used for Na.
5. A Tugtupite Standard is used for Cl.
6. A Fluorite Standard is used for F.

Certified standards are also used for sulphide and oxide analyses, the following standards were used for each element:

a. $Cu\ FeS_2$ for Cu, Fe and S

b. NiO for Ni

c. Pure arsenic and cobalt standards for As and Co

3.2.8 Energy Dispersive Spectrometer (EDS)

An Energy Dispersive Spectrometer (EDS), mounted on the Cameca SX100 Microprobe, was used to find the Platinum Group Minerals (PGM's). The backscatter image contrast was adjusted to reveal minerals consisting of heavy elements. In a backscatter image heavy elements will appear brighter and lighter elements darker. An analysis of the mineral was performed. If the mineral was smaller than 5 micrometers, some of the surrounding host minerals were also analyzed.

3.3. The isocon method

The quantification of changes in the rock volume and elemental concentrations during hydrothermal alteration is an important component of lithogeochemical investigations of alteration zones. It is a simple matter to calculate the relative gain or loss of different components when the altered rocks are distinguished as the least-altered equivalents or source rocks especially in relatively undeformed and unmetamorphosed rocks. Gresens (1967) presented equations for these calculations based on chemical analyses and specific

gravities of altered and unaltered rocks. Grant (1986) suggested a graphical solution to those equations, known as the isocon method. This contributes greatly to a more quantified approach in the study of these phenomena.

Gresens's equations are based on mass rather than the volume (Gresens, 1967). The mass of element after alteration (M_i^A) is defined by the original mass (M_i^O) plus any change in the mass (ΔM_i) of that element during the alteration (Grant, 1986):

$$M_i^A = M_i^O + \Delta M_i$$

Dividing throughout by M^O to get concentration units and multiplying by M^O/M^A to obtain the original concentration, the following equation is derived:

$$M_i^A / M^A = M^O / M^A (M_i^O / M^O + \Delta M_i / M^O)$$

M_i^A / M^A may be substituted for C_i^A and M_i^O / M^O for C_i^O, with C being the abbreviation for concentration and the equation (1) becomes:

$$C_i^A = M^O / M^A (C_i^O + \Delta C_i)$$

For an immobile element $\Delta C_i = 0$, and:

$$C_i^A = M^O / M^A . C_i^O$$

This is a linear equation that passes through the origin with the slope of the resulting line (M^O / M^A), equal to (C_i^A / C_i^O)$_{\text{immobile element}}$. Therefore the final equation for an element is defined as:

$$C_i^A = (C_i^A / C_i^O)_{\text{Isocon line}}[C_i^O + \Delta C_i]$$

This is the general equation for the isocon line. If constant mass is assumed, then $C_{immobile\ element}^A$ will be equal to C^O for an immobile element. If constant volume is assumed, then:

$$C_{immobile\ element}^A = (\rho^O/\rho^A)\ C^O$$

Recognizing the mobile and immobile elements is an important aspect of the isocon method. If elements are immobile during the alteration process, the isocon line will pass through the origin. The concentration of these immobile elements will not vary between the original and altered rocks. The gain and loss of the mobile elements may then be calculated and any volume change can easily be deduced.

The isocon line passes through the origin and immobile elements and oxides i.e., TiO_2, Al_2O_3, Zr, U, Th, Nb, Y, La, and Sc. Those elements, which plot in the upper part of isocon line, represent gain and those elements that plot below the isocon line represent loss. The delta value for each element is calculated based on the following formulae:

$$(\Delta\ value)_i = C_i^A - C_i^O \cdot (\text{Slope value of the isocon line}), \quad _i: \text{the element of interest}$$

If the calculated delta value [$(\Delta\ value)_i$] of an element is positive it is indicative that the concentration of that element in the altered rock is greater than in the least altered rock (i.e. gain). Where the calculated delta value for an element is negative it means that the concentration of the element in the altered rock is less than that of the least altered rock (i.e. loss). The delta value can be converted to percentage based on the following formula:

$$\text{Percentage of gain or loss} = [(\Delta\ value)_i / C_i^O] \cdot 100$$

CHAPTER 4 PETROGRAPHY AND MINERAL GEOCHEMISTRY

4.1 – PRIMARY MAFIC MINERALS

4.1.1. Olivine

Very few preserved olivine grains were encountered in the samples selected for the current investigation, as the study concentrates on the highly altered areas of the Complex. During a preceding reconnaissance study of the harzburgite and wehrlite layers in the LHZBG Unit on the farm Slaaihoek 540 – JT by the author, olivine was encountered in the form of both pristine and completely altered grains (Steenkamp, 2004). The grains encountered during the present investigation were all euhedral and well rounded. Most of the olivine grains examined show signs of alteration, such as cracks in the olivine showing signs of hydrothermal alteration that resulted in the formation of serpentine (lizardite) in contact with the preserved olivine along the edges of the cracks. Since all of the samples were collected at depths that have not suffered any surface weathering effects, it may be inferred that the alteration is due to either syn-magmatic or post-magmatic hydrothermal alteration events. In the central part of internal cracks, in contact with the serpentine, non-continuous stringers of secondary magnetite are sometimes developed (Figure 4.1). The secondary magnetite is formed by topo-metasomatic mobilization of iron oxide from the olivine.

The mineral chemistry of olivine grains encountered during this investigation, as analysed by microprobe, is tabulated and presented in Appendix 2.
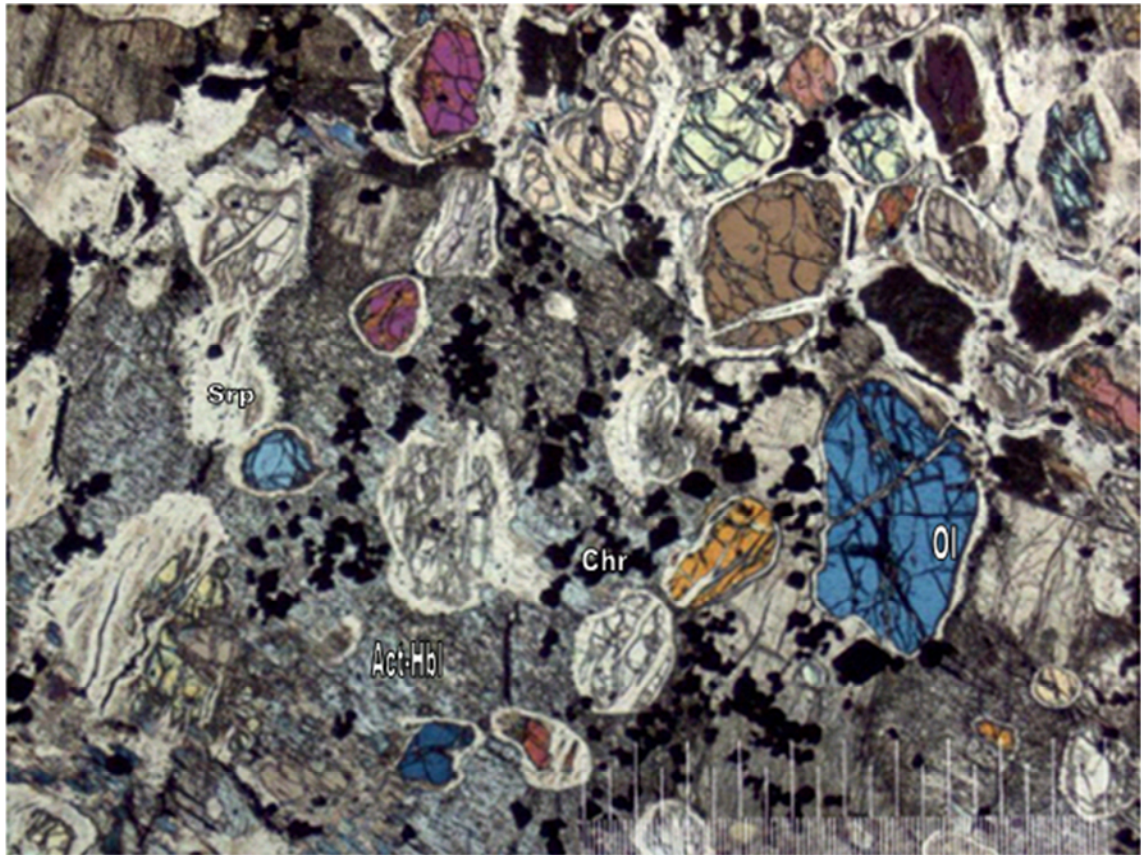
Figure 4.1. Euhedral to subhedral olivine (ol) grains that suffered hydrothemal metamorphism in the PCR Unit. Cracks in olivine grains are filled with serpentine (srp) and secondary magnetite stringers. Serpentine forms in haloes around olivine grains and partly replace them. Euhedral chromite (chr) grains (black) are found in association with the olivine. Olivine and chromite grains are poikilitically enclosed by clinopyroxene (diopside), hydrothermally altered to amphibole of actinolitic (act) to hornblende (hbl) composition. The picture scale bar is 1000. Taken with cross-polarised light. (Sample: UK12D).

In the LHZBG Unit, olivine grains are usually found in two associations. The first is as scattered grains in the harzburgite matrix, with an altered appearance as described above. These grains are poikilitically enclosed by diopside. Olivine grains are also found in the centre of triple junction points formed by larger clinopyroxene grains (Figure 4.2). The second association is in the wehrlite layers within the LHZBG Unit as rounded, euhedral grains surrounded by net-textured sulphides. Most of the olivines in the wehrlite layers have been partially or completely serpentinized and secondary magnetite is also found in and around these serpentinized olivine grains (Figure 4.3). Identifiable olivine grains in the

PCR Unit were only found in UK12, where their appearance is similar to the scattered olivine grains found in the LHZBG Unit (Figure 4.2).
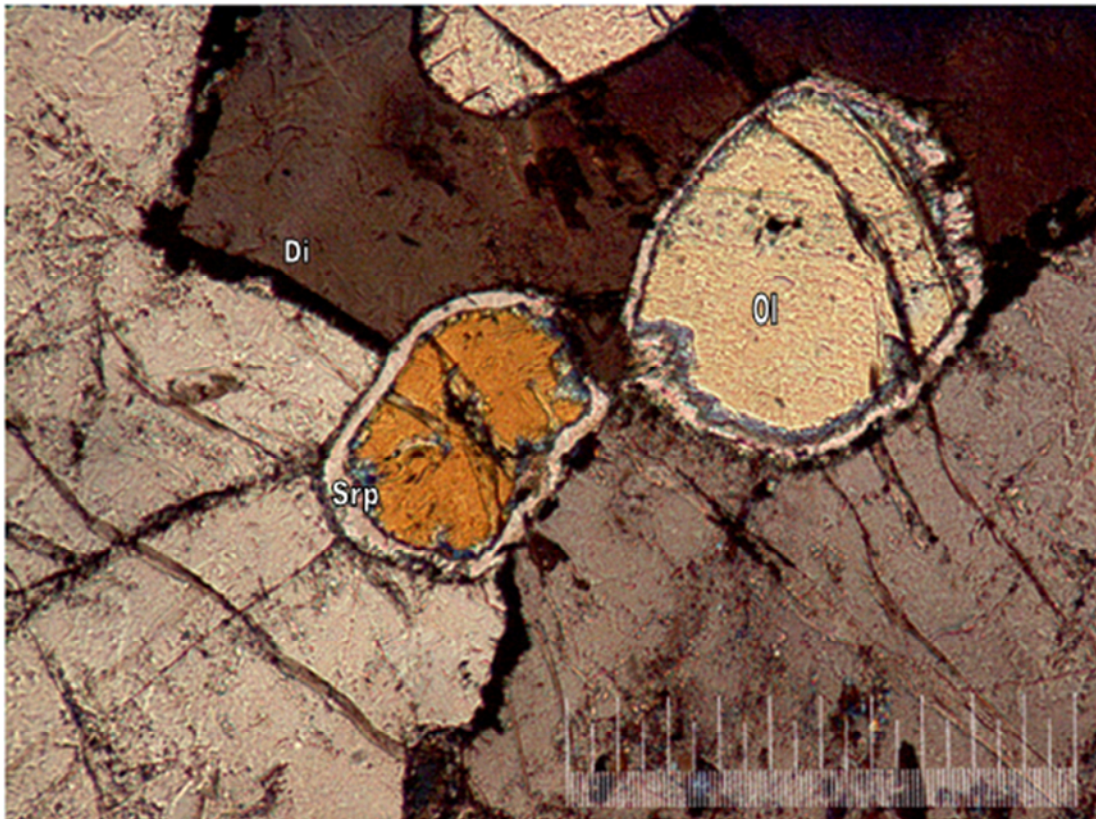
Figure 4.2. Rounded olivine (ol) grains with haloes of serpentine (srp) near a triple junction of diopside (di) grains, found in the LHZBG Unit. The picture scale bar is 1000 micron. Taken with cross-polarised light. (Sample; CS14).
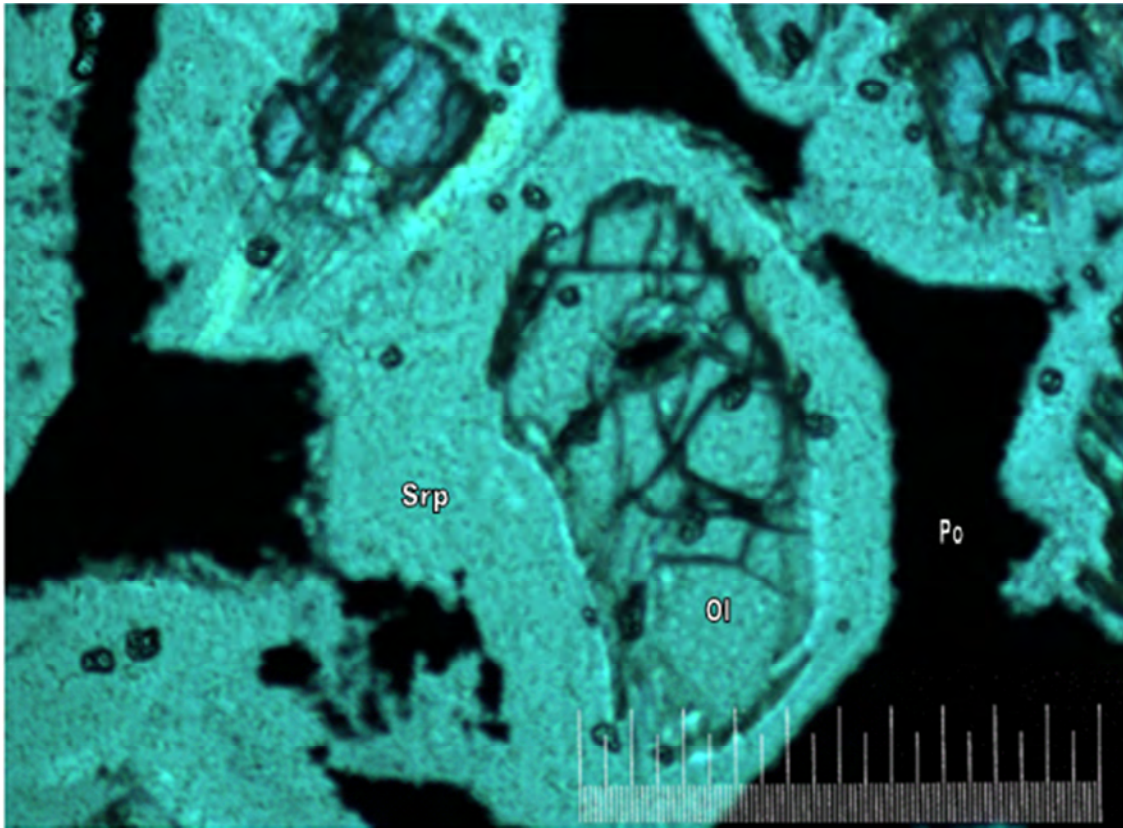
Figure 4.3. Olivine (ol) grains partially replaced by serpentine (srp), enclosed in net-texture sulphides (pyrrhotite – (po)) in the wehrlite layers found in the LHZBG Unit. The picture scale bar is 1000 micron. Taken with plane-polarised light. (Sample; CS 18).

Microprobe analyses (Appendix 2) of olivine grains revealed that the forsterite content of the olivines varies between $Fo_{75.78}$ and $Fo_{82.58}$, with an average of $Fo_{78.13}$ for the LHZBG Unit (n = 15), and between $Fo_{84.04}$ and $Fo_{95.48}$ in the PCR Unit (n = 34), with an average of $Fo_{88.15}$. There does not appear to be a significant difference between the compositions of olivine found in the wehrlite layers within the LHZBG Unit compared to that of the hybrid rock in the same unit. Olivine grains from both wehrlite and harzburgite in the LHZBG Unit contain between 0.1 and 0.23 % NiO and have magnesium numbers (Mg #) of between 0.64 and 0.73 (n = 15). The olivine grains analysed from the PCR Unit contain between 0.01 and 0.17 % NiO and have Mg # values ranging between 0.84 and 0.95 (n = 34).

Figure 4.4 gives a NiO versus Fo % graph showing that the olivine grains analysed from the PCR Unit have a higher forsterite content than olivine grains from the LHZBG Unit. The olivine from the LHZBG Unit has a higher NiO content compared to olivine from the PCR Unit. There are also two groups of olivine compositions in the PCR, one with on average less NiO and has a higher Fo-content and a second with a slightly higher average NiO content and has a lower Fo-content. Both varieties are found in samples with a diopside matrix that has suffered hydrothermal alteration, resulting in partial ampibolisation and chloritisation of the diopside crystals.
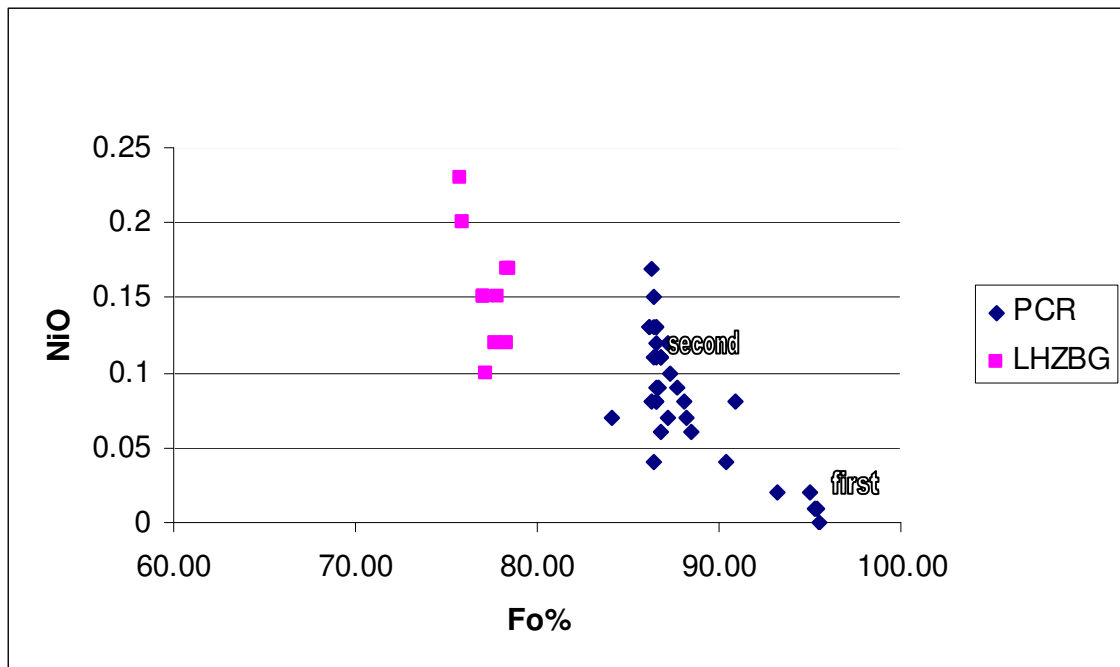
Figure 4.4. Comparison of olivine grain compositions of the LHZBG and PCR Units, based on NiO-content and the percentage forsterite. Data in Appendix 2.
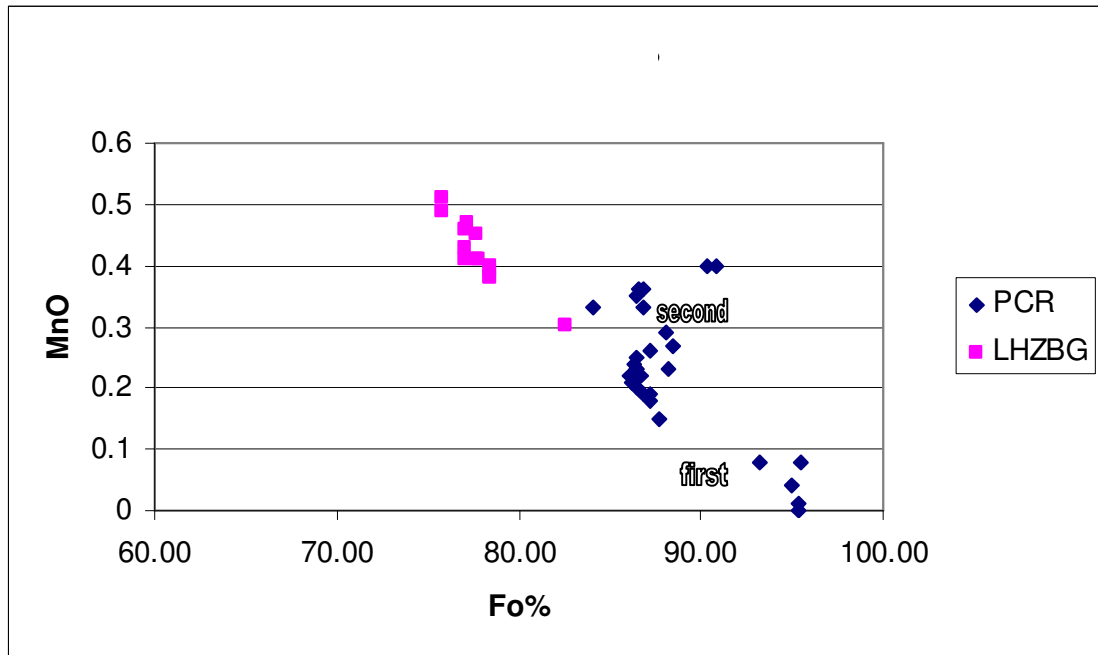
Figure 4.5. Comparison of olivine from the LHZBG and PCR Units on a MnO versus forsterite content diagram. Data in Appendix 2.

From figure 4.5 it may be seen that the olivines from the LHZBG Unit have on average a higher MnO content compared to olivines from the PCR. The two groups of olivine in the PCR Unit identified in Figure 4.4 are also distinguishable in this diagram. The first has a lower MnO content and higher Fo-content and the second a slightly higher MnO content but lower Fo-content.
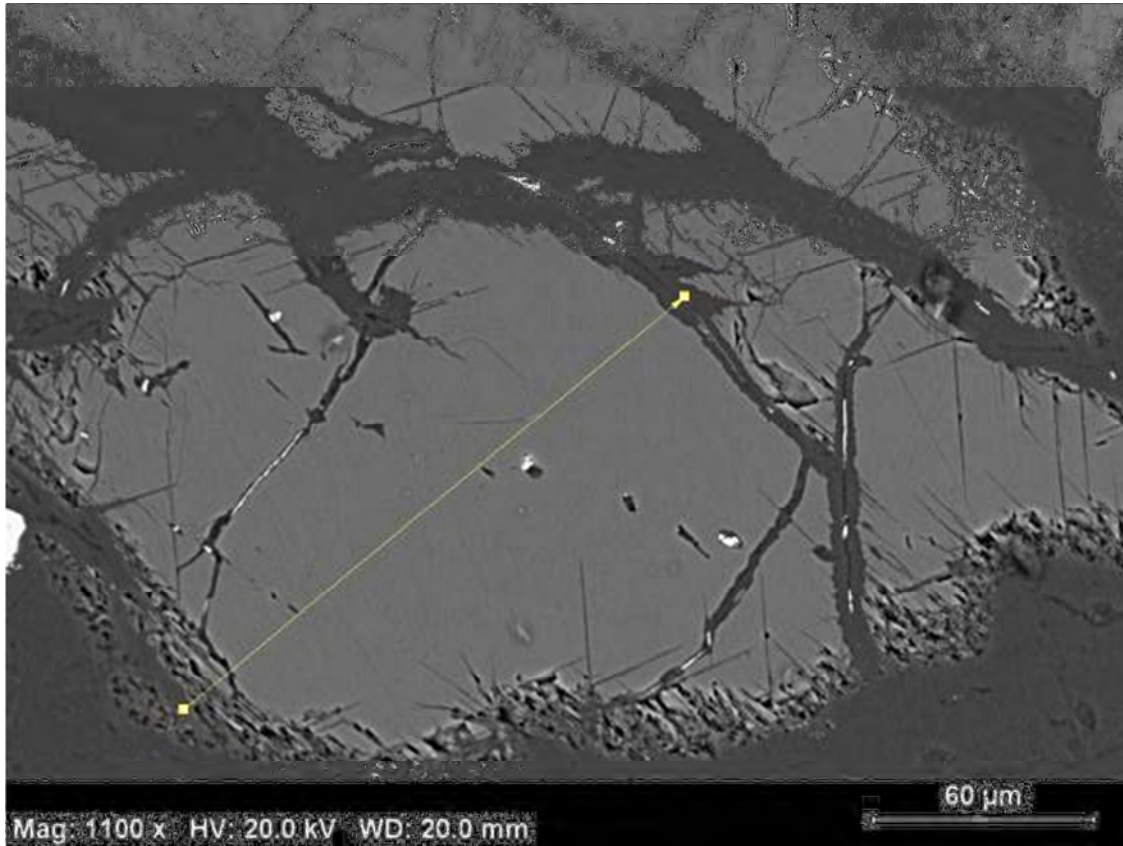
Figure 4.7. Backscatter image of olivine (light grey) with a line indicating the position of a line scan. (Sample: UK12D). Image by P.Graser.

Line scans were performed to determine zonation in the olivine grains, and to determine the effect of hydrothermal alteration or metasomatism of the elements close to and in the affected areas. Figure 4.7 is a backscatter image of an olivine grain tested for zonation.
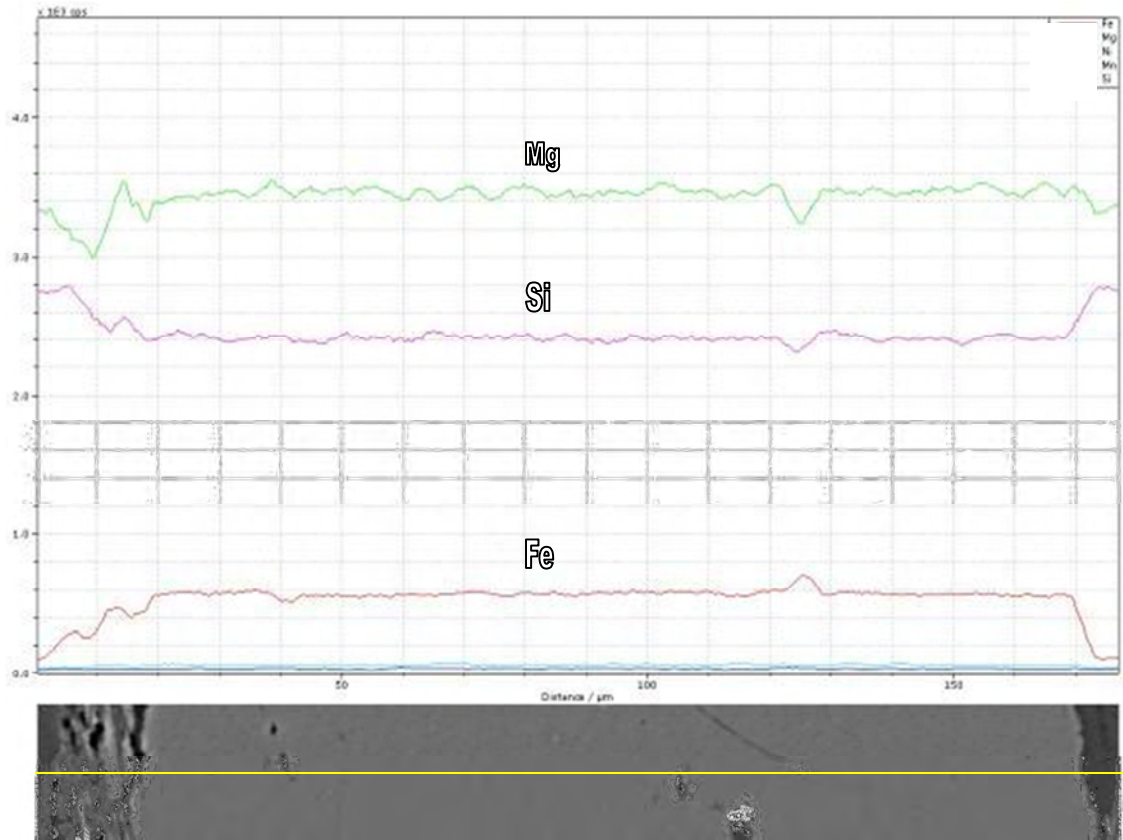
Figure 4.8. Elemental distribution of Mg (top), Si (centre) and Fe (bottom) in line scan of olivine. (Sample; UK12D). Image P.Graser.

In Figure 4.8, it may be seen that the olivine grain shows no evidence of zonation. The increase and decrease of elements on the edges is interpreted as indications of no hydrothermal alteration at the rim of the olivine grain. The depression in the Mg and Si and spike of Fe lines on the grain is most likely an artifact due to the visible scratch. The higher level of Si (purple line, centre) on the rim relative to the rest of the grain is probably due to the formation of serpentine. There is slight depletion of Mg (green line, top) relative to the grain on the edges.
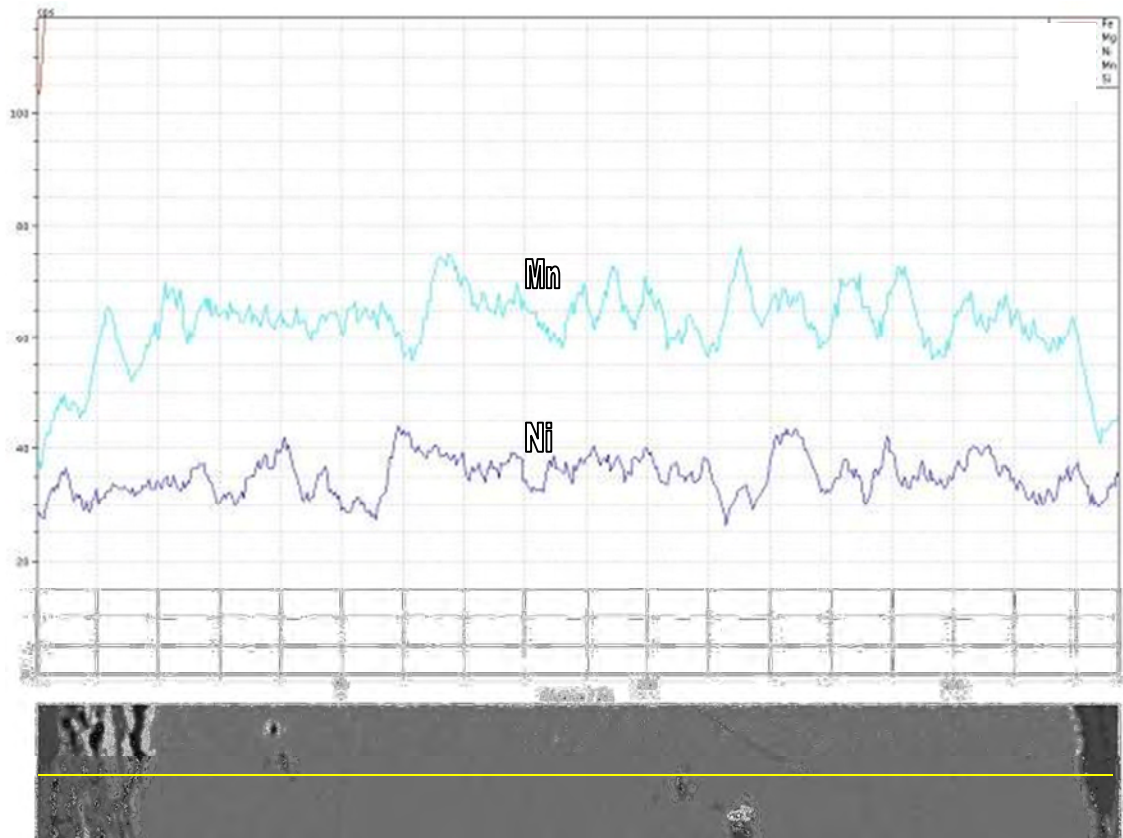
Figure 4.9. Elemental distributions of Mn (top) and Ni (bottom) in line scan of olivine grain. (Sample; UK12D). Image P.Graser.

The greater degree in variation in elemental concentrations is probably "analytical noise" due to lower concentrations of the two minor elements analysed. Slight variations in Mn and Ni content can be seen in Figure 4.9. Although some peaks and dips occur sympathetically, there is no systematic correlation. The Mn content depletes steeply towards the rims. The Ni content on the other hand remains fairly constant, indicating the less mobile nature of Ni.

All the olivine grains that line scans were performed on showed no zonation, suggesting that the olivine was crystallized from a single melt and was not subject to the effects of later pulses.

4.2 Pyroxene

4.2.1 Clinopyroxene and orthopyroxene

The samples studied during the previous reconnaissance of the harzburgite and wehrlite layers from the LHZBG on the farm Slaaihoek showed that the clinopyroxene mineral present is diopside, whereas the orthopyroxene has the composition of enstatite (Steenkamp, 2004). In this early investigation, two types of clinopyroxene were recognized, the first a diopside of magmatic origin and the second a diopside of metamorphic/metasomatic origin. This identification was based on the textural differences and different Cr-contents (Steenkamp, 2004).

A distinction is made here between the three geological environments in which pyroxenes are found in the rocks of the Complex. The first is orthopyroxene and clinopyroxene found in the wehrlite layers and thought to represent the primary magmatic mineralogy. The second is in the harzburgite and hybrid rocks, referred to as pyroxenites. The third is pyroxene (diopside and fassiate) found in the calc-silicate xenoliths. The orthopyroxene grains analysed during this investigation fall in the enstatite composition field, similar to those analysed in the previous project.

Diopside is the main clinopyroxene encountered in the samples analysed. The diopside texturally displays triple junction points in some sections. Some of the diopside from the LHZBG Unit, as well as that from xenoliths, plot above the diopside-hedenbergite (Di-Hb) line (Figures 4.12, 4.13 and 4.16) and indicate that these diopside grains may be of a metamorphic/metasomatic origin. Uralitization of the pyroxene grains is considered to be the result of pneumatolytic action by the water-enriched residual magmatic fluid on the grains (Deer et al., 1992). The pyroxene grains inferred to be of magmatic origin have rounded edges or embayments which may indicate thermal, chemical or mechanical erosion. The analytical results considered here pertain to microprobe analyses done during this investigation. These results are presented in Appendix 2.

The diopside grains in the harzburgites from the talc-rich study area occur in association with olivine and chromite grains, and poikilitically encloses these two minerals (Figure 4.10). In contrast to the findings reported by van Zyl (1996), no poikilitic enstatite grains were encountered in the current investigation. Both enstatite and diopside crystals have been uralitized to the same extent in the LHZBG and the PCR Units and are also associated with secondary minerals, including actinolite-tremolite, hornblende, chlorite, serpentine and secondary magnetite.
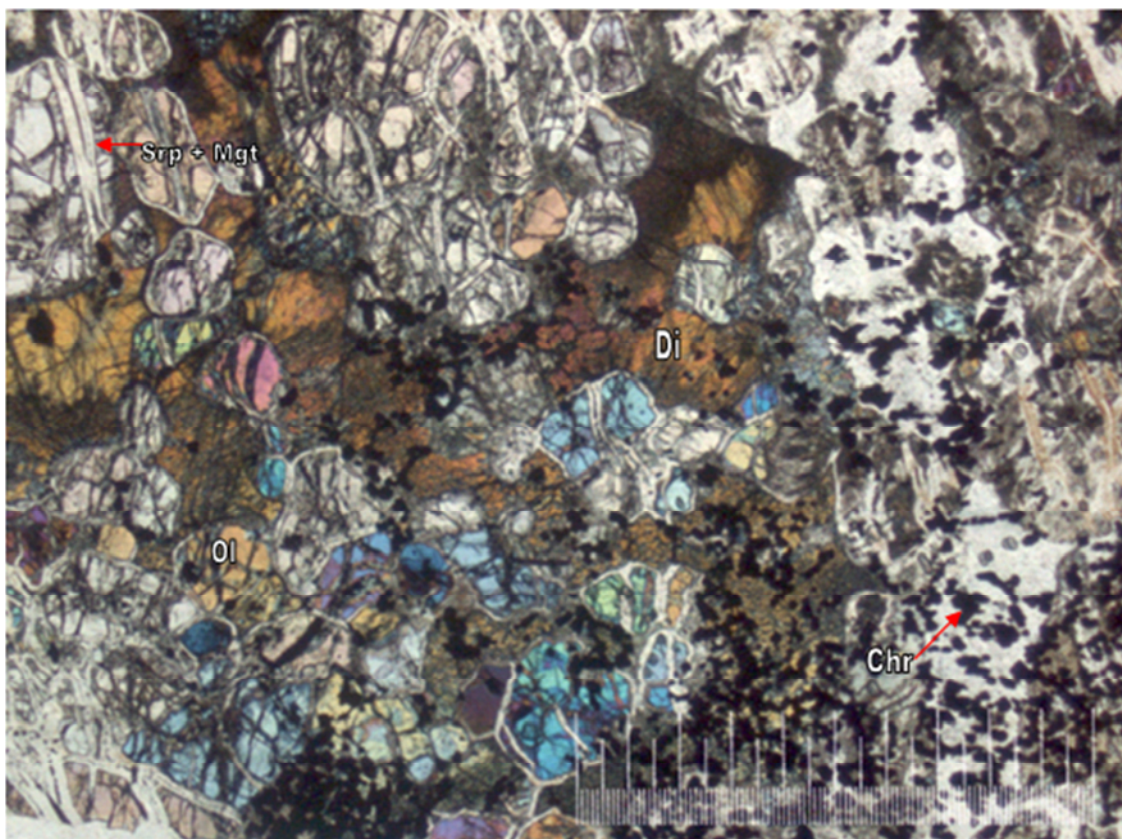
Figure 4.10. Diopside (Di) poikilitically enclosing partially serpentinized (srp) olivine (ol) grains with non-continues secondary magnetite (mgt) stingers and euhedral chromite (chr) grains. This sample is from the PCR Unit. The picture scale bar is 1000 micron. Taken with cross-polarised light. (Sample; UK12G).

The diopside in different varieties of calc-silicate xenoliths is found in association with other minerals formed by thermal metamorphism and metasomatism (Figure 4.11). The xenoliths from borehole UK3 (samples N, Q and U) consist mainly of diopside and calcite

with minor actinolite and chlorite. Xenoliths from borehole SH176 consist of diopside and calcite, but also contain significant amounts of grossular garnet. Calcite is absent from the xenoliths from sample UK12I, but this sample contains significant amounts of plagioclase and minor amounts of muscovite, actinolite and chlorite. This latter variety of xenolith is refered to as a "contaminated" xenolith, as discussed in Chapter 7. Calcite is also absent from the xenolith in sample UK48G, where as it contains significant amounts of epidote and minor actinolite, chlorite and pyrite.
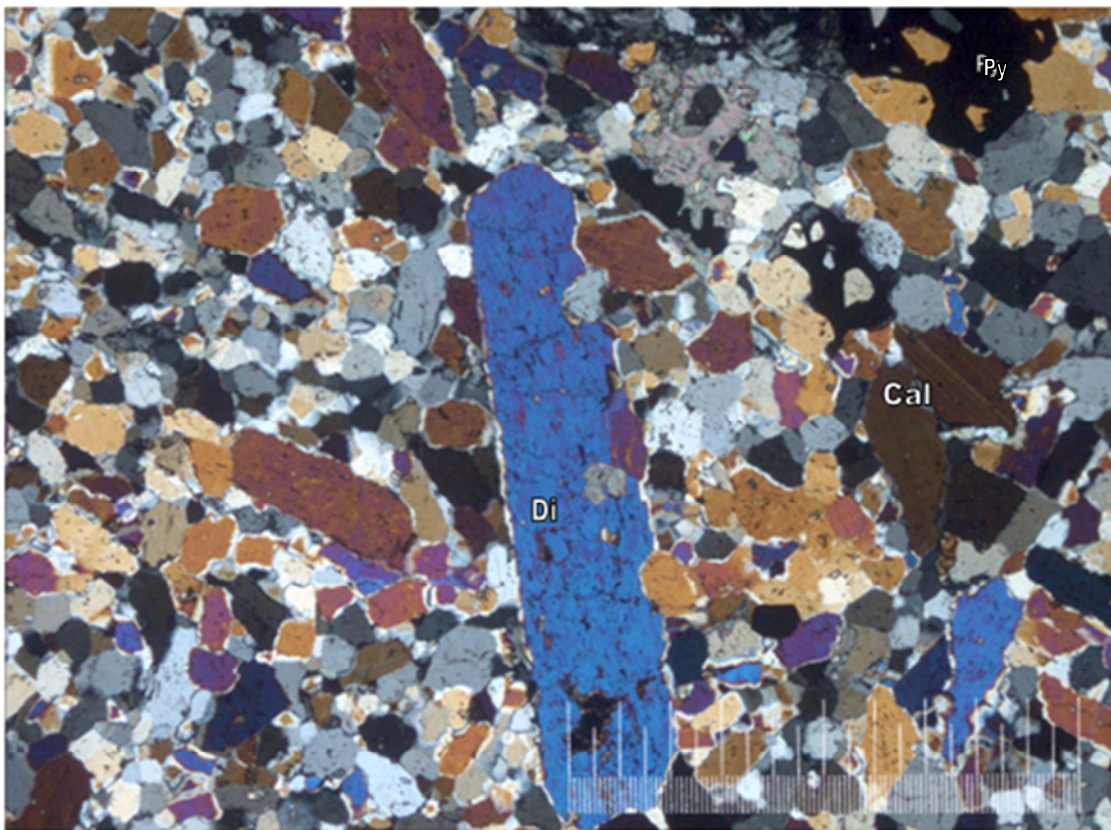
Figure 4.11. Diopside grains in a calc-silicate xenolith from the LHZBG Unit. The minerals depicted are diopside (di), calcite (cal) and pyrite (py). The picture bar scale is 1000 microns. Taken with cross-polarised light. (Sample: CS21H).

The pyroxene compositions determined for this study area can be plotted in various diagrams to characterize them. The pyroxene composition of all the grains analysed are plotted according to AMI-standards as put forward by Morimoto (1989).
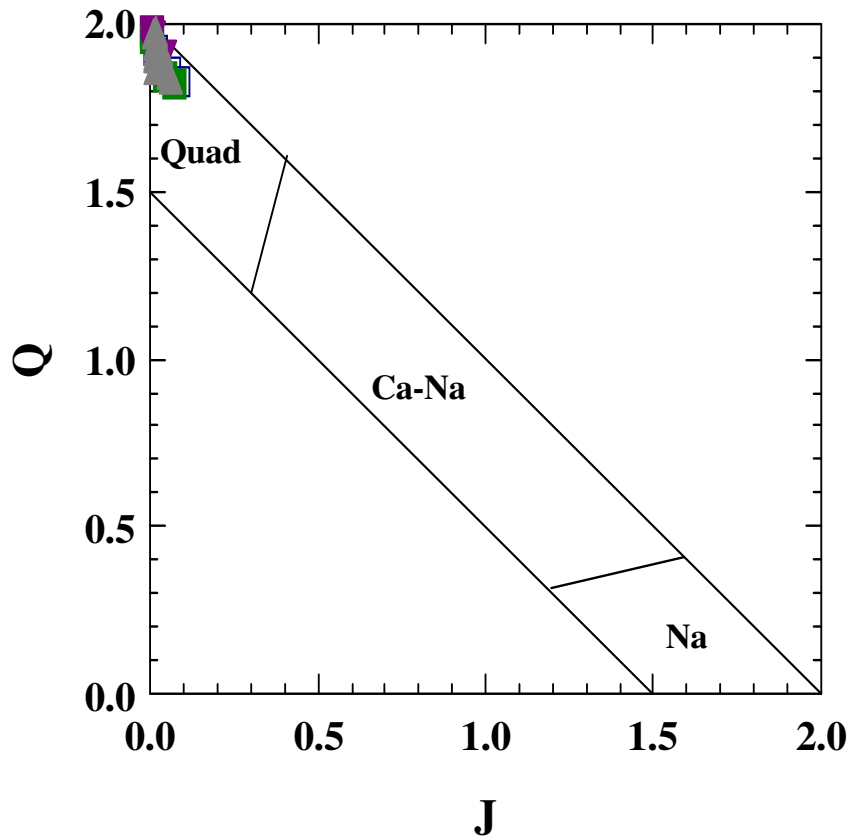
Figure 4.12. Microprobe analyses of pyroxenes from the PCR and LHZBG Units plotted on a Q-J diagram, where $Q = Ca + Mg + Fe^{2+}$ and $J = 2Na$ (After Morimoto, 1989). The legend is the same as presented in Figure 4.13 and 4.14.

Pyroxenes from the PCR and LHZBG Units plot in a tight cluster in the calcium quadrilateral field (Figure 4.12).
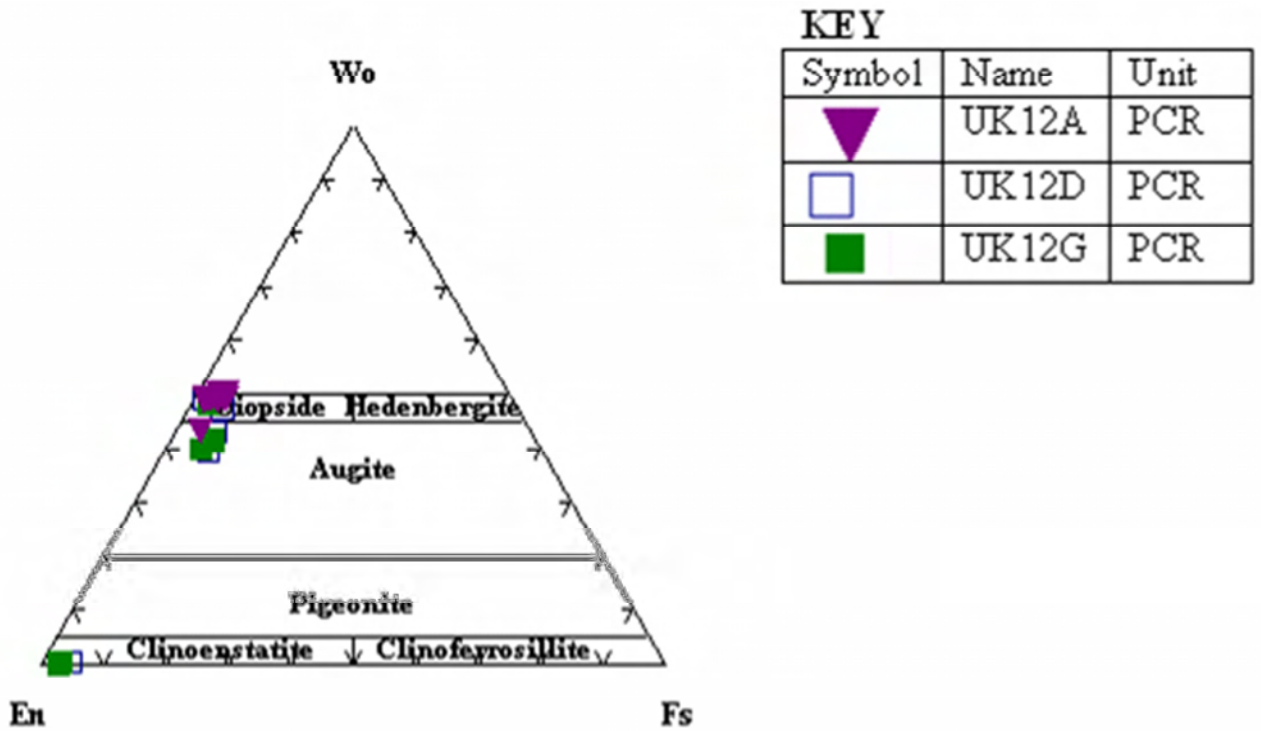
Figure 4.13. Plot of pyroxene minerals from the PCR Unit in the Wo-En-Fs system (After Morimoto, 1989).
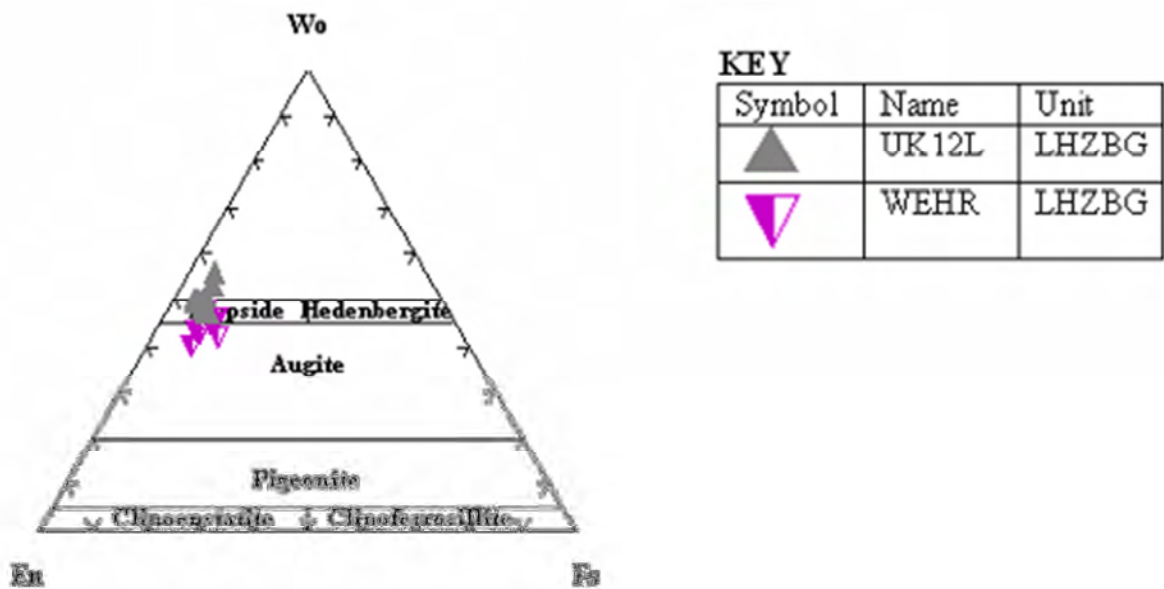
Figure 4.14. Plot of pyroxene minerals from the LHZBG Unit in the Wo-En-Fs system (After Morimoto, 1989).

The graphed data show that pyroxene grains analysed belong to two compositional varieties, diopside and enstatite. The grains of the two types are individually very similar in composition as is demonstrated in Figures 4.13 and 4.14. Pyroxenes from the PCR (Figure 4.13) and LHZBG Units (Figure 4.14) are plotted. In addition, the compositions of the clinopyroxene grains from the wehrlite layers, found in the LHZBG on the farm Slaaihoek 540 - JT, sampled during the previous reconnaissance (Steenkamp, 2004) have been added for comparative purposes (Figure 4.14). During the reconnaissance investigation it was determined that the clinopyroxenes from the parapyroxenites in the LHZBG Unit on the farm Slaaihoek 540 - JT fall in the diopside-augite field and the orthopyroxenes fall in the enstatite field. The wehrlite layers contain clinopyroxene that fall in the diopside-augite field (Figure 4.14).

Pyroxene, analysed from the PCR Unit sampled on the farm Uitkomst 541 - JT, plots in the clinopyroxene and orthopyroxene fields (Figure 4.13). The orthopyroxene falls into the enstatite field and the clinopyroxenes fall into the augite and diopside fields. Clinopyroxene from the upper and central parts of the LHZBG Unit on Uitkomst also plots (Figure 4.14) both the augite and diopside fields, while the clinopyroxenes from the lower part of the unit (near the basal contact) only plot (Figure 4.14) in the diopside field and above the diopside-hedenbergite tie-line.
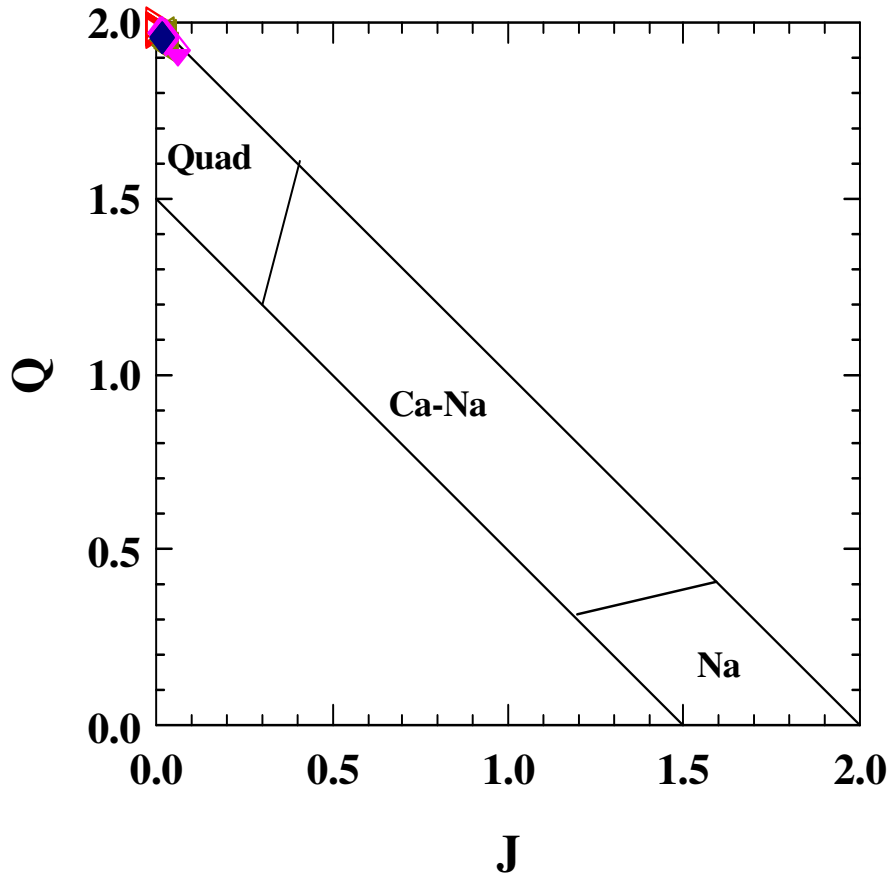
Figure 4.15. Plot of pyroxene compositions in xenoliths, on the Q-J diagram (After Morimoto, 1989). The legend is the as for Figure 4.19.

Pyroxene grains from the xenoliths plots in a very tight cluster in the quadrilateral field of the Q-J diagram (Figure 3.15).

KEY		
Symbol	Name	Unit
◁	UK3N	XENO
◇	UK3U	XENO
◆	UK48G	XENO
▷	SH176	XENO
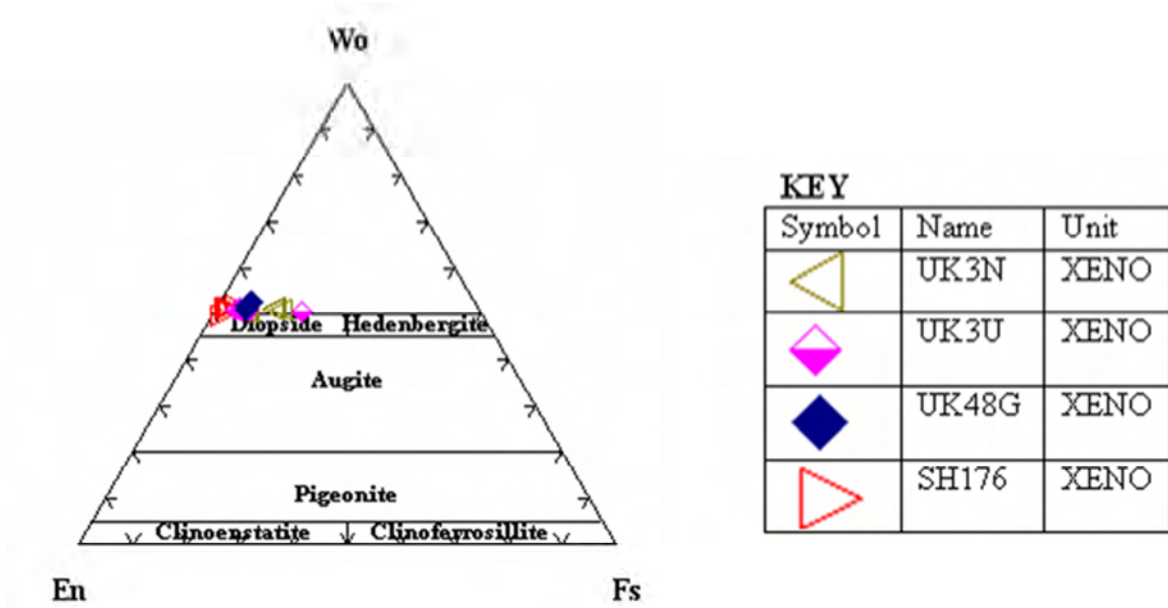
Figure 4.16. Plot of pyroxene compositions of xenoliths in the Wo-En-Fs system (After Morimoto, 1989).

In Figure 4.16 it can be seen that the xenoliths contain no orthopyroxene. The composition of all the grains plot in the diopside field, close to and slightly above the Di-Hb tie-line.

According to Deer et al., (1992) the structure of pyroxene can be expressed in the following way: M2 M1 T_2O_6, where M2 and M1 refer to cations in generally distorted and regular octahedral coordination positions respectively. T refers to tetrahedrally coordinated cations. The composition of Mg-Fe and Ca pyroxenes can be represented by the formula: $M2(R2^+)M1(R^{2+})T(2R^{4+})O_6$. Based on the assumption that more than one R^{4+} cation is present in T sites, the composition of pyroxene containing monovalent and trivalent cations can be described in terms of coupled substitutions. Where $M1(R^{3+})T(R^{3+})$ produces end-member conditions it is commonly termed the "Tschermak" component. In natural minerals the amount of Al in T sites is normally limited to ~0.5. Harris and Chaumba, (2001) ascribe the composition of diopsides found at Sandsloot (PPRust), plotting above the Di-Hb line, as being due to the presence of Al in octahedral sites and that Ca does not exceed one cation per six oxygens. A possible means of formation is given below in the following reactions.

i) $4CaCO_3 + (6CaAl_2Si_2O_8 + 4Mg_2SiO_4) = 4CalAl_2SiO_6 + 6CaMgSi_2O_6 + 2 MgAl_2O_4 + 4 CO_2$

    calcite + anorthite   + forsterite   CaTs-pyx   + diopside   + spinel

ii) $CaMg(CO_3)_2 + 2 CaAl_2Si_2O_8 + Mg_2SiO_4 = CaAl_2SiO_6 + 6CaMgSi_2O_6 + MgAl_2O_4 + 2CO_2$
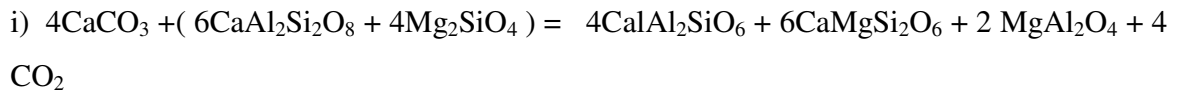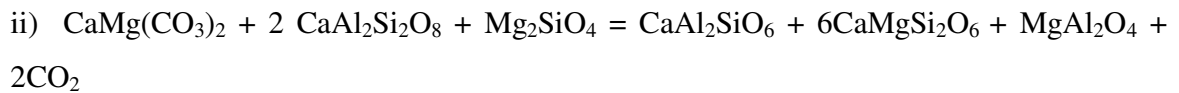
    dolomite   + anorthite   + forsterite = CaTs-pyx   + diopside   + spinel

However, olivine and plagioclase are lacking in the samples analysed. It has been shown by Weeks (1956b quoted in Deer et al., 1992) that diopside may form at temperatures lower than forsterite where the P_{CO_2} is below 1000 atm. according to the following reaction :

$CaMg(CO_3) + SiO_2 = CaMgSi_2O_6 + 2CO_2$
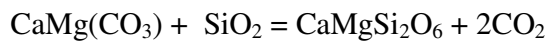
Dolomite + Quartz = Diopside + Carbon dioxide

The occurrence of a non-quadrilateral component, namely CaTs-pyroxene (Ca-Tschermak molecule) has been reported in significant amounts both where assimilation of dolomites took place (e.g. Ioko-Dovyren) and at various limestone-magma contacts (e.g. Abu El-Enen et al., 2004). An increase in the Ca-Tschermak component from the core of clinopyroxene grains to the edge indicates a decrease in silica saturation due to concomitant prograde decarbonation reactions that generally consume SiO_2 (Povoden et al., 2002).

The clinopyroxene that falls above the hedenbergite-diopside line and are described by Gilg et al., (2001) as a subsilicic ferroan aluminian diopside (fassaite) with significant Ca-Al-Tschermak exchange components. Fassaite is a Ca and Al-rich pyroxene found in metamorphosed dolomite and limestone.

4.2.2 Comparison of Pyroxene Compositions in the Uitkomst Complex

Meaningful information is obtained by comparing the compositions of pyroxene grains from different locations and lithological association. Slaaihoek refers to the pyroxene found in the samples from the farm Slaaihoek, and Uitkomst refer to the pyroxene found in samples from the farm Uitkomst. The wehrlite samples are derived from the Slaaihoek section. All comparisons are relative to Ca-content, this provides a very prominent distinction between the species.
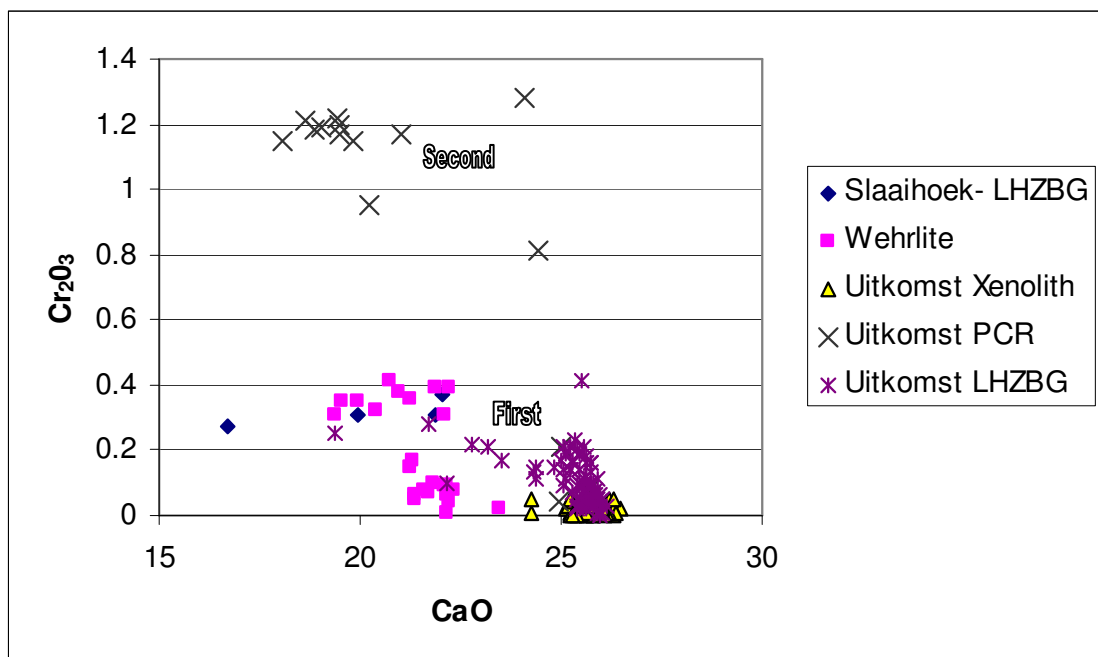
Figure 4.17. Clinopyroxene species from the Uitkomst Complex based on the differences in Cr_2O_3 content of the samples analysed.

There are two distinct groups of clinopyroxene, based on Cr content. The diopside in the PCR Unit is enriched in Cr relative to the clinopyroxenes from the LHZBG Unit's, harzburgite, wehrlite and xenoliths (Figure 4.17) respectively.

There are two species of clinopyroxene present in the wehrlite layers, the first slightly more depleted in Cr than the second. However, the margin of error on analyses and small

difference in content does not make it a diagnostic feature. Diopsides from the LHZBG Unit on Uitkomst 541 - JT and the Uitkomst calc-silicate xenoliths have similar Ca content. The Uitkomst LHZBG clinopyroxenes have higher Cr contents, whereas those from within the xenoliths contain little to no Cr. Some of the Uitkomst LHZBG clinopyroxene grains show an increase in their Cr-content with a decrease in the Ca-content. These Uitkomst LHZBG clinopyroxene compositions tend towards the composition of clinopyroxenes of the Slaaihoek pyroxenites with the Cr-rich clinopyroxene grains present in the wehrlite, being somewhat "transitional" between them.
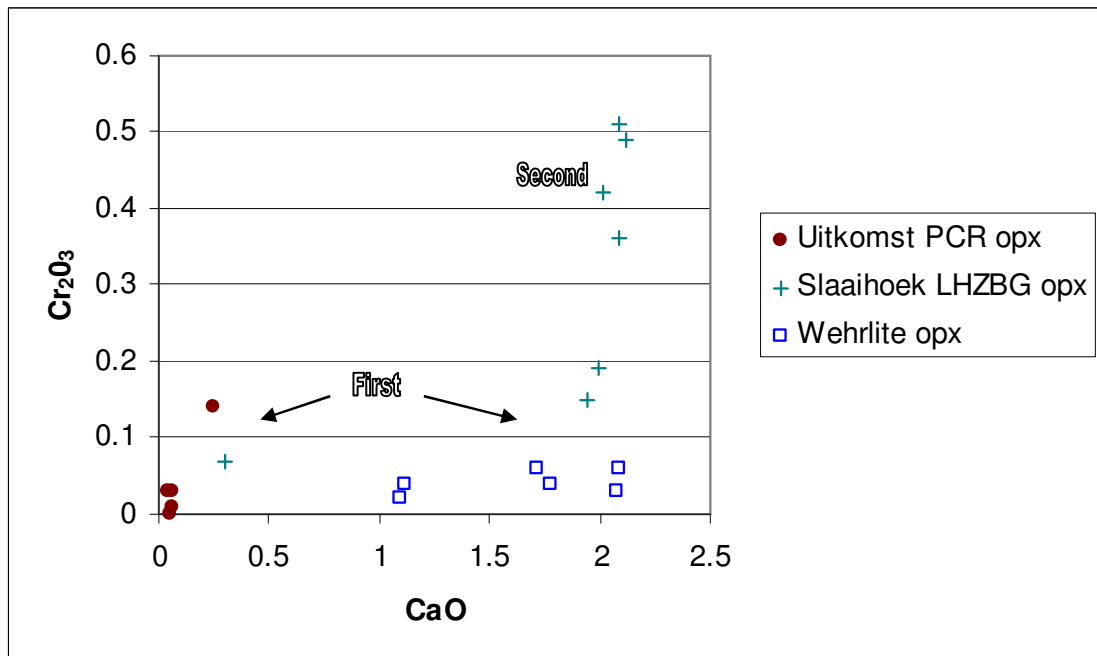
Figure 4.18. Orthopyroxene species from the Uitkomst Complex based on the differences in Cr_2O_3 content of the samples analysed.

The Slaaihoek harzburgite contains two orthopyroxene (enstatite) species (Figure 4.18), the first with a lower Cr-content and the second with a slightly higher Cr-content. The orthopyroxene from the Uitkomst PCR harzburgites and from the wehrlite layers fall in the low Cr-content range of enstatite. The Slaaihoek section samples fall in both. The difference in composition and analytical margin of error may exclude this as a diagnostic

feature. The Cr-content in both ortho- and clinopyroxene in the Slaaihoek samples are higher relative to the Uitkomst section samples.

In Figure 4.19 all the clinopyroxenes analysed form the Uitkomst Complex are compared in a MnO versus CaO diagram. The same comparison for orthopyroxene is made in Figure 4.23.
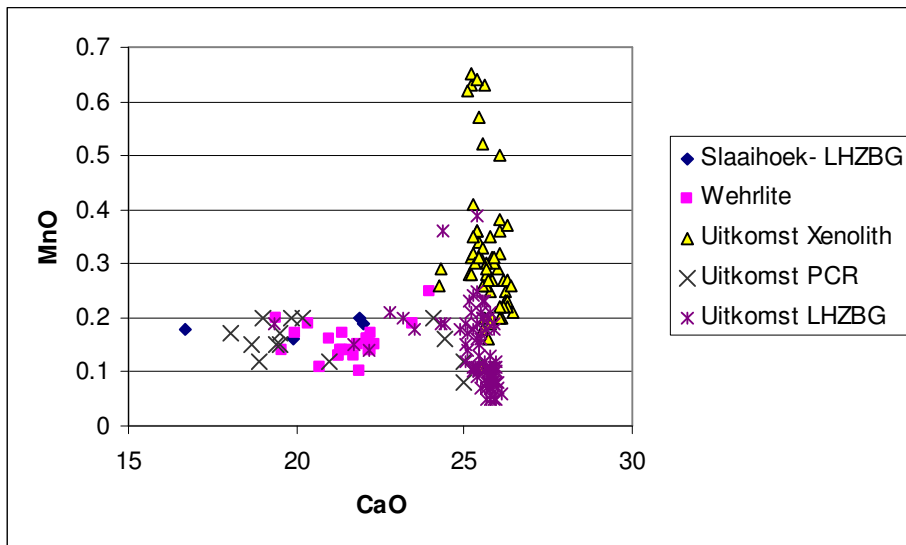
Figure 4.19. MnO against CaO content in clinopyroxene samples from the Uitkomst Complex analysed.
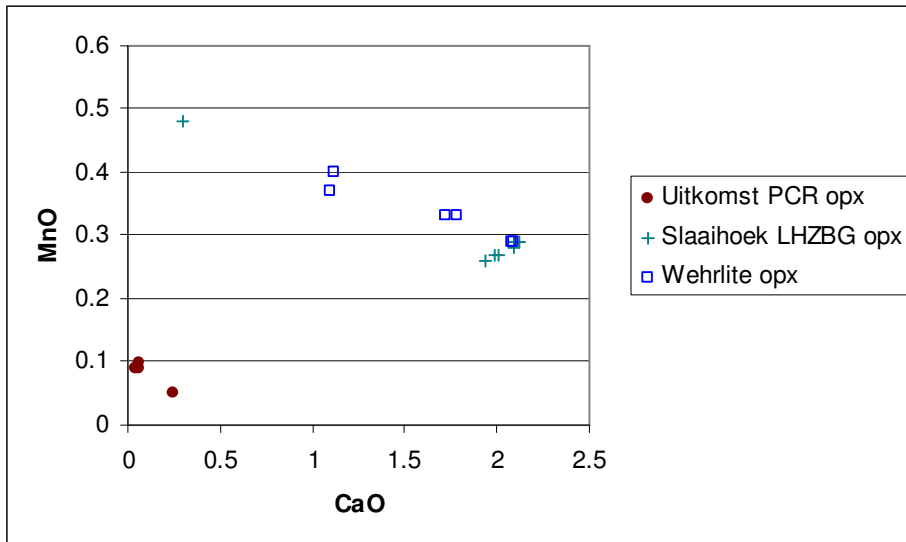
Figure 4.20. MnO against CaO content in orthopyroxene samples from the Uitkomst Complex analysed.

The fassaite diopside (labelled Uitkomst Xenolith) grains from the xenoliths (Figure 4.19) appear to be more MnO enriched relative to the other diopside occurrences. There also appear to be two species of diopside present in the xenoliths, the first with a slightly higher MnO content than the second. The clinopyroxenes found in the Slaaihoek harzburgites, the wehrlite layers and the PCR harzburigites (Figure 4.19) have a lower concentration of CaO relative to the Uitkomst clinopyroxenes, but show approximately the same range of MnO content. There appear to be a "transitional" component between the clinopyroxene composition of the Uitkomst LHZBG and PCR analysed samples. The enstatite (orthopyroxene) grain analyses (Figure 3.20) shows a general trend in the wehrlite and Slaaihoek LHZBG samples. These grains have a slightly higher MnO content relative to the samples from Uitkomst LHZBG (Figure 4.20). However, the compositional difference is again small and considering analytical error, also not considered a diagnostic feature.
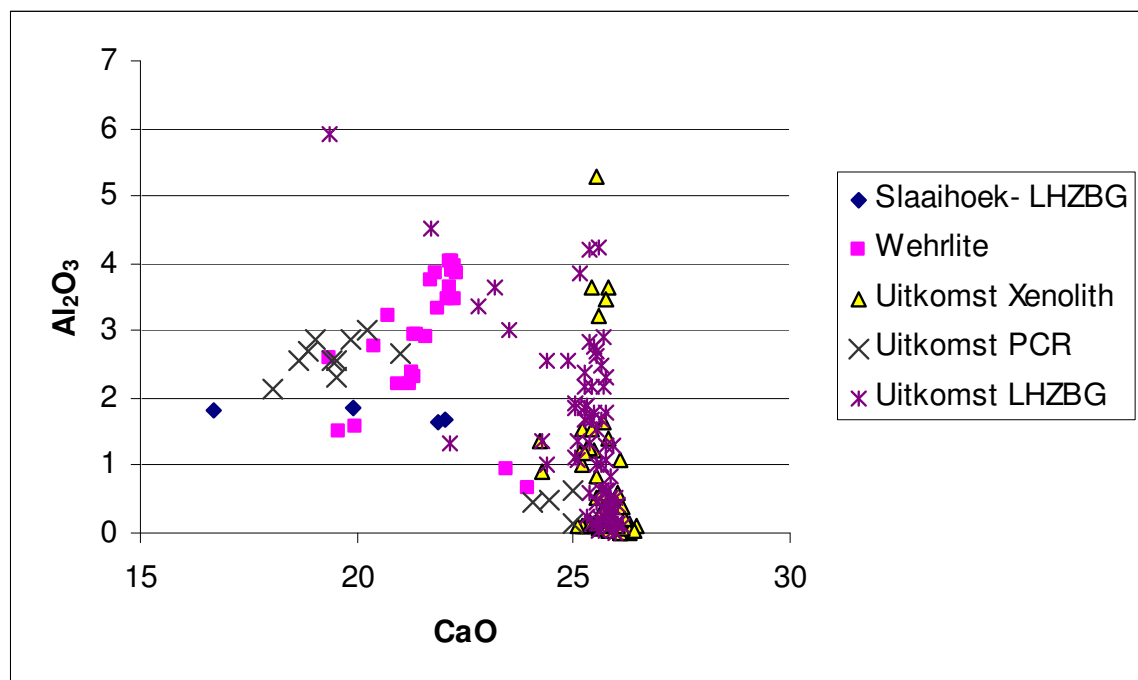
Figure 4.21. Al_2O_3 against CaO contents of clinopyroxenes analysed from the Uitkomst Complex.
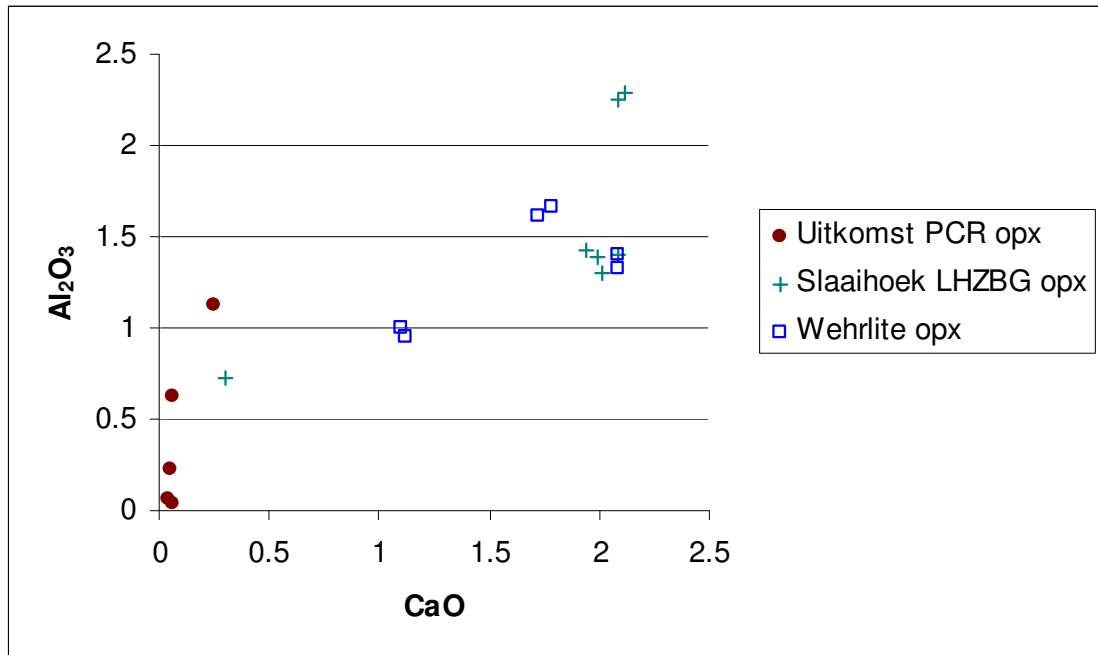
Figure 4.22. Al$_2$O$_3$ against CaO contents of orthopyroxenes analysed from the Uitkomst Complex.

The clinopyroxenes (Figure 4.21) from all of the occurrences have a near similar Al content, ranging from absent to 6 wt%. From the CaO content it may be seen that the clinopyroxene from the Uitkomst, PCR, wehrlite layers and Slaaihoek LHZBG has a slightly lower CaO content, but slightly higher Al$_2$O$_3$ content relative to the majority of clinopyroxene analyses from the Uitkomst LHZBG Unit and Uitkomst xenoliths. Some of the clinopyroxene grains from the Uitkomst LHZBG Unit show an increase in Al-content with decrease in Ca-content. There again appears to be a compositional "transitional" component from the higher Ca-clinopyroxene to the lower Ca-clinopyroxene variety. The enstatite from the Uikomst PCR Unit contains less Al than the orthopyroxene from the wehrlite layers and Slaaihoek LHZBG.

In Figure 4.22 the orthopyroxene compositions are compared in an Al$_2$O$_3$ versus CaO diagram. The enstatite from the Slaaihoek LHZBG and the wehrlite layers has a higher MnO content relative to the orthopyroxene found in the Uitkomst PCR harzburgite. The Slaaihoek LHZBG and wehrlite samples again seem to follow a general positive trend (Figure 4.22)
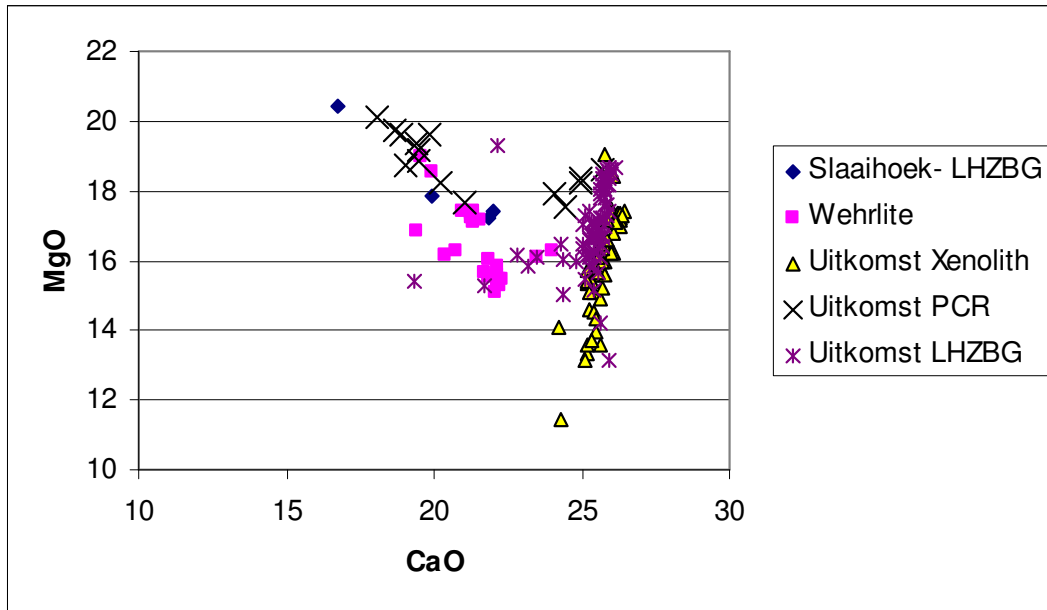
Figure 4.23. MgO versus CaO content of clinopyroxene grains analysed from the Uitkomst Complex.

In Figure 4.23 the clinopyroxene compositions are compared in an MgO versus CaO diagram. In the diopside samples from Slaaihoek LHZBG, wehrlite layers and Uitkomst PCR, there is a negative trend between MgO and CaO content. This may suggest substitution of Mg by Ca. This could be interpreted as indicative of a diopside forming in a dynamic magmatic environment, where a constant supply of mineral forming elements will be supplied. The Uitkomst xenolith and Uitkomst LHZBG diopside grain compositions do not show such a trend, indicative of possible substitution of elements, suggesting formation in a non-dynamic metamorphic environment, owing to depletion of mineral forming elements in the closed environment.

4.3 Plagioclase

Plagioclase was rarely encountered in the rocks sampled and was found to be present only in wehrlite layers within the LHZBG Unit, where it occurs in some samples as a minor mineral. The plagioclase shows evidence of saussuritization, but generally shows less evidence for alteration than the olivine and pyroxene (Figure 4.24). Microprobe analyses of the plagioclase indicated the grains to fall in the labradorite-bytownite compositional field (Steenkamp, 2004). The values correspond to those found by van Zyl (1996) and Gauert (1998).

Kacandes et al. (1989) did an experiment in which a quartz-normative tholeiite basalt (plagioclase, clinopyroxene, mesostasis and magnetite) was subjected to hydrothermal conditions at 300°C and 30 Mpa, and the evolution of the alteration minerals and fluid was monitored. It was found that the resultant secondary minerals, in order of detection were smectite, illite, potassium feldspar and cristobalite. This was followed by an examination of the unaltered minerals, demonstrating that the pyroxene and interstitial glass were the main source of cations, whereas the plagioclase appeared fresh. The fact that the plagioclase remained unaffected would suggest that either dissolution of the primary feldspars was slow or that the plagioclase was in near equilibrium with the fluid.

This would suggest that the near pristine plagioclase grains found in the LHZBG Unit were either in near equilibrium with the deuteric fluids that affected the surrounding precursor mafic minerals, or only suffered partial dissolution during the time it was exposed to the effects of the deuteric fluid.

Wenzel et al., (2001b) suggested that the assimilation of Ca from the country rock, resulted in the formation of Ca-Tschermak-rich interstitial clinopyroxene instead of plagioclase in the Ioko-Dovyren intrusion, Russia. This would suggest that the wehrlite layers represent pulses of primary mafic magma that were not affected by the assimilation of Ca from the dolomite country rock.
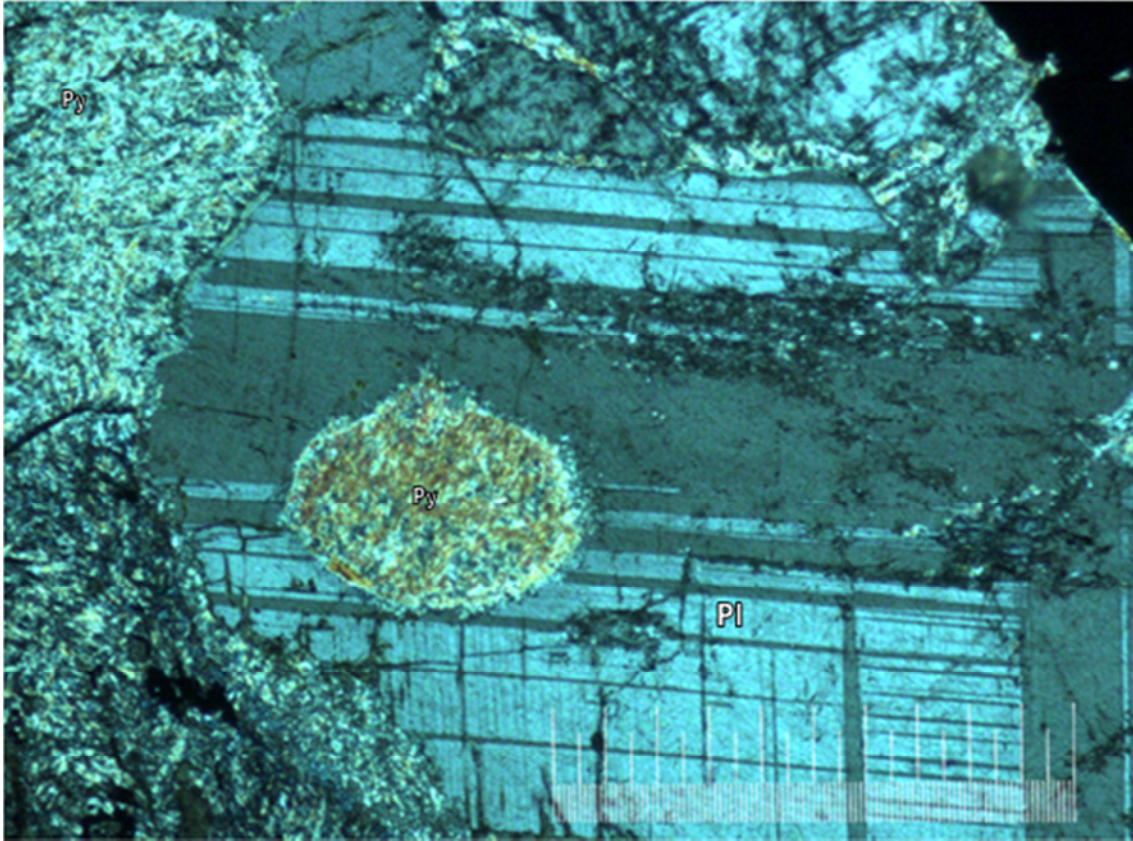
Figure 4.24. Plagioclase (Pl) that has been partially saussuritized. The plagioclase is both enclosing and being enclosed by completely uralitized pyroxene (py). The picture scale bar is 1000 microns. Taken with cross-polarised light. (Sample; CS18).

4.4 Chromite

4.4.1. Chromitite

Chromite is abundant in both the LHZBG and the PCR Units. In the LHZBG Unit chromite is found as disseminated grains and in thin seams within unaltered to altered peridotitic host material. The chromite grains in the LHZBG are usually euhedral and do not show the effects of alteration. The semi-massive chromitite mineralization in the PCR Unit is found in both a highly altered matrix material (Figure 4.25) and a less altered matrix material (Figure 4.26). The chromite grains in the PCR Unit are euhedral and show effects of alteration such as magnetite rims around grains and in cracks. Chromite compositional elements have been shown to be relatively immobile during hydrothermal processes, (Spandler et al. 2005) which may explain the preservation of chromite grains in completely altered matrices. The formation of the chromitite layers in the Uitkomst Complex has been attributed to an increase in oxygen fugacity within the evolving magma pile due to assimilation of dolomite (Gauert, 1998; Dodd, 2004).

Microprobe analyses of the centres of unaltered chromite grains in the PCR Unit reveal the compositional trends evident in Figures 4.27 and 4.28. The mineral chemistry of chromite grains encountered during this investigation, and obtained by electron microprobe analyses, is presented in Appendix 2.
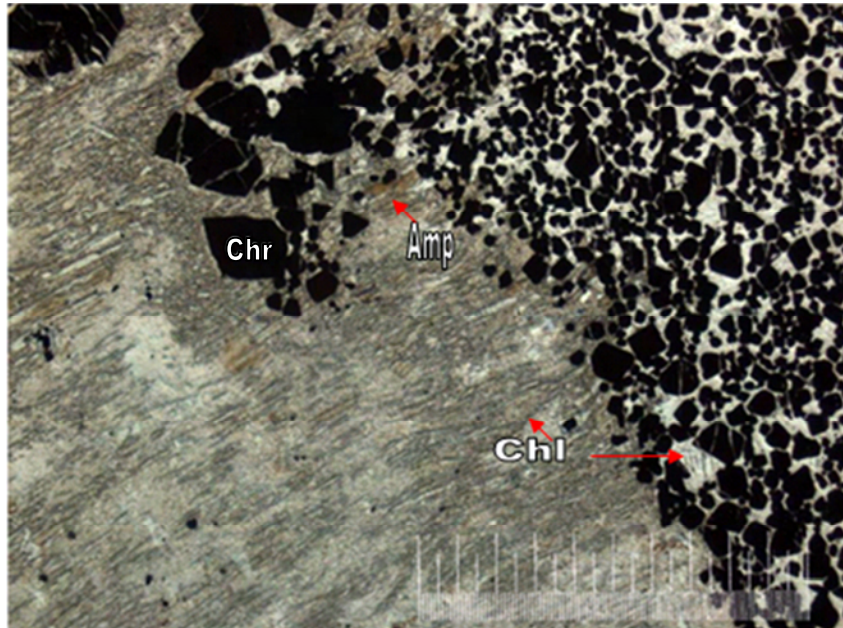
Figure 4.25. Euhedral to subhedral chromite (chr) grains in a matix of chlorite (chl) and relict amphibole (amp) from the PCR Unit. The picture scale bar is 1000 micron. Taken under cross-polarised transmitted light. (Sample: UK12A)
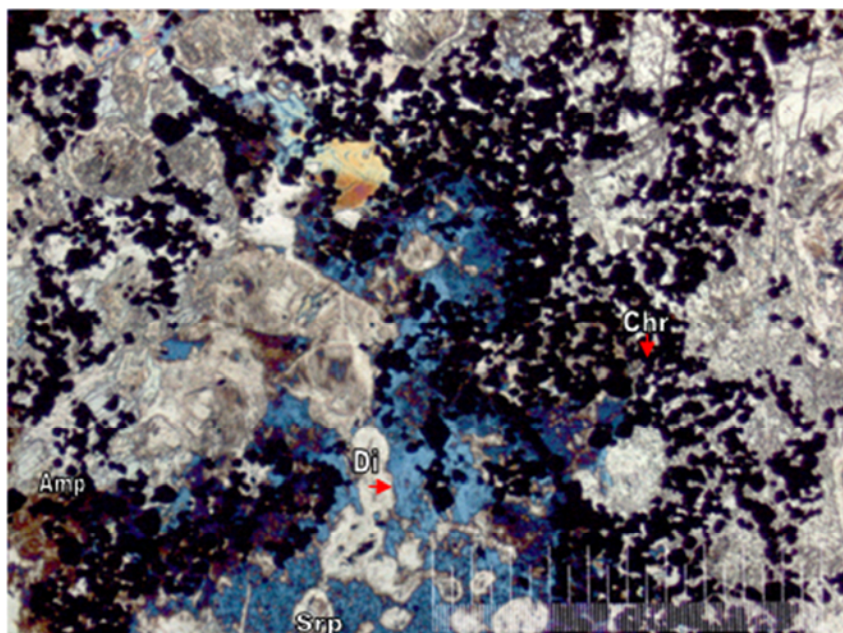
Figure 4.26. Euhedral grains of chromite (chr) (black) associated with serpentinized (srp) olivine and enclosed by diopside (di), partially altered to amphibole (amp), in the PCR Unit. The picture scale bar is 1000 microns. Taken under cross-polarised transmitted light. (Sample: UK12D).
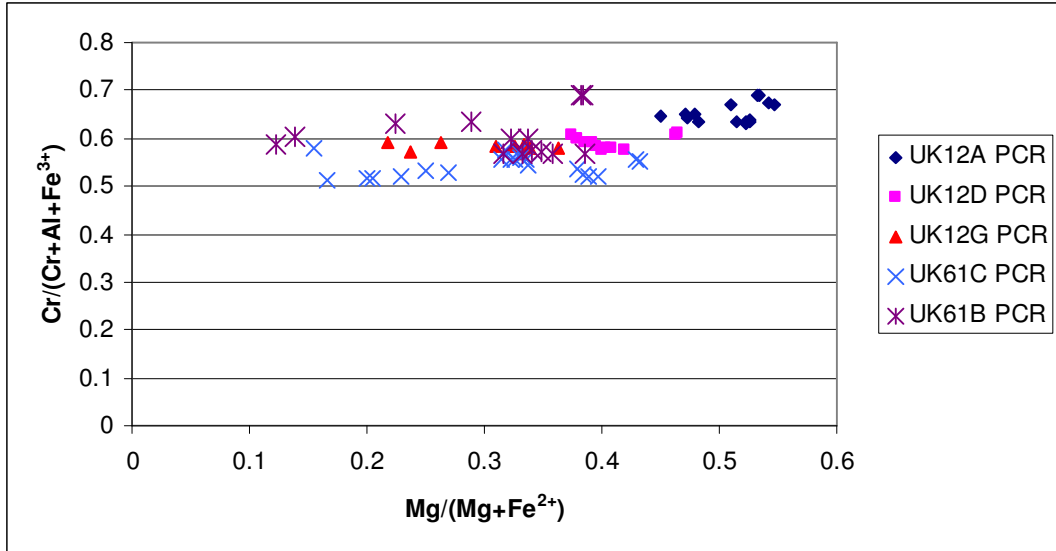
Figure 4.27. $Cr/(Cr+Al+Fe^{3+})$ against $Mg/(Mg+Fe^{2+})$ plot for chromite grains analysed from the PCR Unit.
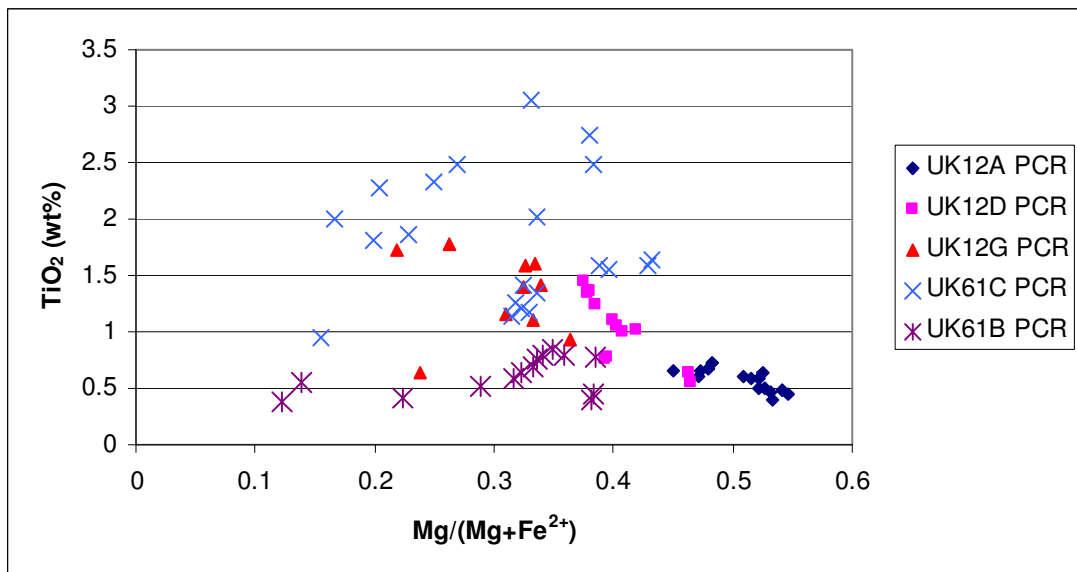
Figure 4.28. TiO2 (wt %) against $Mg/(Mg+Fe^{2+})$ plot for chromite grains analysed from the PCR Unit.

There is a systematic change in $Mg/(Mg + Fe^{2+})$ ratio in the PCR Unit with height (Figure 4.30), in borehole UK12 (where UK12A is near top, UK12D is near centre and UK12G is near the bottom of the unit). The $Mg/(Mg + Fe^{2+})$ ratio increases with height while the $Cr/(Cr + Al + Fe^{3+})$ ratio remains nearly constant. The same applies to borehole UK61. It can bee seen that the TiO_2 content decreases with height in borehole UK61 (Figure 4.28). The results are presented in Table 4.1.

Table 4.1. Comparison of chromite grains from the PCR Unit.

		UK12A	UK12D	UK12G	UK61B	UK61C
	n	15	12	10	14	21
Cr_2O_3 content		50.57	44.04	41.41	44.26	38.00
$Cr/(Cr+Al+Fe^{3+})$	mean	0.65	0.59	0.58	0.60	0.54
	std dev	0.02	0.01	0.01	0.04	0.02
$Mg/(Mg+Fe^{2+})$	mean	0.51	0.41	0.30	0.31	0.31
	std dev	0.03	0.03	0.05	0.08	0.08
TiO_2	mean	0.57	1.02	1.33	0.61	1.81
	std dev	0.09	0.28	0.35	0.16	0.57
Cr:Fe	mean	2.04	1.40	1.14	1.29	0.98
	std dev	0.16	0.14	0.04	0.21	0.17

The Student t-test of $Cr/(Cr+Al+Fe^{3+})$ between UK12A and UK12D yielded a result of 1.32575E-09, between UK12A and UK12G a result of 1.59595E-10 and between UK12D and UK12G a result of 0.043843546. The Student's t-test between UK61B and UK61C yielded a result of 0.000104066. The Student's t-test of $Mg/(Mg+Fe^{2+})$ between UK12A and UK12D yielded a result of 5.86317E-09, between UK12A and UK12G a result of 1.29744E-08 and between UK12D and UK12G a result of 4.296E-05. The Student's t-test between UK61B and UK61C yielded a result of 0.901223189.

4.5 Magnetite

4.5.1 General

Magnetite was encountered within various associations in the LHZBG and PCR Units. In summary, the magnetite is present in the following associations:

a) As secondary stringers associated with serpentinized cracks in olivine, or where the magnetite almost completely pseudomorphically replaces the olivine (Figure 4.29).

b) As secondary rims around sulphide grains, usually pyrrhotite, and along fractures in the sulphide grains.

c) As secondary rims around and along fractures in chromite grains (Figure 4.30).

d) Possibly as primary grains, that suffered alteration (silicification) due to late stage fluid infiltration. Preserved as chamosite pseudomorphs after the primary grains.

No primary magnetite was encountered during the current investigation, but was reported in previous studies (van Zyl, 1996). This would suggest that magnetite is not developed throughout the Uitkomst Complex. The secondary magnetite occurrence is described in the following chapter.

The only evidence of primary magnetite in the LHZBG unit is the pseudomorphs of chamosite after magnetite (Figure 4.29). Ilmenite is persevered as a trellis structure in these grains (Figure 4.30). Trellis structure ilmenite is characteristic of magmatic magnetite. These grains have prominent leucoxene rims where it is in contact with the surrounding pyrrhotite. These occurrences are limited to grain fully enveloped in pyrrhotite. These grains show evidence of having been affected by a late-stage secondary fluid. The host rock is hornblendite.
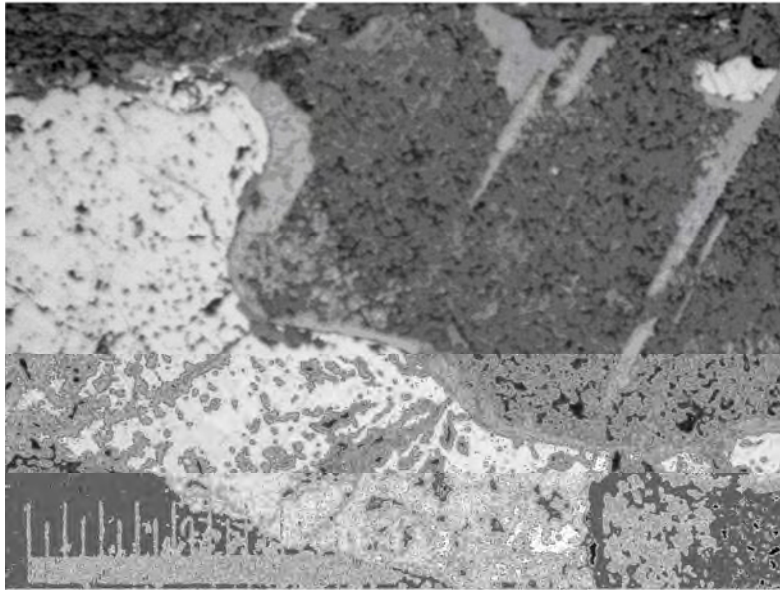
Figure 4.29. Pseudomorphs of chamosite (upper right) after primary magnetite with a leucoxene rim (light grey) and enveloped in pyrrothite (lower left). Photo taken under reflected light, scale bar = 1000 micron (Sample: UK48)
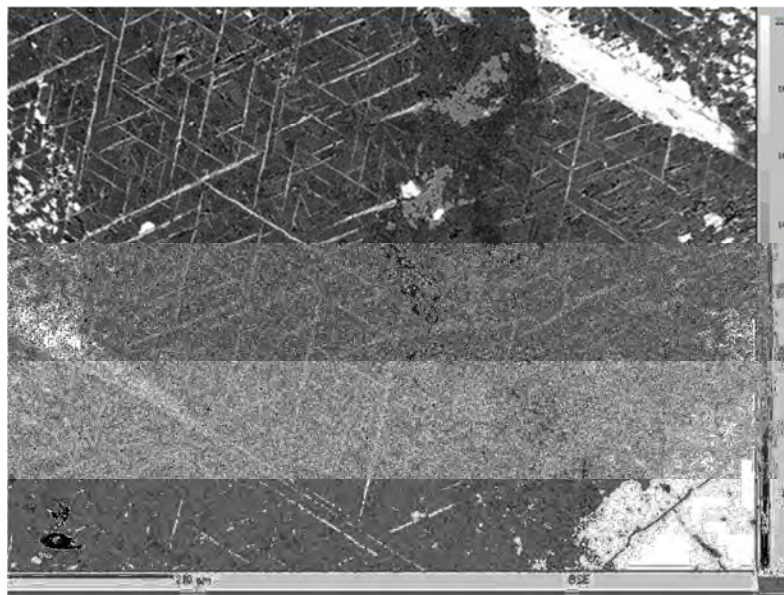
Figure 4.30. Backscatter electron (BSE) image of the preserved trellis structure of ilmenite in the chamosite pseudomorphs. A prominent alteration vein intrudes the grain (left of center in image). The leucoxene rim is visible in the lower left of the image where the grain is in contact with pyrrhotite. There are several pyrrhotite inclusions in the grain. The scale bar is 200 micron (Photo: P.P.H. Gräser).

4.7 Carbonate minerals

The carbonate minerals encountered during the investigation are calcite and dolomite. Calcite is found in the hybrid rocks and calc-silicate xenoliths of the LHZBG Unit. These two minerals are in textural equilibrium with the silicate and sulphide minerals. The carbonate minerals will be assumed to be primary in this context as representing relic primary country rock

4.7.1. Calcite

Where calcite is in contact with a sulphide grain (generally pyrrhotite), the contact is sharp and the sulphide minerals is not intergrown by tremolite often found in proximity to the sulphide mineralization (Figure 4.31).
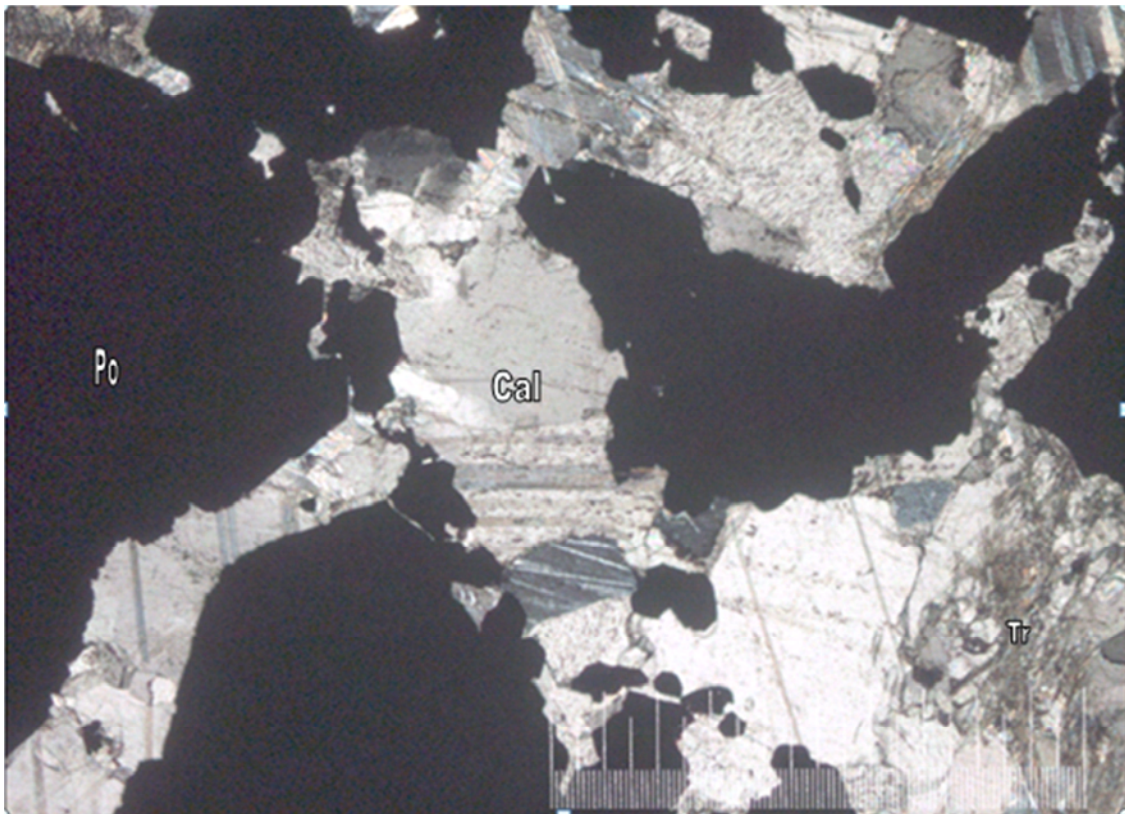
Figure 4.31. Calcite grains enclosing pyrrhotite (black) grains. The calcite (cal) grains appear to be in textural equilibrium with pyrrhotite (po) and tremolite (Tr). The picture scale bar is 1000 micron. Taken with cross-polarized light. (Sample; UK68E).

Calcite is also found in close association with tremolite in the hybrid rock of the LHZBG Unit (Figure 4.32), where the calcite grains are in textural equilibrium with tremolite and pyrrhotite grains.
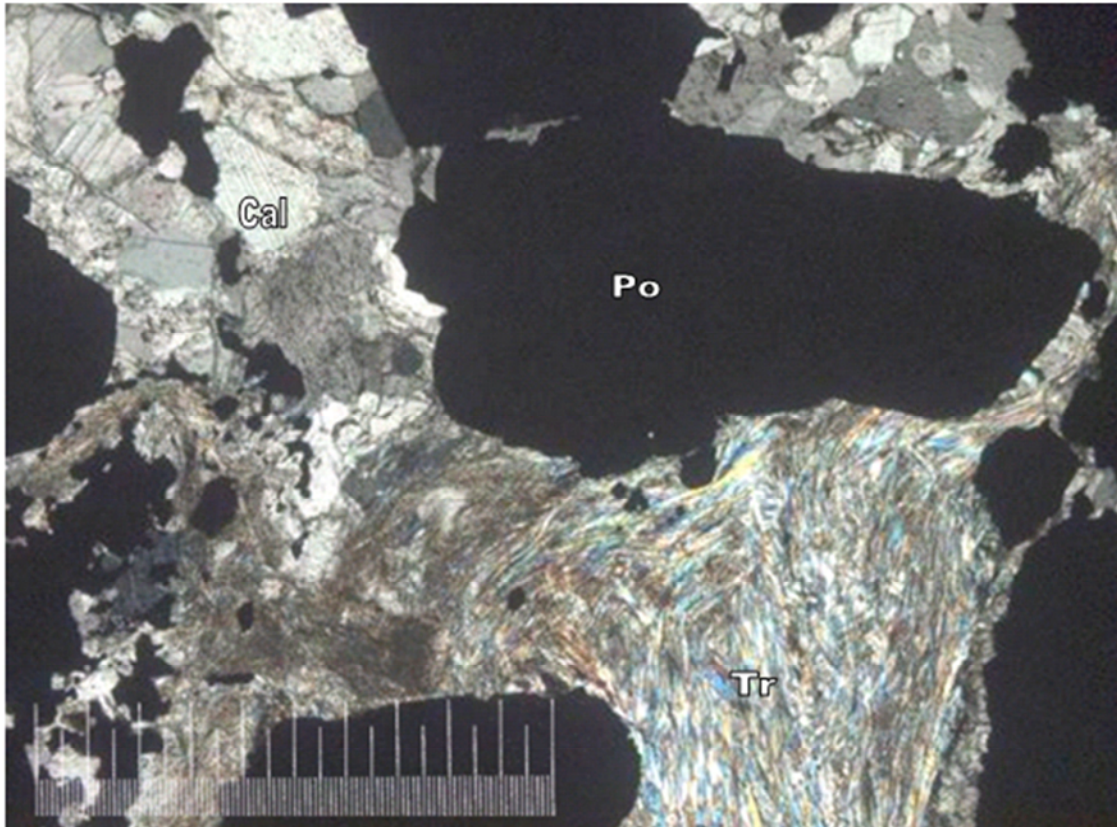
Figure 4.32. Calcite (Cal) and tremolite (Tr) appearing to be in textural equilibrium with each other and with pyrrhotite (Po) (black). The picture scale bar is 1000 microns and it was taken with cross-polarized light. (Sample: UK68E).

Grains of calcite were also found to be enveloped by sulphide in the hybrid rock of the LHZBG Unit (Figure 4.33). Some of the pyrrhotite appears to have infiltrated along the cleavage planes of the calcite grain.
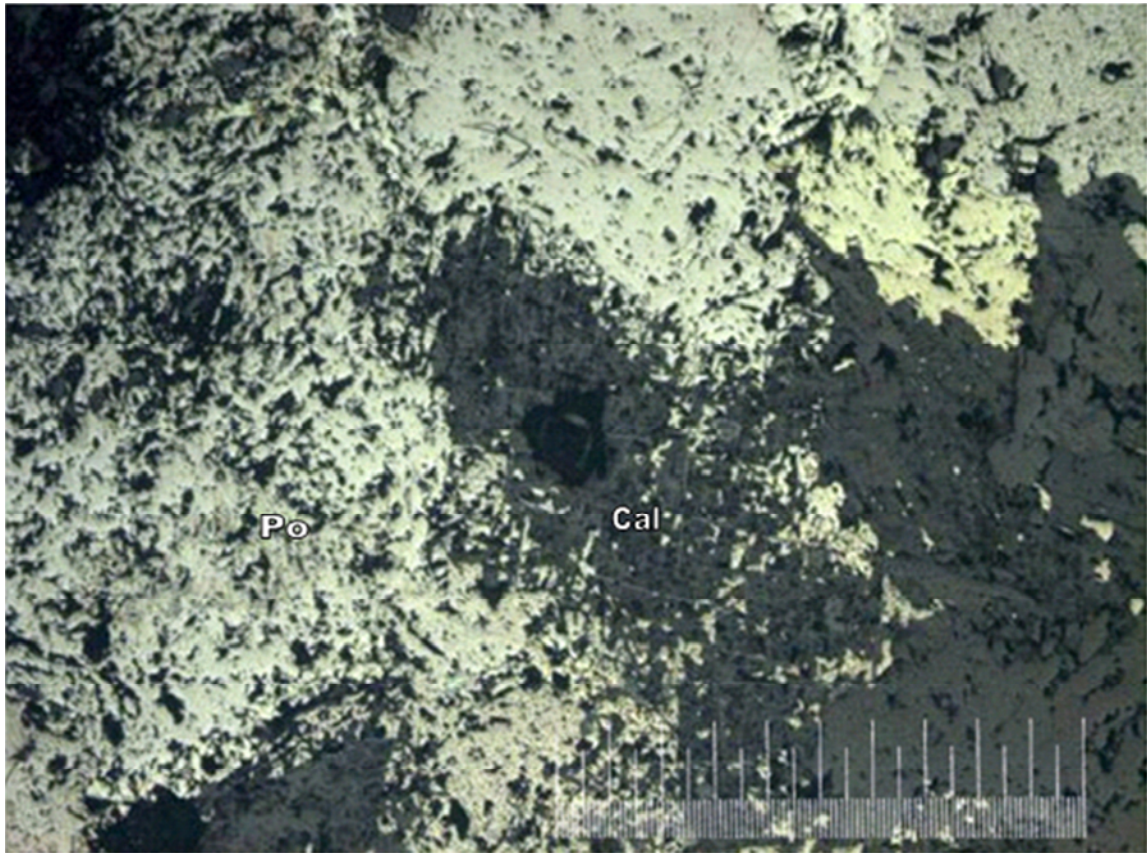
Figure 4.33. A calcite (Cal) grain (in centre of field of view) enveloped by pyrrhotite (Po). The picture scale bar is 1000 micron. Taken with reflected light. (Sample: UK48C).

In the calc-silicate xenoliths calcite encloses diopside grains (Figure 4.34) or occurs in thin veins. Clearly identifiable calcite grains are usually located away from the contact of the xenolith with the hybrid rock.
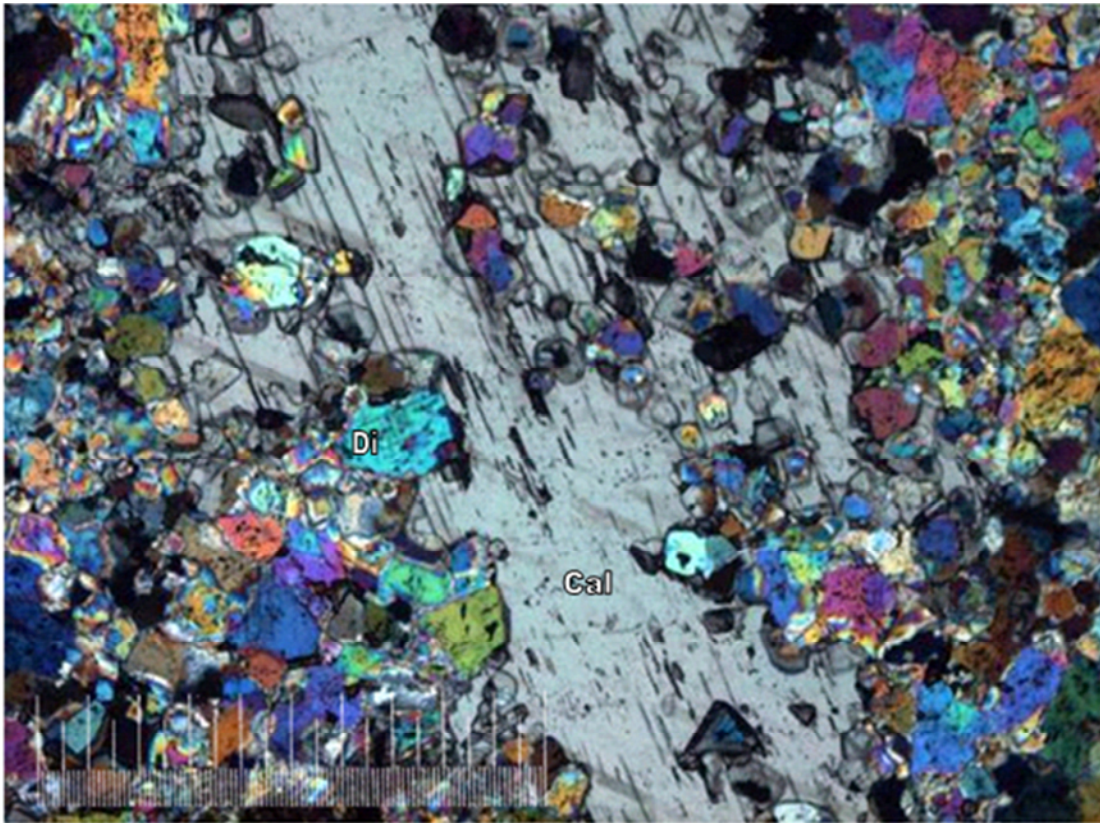
Figure 4.34. A large calcite (Cal) grain, in the center of the view, associated with diopside (Di) in a calc-silicate xenolith from the LHZBG Unit. The picture scale bar is 1000 micron. Taken with cross-polarized light. (Sample: UK3N).

4.7.2. Dolomite

Dolomite was encountered in association with talc, phlogopite and pyrite. The dolomite formed part of the assemblage dolomite-talc-phlogopite or is present as relic grains (Figure 4.35). Dolomite occurs in samples from both the PCR and LHZBG Units, close to the edge of the intrusion.
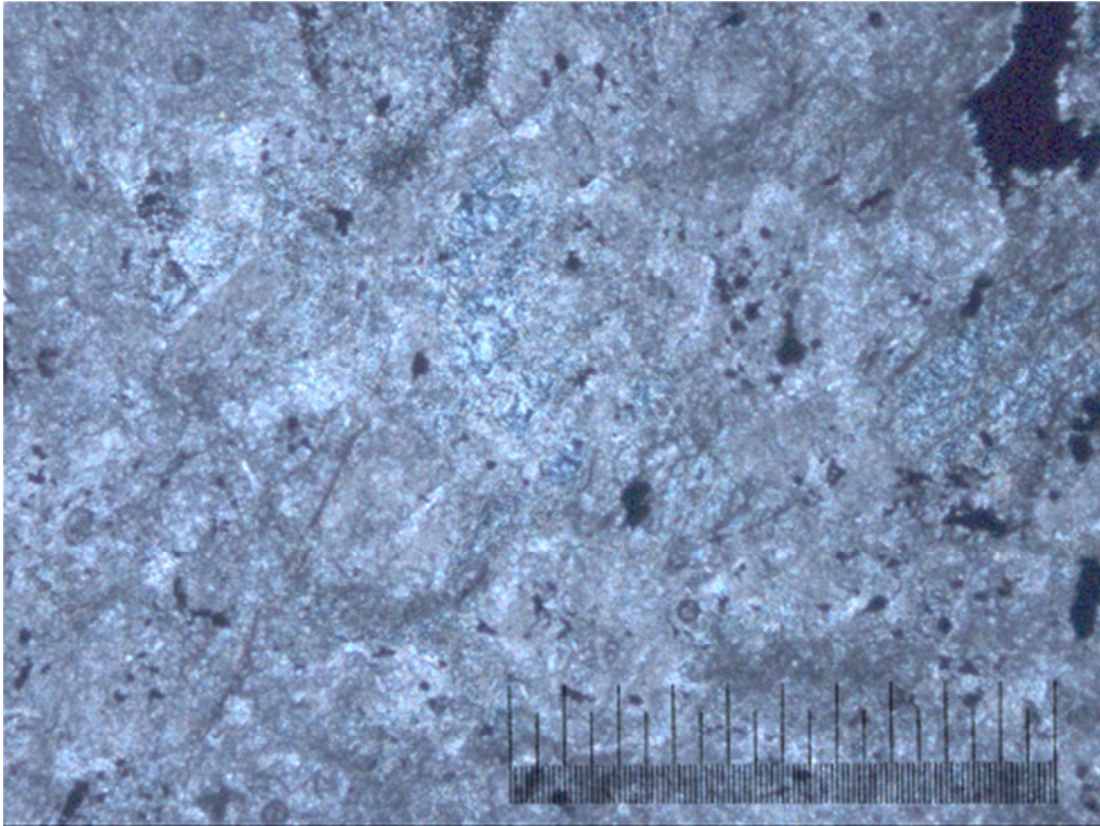
Figure 4.35. Dolomite grains (higher birefringence) occur along with talc and minor sulphides (black). The picture scale is 1000 microns. Taken with cross-polarized light. (Sample: UK61D).

In summary it may be stated that the calcite grains encountered during the investigation are only found in the LHZBG unit and are always in textural equilibrium with the surrounding minerals. In the calc-silicate xenoliths, calcite appeared as discrete, fine veins in close contact with diopside, away from the contact of the xenolith with the surrounding hybrid rock. The calcite grains in the hybrid rock are in textural equilibrium with both silicate (generally tremolite) and sulphide (generally pyrrhotite) minerals. Calcite grains partially enveloped by pyrrhotite are also present.

CHAPTER 5 – SECONDARY MINERALS IN THE LHZBG AND PCR UNITS

5.1 Amphibole

The amphiboles found in the Uitkomst (Figure 5.1) samples are secondary in nature, replacing the original primary mineralogy during retrograde metamorphism of the mafic rocks as well as dolomite. Some pyroxene grains, especially in the LHZBG, have been entirely replaced by fibrous amphibole and may be referred to as uralitized grains. Uralite is the term used to describe the conversion of pyroxene to secondary fibrous amphibole of uncertain composition (Deer et al., 1992). The process of uralitization is ascribed to the action of hydrothermal solutions which may be associated with late stage crystallization of igneous rocks or due to metamorphism or metasomatism (Deer et al., 1992).

5.1.1 Amphiboles of the LHZBG Unit

Amphiboles are the dominant minerals in the LHZBG Unit. These amphiboles (actinolite, tremolite etc.) are less magnesium-rich than amphibole samples of the PCR Unit. Parts of the LHZBG have been altered to such an extent in the boreholes investigated that the entire matrix of the sample is composed of amphibole and the rock type may then be is referred to as amphibolite. Amphiboles in the LHZBG Unit are associated with or replace clinopyroxene grains and are associated with chlorite and brown phlogopite. Some of the uralitized grains also appeared to be pseudomorphic after olivine grains. In borehole UK61, hornblende and tremolite occur in association with dolomite and talc. The sulphide minerals tend to have sharp contacts with the amphibole grains, especially the hornblende grains. Some of the sulphide grains are intergrown with tremolite blades.

5.1.2 Amphiboles of the PCR Unit

The amphiboles (hornblende, magnesio-gedrite, magnesio-cummingtonite etc.) of the PCR unit are very magnesium-rich in composition, with the exception of the PCR unit intercepted in borehole UK12 (sample UK12D), which is located in the narrow part of the intrusion. The grains forming the matrix of these samples are anhedral and some of these grains have pockets of chlorite within them. A few samples are composed completely of amphibole and

chlorite. The amphibole in sample UK48C is associated with remnants of olivine, which are totally serpentinized, containing secondary magnetite. Amphiboles rimming the sulphide minerals are also very magnesium-rich and tend to protrude into the sulphide grains.

5   5.1.3 Microprobe analyses results of amphibole grains

Table 5.1 presents the amphiboles associated with each of the sections that was analysed. The results of the microprobe analyses and mineral formulas are presented in Appendix 2.

Table 5.1 Amphibole minerals in the PCR and LHZBG Units.

Borehole	Unit	Magnesio-anthophyllite	Magnesio-gedrite	Magnesio-cummingtonite	Tremolite	Tremolitic-hornblende	Magnesio-hornblende	Hornblende	Actinolite	Actinolitic-hornblende	Tschermakite	Pargasite-hornblende	Pargasite	Edenite	Edenitic-hornblende	Magnesio-hastingsite
UK12D	PCR							x								
UK12G	PCR		x	x			x					x				x
UK48C	PCR		x	x												
UK48G	PCR			x												
UK48I	PCR	x					x									
UK61A	PCR	x	x	x			x				x					
UK61B	PCR				x											
UK61C	PCR		x	x												
UK12H	LHZBG		x	x			x								x	
UK12J	LHZBG					x					x			x		x
UK12L	LHZBG												x			x
UK48L	LHZBG				x										x	
UK48N	LHZBG				x				x							
UK61E	LHZBG				x	x			x	x						
UK61F	LHZBG	x	x	x												

Microprobe analyses of amphibole grains, presented in Appendix 2, were recalculated and averaged before being plotted. This yields the results presented in figures 5.2 to 5.15.
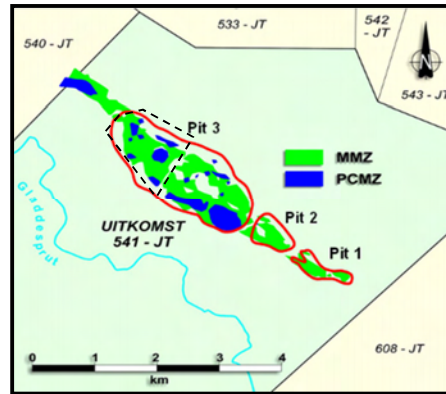
Figure 5.1. Study area located in upper left hand side of pit 3 (black dash line). Figure courtesy Nkomati Mine geological staff.
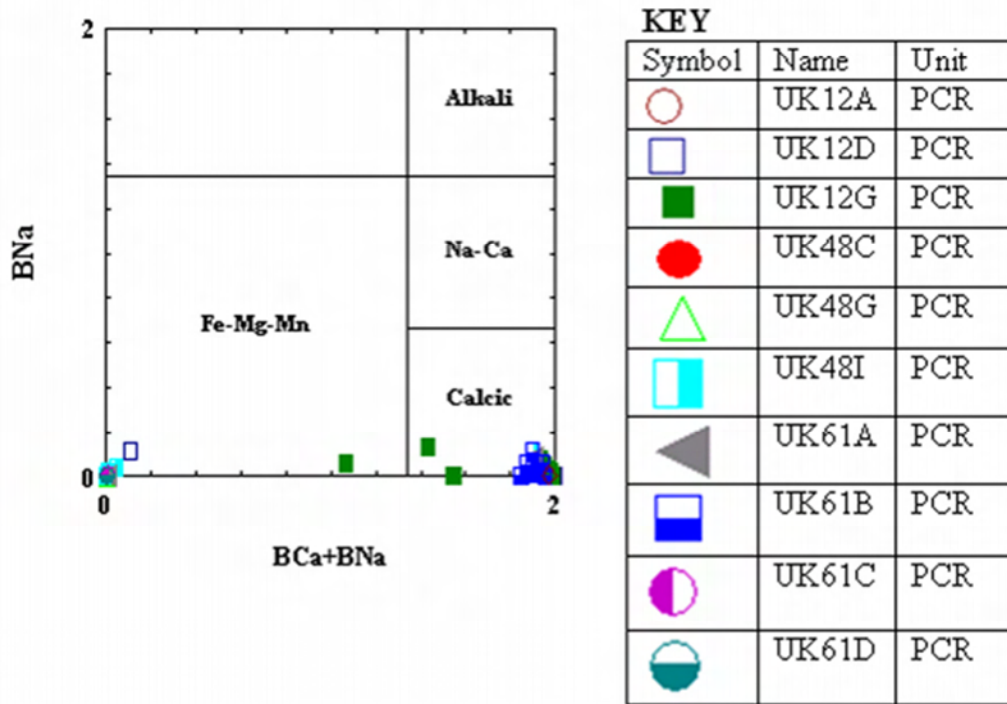
Figure 5.2. Classification diagram for the four principal groups of amphiboles in the PCR Unit (After Hawthorn, 1981).
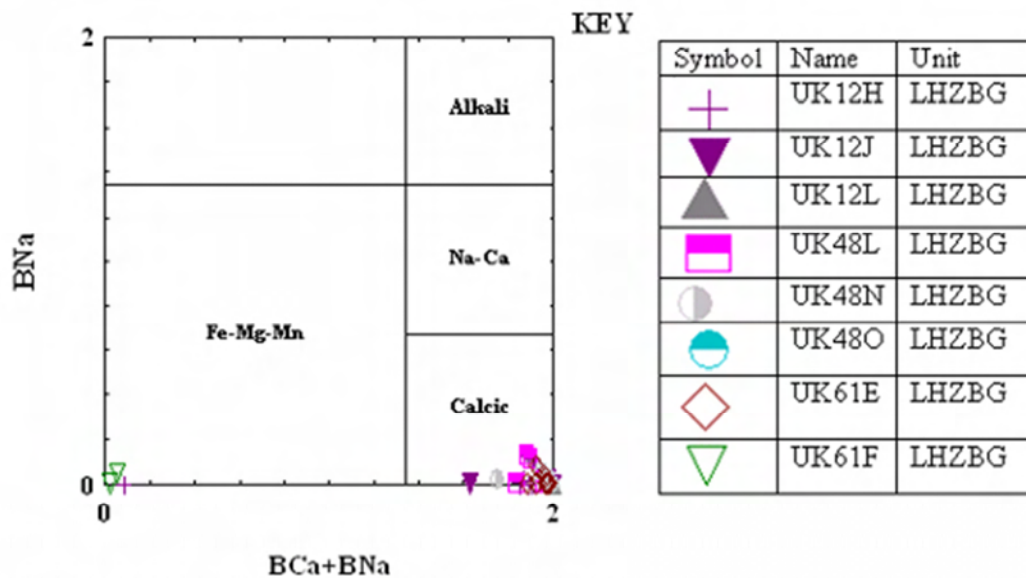
Figure 5.3. Classification diagram for the four principal groups of amphiboles in the LHZBG Unit (After Hawthorn, 1981).

By plotting the recalculated analyses according to Na in the B-position against Ca and Na in the B-position, it is shown that most of the amphiboles are calcic, with some Fe-Mg-Mn amphiboles also being present (Figures 5.2 and 5.3). This correlates with van Zyl's (1996) findings. The dominance of calcic amphiboles may indicate the accommodation of Ca into amphibole species, after assimilation of the dolomitic country rock.
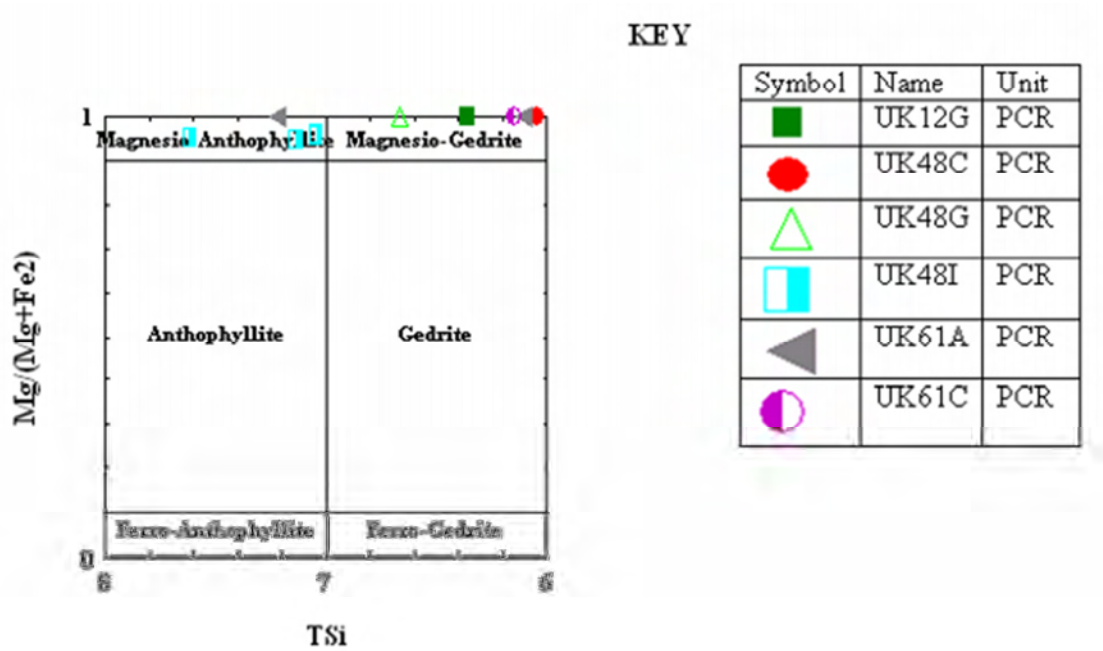
Figure 5.4. Classification diagram for Fe-Mg-Mn group orthorhombic amphiboles in the PCR Unit (After Hawthorn, 1981).
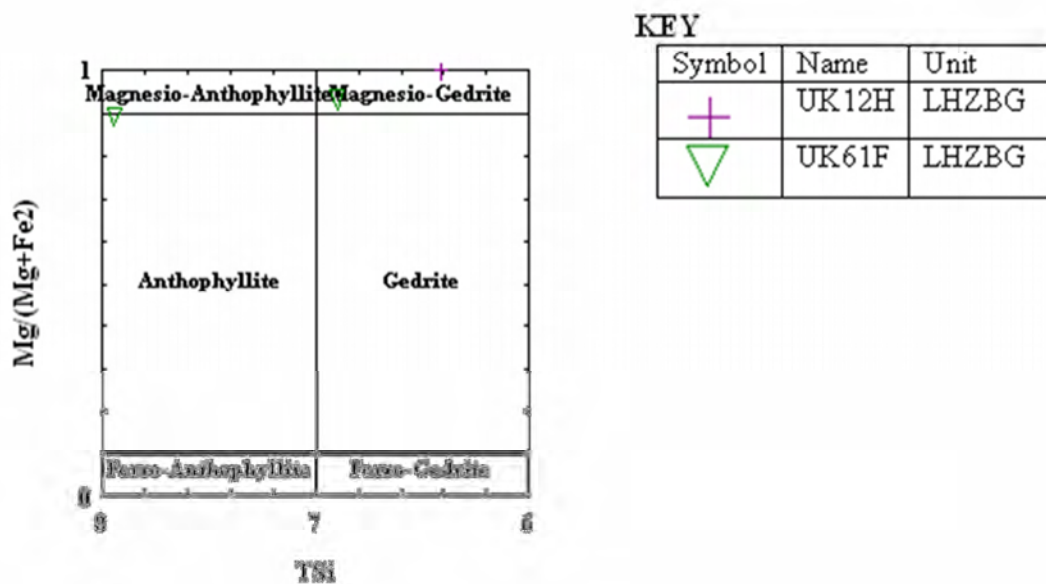
Figure 5.5. Classification diagram for Fe-Mg-Mn group orthorhombic amphiboles in the LHZBG Unit (After Hawthorn, 1981).

84

According to Deer et al., (1992) orthorhombic amphiboles are unknown in igneous rocks. Anthophyllite and gedrite do however occur in metamorphic and metasomatised rocks, and these minerals are also commonly found in the reaction zone between ultramafic rocks and country rocks. These two minerals (presented in Figure 5.4 and 5.5) may also develop during lower amphibolite facies conditions (Deer et al., 1997). Orthoamphiboles may be derived from calcic amphiboles by metasomatism, e.g. hornblende or actinolite, in the latter due to hydrothermal alteration involving the addition of Mg and the loss of Fe, Ti and Ca (Deer et al., 1997). The formation of anthophyllite may also be due to the addition of Fe, Mg or Al and the removal of Ca during metamorphism (Deer et al., 1992). Anthophyllite commonly occur as an alteration product in rocks rich in olivine (Deer et al., 1997). Anthophyllite may also form due to retrograde metamorphism of earlier thermally metamorphosed rocks (Deer et al., 1992).

Magnesio-antophyllite and magnesio-gedrite is found in both the PCR (Figure 5.4) and LHZBG (Figure 5.5) Units. Less evidence of magma-country rock interaction exists in the PCR Unit relative to the LHZBG Unit, thus the possibility of it representing an interaction product is considered unlikely. Samples UK12H and UK61F, from the LHZBG (Figure 5.5) Unit, contain magnesio-antophyllite and magnesio-gedrite. This probably represents interaction between the intruding ultramafic magma and the surrounding dolomitic country rock.

The relict poikilitic texture of the PCR Unit is shown in Figure 5.6. In this unit, magnesio-anthophyllite is found in association with serpentine, likely representing alteration of the precursor mafic minerals orthopyroxene (enstatite) and olivine respectively. Magnesio-gedrite and –anthopyllite is found in PCR samples: UK12G, 48C, 48G, 48I, 61A and 61C (Figure 5.4).
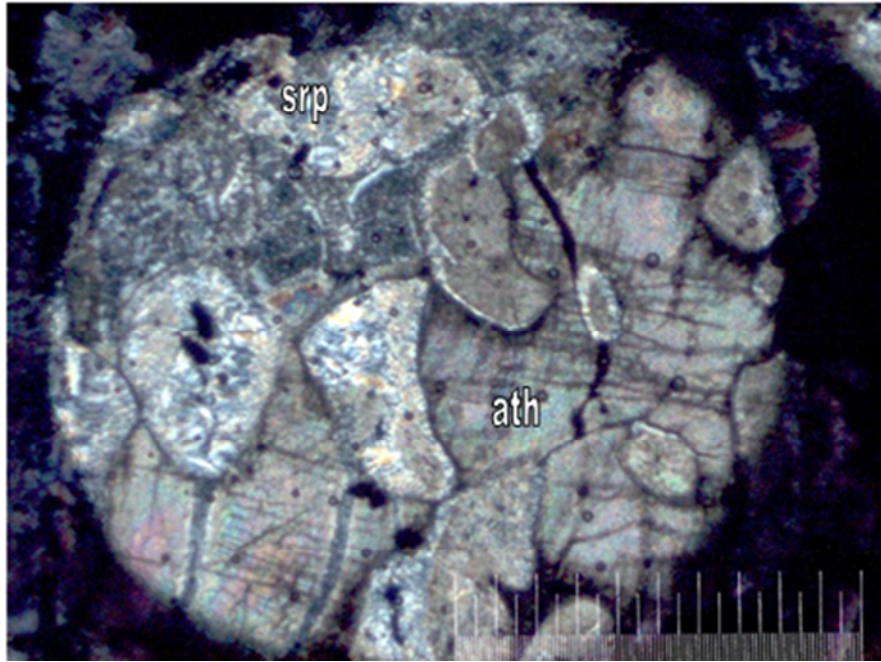
Figure 5.6. Relict pokilitic texture in the PCR Unit. Serpentinised (srp) grains (top left, higher birefringence) probably after olivine and magnesio-anthophyllite (ath) (bottom right, low birefringence) probably after Mg-rich orthopyroxene grains from the PCR. The picture scale bar is 1000 micron. Taken with cross-polarised light. (Sample; UK48I).
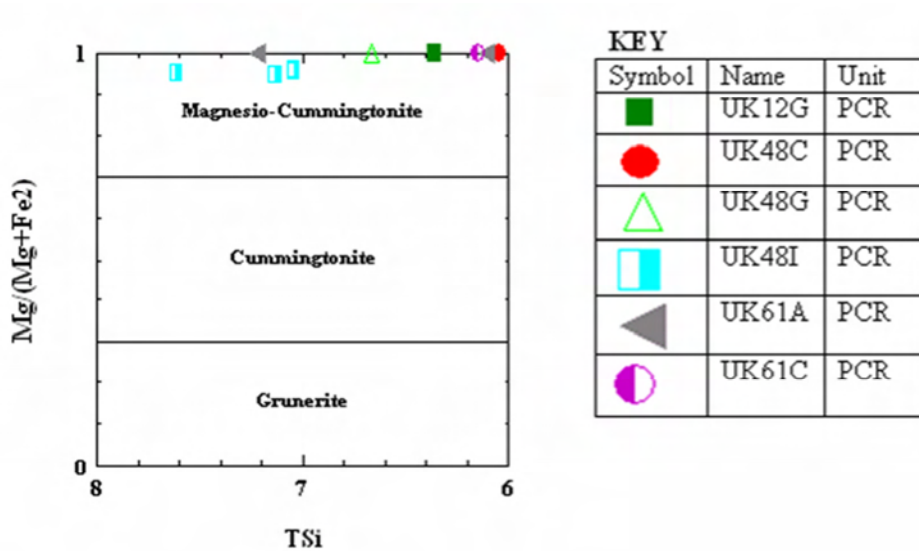
Figure 5.7. Classification diagram for Fe-Mg-Mn Group Monoclinic amphiboles in the PCR Unit (After Hawthorn, 1981).
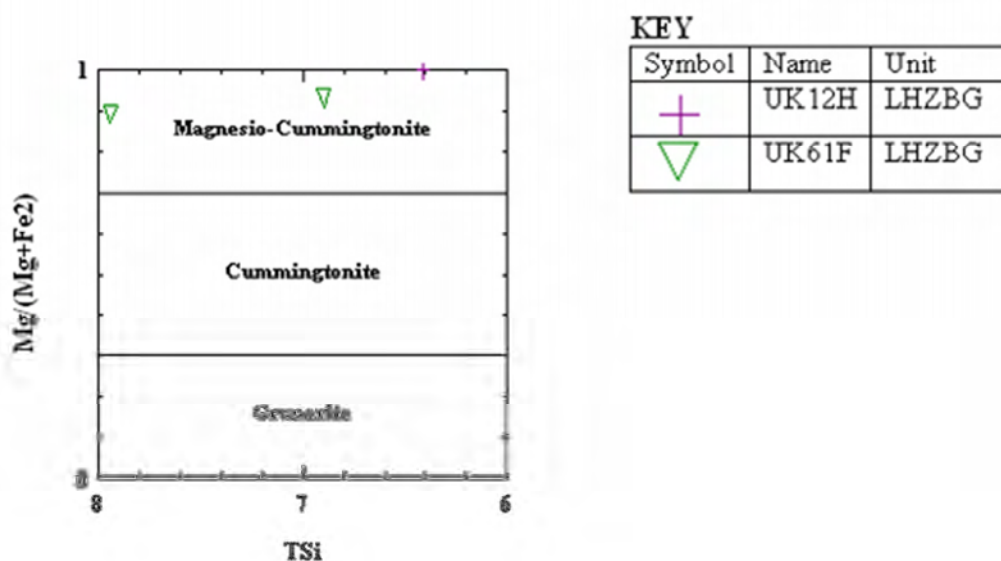
Figure 5.8. Classification diagram for Fe-Mg-Mn Group Monoclinic amphiboles in the LHZBG Unit (After Hawthorn, 1981).

According to Deer et al., (1992) magnesium-rich cummingtonite occurs together with anthophyllite in isochemically metamorphosed ultrabasic rocks. Cummingtonite is also found in hybrid rocks of intermediate composition and may occur as the middle member in the transition of orthopyroxene to hornblende (Deer et al., 1992).

The composition of the Uitkomst samples (magnesio-anthophyllite, magnesio-gedrite and magnesio-cummingtonite) may indicate that the samples represent ultrabasic rocks that suffered metamorphism and metasomatism. The magnesio-cummingtonite samples derived from the PCR Unit, and presented in Figure 5.7, are: UK12G, UK48C, G and I, UK61A, and C. Magnesio-cummingtonite also occurs at the top of the LHZBG Unit (UK12H) and middle (UK61F) of the unit (Figure 5.8). The greater abundance of magnesio-amphiboles in the PCR Unit relative to the LHZBG Unit may indicate the magma that formed the PCR Unit may have been more primitive than the magma that formed the LHZBG Unit or may have suffered less contamination by the dolomite country rock. It is also important to note

that the samples that contain magnesio-cummingtonite are the same samples that contain magnesio-anthophyllite and magnesio-gedrite (Figures 5.4 and 5.5).
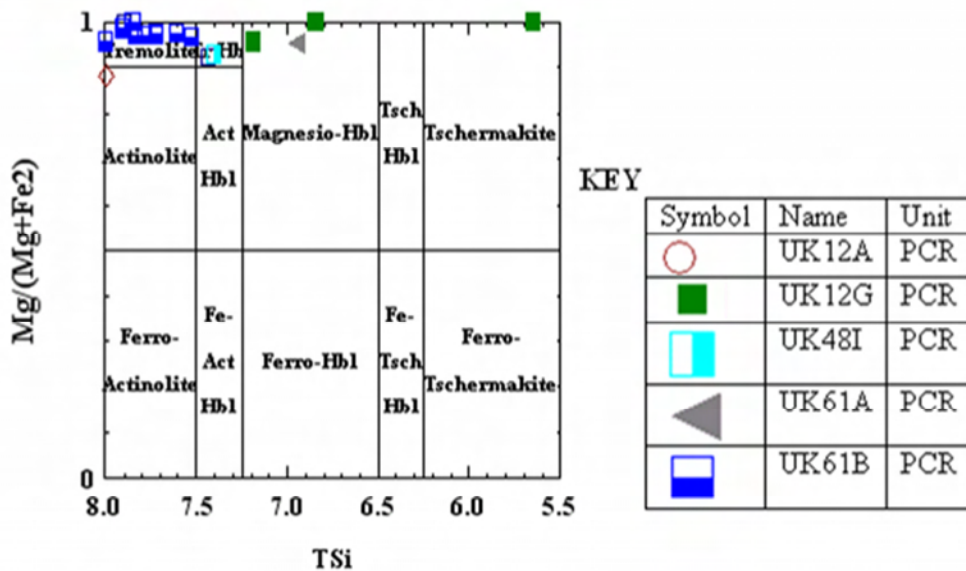
Figure 5.9. Classification diagram for the calcic group of amphiboles where ANa+AK<0.5;Ti<0.5 in the PCR Unit (After Hawthorn, 1981).
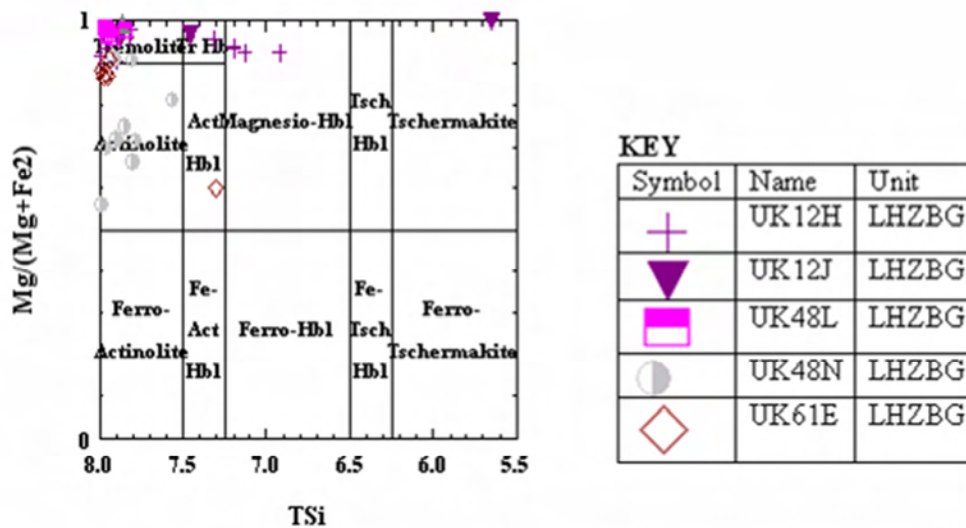
Figure 5.10. Classification diagram for the calcic group of amphiboles where ANa+AK<0.5;Ti<0.5 in the LHZBG Unit (After Hawthorn, 1981).

Tremolite and actinolite are metamorphic minerals that may occur in both contact and regionally metamorphosed rocks. Actinolite is a common product of retrograde metamorphism of ultrabasic rocks. Actinolite usually develops in pyroxene-rich rocks as an alteration product of both orthopyroxene and clinopyroxene (Deer et al., 1997). In ultrabasic rocks actinolite is usually associated with assemblages of tremolite-talc and or tremolite-carbonate-antigorite (Deer et al., 1997).

During thermal metamorphism of impure dolomites, tremolite forms early on in the reaction between dolomite and quartz by the reaction:

$$5CaMg(CO_3)_2 + 8SiO_2 + H_2O = Ca_2Mg_5Si_8O_{22}(OH)_2 + 3CaCO_3 + 7CO_2$$
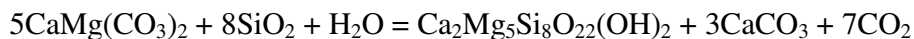
Tremolite forms at the expense of talc and calcite (Provoden, Horacek and Abart, 2002). The reaction for the formation of tremolite as a result of this is:

$$1.5x \text{ Calcite} + 1x \text{ Talc} = 0.5x \text{ Dolomite} + 0.5x \text{ Tremolite} + 0.5x \text{ } H_2O + 0.5x \text{ } CO_2$$
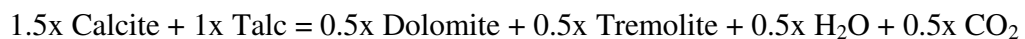
With increasing metamorphic grade, tremolite becomes unstable, and, in the presence of silica and calcite, tremolite will react to form diopside (Deer et al., 1997). Where quartz has been exhausted, the remaining dolomite will react with tremolite to produce fosterite and calcite. Both of these reactions liberate CO_2 and H_2O, but the temperature of reaction will depend on the fluid volume and composition. These reactions do not appear to have occurred in the Uitkomst Complex, as the olivine has been found only as a magmatic phase. The tremolite-actinolite-hornblende assemblages (Figure 5.10) are present in the middle (UK12J and UK48N) to upper parts of the LHZBG Unit (UK12H, UK48L and UK61E) as depicted in Figure 5.10 and in the upper parts of the PCR Unit (UK12D, UK61A and B) and bottom part of the PCR (UK12G) as depicted in Figure 5.9. Amphiboles of this composition are occasionally intergrown with sulphide grains.

Tremolite is the dominant amphibole mineral found in the LHZBG Unit, in the Uitkomst Complex, on the farm Slaaihoek 540 - JT (Steenkamp, 2004). The Slaaihoek samples appeared more pristine relative to samples from the current study area. In the Slaaihoek samples the tremolite pseudomorphically replaces pyroxene and olivine. Steenkamp (2004) also describe hybrid rocks that consist predominantly of tremolite and classify them as amphibolites.

The occurrence of the actinolite-tremolite in the middle- and upper parts of the LHZBG Unit (Figure 5.10) and lower part of the PCR Unit (Figure 5.9) may indicate that the H_2O-rich fluid migrated upward and affected the minerals above and below the contact between the two units. In contrast, the abundance of actinolite-tremolite only again in the upper part of the PCR may indicate that the H_2O-rich fluid was trapped below the MCR Unit developed on the contact between the PCR and MHZBG Units.
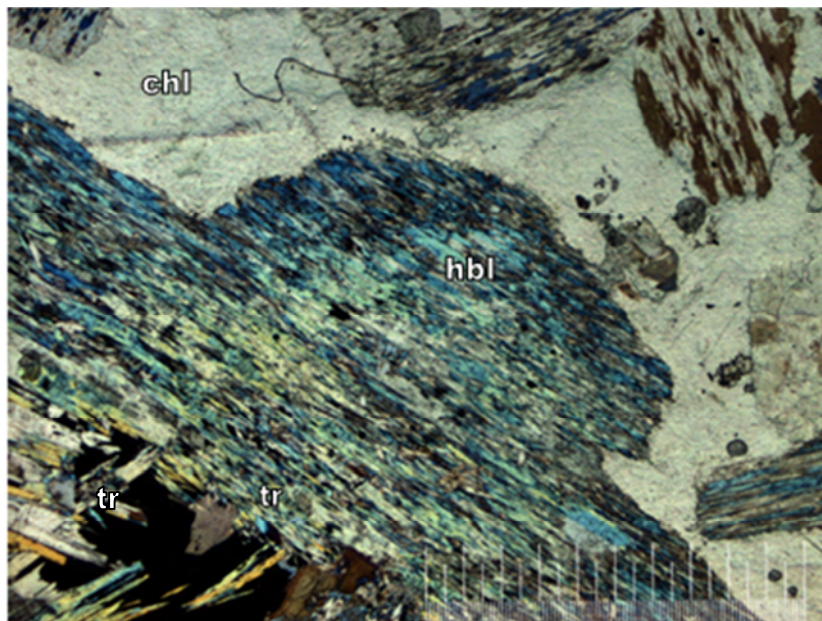
Figure 5.11. Diopside grains entirely replaced by tremolite (tr), magnesio-hornblende (hbl) (acicular grains, high birefringence) in centre of view. Chlorite (chl) is associated with the tremolite and magnesio-hornblende grains and forms the surrounding matrix material. Tremolite also protrudes into a sulphide grain (black, bottom left). The picture scale bar is 1000 micron. Taken with cross-polarised light. (Sample: UK12H).
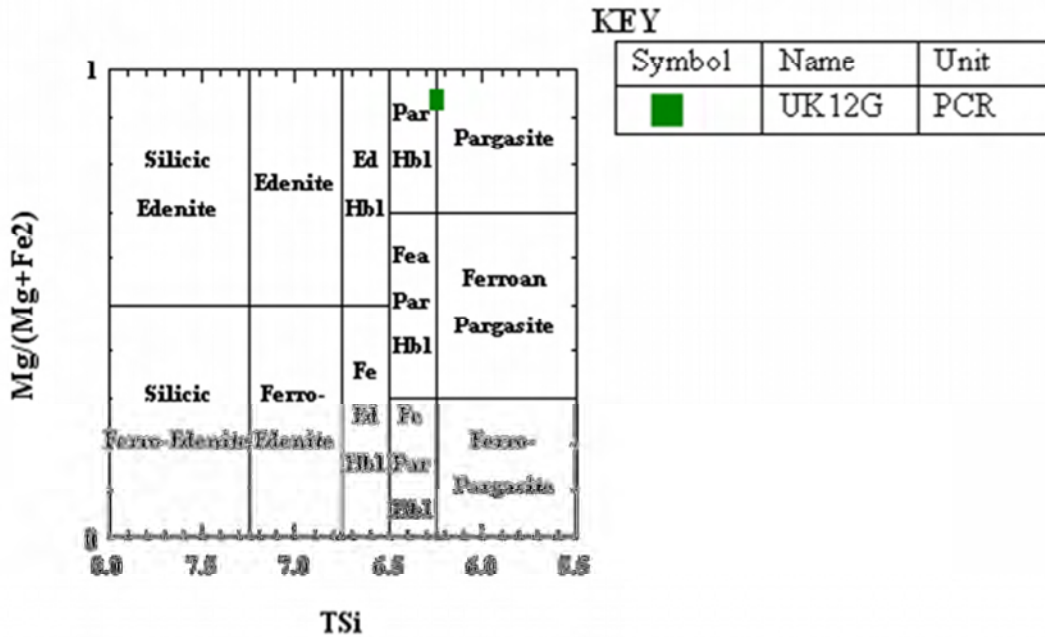
Figure 5.12. Classification diagram for the Calcic Group of amphiboles where Ana+AK>0.5;Ti<0.5;Fe3<Alvi in the PCR Unit (After Hawthorn, 1981).
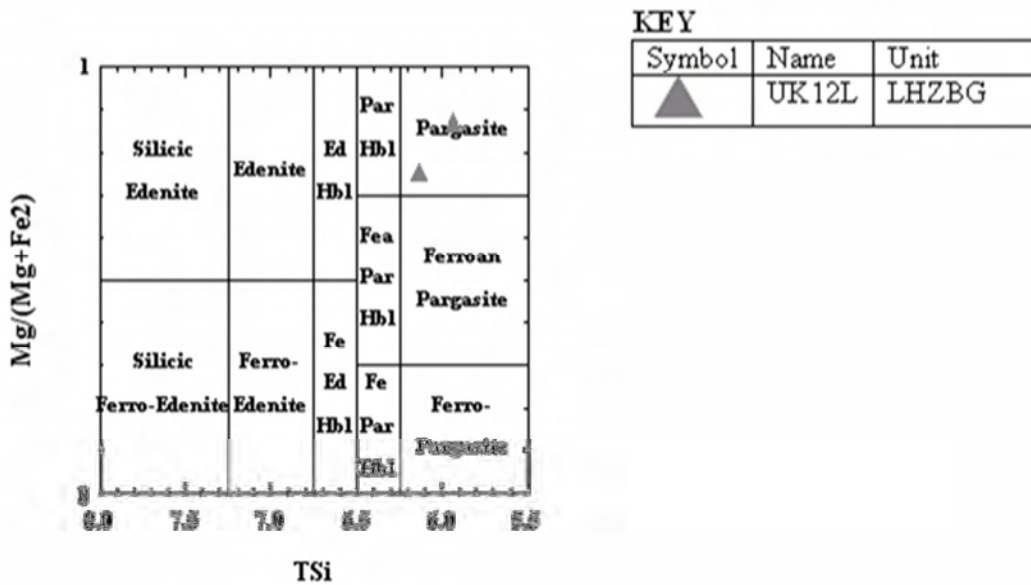
Figure 5.13. Classification diagram for the Calcic Group of amphiboles where Ana+AK>0.5;Ti<0.5;Fe3<Alvi in the LHZBG Unit (After Hawthorn, 1981).

Pargasite-hornblende and pargasite also occur in metamorphosed impure dolomites and limestone (Deer et al, 1992). The composition of hornblende and pargasite is sensitive to pressure and temperature, but this relationship is affected by the bulk rock composition, fluid phase and the oxygen fugacity (Deer et al., 1997).

Pargasite is found only in sample UK12G from the lower part of the PCR Unit and in sample 12L from the lower part of the LHZBG Unit. This may indicate xenolithic material of metamorphosed impure dolomitic material is associated with the samples from the narrower part of the intrusion. This may represent finger structures of penetrating or preserved country rock in the narrow part of the intrusion in the study area.
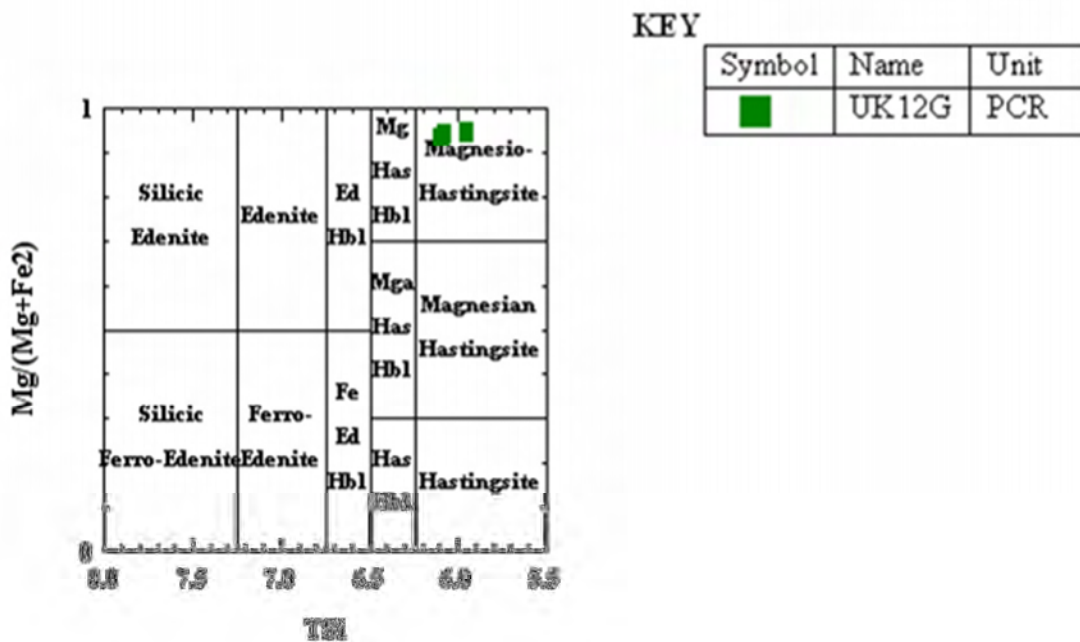
Figure 5.14. Classification diagram for the Calcic Group of amphiboles where ANa+AK>0.5;Ti<0.5;Fe3>Alvi in the PCR Unit (After Hawthorn, 1981).
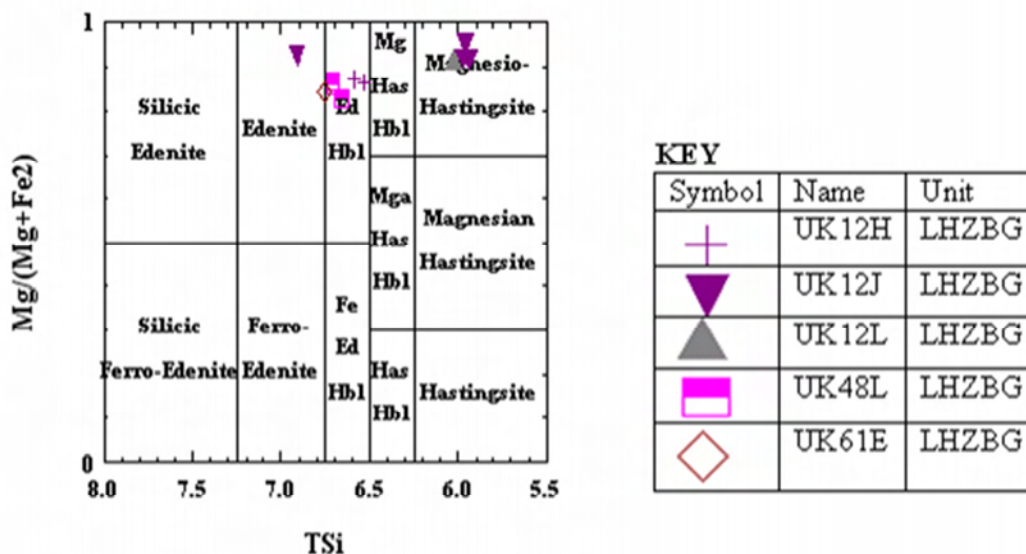
Figure 5.15. Classification diagram for the Calcic Group of amphiboles where ANa+AK>0.5;Ti<0.5;Fe3>Alvi in the LHZBG Unit (After Hawthorn, 1981).

According to Deer et al., (1992), the wide range of chemical substitution possible in hornblende leads to its existence in a wide variety of igneous and metamorphic petrogenetic conditions. Magnesio-hastingsite usually only occurs in alkali basalt and calc-alkaline rock (Deer et al., 1992). In andesitic rocks hornblende is usually accompanied by olivine and has been suggested to form due to interaction between olivine and the andesitic fluid (Deer et al., 1992). It was suggested by de Waal et al. (2006) that the edenite and magnesio-hastingsite amphiboles found in the high-Ti suite samples stabilized after clinopyroxene in the paragenetic sequence, and its concentrations are directly proportional to the amount of trapped liquid. It was indicated by Arndt et al. (2005) that the presence of H_2O and CO_2 in magma will manifest mineralogically as phlogopite and magmatic amphibole in the groundmass.

The magnesio-hastingsite mineralization in the Uitkomst Complex is found in the lower and middle part of the LHZBG Unit (Figure 5.15) and the lower parts of the PCR Unit (Figure 5.14) in the narrow part of the intrusion. Edenite-hornblende, also indicated in Figure 5.15, is found in the upper part of the LHZBG Unit in all three of the analysed boreholes. The

only edenite (Figure 5.15) found is in the middle part of the LHZBG Unit in the narrow part of the intrusion. Pargasite, magnesio-hastingsite and edenite are in contact with, but are not intergrown with sulphide grains.

Following de Waal et al. (2006), it is suggested that the magnesio-hastingsite and edenite-hornblende may represent amphiboles formed as part of the paragenetic sequence of mineralization of the magma due to trapped liquids. This hypothesis is supported by the presence of the magnesio-hastingsite and edenite in proximity to preserved olivine grains (Figure 5.16). The magnesio-hastingsite, edenitic-hornblende and edenite are also found in greater abundance in the LHZBG Unit relative to the PCR Unit, suggesting more interaction with trapped fluids in the LHZBG Unit. The magnesio-hastingsite found in the PCR Unit comes only from sample UK12G, the lower part of the PCR Unit. This may suggest interaction with trapped fluids took place only in the lower part of the PCR Unit, in the narrower part of the intrusion in the study area.
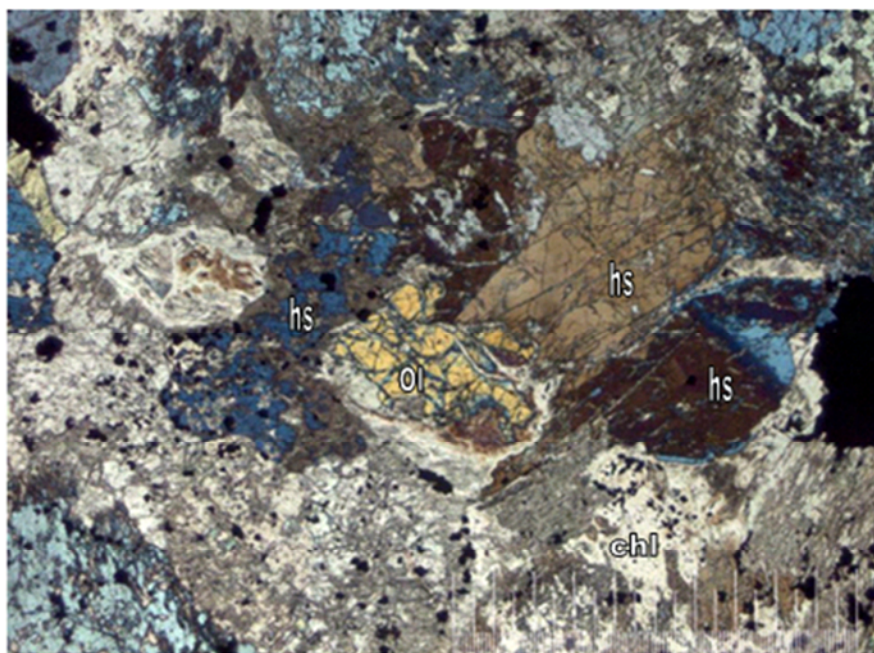
Figure 5.16. Olivine (ol) (yellow grain, centre of view), magnesio-hastingsite (hs) (light brown grain, to top right of olivine) and the combination blue-brown grains are mainly magnesio-hastingsite (hs) with minor edenite (ed). The low birefringence mineral is chlorite (chl). The black mineral is a sulphide grain. The picture scale bar is 1000 micron. Taken with cross-polarised light. (Sample: UK12J).

5.2 Chlorite

Chlorite is a secondary mineral that forms due to deuteric or hydrothermal alteration of primary ferromagnesian minerals such as mica, pyroxenes, amphiboles, garnets and olivines at temperature of up to 400 ˚C (Deer et al., 1992). The composition of the chlorite is often related to that of the original minerals, but the ideal formula of chlorite is $(Mg, Fe^{2+}, Fe^{3+}, Mn, Al)_{12}[(Si,Al)_8O_{20}](OH)_{16}$ (Deer et al., 1992).

Chlorite is found in the all of the analysed (XRD) samples of the BGAG, LHZBG and PCR Units. In the PCR Unit the chlorite has a white-green colour. In some instances, chlorite and talc form the entire matrix (e.g. UK12A). Chlorite also occurs in association with serpentine and talc (e.g. UK48G). Chlorite and amphibole also occur together in relic dolomite grains (UK61C) along with talc (e.g. UK61F). Chlorite in the LHZBG Unit appears green-white to white. Here it is associated with amphibole and is present as pockets within amphibole (e.g. UK12J presented in Figure 5.17) and diopside. Chlorite also forms part of rims surrounding sulphide grains, but the sulphides are not intergrown by the chlorite.
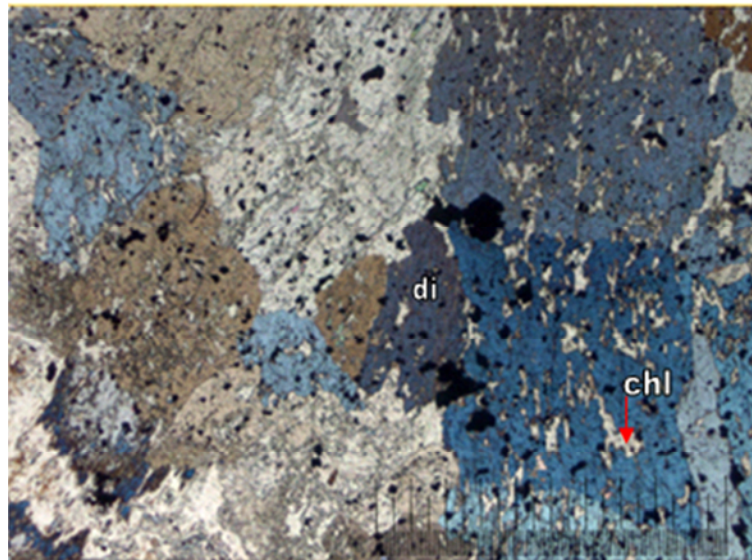
Figure 5.17. Pockets of chlorite (chl) (off-white) in diopside (di) grains (blue and brown) with associated subhedral pyrite (black) grains form the Lower Harzburgite Unit. Note the triple junctions between the diopside grains. The picture scale bar is 1000 micron.Taken with cross-polarised light. (Sample: UK12J).

The average chlorite content (based on semi-quantitative XRD analyses) is 17 wt% in the BGAB Unit, 19 wt% in the LHZBG Unit and 21.6 wt% in the PCR Unit. This shows a progressive increase in chlorite content with stratigraphic height in the lower part of the Complex. Microprobe analyses of chlorite are provided in Appendix 2. The data was recalculated and plotted using *MinPet* software.
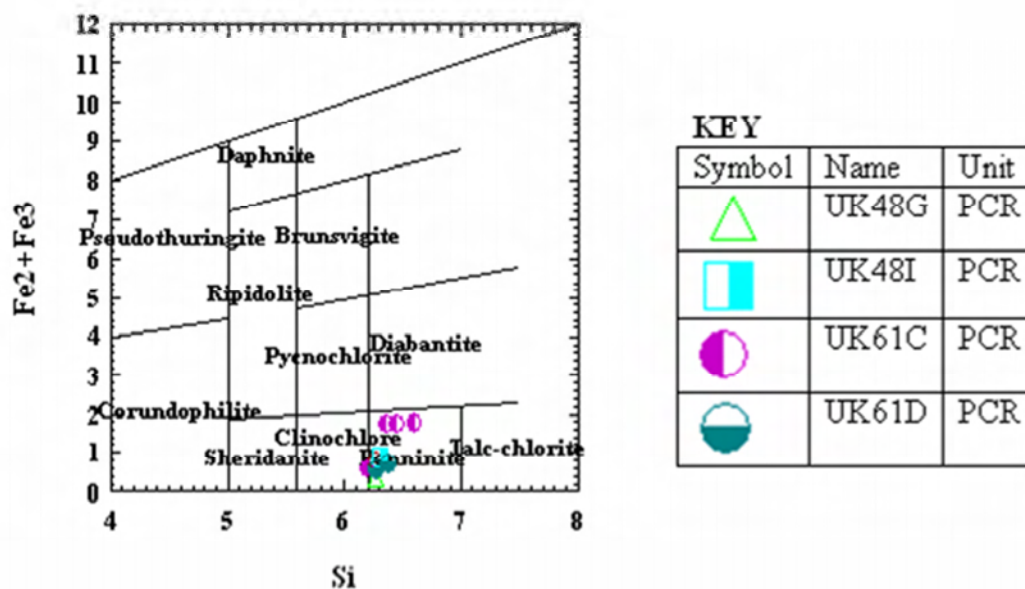
Figure 5.18. Chlorite classification diagram of Deer et al. (1972) showing chlorite grains analysed in the PCR Unit.

Using the classification scheme proposed, for the chlorite grains analysed, it may be seen that the chlorite composition fall mainly into the clinochlore, pycnochlorite and penninite composition range. Penninite is a manganese chlorite and clinochlore is an Mg-rich chlorite (Deer et al., 1992).

In the PCR Unit (Figure 5.18) all of the analysed chlorite grains fall in the penninite compositional range. In the LHZBG Unit (Figure 5.19) the chlorite composition range is

highly varied. The chlorite species in the LHZBG Unit are talc-chlorite, penninite, clinochlore, pycnochlorite and diabantite. The chlorite found in the xenoliths from the LHZBG Unit (Figure 5.20) falls in the ranges of clinochlore and pycnochlorite.
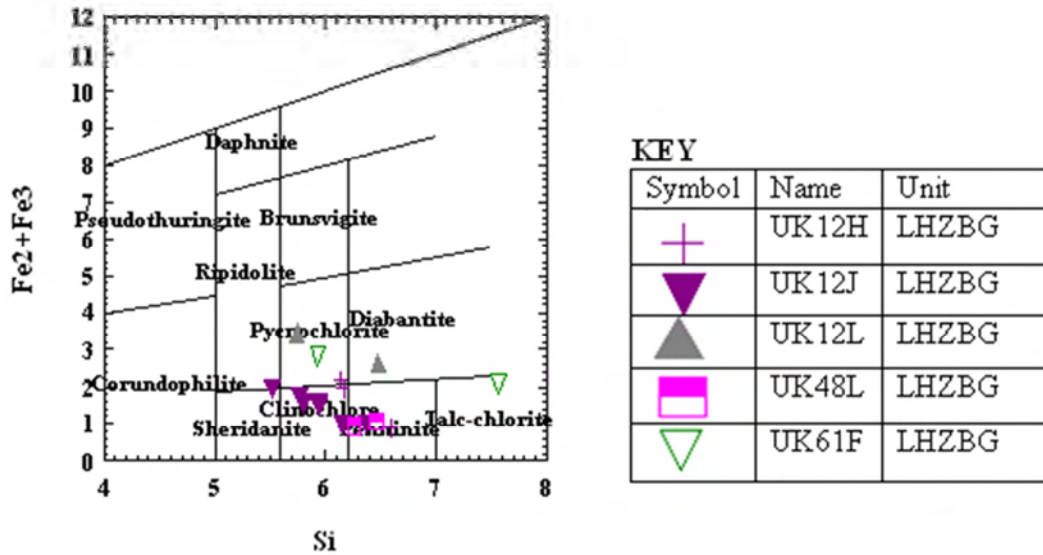
Figure 5.19. Chlorite classification diagram of Deer et al. (1972) showing chlorite grains analysed in the LHZBG Unit.
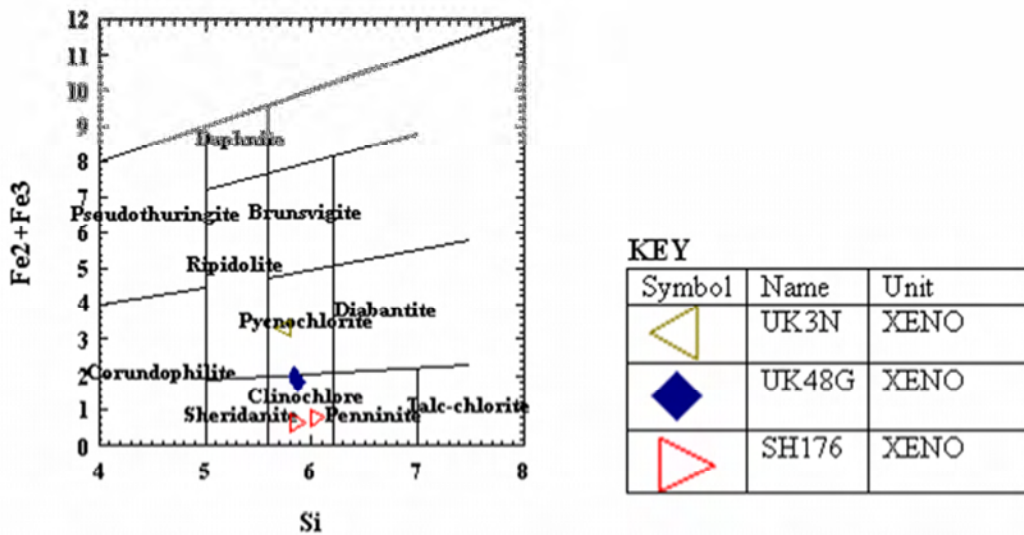
Figure 5.20. Chlorite classification diagram of Deer et al. (1972) showing chlorite grains analysed in the xenoliths from the LHZBG Unit.

The occurrence of the different species of chlorite is presented in Table 5.2

Table 5.2. Classification of chlorite in the different units.

Borehole	Unit	Pycnochlorite	Clinochlore	Penninite	Ripidolite	Diabantite	Talc-chlorite
UK12H	LHZBG	X	X	X			
UK12J	LHZBG		X		X		
UK12L	LHZBG	X				X	
UK48G	PCR			X			
UK48I	PCR			X			
UK48L	LHZBG			X			
UK61C	PCR			X			
UK61D	PCR			X			
UK61F	LHZBG	X					X
SH12H	XENO		X				
UK44G	XENO		X				

Chlorite in the calc-silicate xenoliths from the LHZBG Unit is of a clinochlore composition and those in the LHZBG are pycnochlorite, and clinochlore, with the exception of sample UK48L from the LHZBG Unit where the chlorite compositions plot predominantly in the penninte field. The chlorite from all samples of the PCR Unit, has the composition of penninite. These findings differ from those of van Zyl (1996) who found that the chlorite compositions are only of a pycnochlorite-diabantite composition.

The average compositions of chlorite from the LHZBG, PCR and xenoliths form the LHZBG Units are presented in Table 5.3. The results and calculated formulas are presented in Appendix 2.

Table 5.3. The average chlorite composition in the PCR, LHZBG and xenoliths from the LHZBG Units.

PCR	Al_2O_3	FeO	MnO	MgO
Mean	15.28	7.89	0.05	30.61
Std Dev	1.04	3.42	0.04	2.40
LHZBG				
Mean	17.46	11.79	0.23	25.85
Std Dev	2.19	4.67	0.13	4.44
Xeno				
Mean	19.63	10.54	0.56	24.65
Std Dev	0.77	5.56	0.23	3.85

The Al- and Mn content in the chlorite present in the xenoliths from the LHZBG Unit is the highest amongst the sampled rocks. The chlorite in the LHZBG Unit has the highest Fe content and the chlorite from the PCR Unit has the highest Mg content. The chlorite from the LHZBG Unit and the xenoliths from the LHZBG Unit have near similar composition, but differ notably from the composition of chlorite from the PCR Unit.

5.3. Serpentine

Retrograde metamorphism of ultramafic rocks requires the presence of H_2O and or CO_2. The most common hydrothermal alteration product of olivine is the serpentine mineral lizardite with pseudomorphic textures, with or without brucite, magnesite and magnetite. Serpentine is only stable at very low values of X_{CO_2}, which implies that the fluid phase that dominated at the time of its formation contained very little CO_2. The X_{CO_2} must be <10 mole%, otherwise serpentine would be converted to magnesite and quartz or talc (Winkler, 1974; Bucher-Nurminen, 1982; Provoden et al., 2002).

Of importance are the following reactions that take place at extremely low concentrations of CO_2 (Winkler, 1974):

1) 1 Serpentine + 1 magnesite = 2 fosterite + 2 Water + $1CO_2$

3) 2 Serpentine + 3 CO_2 = 1 talc + 3 magnesite + $3H_2O$

5) 1 Serpentine + 3 CO_2 = 2 quartz + 3 magnesite + $2H_2O$

6) 1 Serpentine + 1 brucite = 2 fosterite + $3H_2O$

7) 5 Serpentine = 6 fosterite + 1 talc + $9H_2O$

8) 1 Serpentine + 2 quartz = 1 talc + $1H_2O$

19) 1 Brucite $+1CO_2$ = 1 magnesite $+1H_2O$

20) 1 Brucite = 1 periclase + H_2O

Introduction of H_2O and small amounts of CO_2 results in the formation of rims of talc and magnesite around the serpentine. The talc and magnesite may then enclose pre-existing serpentine which formed in H_2O-rich environments alone (Winkler, 1974). If the X_{CO2} is not known, mineral parageneses formed in serpentines at higher temperatures do not constitute reliable temperature indicators (Winkler, 1974).

In the samples studied here, serpentine is closely associated with cracks in relict olivine grains and in some instances serpentine completely replaces the olivine grains pseudomorphically. Stringers of secondary magnetite are associated with this serpentine (Figure 5.21). Serpentine has also been found to be present as a rim around sulphide grains, with some of the needles penetrating into the sulphide grain. These serpentine rims have been found to have a talc halo, indicating a change in H_2O-CO_2 conditions (reaction 3).

XRD analyses indicate that amesite is the principal serpentine mineral present in the BGAB Unit. Amesite occurs as a metamorphic mineral in environments rich in Al, and its ideal formula is $(Mg_2Al)(SiAl)O_5(OH)_4$ (Deer et al., 1992). Amesite is chemically similar chlorite, but is structurally similar to serpentine with major substitution of Al for Mg and Si (Deer et al., 1992). According to Deer et al., (1992) there appears to be a complete solid solution range between serpentine and amesite due to this Al substitution. The average serpentine content of the BGAB Unit in this area is 3.7% (based on semi-quantitative XRD analyses).

Semi-quanitative XRD analyses show that detectable serpentine is not present in all samples of the LHZBG and PCR Units. These analyses indicate that lizardite is the principal

serpentine mineral in the LHZBG and PCR Units, with an average content of 3.8 and 5 % respectively.

Van Zyl (1996) indicates that microprobe analyses reveal serpentine from the Uitkomst Complex to have higher FeO and Al_2O_3 values than examples given by Deer et al., (1992) and ascribed it to the presence of chlorite on a sub-microscopically intermixed scale with the serpentine. It was also argued that the elevated levels of FeO may be due to a low oxygen fugacity and of a high SiO_2 activity during serpentinization. The serpentine (senso stricto) encountered in the present study was found only in the PCR Unit. The Al_2O_3 content of the serpentine in UK12 place it closer in composition to chrysotile, while the composition of the serpentine in UK61 place it close to Lizardite and that of UK48 to antigorite. The FeO content in all the samples were also found to be higher than values given by Deer et al., (1992).

The variation in composition of serpentine from the PCR Unit is shown in Table 5.4. The microprobe results and calculated formulas are presented in Appendix 2.

Table 5.4. The average composition of serpentine from the PCR Unit in different boreholes (n = number of grains analysed).

		Al_2O_3	FeO	MgO
UK12	Mean	0.14	2.73	40.94
	Std Dev	0.14	4.67	0.89
UK48	Mean	1.05	4.86	37.95
	Std Dev	0.52	0.49	0.53
UK61	Mean	0.74	6.07	37.12
	Std Dev	1.07	2.24	1.92

The Fe and Al content of the serpentine increases from the NW to the SE of the complex and the Mg content slightly decrease from the NW to the SE.

5.4 Secondary Magnetite

Secondary magnetite is found mainly as stringers in the internal cracks of preserved olivine grains. The secondary magnetite stringers are associated with serpentine in all cases (Figure

5.21). Secondary magnetite is also developed around primary chromite grains, in highly altered matrix material, mostly chlorite-talc assemblages in the PCR unit (Figure 5.22).

The mineral chemisty of the secondary magnetite grains encountered during this investigation, and obtained by microprobe analyses, is presented in Appendix 2. Summarized statistics of these analyses are presented in Table 5.5.

Table 5.5. Secondary magnetite grains from the PCR Unit.

n = 15	SiO_2	TiO_2	Al_2O_3	FeO	MnO	MgO	CaO	Na_2O	K_2O	Cr_2O_3	NiO
mean	0.34	0.04	0.03	87.78	0.03	0.22	0.17	0.01	0.01	0.08	0.05
std dev	0.54	0.03	0.04	1.29	0.02	0.49	0.56	0.01	0.01	0.14	0.05

n = number of analysis.

The alteration magnetite product around sulphide grains was not considered in the statistical evaluation, due to the difference in analytical set-up used as two different sets of standards, one for silicates and the second for sulphides and oxides, were used.
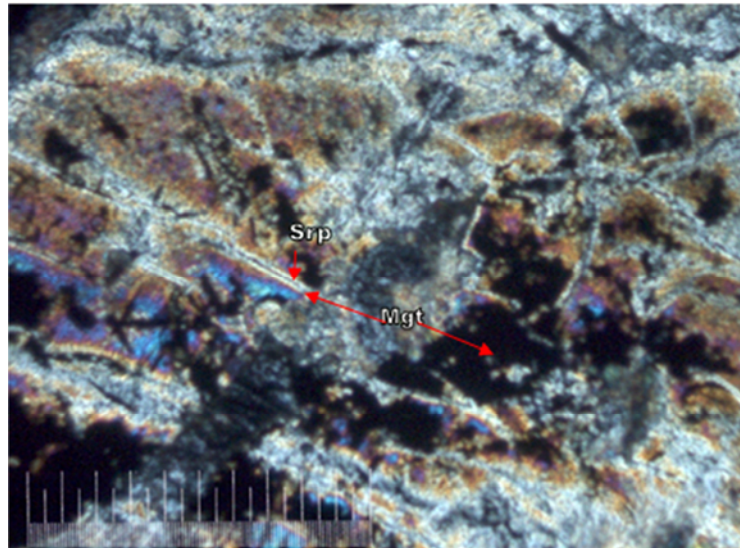
Figure 5.21. Magnetite (mgt) (black) occurring as non-continues stringers between serpentine (srp) visible in the grain on the left and almost completely pseudomorphically replacing olivine near the center of the picture. The picture scale bar is 1000 micron. Taken with cross-polarised light. (Sample: UK48C).

The formation of secondary magnetite stingers in the altered olivine grains are the product of topo-metasomatic mobilization of iron oxide from the olivine. It is suggested that this is the product of late-stage, low temperature hydrous retro-grade metamorphism.

In the case of secondary magnetite after primary magnetite, the association is with talc-dolomite assemblages in the PCR unit. This would suggest that alteration took place in an environment with higher CO_2-partial pressures. In most instances a core of relict chromite is preserved. No secondary magnetite after chromite were observed in the LHZBG Unit.
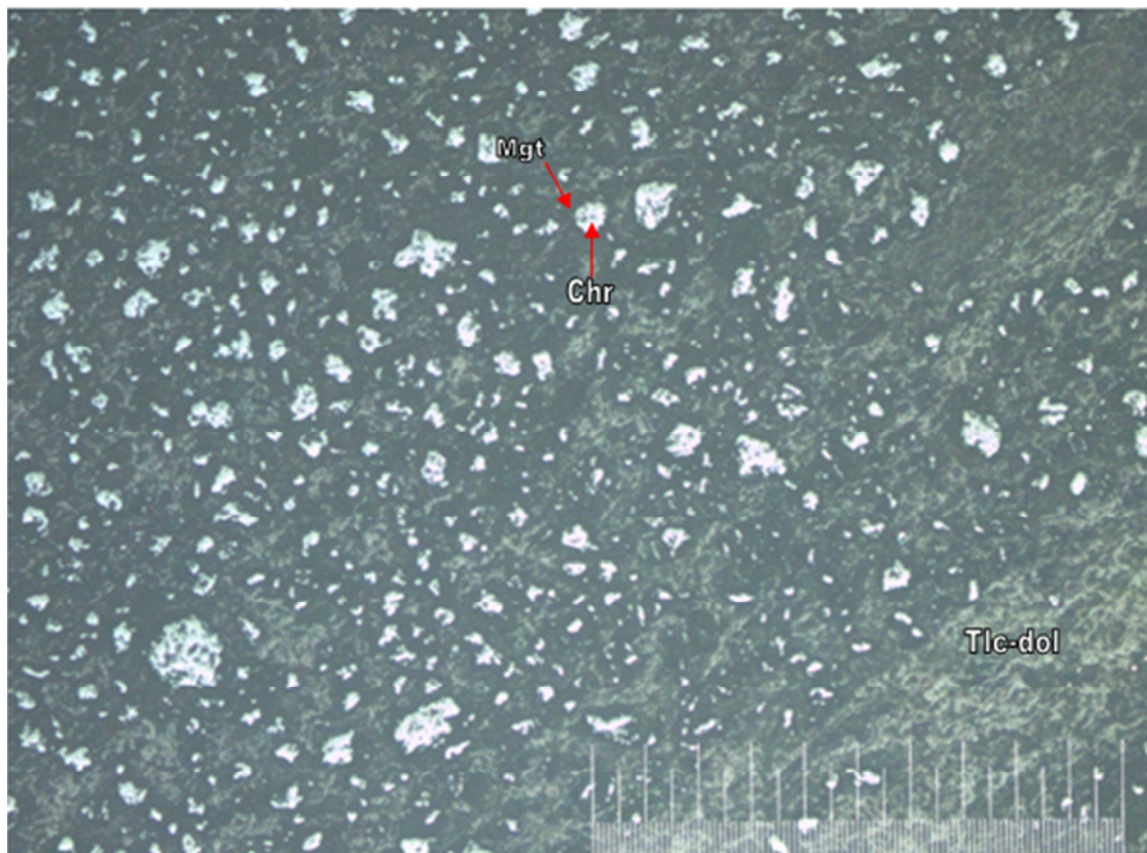
Figure 5.22. Chromite (chr) grains that show the effect of alteration. The chromite (white) grains are partly replaced by magnetite (gray) in a talc-dolomite (tlc-dol) matrix. The picture scale bar is 1000 micron. Taken with reflected light. (Sample; UK61C).

5.5 Talc

Microscopic investigation and microprobe analyses show that talc is closely associated with chlorite, phlogopite and amphiboles (Figure 5.23). Talc is also closely association with relic dolomite and pyrite grains that has the "orange skin-like" appearance (Figure 5.26). In various instances talc was found as part of a halo consisting of serpentine, talc and calcite around sulphide grains.
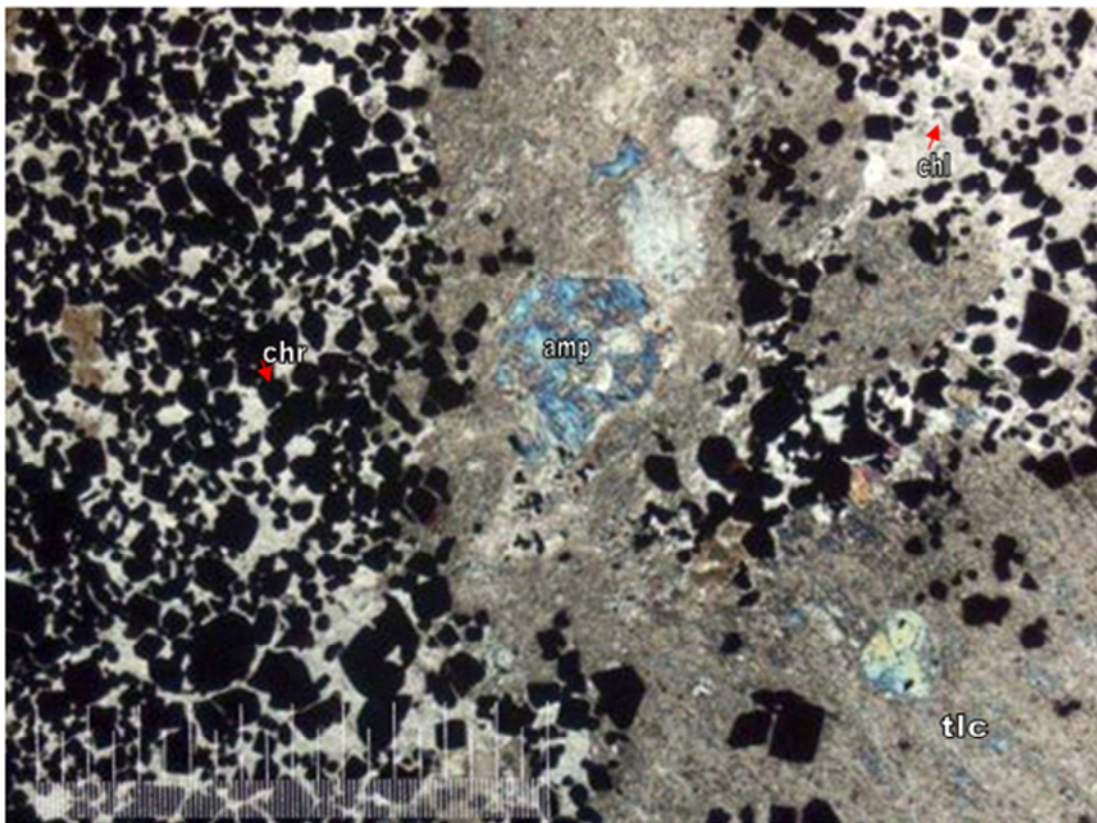
Figure 5.23. The alteration assemblage in the PCR, consisting of talc (tlc) (brown, low birefringence), chlorite (chl) (interstitial to chromite) and amphibole (amp) (high birefringence). Large to small euhedral chromite (chr) grains (black) are concentrated together. The picture scale bar is 1000 micron. Taken with cross-polarised light. (Sample: UK12A).

The occurrence of talc depends on the availability of sufficient Mg in the bulk rock composition. The paragenesis of talc can either be through low grade metamorphism (like hydrothermal alteration) of ultramafic rocks or by contact and regional metamorphism of

siliceous dolomites (Deer et al., 1992). However, the abundance of elements (Al, Ca and K) will favour the formation of minerals such as: Al = Chlorite, Ca = tremolite and K = phlogopite (Deer et al., 1992). In ultra-basic rocks talc is usually accompanied by serpentine and olivine forming lenticular veins (Deer et al., 1992).

Talc commonly forms at the expense of quartz and dolomite (Provoden et al., 2002). Steatization, the process through which serpentine is converted to talc is usually associated with serpentinization. During steatization talc is the main product with chlorite, serpentine and carbonates being accessories. Steatization may occur through the addition of silica and removal of magnesia, or by addition of CO_2.

$$2Mg_3Si_2(OH)_4 + 3CO_2 = Mg_3Si_4O_{10}(OH)_2 + 3MgCO_3 + 3H_2O$$

serpentine   talc   magnesite
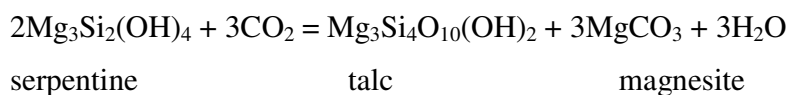
At low temperatures both tremolite and chlorite may be converted to talc by CO_2 metasomatism. Talc is stable in the binary H_2O-CO_2 fluid up to X_{CO_2} of about 0.95. In the presence of magnesite, dolomite and calcite the stability of talc is progressively reduced to more restricted portions of the T-X_{CO_2} diagram.

If talc rather than tremolite is present, it implies that the X_{CO_2} of the original pore fluid was below 0.73 (Provoden et al., 2002). As H_2O is consumed and CO_2 produced, talc formation tends to shift the composition of the pore fluid along towards higher X_{CO_2} levels, this process results in internal buffering (Provoden et al., 2002). The reaction temperature for talc formation however varies significantly as a function of X_{CO_2} (Provoden et al., 2002).

The variation in composition of talc from the PCR and LHZBG Units is given in Table 5.6. The microprobe results and calculated formulas are presented in Appendix 2.

Table 5.6. Variation in composition of talc from the PCR and LHZBG Units (n = number of grains).

PCR		Al_2O_3	FeO	MgO
UK12	Mean	0.67	1.16	31.00
	Std Dev	0.46	0.10	0.54
UK48	Mean	1.08	4.02	29.16
	Std Dev	0.35	0.06	0.42
UK61	Mean	1.22	6.32	27.78
	Std Dev	1.49	1.84	0.95
LHZBG	Mean	0.61	5.70	27.75
UK61	Std Dev	0.74	1.72	1.32

The talc from UK12 in the PCR Unit and UK61 from the LHZBG Unit has a lower Al_2O_3 content relative to UK48 and 61 from the PCR Unit. The FeO content of talc in the PCR Unit intersected by UK12 is lower than in the PCR Unit intersection of UK48 and UK61 and than the talc within the LHZBG Unit intersected by UK61. The MgO content of all of the samples is fairly consistent. As these samples were collected from borehole closer to the inferred margin of the intrusion, the variation may be due to the variable degrees of assimilation.

Semi-quantitative XRD analyses shows that talc is virtually absent from the BGAG, while the talc content in the LHZBG and PCR Units are highly variable. Talc, however always attains its highest content in the PCR Unit.

5.6 Mica

The most common mica encounted during the present investigation is phlogopite. The ideal formula of phlogopite is $KMg_3AlSi_3O_{10}(OH)_2$ (Deer et al., 1992). Deer et al. (1992) noted that phlogopite occurs mainly in ultrabasic igneous rocks and particularly in kimberlites. Phlogopite and biotite are also found in metamorphic rocks that may form under a wide range of temperature and pressure conditions and phlogopite is common in metamorphosed pelites, basic and ultrabasic rocks, siliceous limestone and dolomite (Deer et al., 1992).

During this investigation phlogopite was encountered in the LHZBG and PCR Units. The phlogopite is usually found as part of the association talc-chlorite-phlogopite (Figure 5.24)

and in association with amphibole and carbonate. Phlogopite usually constitutes minor amounts of the investigated rock, but in sample UK32D of the PCR Unit, phlogopite and hornblende are the dominant minerals.
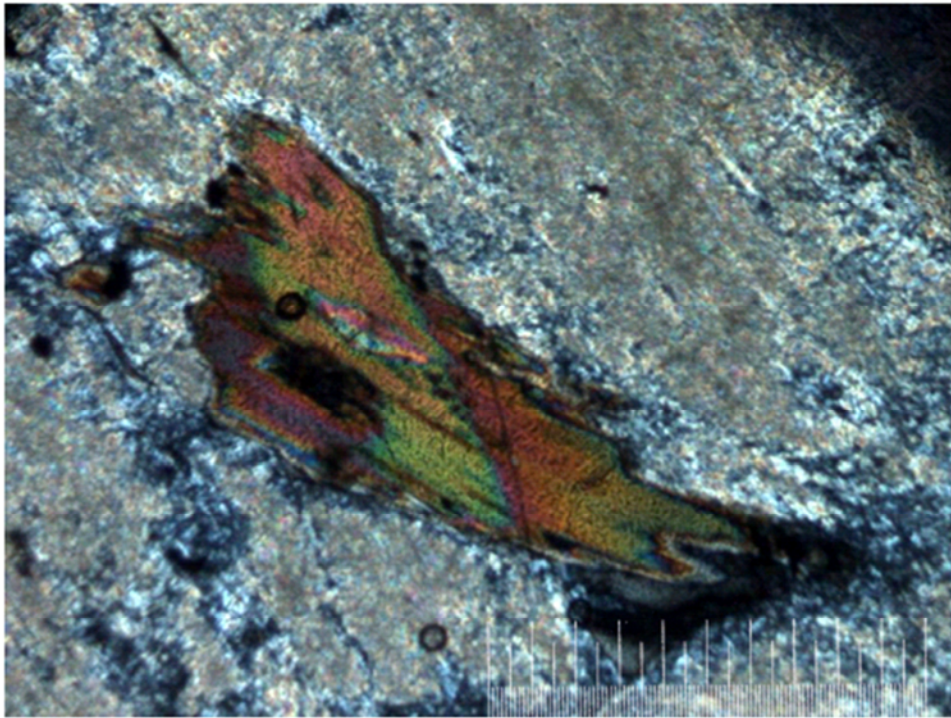
Figure 5.24. Phlogopite (brown) blade associated with talc and chlorite. The picture scale bar is 1000 micron. Taken with cross-polarized light. (Sample: UK48G).

Muscovite is generally present in the xenoliths of the LHZBG Unit. The muscovite occurs along with diopside, actinolite and chlorite in the "contaminated" variety of xenoliths. Muscovite and biotite is also found in the BGAB Unit. The muscovite in xenoliths from the LHZBG and BGAB Units is always associated with chlorite.

Microprobe analyses preformed on samples from the LHZBG and PCR units indicate the micas analysed to be phlogopite. The results are provided in Appendix 2 and summarized in Table 5.7 and 5.8.

Table 5.7. Average composition of phlogopite from the LHZBG Unit.

n=13	TiO_2	Al_2O_3	Cr_2O_3	FeO	MnO	MgO	CaO	Na_2O	K_2O	NiO
Mean	4.09	12.96	0.29	8.35	0.24	23.98	0.14	0.21	5.51	0.08
Std Dev	1.82	1.08	0.16	1.73	0.12	4.71	0.46	0.23	2.96	0.02

n = the number of analyses.

Table 5.8. Average composition of phlogopite from the PCR Unit.

n=21	TiO_2	Al_2O_3	Cr_2O_3	FeO	MnO	MgO	CaO	Na_2O	K_2O	NiO
Mean	3.41	13.40	0.72	6.68	0.04	24.39	0.01	0.14	6.59	0.06
Std Dev	2.66	0.47	0.48	2.95	0.03	5.49	0.03	0.15	2.98	0.03

n = the number of analyses.

Table 5.9. The Fe/Mg ratio of phlogopite from the LHZBG and PCR Units.

Fe/Mg	LHZBG	PCR
Minimum	0.19	0.12
Maximum	0.56	0.79
Average	0.37	0.31
Std Dev	0.15	0.20

No significant difference could be found between the compositions of phlogopite grains from in the LHZBG and PCR Units. The average Fe/Mg ratio of the analysed phlogopite grains (Table 5.12) show the ratio to be slightly higher in the LHZBG Unit compared to the PCR Unit. The calculated mineral formula for phlogopite is presented in Appendix 2.

5.7 Discussion

5.7.1. Growth of retrograde metamorphic mineral crystals

It has been noted that sulphide minerals in the LHZBG and PCR Units have been intergrown with fibrous minerals. It has been determined through optical and microprobe investigation that the majority of these minerals are actinolite-tremolite amphibole (Figure 5.25) and minor amounts of serpentine. The process which may have been responsible for this phenomenon is discussed in this section.
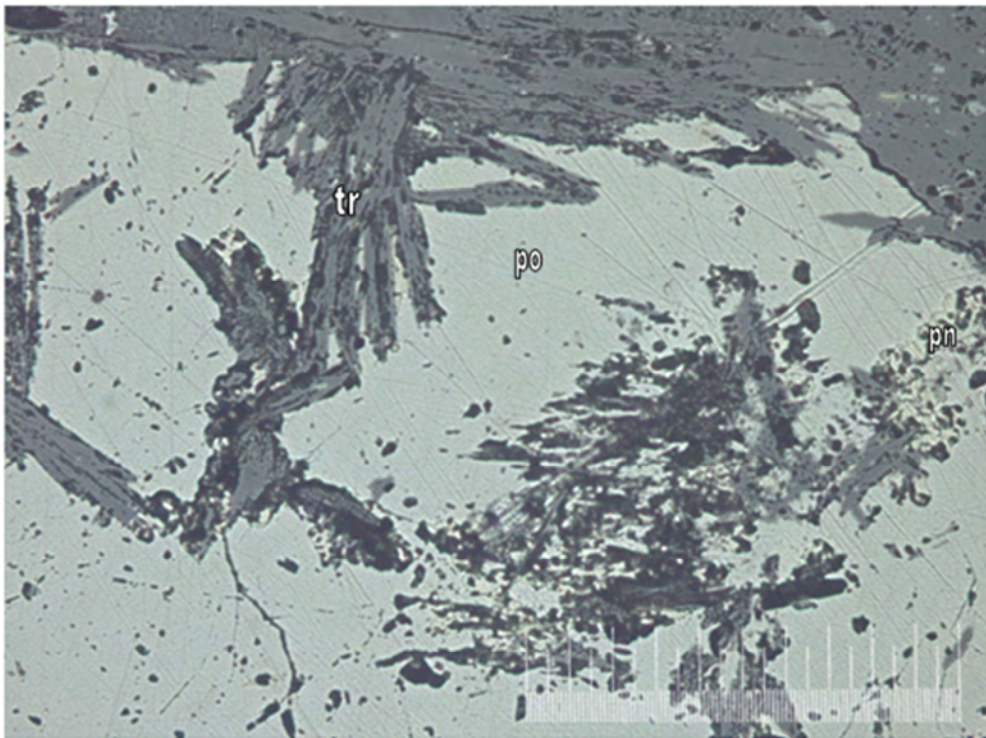
Figure 5.25. Granular pentlandite (pn) (light yellow) associated with tremolite (tr) blades (grey-black) intergrown with a pyrrhotite (po) grain (cream). The lines visible on the suface of the sulphide grain is due to poor polish. The picture scale bar is 1000 micron and it was taken with reflected light. (Sample; UK48L).

Secondary minerals intergrowths with sulphide grains have also been observed in the Stillwater Complex, Montana (Polovina et al., 2004). Here the sulphide grains have intergrowths of clinoziosite and Cl-rich ferropargasite, along with secondary sulphide minerals. This texture has been interpreted as representing a low temperature hydrothermal

event. Since secondary sulphides in association with the amphibole grains are absent in the Uitkomst Complex, a low temperature hydrothermal event, similar to that proposed for the Stillwater Complex is not considered.

Retrograde metamorphism happens where fluid and product minerals are in equilibrium during a mineral-fluid reaction (Ferry, 2000). This reaction will eventually lead to a state where the fluid and mineral products are in equilibrium with the mineral reactants. In the final stage where all of these are in local equilibrium, is assumed to give rise to the retrograde metamorphism, i.e. texture and assemblage. The mineral reactions during retrograde metamorphism will almost always involve carbonation or hydration.

Ferry (2000) indicates that one of the most distinctive features of retrograde metamorphism is the development of pseudomorphs. The pseudomorph will develop by the direct replacement of a reactant in a mineral reaction by one or more of the reaction products. In the case of a pseudomorph the outward crystal shape of the reactant will be preserved in the product. Ferry (2000) notes that pseudomorphs in prograde metamorphic reactions are relatively uncommon. Pseudomorphs are furthermore considered significant by Ferry (2000), as they records a novel phenomenon that results from the coupling of a chemical process, i.e. a mineral reaction, with a mechanical process and the force of crystallization during metamorphism. Force of crystallization is defined by Ferry (2000) as "the force exerted by a growing crystal against its surroundings, if those surroundings have finite yield strength". He therefore suggests that force of crystallization will promote the formation of pseudomorphs during retrograde metamorphism.

It is suggested here that the actinolite-tremolite grains that are intergrown with the sulphide represent retrograde metamorphism of diopside grains. Possible multiple overprints of metamorphic events, coupled with hydrothermal fluids, will hamper any effort to empirically prove this relationship e.g. ratio of Ca:Fe:Mg in both due to possible different mobilization of elements in preserved diopside and actinolite-tremolite. It is however reasonable to suggest this particular primary to secondary mineral relationship. The

mechanism by which the diopside was transformed to actinolite-tremolite and the resultant growth into the spaces between discrete pentlandite and chalcopyrite is discussed in detail in the next section.

5.7.2. Retrograde metamorphism in the Uitkomst Complex

For the Uitkomst Complex, the most likely scenario of retrograde metamorphism envisaged is where the initial contamination of the magma responsible for the formation of the LHZBG and PCR Units caused the super saturation of sulphur resulting in the separation of an MSS phase. These MSS droplets accompanied by hydrous carbonate-rich fluids then accumulated interstitially to the semi-solid mush of silicate minerals. The MSS droplets may originally have been bordered by diopside that formed as an assimilation product in the contaminated magma. The diopside grains would then have been subjected to the effects of a carbonate-rich deuteric fluid that resulted in retrograde metamorphism of the diopside to actinolite-tremolite at the temperature where the MSS itself started crystallizing. The newly grown amphiboles of actinolite-tremolite composition then formed intergrowths with the last phases of the MSS to crystallize, namely the copper-rich phase.

The actinolite-tremolite grains probably suffered less resistance when crystallizing towards the sulphide grains and may have been able to slightly displace pentlandite when it encountered a fracture in the coarse grained pentlandite rims surrounding the main pyrrhotite grain. This would have resulted in the texture observed in Figure 5.6. The actinolite-tremolite grains may also have been able to mobilize some of the chalcopyrite rims surrounding the main pyrrhotite grains. The copper-rich MSS phase may have been relocated during growth of the actinolite-tremolite grains.

Pyrrhotite is not intergrown by the actinolite-tremolite grains. If the pyrrhotite crystallized out first from the MSS, it would have offered more resistance to growth than the non-cohesive coarse grained pentlandite or late phase chalcopyrite exsolution rims. The film on the surface of the growing actinolite-tremolite grain may then have been broken and expelled. The film may, as an alternative, have been retarded to such an extent that it was

not able propagate into the slightly harder pyrrhotite main grain. The well known hydrophobic character of sulphur may also have played a role if it may be assumed that fluid responsible for the retrograde metamorphism was hydrated. There may have been limited dissolution and recrystallization of the sulphide minerals, especially chalcopyrite, in the associated hydrothermal fluid. The effect was however limited and the magmatic disseminated texture were largely retained in the rock. However the possible interaction between the sulphide minerals and the solution that induced the growth of the actinolite-tremolite grains is beyond the scope of this investigation.

5.7.3. Petrogenetic significance of olivine

The lack of zoning in the olivine in addition to the high Ni content and Mg # of the olivine from both the LHZBG (including the wehrlite layers) and PCR Units indicate that the olivine is probably magmatic in origin. In the case of the LHZBG Unit it was not the result/product of metamorphism or metasomatism of siliceous dolomite, although the primary olivine grains probably equilibrated to variable degrees with the surrounding magma.

5.7.4. Petrogenetic significance of pyroxene

It is suggested that the diopside grains from the LHZBG Unit on the farm Slaaihoek 540 - JT, along with those in the wehrlite layers from within the PCR Unit represent clinopyroxene that crystallized from a magma that was less affected by assimilation of dolomitic country rocks. It may be inferred that the diopside in the PCR Unit is derived from a relatively uncontaminated magma, based on the petrographic descriptions and geochemical composition. The diopside grains from the LHZBG Unit on the farm Slaaihoek 540 - JT and from the wehrlite layers, are suggested to represent a mixture of diopside derived from primary magma and magma that assimilated some carbonate wall rocks. The greater similarity between the diopside grains from the LHZBG Unit on the farm Uitkomst 541 - JT and those within calc-silicate xenoliths may also indicate a greater degree of country rock assimilation by the magma in that area where the Complex widens. The grains showing a "transitional" feature between the two types of diopside may represent

clinopyroxene crystallizing from flows that suffered slightly less assimilation of country rock, possibly due to the formation of solidification fronts (discussed later in subsequent sections).

The differences in the composition of enstatite grains from the PCR Unit relative to enstatite grains from the wehrlite layers and LHZBG from the farm Slaaihoek may indicate a difference in either the magma composition between the two units, or a difference in crystallization environment, possibly due to differences in oxygen fugacity during the degassing of assimilating dolomite country rock. The higher Cr-content on the Slaaihoek section relative to the Uitkomst section indicates a more "primitive" composition, supporting the field evidence that intrusion of the conduit was from the northeast to the southwest.

5.7.5. Petrogenetic significance of plagioclase

It is suggested here that the near pristine plagioclase grains found in the LHZBG Unit were either in near equilibrium with the deuteric fluids that affected the surrounding precursor mafic minerals, or only suffered partial dissolution during the time it was exposed to the effects of the deuteric fluid. The resistance of the plagioclase, relative to its surrounding highly altered mineral matrix, is similar to that observed in the fassaite-diopside and phlogopite grains. This would suggest that a slight addition of an element to these minerals, not found in the surrounding matrix minerals, gives it an increased refractory property. In the light of the presence of fassaite-diopside it is suggested here that the accommodation of aluminium in their mineral structure is responsible for this property.The assimilation of Ca also resulted in the crystallization of clinopyroxene at the expense of orhtopyroxene and plagioclase. This is evidence of disruption of the original mafic magmatic composition.

5.7.6. Petrogenetic implications of chromite in the Uitkomst Complex

The formation of chromitite seams in magma chamber is not completely compatible with the formation of chromitite seams in a magma conduit. If it is assumed that a broadening of the magma conduit during the emplacement of further magma may in some respects

influence the physical conditions in a magma chamber, the formation of chromitite seams in the Uitkomst Complex may be explained in part. Two models are presented:

Firstly, it is suggested that the increase in oxygen fugacity in the Uitkomst Complex may be due to the assimilation of dolomite country rock (Gauert et al., 1996; Gauert, 1998) where CO_2 and H_2O may serve as agents for the precipitation of spinel (de Waal, 1977). It is suggested that the chromitite seams in the LHZBG Unit, but especially in the PCR and MCR Units may be due to the influx of fresh pulses of magma. These fresh pulses of primitive magma were then subjected to reaction with increased CO_2- and H_2O-enriched magma, resulting in periodic formation of chromite grains, that sank down to the top of the underlying cumulate mush to form a chromitite seam.

It is suggested here that the MCR Unit may have formed in reaction to the influx of the MHZBG magma over the residual PCR magma. The presence of chromitite seams in the MHZBG Unit may represent influxes of fresh magma into the conduit system, during the formation of the lower part of the unit, before the conduit system came to an end and development of the closed system.

It is further suggested that the more voluminous chromite mineralization in the SE relative to the NW part of the intrusion may have formed due to a sudden increase in oxygen fugacity in the south-eastern part of the Uitkomst Complex, where the intrusion broadens. The increase in oxygen fugacity in the south-eastern part of the intrusion relative to the north-western part of the intrusion may be due to the formation of reaction fronts and the direction of emplacement, namely from the north-west to the south-east. The combination of more rapid flow of magma in the narrow part, coupled with the development of reaction fronts (discussed in later sections) which prevented further degassing of the xenoliths and may have inhibited the settling of large amounts of chromite grains. The broadening of the intrusion on the Uitkomst section, leading to less rapid flow of magma and possible accumulation of CO_2-rich fluids and may have collectively led to an increase in oxygen fugacity as the magma flowed into this area. This resulted in the thicker chromite seams in

the Uitkomst section of the Complex. This decreased flow rate of the magma in the broader part of the Uitkomst Complex in the Uitkomst section, may have contributed to the settling out of the denser chromite crystals especially if a portion of the chromite grains, which settled out in this area, was initially carried in the streaming magma as suspension load.

The second model is based in part on the Stillwater Complex model proposed by Spadler et al. (2005). It is proposed that the magma that formed the PCR Unit was also responsible for the formation of the MHZBG Unit. As the magma stoped through the Rooihoogte sediments into the Timeball Hill shales, the magma began to interact with country rock richer in silica. This may have led to an increase in the amount of chromite crystallizing out of the system. As the conduit broadened, due to increased stoping of the shale country rock and a broadening of the conduit in the study area, the ability of the magma to suspend the chromitite load decreased. This would result in the formation of a thick layer of chromite at the base of the cumulate mush, represented by the PCR Unit. The result was the formation of the MCR layer. The subsequent formation of chromite stringers may indicate further stoping of the shales by the intruding magma, causing assimilation of the country rock, and thus formation of chromite grains, which would settle out on top of the cumulate mush present during that stage of development of the MHZBG Unit.

The absorption of CO_2-rich fluids in the Uitkomst magma may have been very limited. Most of the CO_2-rich fluids might have migrated upwards, and being trapped by the Massive Chromitite layer which served as a permeability barrier. These fluids would have been responsible for most of the alteration of the primary magmatic silicate minerals of the PCR Unit to a talc-chlorite-carbonate assemblage. Where the Massive Chromitite is not developed, especially in the NW, the CO_2-rich fluid was still able to stream or steam out of the system, resulting in the formation of the LrPRD Subunit. The chromite seams found in the LrPRD Subunit might be due to increased oxygen fugacity, caused by the influx of CO_2-rich fluids into the MHZBG Unit.

5.7.7. Petrogenetic significance of calcite

It is suggested here that the calcite encountered in the hybrid rocks represent the calcite melt forced out of the xenoliths, when the xenoliths suffered loss of volume and reacted with the magma. The calcite grains may have formed where the addition of Ca was not immediately accommodated by the magma or due to local cooling of a CO_2-rich fluid.

5.7.8. Petrogenetic significance of dolomite

Dolomite encountered in this investigation either forms part of the assemblage dolomite-talc-phlogopite or relic grains. It is encountered in minor amounts in both the PCR and LHZBG Units. The higher content of dolomite in some samples closer to the edge of the intrusion suggests that it may be derived from the dolomite country rock protruding into the Uitkomst Complex. An excess of dolomite that did not interact with the intruding magma appears to have survived the alteration processes affecting the Uitkomst Complex.

5.7.8 Petrogenetic implications of amphibole composition

It has been determined that the amphiboles were derived from a variety of metamorphic and or retrograde conditions. It is suggested that the "high-grade" amphiboles (e.g. edenite and magnesiohastingsite) may have crystallized out of trapped magmatic fluids that became enriched in volatiles. These amphiboles would thus have formed in a CO_2-rich environment that was not affected, or insignificantly affected by assimilation of the country rocks. These amphiboles may represent a "first generation" amphibole where it is found in the LHZBG Unit. In the PCR it may represent a remnant of the amphiboles associated with the original ultramafic rock, or as a product of metasomatic alteration of these ultramafic rocks.

The "lower-grade" amphiboles (e.g. tremolite and actinolite) are interpreted as being the result of retrograde metamorphism and metasomatic replacement of the precursor ultramafic minerals and hybrid rocks in an H_2O-enriched environment, where there might have been more extensive assimilation of country rock. The occurrence of actinolite-tremolite may be interpreted as resulting from retrograde metamorphism, as the actinolite-tremolite assemblage occur as pseudomorphs, and pseudomorphs are only present in retrograde metamorphic rocks (Ferry, 2000). These amphiboles may represent a "second generation"

of amphibole in especially the LHZBG Unit, where the "first generation" amphiboles or precursor clinopyroxene (diopside) may have been affected by hydrothermal alteration at lower temperatures. It may also represent the interaction product of an ultramafic magma with siliceous dolomite country rock in a H_2O-rich environment, especially where there is a close spatial association with calc-silicate xenoliths.

Sulphide mineralization is commonly associated with amphiboles of hornblende or magnesio-gedrite composition. Where the sulphide minerals are associated with these amphiboles, the contact between them tend to be sharp. Some sulphide grains are intergrown by amphiboles of a tremolite-actinolite composition. These amphiboles tend to only be intergrown with the chalcopyrite and pentlandite portions of the grain and not the main pyrrhotite grain. The origin of actinolite-tremolite is discussed in the following section. If it is accepted that the crystallization of the amphiboles requires an abundance of H_2O it may be inferred that the textural setting of the disseminated sulphide blebs are also associated with the same hydrous environment, especially the Cu-rich phase of the mono sulphide solid solution.

5.7.9. Petrogenetic significance of chlorite

The chlorite varieties occurring in the LHZBG Unit and in xenoliths from this unit have similar compositions and may reflect the same direct environment in which the hydrothermal event, responsible for the formation of the chlorite, took place. The Al and Fe-contents suggest a skarn as source, when compared to values given by Deer et al., (1992). In contrast, chlorite from the PCR contains less Fe and Mn but more Mg. This composition reinforces the fact that the alteration mineral assemblages in the PCR formed from an ultramafic igneous precursor.

The fact that chlorite occurs as pockets in amphibole may also indicate that the fluid responsible for the formation of chlorite passed through the rock at a later stage and possibly at a lower temperature than the fluid responsible for the formation of the amphibole. The fact that chlorite is not intergrown with the sulphide minerals also supports this hypothesis.

The close association of chlorite with especially talc and dolomite may indicate that the fluid was still carbonate-rich and deuteric.

It is also proposed here that at least two chlorite events affected the Uitkomst Complex. The first event is recorded by the chamosite after magmatic magnetite. The unusual preservation of the chamosite after magmatic magnetite was discussed earlier. It is considered unlikely that other remnants from this event would be persevered. The second event is recorded by the chlorite occurrence discussed in this section.

5.7.10. The petrogenetic significance of serpentine

Sakar, Ripley and Li, (2005) used oxygen and hydrogen isotopic analyses of samples from the Uitkomst Complex to determine that the fluids involved in the serpentinization process may have been of meteoric origin, but that the isotopic exchange occurred over a long period, at relatively low water/rock ratios. The evolved meteoric water stays in the country rock before mixing with later generated magmatic or hydrothermal water along the fluid path.

This implies that the hydrothermal alteration process, reflected in the samples collected, is responsible for the formation of the alteration assemblage minerals. Amongst others, the serpentine occurrences may have resulted from fluid derived by assimilation from the fluids present in the dolomite at the time of the intrusion. The assimilation of these fluids, rather than circulation of surface meteoric water, may be assumed to have been responsible for the formation of the serpentine in the fresh samples collected well below the limit of weathering and the current water table. The implication is that the initial fluid that resulted in the first alteration event may have been enriched in water derived from the assimilated dolomite country rock.

5.7.11 Petrogenetic significance of talc

It is suggested that the talc found in the PCR Unit represents the low grade retrograde hydrothermal alteration of the ultramafic rock by a carbonate-rich deuteric fluid. As talc

always attain it highest content in the PCR Unit, it may be inferred that the effects of this carbonate-rich deuteric fluid was more pervasive in this unit.

The occurrence of talc in the LHZBG Unit may also suggest the presence of a carbonate-rich deuteric fluid affecting the ultramafic rocks here, but that it was not as pervasive as in the PCR Unit. An alternative interpretation is that the origin of talc in the LHZBG Unit is related to contact metamorphism of the dolomitic country rocks rather than secondary alteration. This interpretation is supported by the occurrence of talc associated with dolomite and pyrite with an "orange skin" texture.
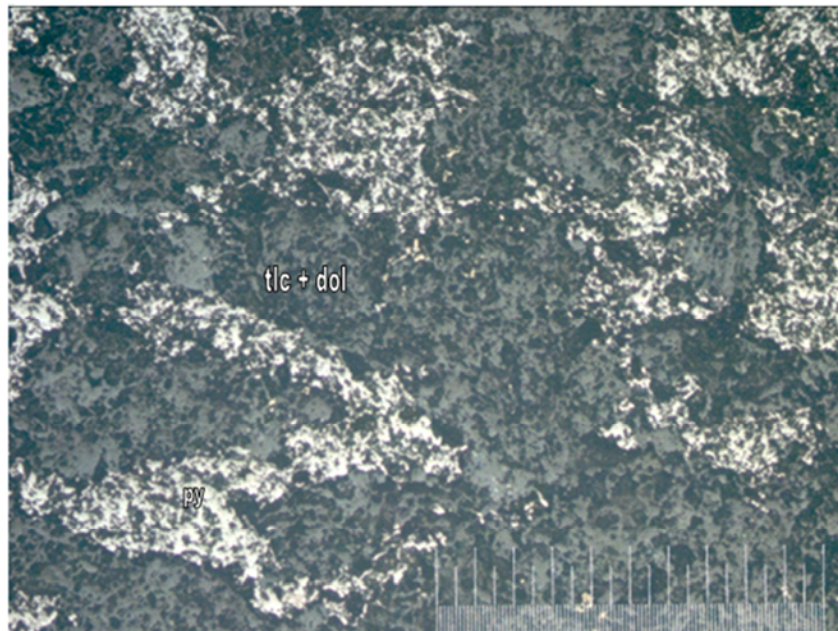
Figure 3.60. Anhedral pyrite (py) exhibiting a pitted "orange-skin" texture. The pyrite is found in a matrix of talc (tlc) and dolomite (dol). The picture scale bar is 1000 micron and it was taken with reflected light. (Sample; UK61F).

5.7.12 Petrogenetic significance of phlogopite and mica

Phlogopite and the occurrence of mica in the Uitkomst Complex is mainly associated with calc-silicate xenoliths and talc-dolomite assemblages. This would suggest that the mica and especially phlogopite minerals are the products of metamorphism of dolomitic country rock. This is demonstrated by the similar composition of the grains in the LHZBG and PCR. The

preservation of these grains and lack of over-printing, may as the case with plagioclase be, that the Al-content makes it more resistant to the effects retrograde metamorphism.

5.7.13 Petrogenetic significance of secondary magnetite

The stringers of secondary magnetite associated with olivine and serpentine would indicated the effect of a late-stage hydrous metasomatic event that affected both the LHZBG and PCR units. This event may be the same event that resulted in the formation of chlorite pockets in the these units. The secondary magnetite rims associated with chromitite grains in the PCR in the dolomite-talc assemblages may indicated that the fluid that led to the complete replacement of the precursor magmatic minerals affected the chromite grains, but did not completely replace it. All of these grains still have a chromite centre.

CHAPTER 6 - REACTION OF THE INTRUSIVE ROCKS WITH THE COUNTRY ROCKS AND WITH XENOLITHS

6.1 Previous work on xenoliths

In the Uitkomst Complex the dominant xenolith type is a calc-silicate rock of variable composition derived from the Malmani Subgroup (Gomwe, 2002; van Zyl, 1996; Gauert, 1996; de Waal et al. (2001), Maier et al., 2004). The contact aureole of the Uitkomst Complex extends 50 to 100 m from the contact into the country rock. Within the aureole, the Malmani Dolomite has been transformed to calc-silicate hornfels grading to talc-tremolite-bearing carbonate rock (Gauert et al., 1996; Gomwe, 2002). The calc-silicate xenoliths are composed mainly of diopside, epidote, calcite and tremolite (Gomwe, 2002). As indicated before, the calc-silicate rocks seem to have suffered very little or no rotation, with the preserved internal layering being sub-parallel to the igneous layering (Gomwe, 2002). The pelitic roof material of the complex underwent medium- to high-grade metamorphism extending 10 to 50 meters above the Complex, represented by a rim of corundum-andalusite-hornfels (Gauert et al., 1996; Hornsey, 1999; Gomwe, 2002). The interaction between the xenoliths and the LHZBG magma and inferred influence on mineralization within this unit was the subject of a dissertation by Hulley (2005).

Considering other intrusions of a similar nature, the Platreef is the most relevant. Gain and Mostert (1982) found that the main mineral assemblages of the xenoliths in the Platreef consist of variable amounts of fosterite, diopside and monticellite. Retrograde metamorphism of these xenoliths led to the alteration of the original minerals assemblage in the following manner: fosterite alters to serpentine, monticellite alters to hydrogrossular, talc and serpentine and diopside alter to hydrogrossular, talc and tremolite. Brucite was found to be the most common alteration product of dolomite xenoliths (Gain and Mostert, 1982). The contacts between the xenoliths and the Platreef rocks are rarely sharp, but pegmatoidal (Gain and Mostert, 1982).

6.2 Xenoliths investigated during the current investigation

There are two types of calc-silicate xenoliths present in the core samples investigated from the Uitkomst Complex. The first type is "clean" xenoliths (Figure 6.6) with a white appearance, usually displaying a sharp contact relationship with the host pyroxenite. White xenoliths usually appear "cleaner" due to the expulsion of contaminants such as carbon during thermal metamorphism (Park and MacDiarmid, 1975). A petrological investigation of these xenoliths reveals that they consist mainly of clinopyroxene and calcite (Figure 6.1). Zones of larger clinopyroxenes (diopside) that show signs of uralitization occur near the contact between the xenolith and the pyroxenite, while smaller subhedral crystals of clinopyroxene and calcite showing no signs of alteration (Figure 6.2 and 6.3) are in close contact with these larger clinopyroxene grains, and occur towards the centre of the xenolith. It has been determined by Tilley and Harwood (1931) that by the addition of CO_2 during breakdown of carbonate rocks assists in decreasing the viscosity of the melt and this allows free growth of comparatively large crystals. Similar decarbonation reactions are probably responsible for the development of the larger diopside crystals near the xenolith-pyroxite contact, relative to the interior of the xenolith. Minor amounts (<10 %) of blebby pyrite are present in these xenoliths (Figure 6.2). These pyrite grains generally occur along the preserved bedding of the dolomite protolith (Figure 6.9). The pyrite grains are interstitial to the clinopyroxene grains and show no alteration features.
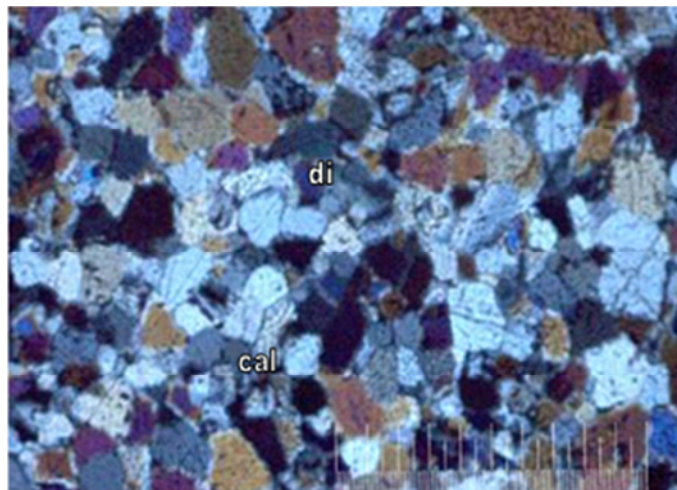
Figure 6.1. The"clean xenolith" consist mainly of small diopside (di) (high birefringence minerals) and calcite (cal) (blue-grey low birefringence minerals) grains. The picture scale bar is 1000 micron and the image was taken with cross-polarized light. (Sample CS21).
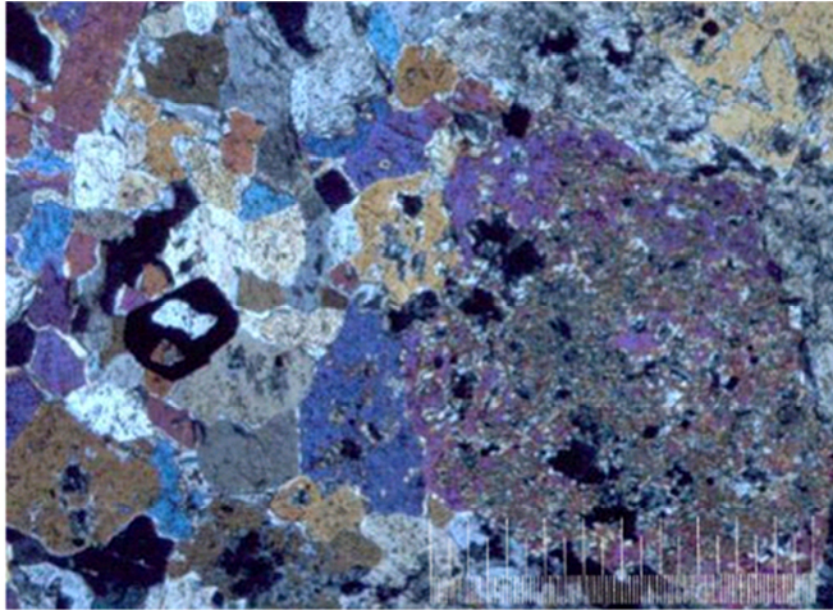
Figure. 6.2. Photomicrograph showing large clinopyroxene (high birefringence) grains that has been uralitized (right side of picture) in contact with smaller, unaltered clinopyroxene grains (left side of picture). There is no compositional difference between the two textures. Also present are carbonate minerals (low birefringence) and sulphide (pyrite) grains (black). The picture scale bar is 1000 micron and the image was taken with cross-polarised light. (Sample UK44G).
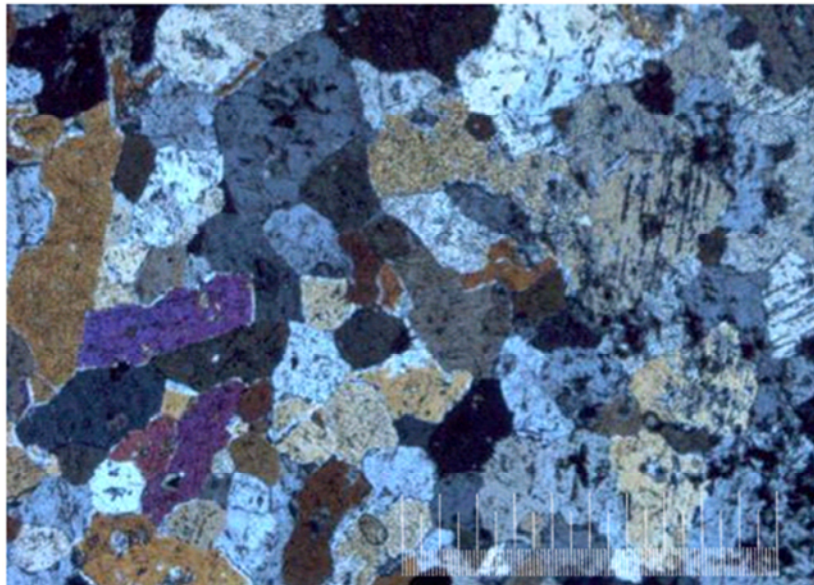
Figure. 6.3. Photomicrograph showing slightly uralitized clinopyroxene (high birefringence) and carbonate (low birefringence) grains. The picture scale bar is 1000 micron and the image was taken with cross-polarized light. (Sample CS21).

The second variety of xenoliths is described as "contaminated" xenoliths. These xenoliths have a grey colour and contain apophyses of pyroxenite running through them (Figure 6.7). The xenoliths have slightly larger amounts (> 10%) of pyrite present. They consist largely of altered pyroxene, amphiboles and muscovite and phlogopite (Fig.6.4 and 6.5).
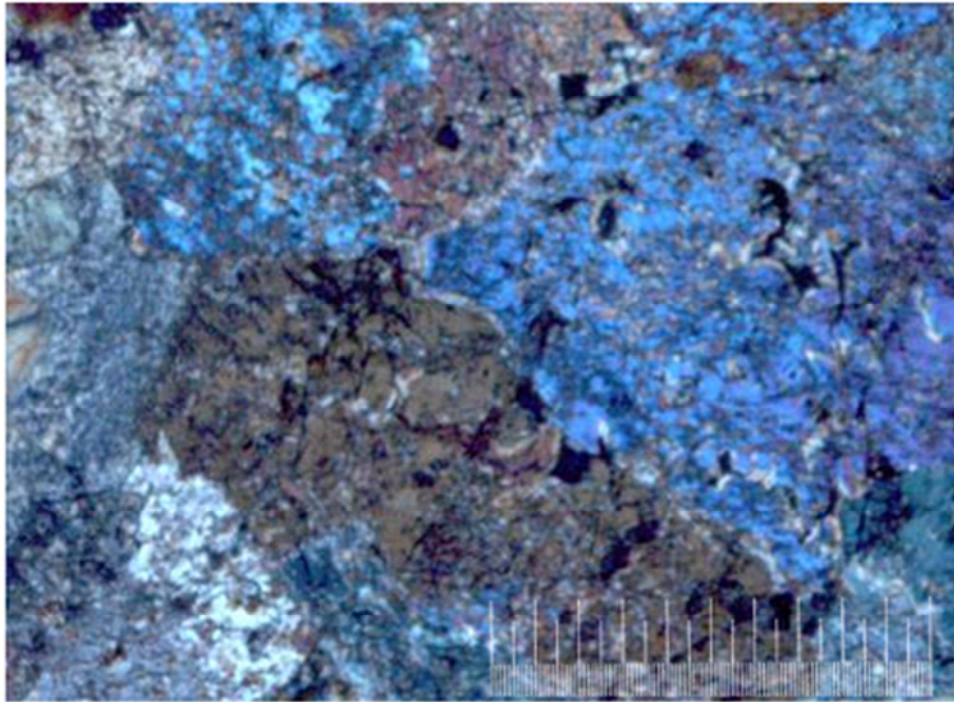
Figure 6.4 Large grains of uralized clinopyroxene in a "contaminated" xenolith. The picture scale bar is 1000 micron and the image was taken with cross-polarized light. (Sample UK3N).

Figure 6.5. A highly altered "contaminated" xenolith. Pseudomorphous serpentine (fiberous white), magnetite (black stingers) after olivine and amphibole, chlorite (high to intermediate birefringence) after pyroxene respectively. Some phlogopite (phl) (brown mineral, top right) are also present in this section. The picture scale bar is 1000 micron and the image was taken with cross-polarised light. (Sample CS4).

The xenoliths display a variety of textural relationships at their contacts with the magmatic material. The first relationship is formed by a very fine-grained zone, dark in colour and consisting of highly altered minerals (Figure 6.6). This is associated with the "clean" xenoliths. A zone of what appears to be primary phase minerals forms the second type of contact relationship, consisting mainly of pyroxene grains inside the xenolith which are, altered to actinolite (Figure 6.7). Some muscovite, phlogopite, pyrite and pyrrhotite are also present. The third contact relationship comprises pegmatoidal material, consisting of coarse large pyroxene (diopside) grains and calcite, with interstitial coarse grains of sulphide minerals (Figure 6.8). The massive sulphide bordering the pegmatoidal material consists mainly of pyrrhotite with minor chalcopyrite and pentlandite with small Platinum Group Mineral (PGM) grains. This is in direct contrast to the sulphides inside the xenolith that consist of pyrite only. There appears to be no difference in the development or abundance

of pegmatoidal material at the bottom or top of the xenoliths, as determined during the current and previous investigations (Steenkamp, 2004).

Figure 6.6. Sharp contact between a clean xenolith and pyroxenite from the LHZBG in a quartered core sample. The contact is fine grained, dark and consists of a highly altered material. Where a "clean" xenolith can be seen on the right and pegmatiodal pyroxenite to the left. (Sample CS21).

Figure 6.7. A vein of pyroxenite penetrating a xenolith. On the contact a layer of uralized pyroxenes are developed. Disseminated sulphides may also be seen close to the contact. (Sample CS21).

Figure 6.8 An example of a pegmatiodal contact. The xenolith was situated to the left side (not sampled) of the sample. Large uralized clinopyroxene grains occur on the contact and extend away from the contact. Massive sulphides surround them. A large white calcite grain is also present. The pegmatoidal material grades into wehrlite on the far right hand side of the sample. (Sample CS13).

Figure 6.9. Blebby pyrite mineralization in a xenolith. The pyrite mineralization occurs along the preserved original bedding of the dolomite protolith. (Samples UK3R top and UK3S bottom).

6.3 Melting rate of xenoliths

It is important to consider the melting rate of xenoliths in magma to explain some of the inferred textural observations in the Uitkomst Complex. The melting of crustal xenoliths is rapid compared to other magmatic processes. The rate is however controlled by the magmatic temperature, initial xenolith temperature, melting temperature and melt viscosity and the composition of the xenolith. This provides an efficient mechanism for producing

changes in the compositional as well as thermal properties of the intruding magma. Cooling of magma in the thermal boundary layer adjacent to the xenolith is relatively restricted, thus any induced crystallization will be limited and unlikely to have an appreciable direct influence on the dynamics of the magma's thermal convection around the xenolith. The thickness of the mobile mush layer around the xenolith is predicted to be typically only a few centimetres. The melting rate of continental crust xenoliths has been determined McLeod, Stephen and Spark, (1998) to be about 2mm/hr, based on experiments done involving stationary and sinking wax balls in hot liquid.

Partial melting of non-eutectic compositions may produce a layer of crystal melt mush at the contact with the xenolith. Such processes may have given rise to the pegmatoidal material surrounding some of the xenoliths in the LHZBG Unit.

It should however be noted at this point that most work pertaining to skarn formation have been based on the interaction between felsic (granitic) intrusion and dolomitic country rocks. Dolomite only melts at very high temperatures, but undergoes a series of decarbonation reactions at lower temperatures (Bowen, 1940). Care should be taken to distinguish the difference in interaction and in product between a volatile-rich felsic- and volatile-poor mafic magma. The effects of assimilation and the collapse of dolomitic xenoliths in a mafic magmatic environment is described in locations such as Ioko-Dovyren intrusion in Russia (Wenzel et al., 2004 and Wenzel et al., 2005) and at the Panzhihua deposit in China (Ganino et al. 2008).

It was determined by Glazner (2007) that the assimilation of wall rock by an intruding mafic magma would be limited due to the energy required. Glazner suggest that the process of disaggregation without melting will result in greater assimilation, without requiring as much energy. The experimental data (Glazner, 2007) suggest that during disaggregation, the assimilation of cool xenoliths requires significant crystallization of the host magma. Larger crystallization is observed during disaggregation, relative to a fully reacted case. This is suggested (Glazner, 2007) to be as a result of partial crystallization of the host magma in

order to heat the xenolith, without xenolithic crystals being resorbed. The amount of crystallization by the host magma becomes important because it influences the ability of the host magma to incorporate the xenolith material and its own ability to rise. Crystallization above 50% also significantly changes the viscosity of the magma by several orders of magnitude, making the magma semi-rigid. At this level of crystallization any segregation of magmatic liquid would be very limited. It is also suggested by Glazner (2007) that addition of new magma is required to counter the effect of heat loss that will otherwise create an upper boundary for the assimilation of xenoliths.

A semi-quantitative estimation may be made based on the information contained in the borehole logs of to the period during which the magma was exposed to the effect of assimilation of dolomite. This is done by measuring the vertical thickness of the host rock between the preserved xenolith inclusions in the LHZBG Unit. The thickness of these intervals is then related to the calculated assimilation time and a period of static exposure is calculated. Assumptions for these calculations are:

1) That dolomites were present up to the level represented by the current top contact of the LHZBG Unit.

2) That all of the dolomite country rock was either assimilated or removed from the system.

3) Accepting that thin pyroxenite layers within xenoliths were not included as separate layers in the logs.

4) Static system is assumed, whereas in reality the magma was probably flowing through a conduit.

The calculated values are given in Table 6.1. As could be expected the top of the LHZBG Unit was exposed to the longest period of interaction and assimilation of dolomite by the intruding magma. The calculated periods for the succession lower in the unit are highly variable with height and spatial distribution.

Table 6.1. The thickness of the area between xenoliths is indicated under the borehole number from the top to the base of the LHZBG Unit and the hours (calculated for 2mm/hour) indicated in bold.

UK3	Hours	UK12	Hours	UK20	Hours	UK32	Hours	UK39	Hours
1.8	**90**	6.64	**332**	19.41	**970.5**	7.79	**389.5**	25.06	**1253**
3.59	**179.5**	0.43	**21.5**	1.36	**68**	0.36	**18**	1.12	**56**
0.55	**27.5**	1.44	**72**	3.43	**171.5**	3.12	**156**	3.97	**198.5**
2.44	**122**	0.72	**36**	0.76	**38**	0.26	**13**	1.49	**74.5**
3.05	**152.5**	2.66	**133**	3.92	**196**	0.41	**20.5**	4.55	**227.5**
4.08	**204**					0.91	**45.5**	0.21	**10.5**
1.38	**69**					1.31	**65.5**	2.01	**100.5**
1.23	**61.5**					0.2	**10**	0.66	**33**
0.64	**32**					23.73	**1186.5**		
2.04	**102**					6.38	**319**		
2.84	**142**								
1.52	**76**								
0.97	**48.5**								

Table 6.1. Cont.

UK40	Hours	UK43	Hours	UK44	Hours	UK55	Hours	UK57	Hours
13.65	**682.5**	6.97	**348.5**	7.02	**351**	6.09	**304.5**	0.57	**28.5**
0.29	**14.5**	0.17	**8.5**	1.15	**57.5**	6.08	**304**	1.31	**65.5**
4.32	**216**	30.41	**1520.5**	0.66	**33**	0.23	**11.5**	2.62	**131**
0.16	**8**	0.28	**14**	0.7	**35**	0.6	**30**	0.2	**10**
0.17	**8.5**	3.43	**171.5**	0.52	**26**	4.34	**217**	2.26	**113**
6.61	**330.5**	0.44	**22**	0.54	**27**	3.2	**160**	0.53	**26.5**
0.99	**49.5**	7.95	**397.5**	0.19	**9.5**	0.17	**8.5**	1.23	**61.5**
		0.17	**8.5**	0.79	**39.5**	2.09	**104.5**	0.55	**27.5**
		3.88	**194**	0.22	**11**	9.36	**468**	6.77	**338.5**
				5.32	**266**			1.11	**55.5**
				0.26	**13**			1.86	**93**
				0.28	**14**			0.33	**16.5**
				4.82	**241**			0.97	**48.5**
				2.93	**146.5**			2.43	**121.5**
				2.88	**144**			5.29	**264.5**

Table 6.1. Cont.

UK60	Hours	UK61	Hours	UK 63	Hours	UK 65	Hours	UK68	Hours
17.73	**886.5**	9.31	**465.5**	24.03	**1201.5**	2.27	**113.5**	8.44	**422**
2.94	**147**	2.99	**149.5**	7.86	**393**	11.48	**574**	0.06	**3**
0.45	**22.5**	4	**200**	2.19	**109.5**			15.27	**763.5**
1.65	**82.5**	0.54	**27**						
2.78	**139**	28.64	**1432**						
2.94	**147**								
0.61	**30.5**								
0.44	**22**								
6.44	**322**								
1.34	**67**								

6.4. Distribution of Xenoliths and their Effect on the Development of the Uitkomst Complex

The distribution of boreholes is indicated by Figure 6.10. The true thickness of the LHZBG Unit and the percentage of xenoliths in the LHZBG Unit for certain sections were calculated. The true thickness of the BGAB was also calculated. The results are presented in figure 6.11 to figure 6.13.
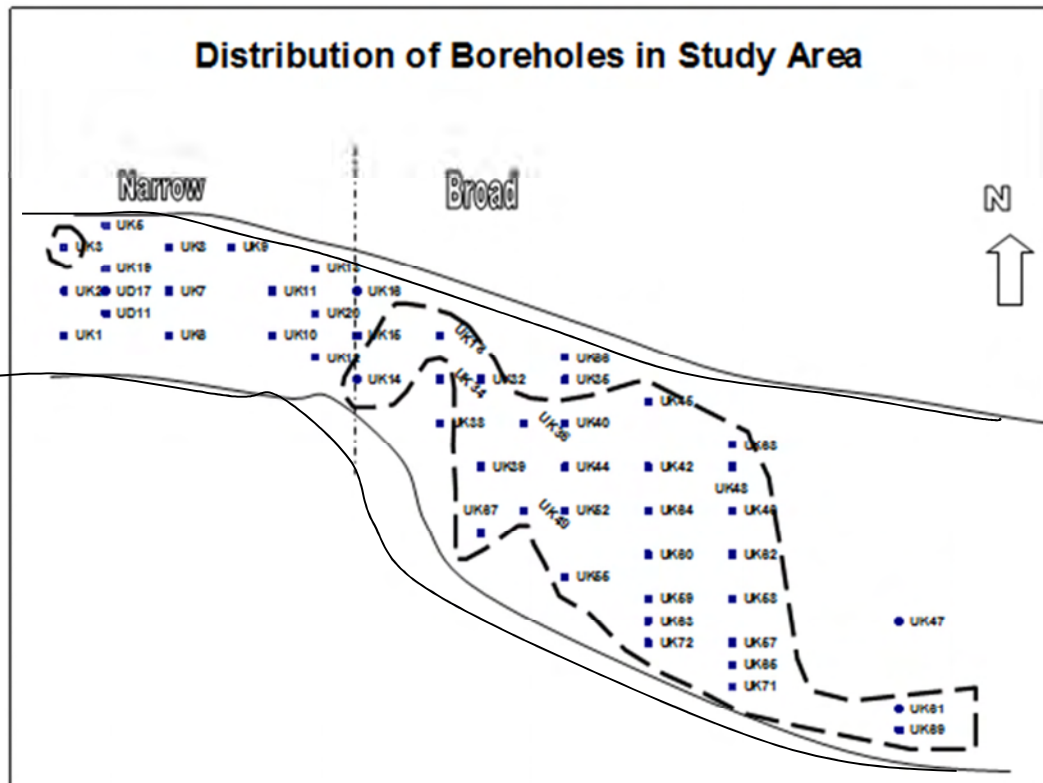
Figure 6.10. The position of boreholes in the study area. The "talc-rich" zone is indicated by the dashed line (After L. Bradford, 1996). The inferred margins of the Uitkomst Complex are indicated by the solid black lines. To the left of the stripe-dash line is the narrow part of the intrusion and to the right the broad part. The base of the picture represents approximately 2 kilometers.

First the percentage of xenoliths in the LHZBG Unit in the study area is compared to the thickness of the LHZBG and BGAB Units in the study area by looking at selected sections (north-south) through the Complex. These calculations are based on the borehole logs prepared by the AVMIN geologists during the feasibility programme during the 1990s. Secondly, these will be evaluated in terms of the distribution of the "talc-rich" zone located in the study area.
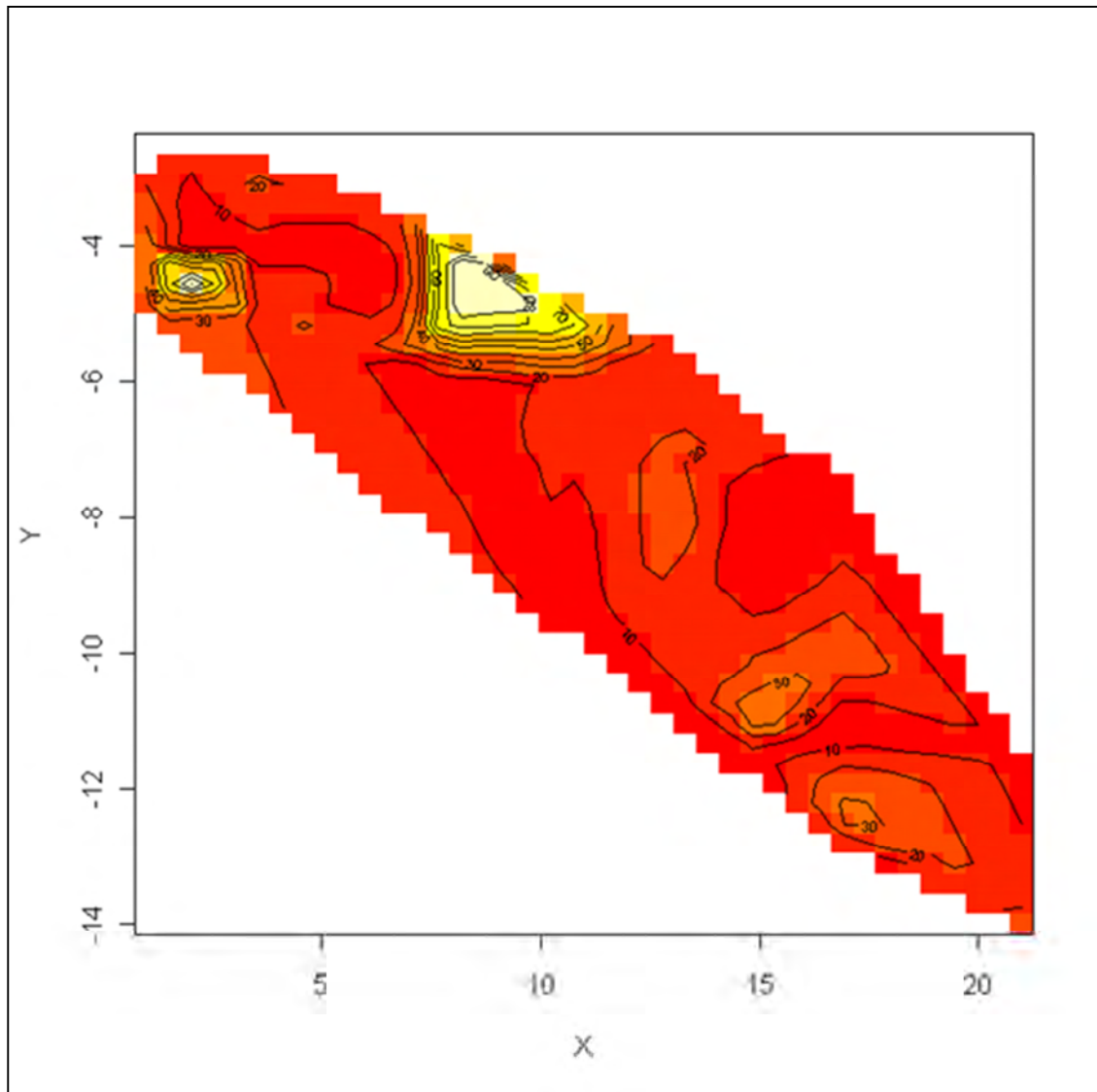
Figure 6.11. Contour map indicating the percentage distribution xenoliths in the study area of the Complex. The graph was constructed using an interpolation routine included as part of the "AKIMA" package for the functional language "R" and based on Akima (1978). A false X- and Y-coordinate system is applied.

The percentage of xenoliths (figure 6.11), the true thickness of the LHZBG Unit (figure 6.12) and of the BGAB Unit (figure 6.13) is considered in this discussion. The true thickness refers to the thickness of the unit after the thickness of post-Uitkomst diabase intrusions has been subtracted. The figures were constructed utilizing the "AKIMA"

package and show contour intervals of ten. A false X- and Y-coordinate system was used to construct the graphs.
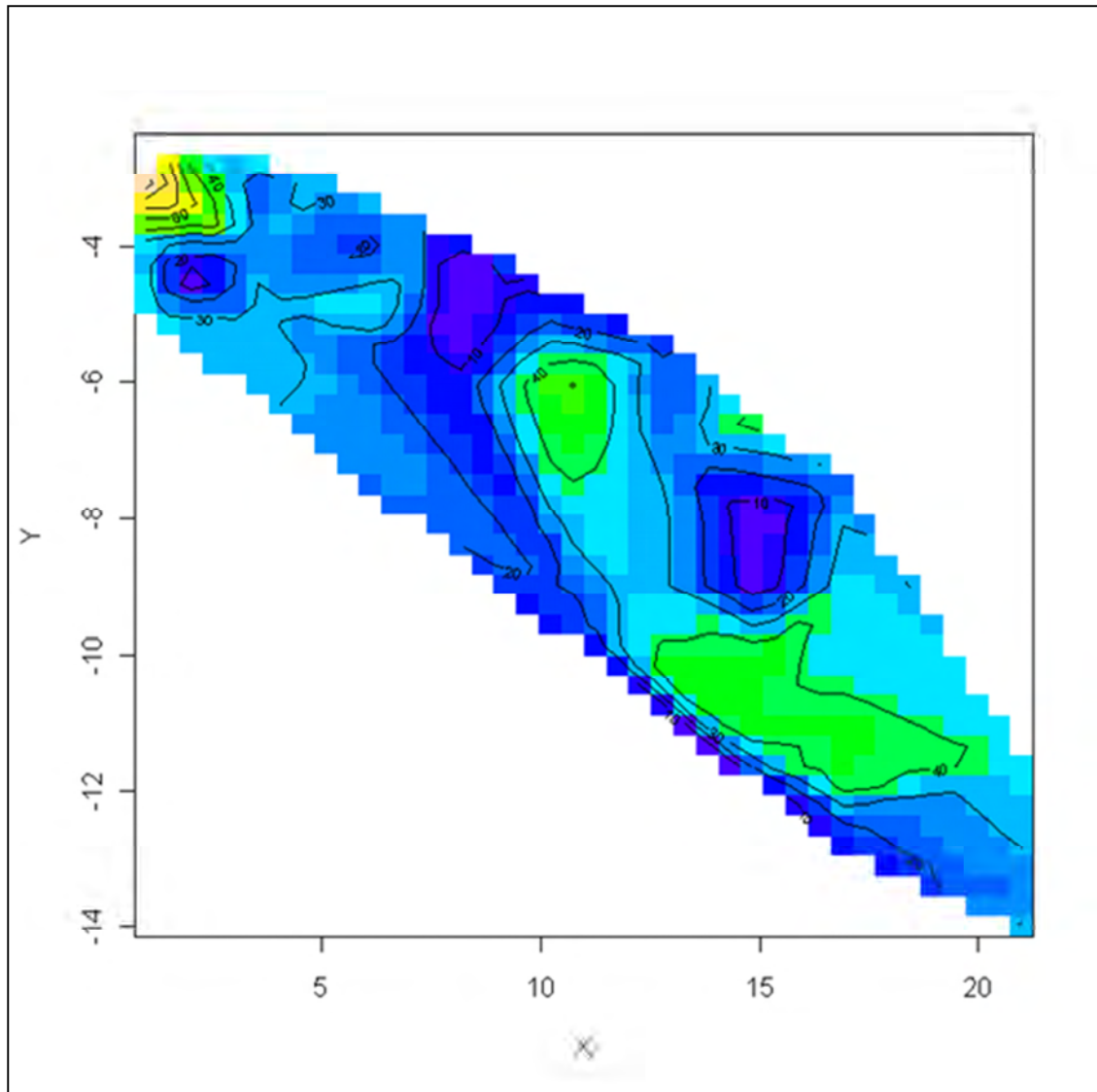
Figure 6.12. Contour map indicating the true thickness distribution of the LHZBG Unit in the study area of the Complex. The graph was constructed using an interpolation routine included as part of the "AKIMA" package for the functional language "R" and based on Akima (1978). A false X- and Y-coordinate system is applied.
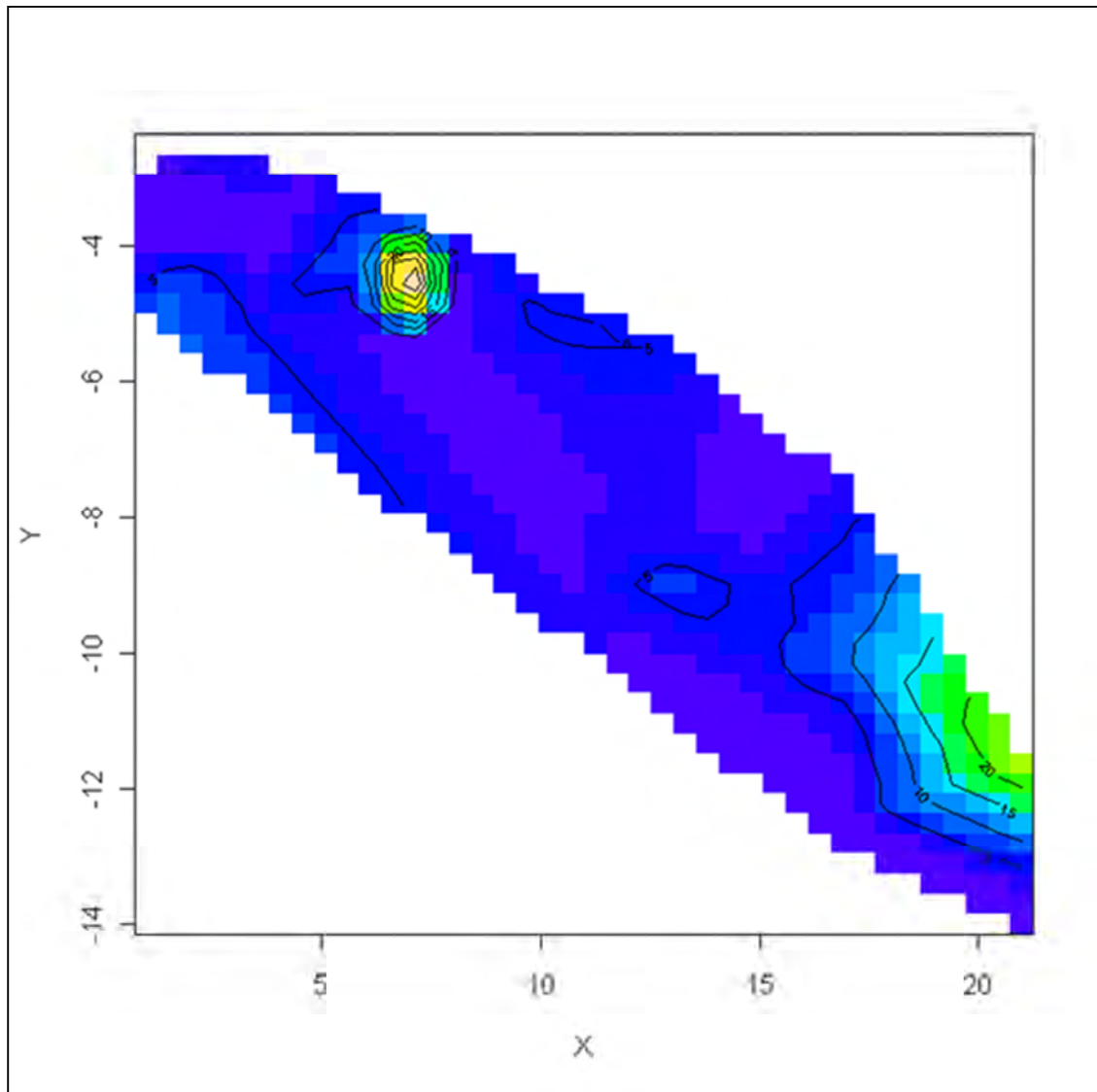
Figure 6.13. Contour map indicating the true thickness distribution of the BGAB Unit in the study area of the Complex. The graph was constructed using an interpolation routine included as part of the "AKIMA" package for the functional language "R" and based on Akima (1978). A false X- and Y-coordinate system is applied.

In the narrower part of the intrusion, in the upper northwest of the study area, there appears to be a weakly defined relationship between the percentage of xenoliths in the LHZBG Unit and the thickness of the LHZBG Unit. Where the LHZBG Unit is the thickest, the percentage xenoliths are lower than where the LHZBG Unit is the thinnest. It also appears as if the intrusion "meandered", from the northeast of the complex, first toward the north

and then to the south and then to the center, relative to the inferred margins of the Complex. There also appear to be a weak correlation between the distribution and thickness of the BGAB Unit and the distribution of the xenoliths. Where the BGAB Unit is thickest, the percentage of xenoliths also appears to attain its maximum occurrence in the LHZBG Unit. There is also a very weak correlation between the distribution and thickness of the BGAB Unit and the overlying LHZBG Unit. Where the BGAB Unit is thickest, the LHZBG Unit appear thinnest and where the BGAB Unit is thinnest, the LHZBG Unit appears thickest. The BGAB Unit appear to be thickest in the southern part of the study area.

In the broader part of the intrusion in the study area, the weakly defined relationship between the percentage of xenoliths present in the LHZBG Unit and the thickness of the LHZBG Unit defined above cannot be discerned. However, it appears as if the intrusion also "meandered" in the broad part of the intrusion. From the northwest of the Complex, the intrusion appear to have first "meandered" to the south, then to the north, back to the south and finally more consistently to the north in the southeast of the Complex. In the broader part of the Complex the percentage xenoliths attains its maximum percentage towards the northern inferred margin of the Complex in the northwest. Where the xenoliths constitute 100%, it is inferred to represent a part of the Complex that only has finger-structures into the surrounding country rock. Towards the south-west part, of the broader part of the Complex, the xenoliths appear to maintain its maximum percentage to the south of the idealized center of the Complex, relative to the inferred margins of the Complex.

As in the narrow part of the Complex there appear to be a weak correlation between the distribution of the BGAB Unit and the distribution of xenoliths in the broader part of the Complex. Where the BGAB Unit is thickest, the percentage xenolith in the LHZBG Unit attains it highest occurrence. This correlation is however completely reversed in the south east part of the study area. In the south east of the broader part of the Complex, the percentage xenoliths now attain its maximum where the BGAB Unit is thinnest. There also appear to be a weak correlation between the distribution and thickness of the BGAB and the LHZBG Units. In the broader area the BGAB Unit is thickest, the LHZBG Unit is also

thickest. The BGAB Unit have been preserved in the southern and south-central parts of the intrusion in the broader part of the Complex.

There is no apparent correlation between the location of the "talc-rich" zone in the study area relative to the percentage of xenoliths in the LHZBG Unit, nor to the distribution of the LHZBG Unit in the study area. Nor is there any correlation between the thickness or distribution of the BGAB Unit and the "talc-rich" zone in the study area. It may be noted that the "talc-rich" zone is located in the area where the LHZBG Unit of the intrusion is thickest in the central part of the Complex. It is also considered significant that the "talc-rich" area is located in the broadest part of the intrusion in the study area. The effect of the broadening of the Complex, and the distribution of the MCR layer will be considered in a later section.

The formation of the skarn aureole may also have been instrumental in the formation of an economically viable LHZBG Unit. At the Noril'sk intrusion, Arndt et al. (2005) suggested that the magma parental to the ore deposit is related to the physical factors which influenced interaction with the wall rock. The first is a magma with a high metal tenor and low volatile content which was able to interact with the wall rocks. The second is that the magma bypassed the magma chamber, not interacting with the granitic crust, which would have resulted in sulphide segregation at an inaccessible depth. This magma was then left relatively uncontaminated and able to assimilate evaporates and segregate sulphides at a shallow (mineable) level.

The Uitkomst Complex is intruded between the Archean basement granite and the overlying sedimentary sequence of the Transvaal basin. Intrusion of the LHZBG magma and the resultant formation of a skarn aureole below it, would have shielded the main intruding LHZBG magma from direct interaction with the Archean granite. Had the LHZBG magma intruded directly on the Archean granite, it is possible that the magma would have segregated sulphides at depth. The magma however was now able to intrude to much shallower levels. Here the magma partially assimilated dolomite country rock, which led to

an increase of oxygen fugacity and addition of sulphur, which resulted in the segregation of the sulphides at shallow (mineable) depth. The skarn floor would also have increased turbulent magma flow in the conduit and the opportunity for segregated sulphide droplets to accumulate. It is suggested in section 2.1.3 that where the LHZBG is in contact with the floor rocks, it is due to scouring of the BGAB.

It was noted that blebby pyrite occur along the preserved bedding of the xenoliths. The formation of this feature may be due to the intrusion of the LHZBG magma which mobilized a fluid in the dolomitic precursor rock, resulting in pyritization taking place along the preserved bedding in the xenoliths. This phenomenon may also be used as prove that the skarnification event took place synchronous to the intrusion of the LHZBG magma.

6.5 Petrogenetic implication for the Uitkomst Complex

In the Uikomst Complex the xenoliths consist dominantly of diopside. The diopside composition suggests thermal metamorphism of siliceous dolomite. The xenoliths also contain minor amounts of calcite, actinolite and chlorite. The presence of these alteration minerals suggests the presence of hydrous fluids, either inside the xenoliths during skarn mineralization or a late stage fluid infiltrating the xenolith as suggested by Hulley (2005). The increase in grain size of the diopside closer to the edge of the xenoliths may indicate annealing of the grains due to the presence of a CO_2-rich fluid. Such a fluid could have concentrated near the contact of the xenolith and the intruding magma. The CO_2-rich fluid initially lowers the viscosity favouring the growth of the diopside, but it also leads to the subsequent uralization of the grains. The variability of the CO_2 content during the skarn mineralization is demonstrated by the variation of in mineralogy of the xenoliths. In xenoliths from borehole SH176 (studied during the author's reconnaissance investigation on Slaaihoek) the presence of grossular and complete lack of sulphide mineralization would suggest lower CO_2 concentration at the time of formation relative to xenoliths from the current study area.

The role of temperature and CO_2 pressure in the formation of skarns, and its bearing on mineralization was investigated by Shoji (1975). This study determined that the most favourable skarn-forming conditions exist below 400 ˚C and at a CO_2 pressure with upper and lower limits determined by the stability of grandite garnet and the instability of hydrogrossular respectively. The amount of CO_2 in the fluids was thus inferred to be between 0.7 and 2.0 mole percent at 400 ˚C. These values need to be revised for the formation of iron-rich clinopyroxene. It was also pointed out that CO_2 needs to be released efficiently for skarn mineralization to proceed. Shoji (1975) stressed the importance of the availability of iron in the ore-forming fluid, as the ore-minerals are found in association with pyroxene and garnet skarns.

It appears from borehole logs that more xenoliths may have been preserved in the broader part of the intrusion away from the edge of the Uitkomst Complex, with the exception of finger-structures protruding from the Complex into the country rock, in the narrow part of the Complex. The preservation of horizontal bedding would suggest a more passive style of intrusion.

The presence of pyrite mineralization along the original bedding of the dolomite precursor rock and chlorite in the xenoliths may indicate a later intrusion of the xenoliths by a sulphur-rich hydrothermal fluid with a temperature of up to 400 ˚C and low to intermediate CO_2 content (Hulley, 2006). An alternative to this model is discussed below.

The concentration of iron sulphides in sediments is usually sparsely disseminated crystal and crystalline aggregates of pyrite or marcasite (Stanton, 1972). Enrichment may be due to pyritization of sedimentary iron oxide concentrations which already deposited during sedimentation (Stanton, 1972). This may be due to "leaking" of H_2S from underlying sediments. Alternatively, the iron accumulated during sedimentation will aid in the precipitation of sulphide from pore water. It is known that magmatic material contains heavy metal halides (mainly chlorides), which will dissolve in pore water. The pore water will be driven away form the intrusion and dispersed. As this pore water, laden with iron and other elements like copper lead and zinc, is dispersed it may encounter the disseminated iron

sulphides. These metals will displace some of the iron from the existent iron sulphides and precipitate as sulphides themselves. This metamorphic concentration is expected to cease once the rock ceases to contain free water (Stanton, 1972). The formation of pyrite cubes in this type of low-grade metamorphic environment is not well understood, but it is suggested that these grains form due to "retexturing" of concretions or by coalescence of closely packed groups of smaller crystals (Stanton, 1972).

In the alternative model suggested here, the pyrite occurring along the preserved bedding of the xenolith formed during emplacement of the LHZBG magma and the resultant skarnification process which affected the dolomitic precursor rock. The implication is that the LHZBG intruded at a level above the current preserved xenolith horizon, stoping downward into the country rock. The intruding LHZBG magma may have contained Fe-rich halides, which would then dissolve in the pore water present in the dolomite country rock. The pore water would be driven away from the intruding magma, into the surrounding country rock. As the pore water, now laden with Fe-rich halide complexes, was dispersed through the underlying country rock it encountered pyrite or marcasite, likely deposited during diagenesis of the dolomite along the original bedding planes. The pore water would interact with these pyrite or marcatite grains, displacing some of the iron in the sulphides and precipitating as sulphides themselves. This process may have been active while free water was still able to circulate in the forming xenoliths. The mineralogy of the xenoliths, dominated by fassaite diopside, suggests further contact thermal metamorphism of the xenoliths as the LHZBG magmas continued to flow through the conduit. This would have resulted in modification (coalescence) of the pyrite grains, giving the blebby texture observed in the xenoliths.

The xenoliths' precursor minerals, such as fassaite diopside, may have suffered retrograde metamorphism as any water remaining in the xenolith was driven off by the intrusion of the LHZBG magma. The finger structures of LHZBG Unit material in the xenoliths suggest that the LHZBG magma may have been able to intrude the xenoliths, possibly allowing the introduction of late stage fluids into the xenoliths. The chlorite occurrence in the xenoliths may reflect this.

CHAPTER 7 GEOCHEMISTRY OF THE TALC-RICH PART OF THE UITKOMST COMPLEX

7.1 Introduction

The genesis of the Uitkomst Complex may be divided into to two stages according to Gauert (1998) and de Waal et al., (2001). The first is the conduit stage and consists of the LHZBG, PCR and the MHZBG Units, excluding the top 20 meters (Gauert, 1998; de Waal et al., 2001). The second is the closed-system stage and consists of the upper 20 meters of the MHZBG, the PXNT and GN Units (Gauert, 1998; de Waal et al., 2001). In the conduit stage the parental magma has been determined to most likely be B1-type Bushveld magma that flowed through the conduit. This magma may have been saturated in sulfur and precipitated small quantities of sulfide together with chromian spinel and olivine (de Waal et al., 2001). The small variations in chemical composition in the LHZBG, PCR and MHZBG Units with height, is taken by these authors as supporting the conduit nature of continual replenishment of the magma (de Waal et al., 2001). With the exception of Ti, all the major elements have concentrations closely comparable to B1-magma in the closed-system stage (de Waal et al., 2001). The trace elements Zn, Co, Zr, Y, Sr and Rb show some deviation from the average B1 composition (de Waal et al., 2001). The fractionated trend of the upper part of the MHZBG, the PXNT and GN units was used by de Waal et al. (2001) to confirm the suggested closed-system stage.

In van Zyl's (1996) investigation, the chemical analyses of the primary and secondary silicate minerals associated with the sulphide mineralization show that the complex is enriched in iron towards the base of the LHZBG Unit. The enrichment in iron is interpreted as a combined effect of fractionation and the cooling effect of the country rock on the intruding magma. The sulphide grains also increase in size towards the base of the Lower Harzburgite Unit to >450 microns. The Cu-Ni ratio of the sulphides also increases towards the base of the complex. Van Zyl (1996) also found that there is an increase in the incompatible element content in the bulk rock composition towards the top of the closed system.

Gomwe (2000) determined that there is a decrease in the Na_2O, K_2O, TiO_2 and SiO_2 and an increase in MgO content with increasing height from the base of the complex to the MHZBG Unit. Reflecting the inverse sequence, also observed by Kenyon (1986), the lack of variation with stratigraphic height in the MHZBG Unit indicates that the magma was not differentiated. Gomwe (2000) calculated that the magma contained 20-30% trapped melt, decreasing with height. The Cu-content of >10-20ppm indicate the presence of excess sulphide relative to the trapped melt, which suggest the presence of cumulus sulphide. Gomwe (2000) also noted that the LHZBG and PCR Units have a slightly negative correlation between S and MgO, in that the least Mg- rich rocks are the most S-rich. The negative Sr excursions found in the investigation allude to possible mobilization of Rb during pervasive alteration of the LHZBG, PCR and lower MHZBG Units. Gomwe (2000) also found that the sulphide-bearing rocks have higher values of εNd and lower ratios of [Sm/Ta] than the remainder of the complex, leading to a suggestion of less crustal contamination in these horizons. This could possibly be explained by selective contamination of external sulfur or oxygen from the country rocks, triggering sulphur-segregation. It was also found by Gauert (1998) that Slaaihoek samples showed somewhat higher V/Cr ratios than Uitkomst samples, which may reflect the more evolved nature of the cumulates at Slaaihoek, and higher Zr/Y ratios which may indicate less contamination with dolomitic country rock.

Sakar et al. (2008) indicated that crustal sulphur was assimilated and impacted on the sulphur isotopic signature. It is also deemed to have contributed to the mineralization in the Uitkomst Complex. The sulphur is suggested to have been transported by the fluid derived from pro-grade metamorphism of the country rock. The oxygen isotopes on the other hand indicated country rock derived fluid not to have influenced the signature of the magma, it is suggested to be a result of late-stage meteoric water infiltration.

7.2 Background

In this section the lower units of the Uitkomst Complex are investigated to find out if there is a relationship between mineralogical variation in the LHZBG Unit and the overlying PCR

Unit. Secondly, the possibility that the mineral abundances in the different units may be related to the position sampled in the Complex relative to the inferred margins of the intrusion in the study area. A semi-quantitative approach in the evaluation of the distribution of secondary minerals with height and spatial distribution is used to answer these questions.

As part of the discussion, a mineralogical report compiled for ARM by Moruo Mineralogical Services (Singh and de Nooy, 2003) is also considered. This report was made available for this study by Mr. J. Woolfe of ARM, and refers to Pit 1 and Pit 2, areas outside of the current study area which is confined to Pit 3 area (Figure 7.1). All the lower and central data points in this report refer to the LHZBG, or are assumed to refer to the LHBZG as it is the only unit preserved in that part of the intrusion and no unit indicators are given in the report.
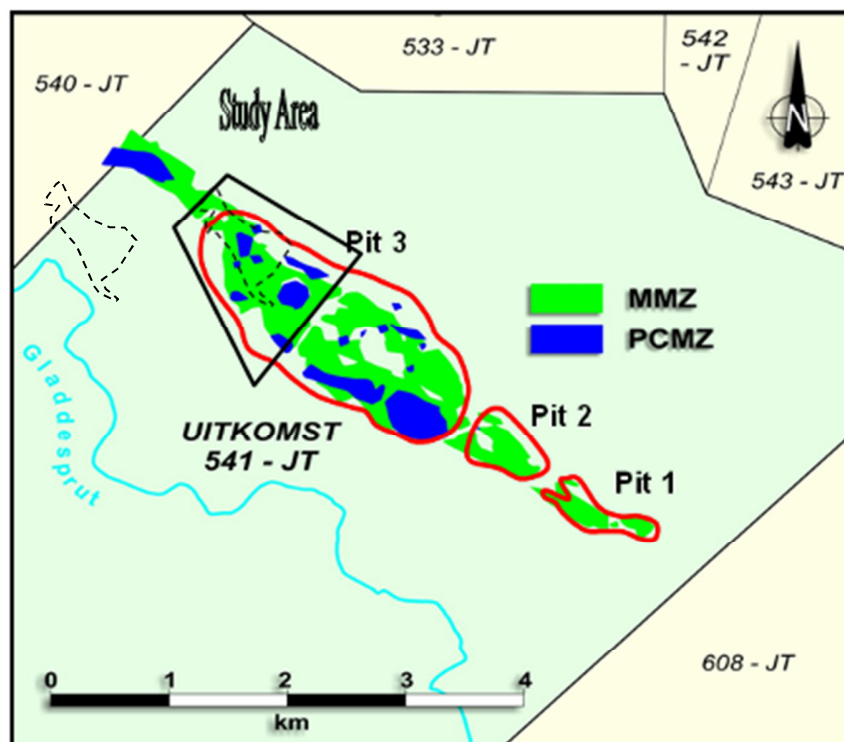
Figure 7.1 Outline of the open pits planned as part of the extension programme. The extent of the study area is indicated. The high alteration mineral assemblage area is indicated by the dashed line. Figure courtesy Nkomati Mine.

7.3 Vertical distribution of amphibole, chlorite and talc

The mineral distribution, based on semi-quantitative mineral abundances determined by XRD, is presented for individual boreholes. The data is presented in such a way to indicate the vertical variation of the secondary minerals. The unit is given with the section number in brackets.

Amphibole, talc and chlorite are grouped together, as these minerals may collectively represent the alteration products of the same primary minerals, i.e. olivine, orthopyroxene and clinopyroxene. The composition of the alteration minerals has already been discussed in the chapters dealing with the petrography and mineral chemistry. Serpentine is not considered a diagnostic mineral as it generally below 5 % occurrence and its presence is solely due to the hydrothermal alteration of olivine at low CO_2 concentrations.

The Loss On Ignition (LOI) is also presented as a separate graph to indicate the presence of volatiles associated with the afore mentioned alteration minerals, with height.
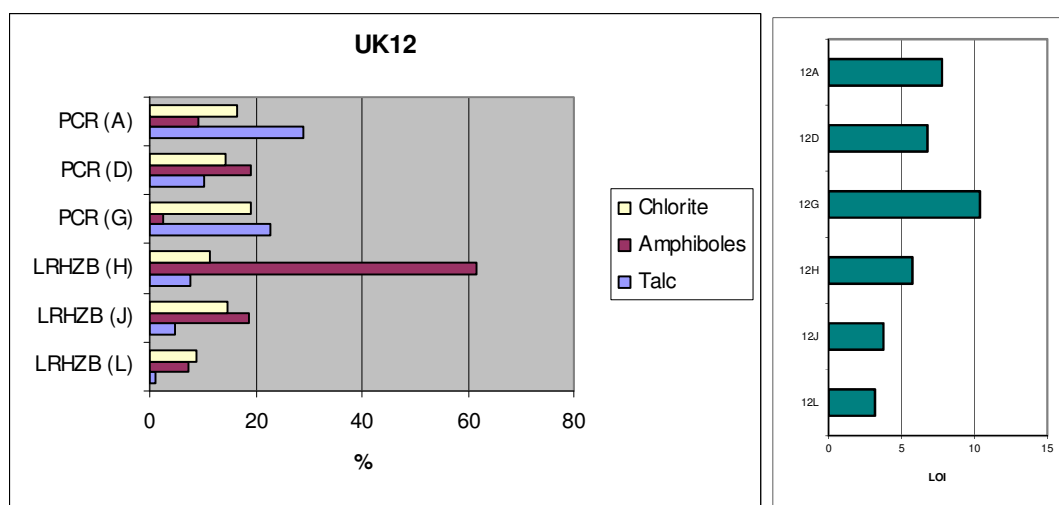
Figure 7.2. Bar-graph indicating the relationship between talc, amphibole and chlorite, as well as the variation of these minerals with height in borehole UK12. The LOI value with height is also presented.

In UK12 (Figure 7.2), there does not appear to be a systematic relationship between the occurrence of talc and amphiboles. The amphibole content increases with height in the LHZBG Unit, between point L and H. The amphibole content in the PCR Unit in contrast

shows an almost inverse relationship with talc, with height. The talc content increases with height in the LHZBG Unit and appears to continue the trend into the basal part of the PCR Unit (point L to G) before decreasing and then increasing again with height (point D to A). Talc reaches its highest abundance in the PCR Unit. Talc and amphibole both increase in abundance with height in the LHZBG Unit. There appears to be no systematic variation in the chlorite content with height in either the LHZBG or the PCR Units. In the PCR Unit, chlorite shows a very subtle relationship with talc and shares the inverse relationship of talc with amphibole. The increase of volatiles is demonstrated by the increase in LOI values with height, tapering out near the top of the unit. No specific correlation is made with any of the alteration minerals, but talc show the closest correlation.
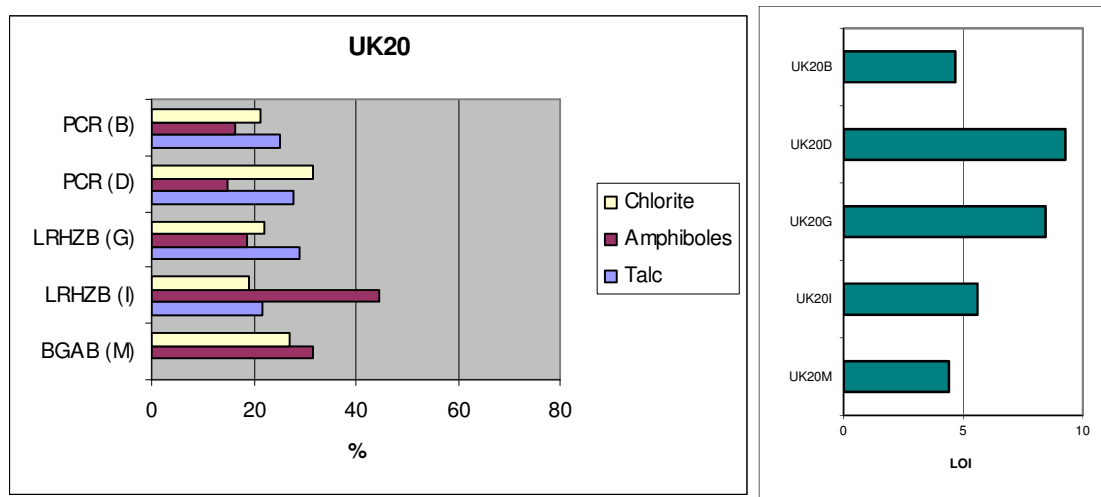
Figure 7.3. Bar-graph indicating the relationship between talc, amphibole and chlorite, as well as the variation of these minerals with height in borehole UK20. The LOI value with height is also presented.

In UK20 (figure 7.3), there appears to be no systematic relationship between the occurrence of amphiboles and talc. There is an increase in the amphibole content from the BGAB Unit to the lower part of the LHZBG Unit, before dropping off and remaining nearly constant in the upper part of the LHZBG and PCR Units. There is no talc present in the BGAB Unit and there is a consistent content of talc from the bottom of the LHZBG Unit through to the top of the PCR Unit. The chlorite content decreases from the BGAB Unit to the base of the LHZBG Unit before steadily increasing to the base of the PCR Unit (point I to D) before

decreasing at the top of the PCR Unit. The presence of volatiles increases with height up to the lower contact of the PCR before decreasing again. The closest correlation is with talc.
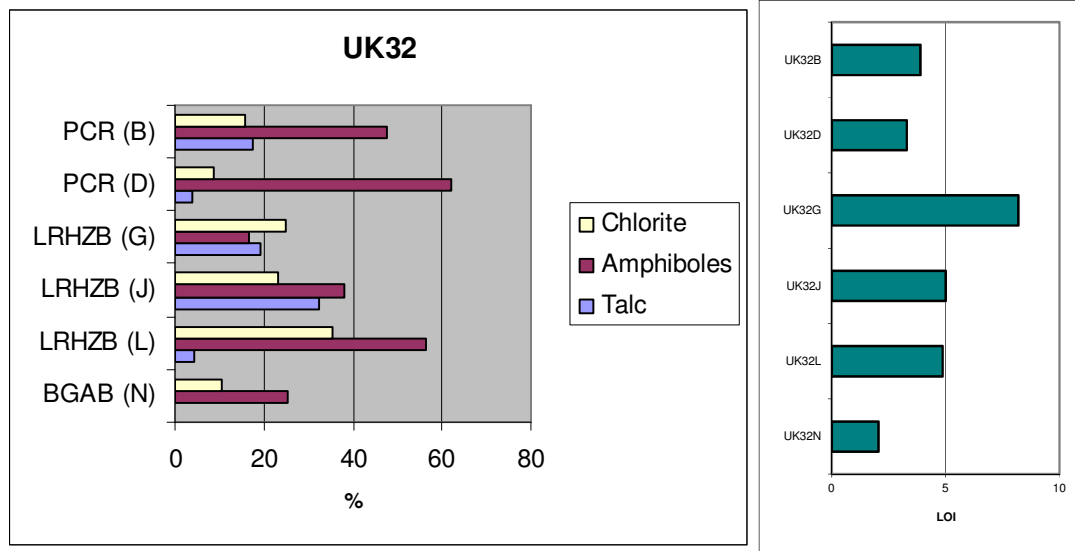
Figure 7.4. Bar-graph indicating the relationship between talc, amphibole and chlorite, as well as the variation of these minerals with height in borehole UK32. The LOI value with height is also presented.

In UK32 (figure 7.4), there again appears to be no relationship between the talc and amphibole content. There is an increase in amphibole content from the BGAB Unit to the lower part of the LHZBG Unit before there is a steady decline in amphibole to the top of the unit (point N to G). The amphibole content then increases in the bottom part of the PCR Unit before decreasing again (point D to B). There does not appear to be a systematic increase or decrease of talc with height. The chlorite content increase from the BGAB Unit to the bottom of the LHZBG Unit then decreases and remains fairly constant to the top of the LHZBG Unit (point N to G). The chlorite content decreases at the bottom of the PCR Unit then increases with height. The LOI increases with height up to the top of the LHZBG, before decreasing in the PCR. The closest correlation is again with the abundance of talc.
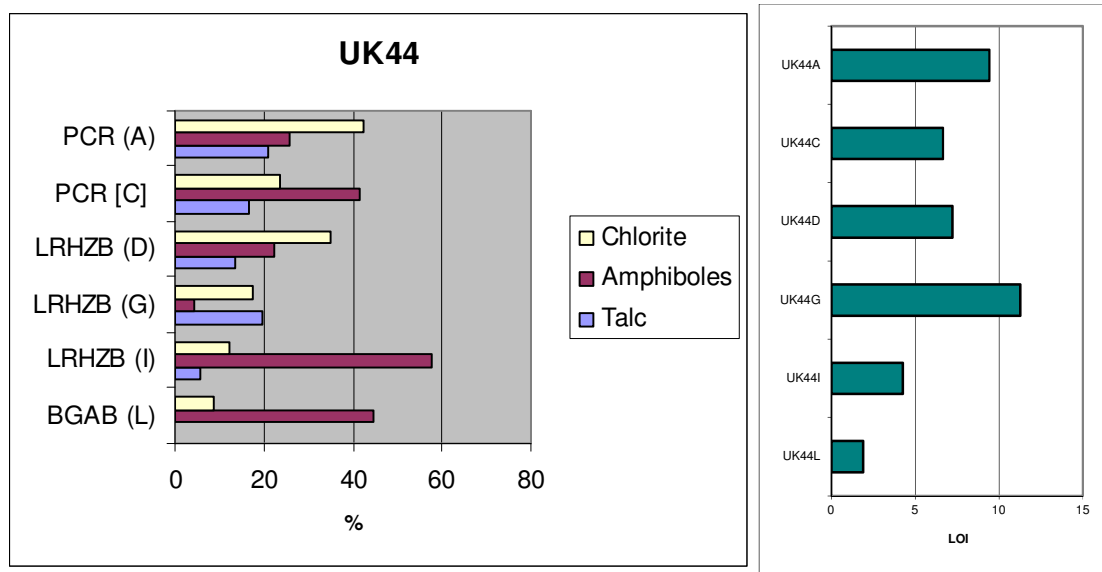
Figure 7.5. Bar-graph indicating the relationship between talc, amphibole and chlorite, as well as the variation of these minerals with height in borehole UK44. The LOI value with height is also presented.

In UK44 (figure 7.5), there appears to be no relationship between the distribution of amphiboles and talc. There is a increase in amphibole content from the BGAB Unit to the lower part of the LHZBG Unit (point L to I) before a rapid decrease and then a steady increase in amphibole with height (point G to C) through the top of the LHZBG Unit to the bottom of the PCR Unit, followed by a decrease of amphibole in the top of the PCR Unit. There is no talc present in the BGAB Unit and the talc content appears to increase with height from point I to G, before decreasing and then steadily in crease from point D (top of the LHZBG Unit) to the top of the PCR Unit. The chlorite content increases steadily from the BGAB Unit to the top of the LHZBG Unit (point L to D) before decreasing in the bottom of the PCR Unit and then increasing again with height (point C to A). The volatile content demonstrated by the LOI values increase from the bottom to the middle of the LHZBG, decreasing before increasing again with height in the PCR. The closest correlation is with the distribution of talc.

147
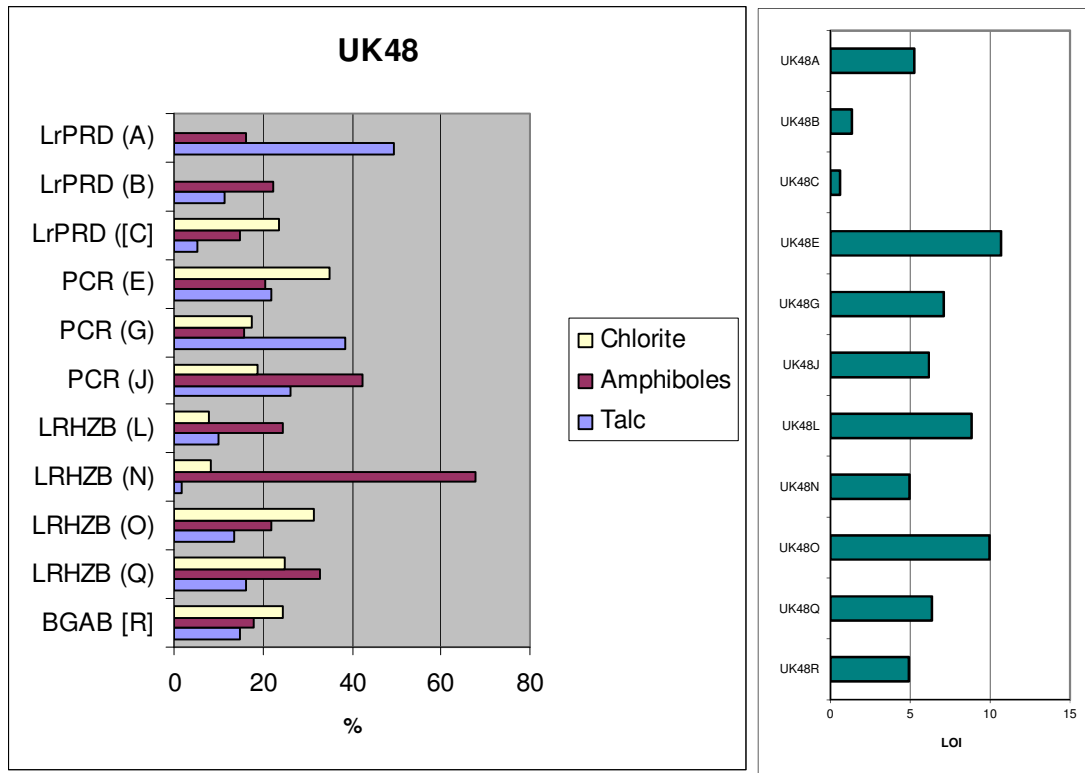
Figure 7.6. Bar-graph indicating the relationship between talc, amphibole and chlorite, as well as the variation of these minerals with height in borehole UK48. The LOI value with height is also presented.

In UK48 (figure 7.6), there does not appear to be a relationship between the occurrence of talc and amphibole. There is no systematic variation in amphibole content with height. The amphibole content is fairly constant with height, with the exception of points J and N. The talc content is fairly constant from the BGAB Unit to the lower part of the LHZBG Unit (point R to O). The talc content then sharply decreases before steadily increasing from the top (point N to G) of LHZBG Unit to the lower PCR Unit. The talc content then steadily decreases from the top of the PCR Unit to the bottom of the LrPRD Sub-unit (point G to C). The talc content then increases with height to the top of the LrPRD Sub-unit (point C to A). The chlorite content slightly increases from the BGAB Unit to the bottom and lower central part of the LHZBG Unit (point R to O). The chlorite content then decreases sharply in the upper central part and top of the LHZBG Unit (point N to L). The chlorite content then increases from the bottom to the top of the PCR Unit (point G to E). The chlorite content

then decreases at the bottom of the LrPRD Sub-unit and is completely absent in the upper part of the LrPRD Sub-unit.

The volatile content shows four cycles of increase followed by a sudden decrease. The correlation between LOI values and the percentage talc is again evident.
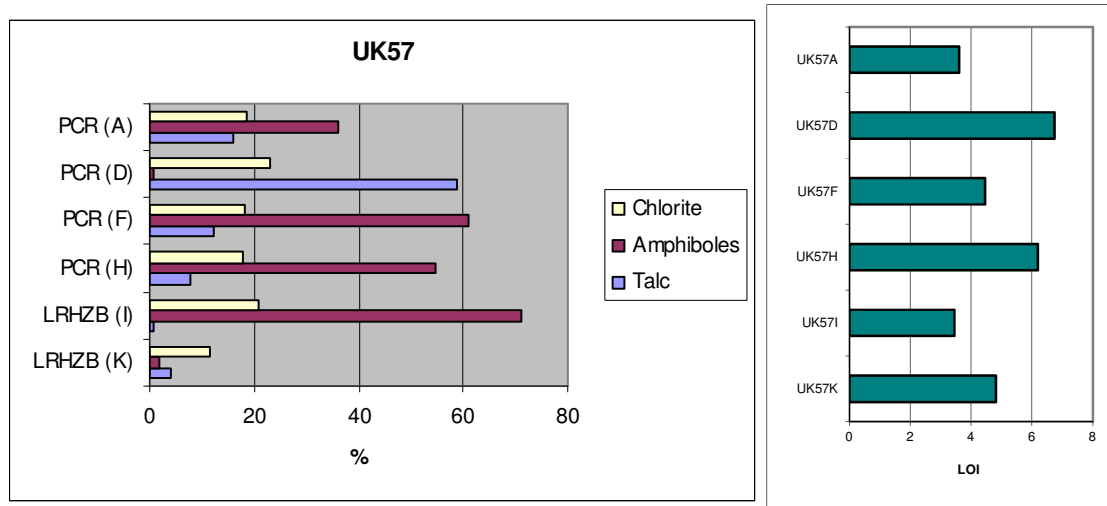
Figure 7.7. Bar-graph indicating the relationship between talc, amphibole and chlorite, as well as the variation of these minerals with height in borehole UK57. The LOI value with height is also presented.

In UK57 (figure 7.7), there does not appear to be a specific relationship between the occurrence of amphibole and talc. The amphibole content steeply increases from the bottom to the top of the LHZBG Unit. The amphibole content decreases at the bottom (point H) of the PCR Unit then increases slightly with height (point F) before a rapid decrease (point D) and increase at the top (point A) of the PCR Unit. The talc content decreases with height in the LHZBG Unit (point K to I) before increasing with height in the PCR Unit (point H to D) before decreasing at the top (point A). The chlorite content increases from bottom of the LHZBG Unit to the top, then decreases at the base of the PCR Unit. The chlorite content of the PCR Unit increases with height (point H to D) before decreasing at the top. The LOI-along with the correlating talc value is erratic with height.
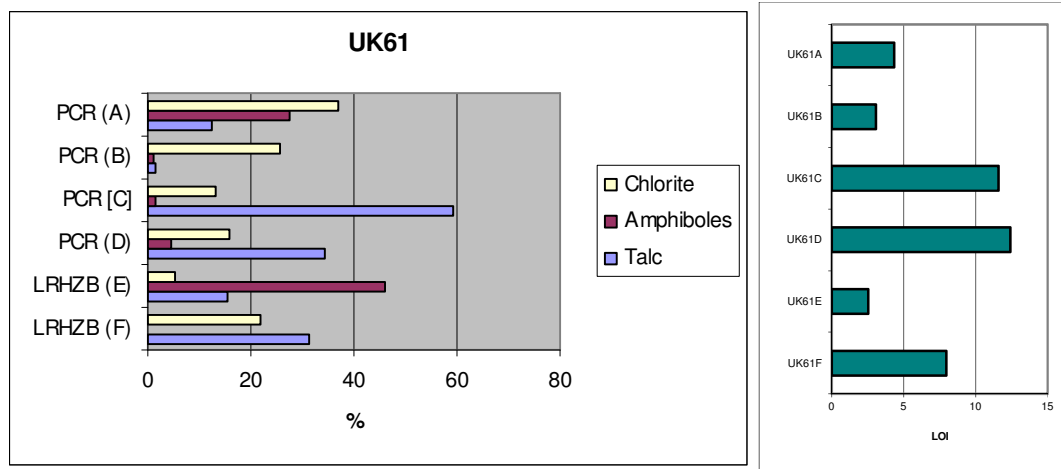
Figure 7.8. Bar-graph indicating the relationship between talc, amphibole and chlorite, as well as the variation of these minerals with height in borehole UK61. The LOI value with height is also presented.

In UK61 (figure 7.8), there appears to be no relationship between the occurrence of talc and amphibole. The amphibole content in the LHZBG Unit goes from being absent in the bottom to maximum in the top. The amphibole content decreases with height in the PCR Unit from point D to B before increasing at the top. The talc content of the LHZBG Unit decreases with height. The talc content of the PCR Unit increases with height (point D to C), before rapidly decreasing (point B) and then increases at the top. The chlorite contents decreases with height in the LHZBG Unit. The chlorite content increases at the bottom to the PCR Unit then slightly decrease and then increase with height (point D to A). In contrast to the other units, the LOI shows cycles of decrease with height, along with talc, although distribution still appears erratic.
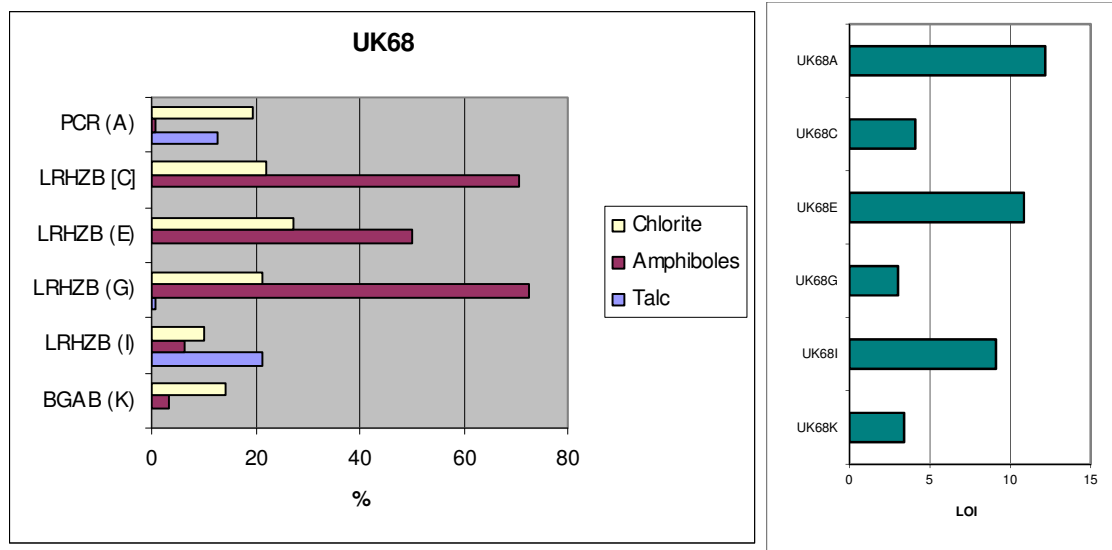
Figure 7.9. Bar-graph indicating the relationship between talc, amphibole and chlorite, as well as the variation of these minerals with height in borehole UK68. The LOI value with height is also presented.

In UK68 (figure 7.9), there appears to be no relationship between the talc and amphibole content. The amphibole content increases with height from the BGAB Unit to the central part of the LHZBG Unit (point K to G) before slightly decreasing and then increasing again towards the top of the unit. The amphibole content then decreases significantly in the PCR Unit. Talc is absent in the BGAB Unit. The talc content decreases with height to absent in the upper part of the LHZBG Unit. Talc is only present again in the PCR Unit. The chlorite content decreases from the BGAB Unit to the bottom of the LHZBG Unit before increasing with height (point I to E) then decrease to the top of the LHZBG Unit through to the PCR Unit (point E to A). The volatile content reflected by LOI values show three increments of increase and decrease with height.

7.4 Lateral distribution of amphibole, chlorite and talc

Only the lateral distribution of the average alteration minerals in the BGAB, LHZBG and PCR Units will be discussed in this section. The aim of this section is to determine the lateral distribution, if any, of the alteration minerals in the study area by looking at the average distribution per mineral per borehole. A summary of the averages, per mineral per borehole, is presented in Tables 7.1, 7.2 and 7.3.

151

Table 7.1. The average alteration mineral per borehole in the BGAG Unit.

	UK20	UK32	UK44	UK48
Amphibole	30.37	20.23	44.6	5.97
Chlorite	26.86	10.52	8.73	24.61
Talc	0	0	0	14.97

A longitudinal section is given in Figure 7.10, representing the average alteration mineral distribution in the BGAB Unit of the Uitkomst Complex.
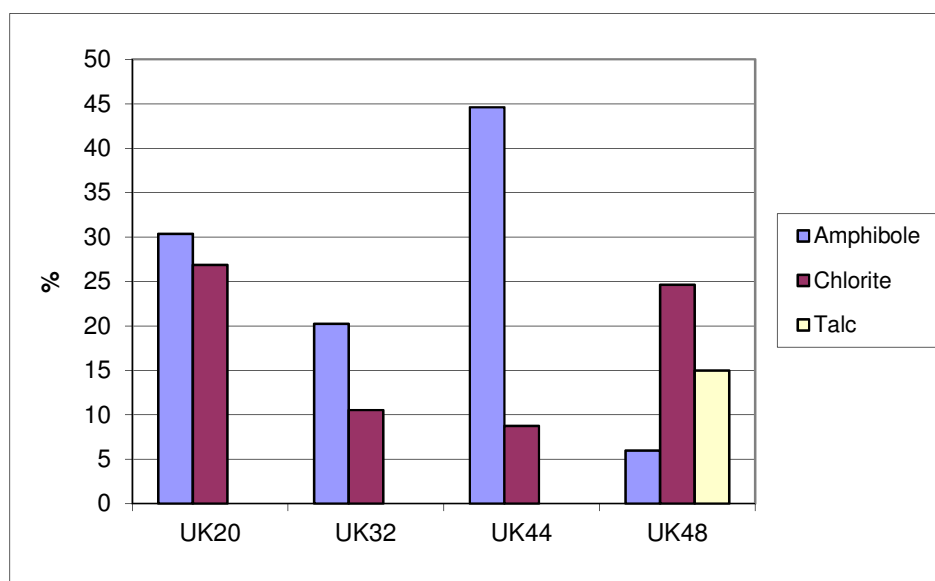
Figure 7.10. The average alteration mineral abundance, expressed in weight percent, in a partial longitudinal section through the Uitkomst Complex in the BGAB Unit. From UK20 (NW) to UK 48 (SE).

From Figure 7.10 it can be seen that the amphibole content varies from the NW to the SE. It can also be seen that the chlorite content decreases from the NW to the SE, before increasing again in the SE corner. Lastly, talc only occurs in the SE portion of the Uitkomst Complex in the BGAB in the study area.

Table 7.2. The average alteration mineral per borehole in the LHZBG Unit.

	UK12	UK20	UK32	UK44	UK48	UK57	UK61	UK68
Amphibole	29.23	31.62	37.18	28.13	36.62	36.46	23.00	49.93
Chlorite	11.63	20.53	27.87	21.60	18.16	16.17	13.47	20.27
Talc	4.56	25.28	18.60	12.99	10.40	2.43	23.40	5.63

A longitudinal section is given in Figure 7.11, representing the average alteration mineral distribution in the LHZBG Unit of the Uitkomst Complex.
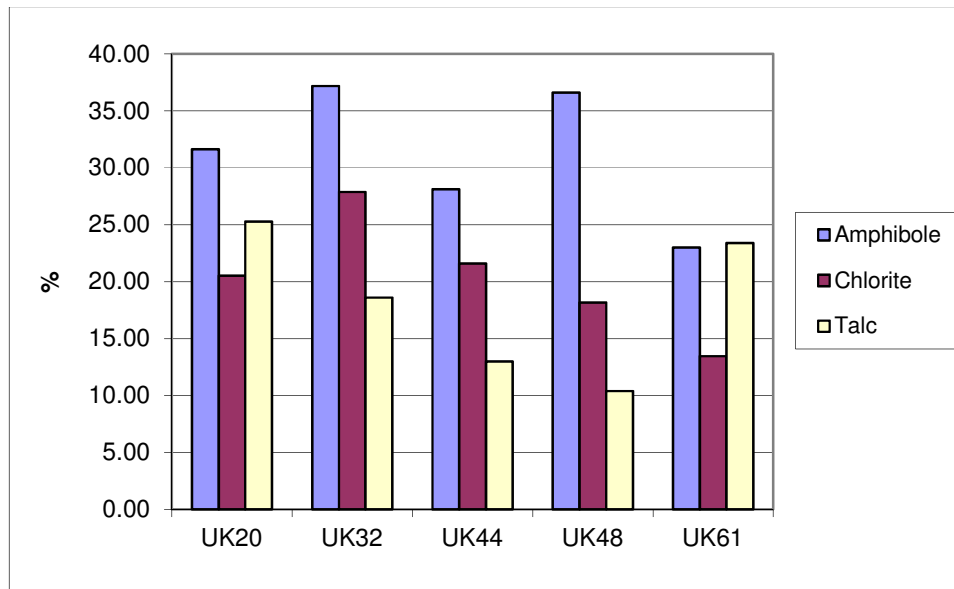
Figure 7.11. The average alteration mineral abundance, expressed in weight percent, in a partial longitudinal section through the Uitkomst Complex in the LHZBG Unit. From UK20 (NW) to UK 61 (SE).

From Figure 7.11 it may be seen that the amphibole content varies from the NW to the SE. It can also be seen that the chlorite content decreases from the NW to the SE in the broad part of the study area. Lastly, the talc content also decreases form the NW to the SE in the study area, before increasing again in the SE corner. A transverse section is given in Figure 7.12, representing the average alteration mineral distribution in the LHZBG Unit of the Uitkomst Complex.
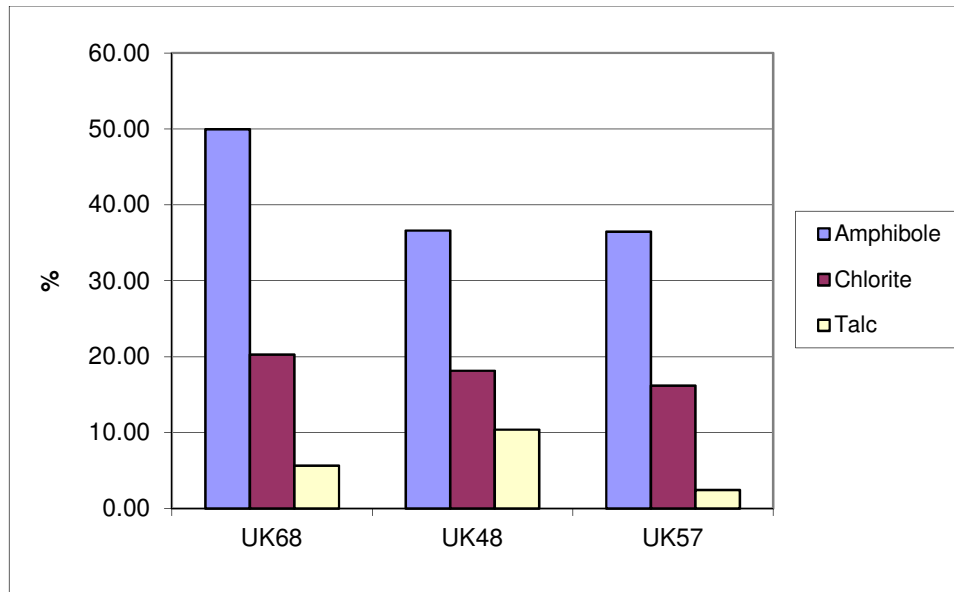
Figure 7.12. The average alteration mineral, expressed in weight percent, in a partial transverse section through the Uitkomst Complex in the LHZBG Unit. From UK68 (N) to UK57 (S).

From Figure 7.12 it can be seen that the amphibole content is higher closer to the inferred margins of the complex and the talc content slightly lower at the edges of the complex. The chlorite content decreases slightly from from the N to the S in the transverse section.

Table 7.3. The average alteration mineral per borehole in the PCR Unit.

	UK12	UK20	UK32	Uk44	UK48	UK57	UK61	UK68
Amphibole	10.34	15.72	54.90	33.58	26.11	38.11	22.17	0.69
Chlorite	16.62	26.44	12.41	33.15	23.71	19.59	22.94	19.32
Talc	20.64	26.41	10.70	18.77	28.87	23.81	26.82	12.72

A longitudinal section is given in Figure 7.13, representing the average alteration mineral distribution in the PCR Unit of the Uitkomst Complex.
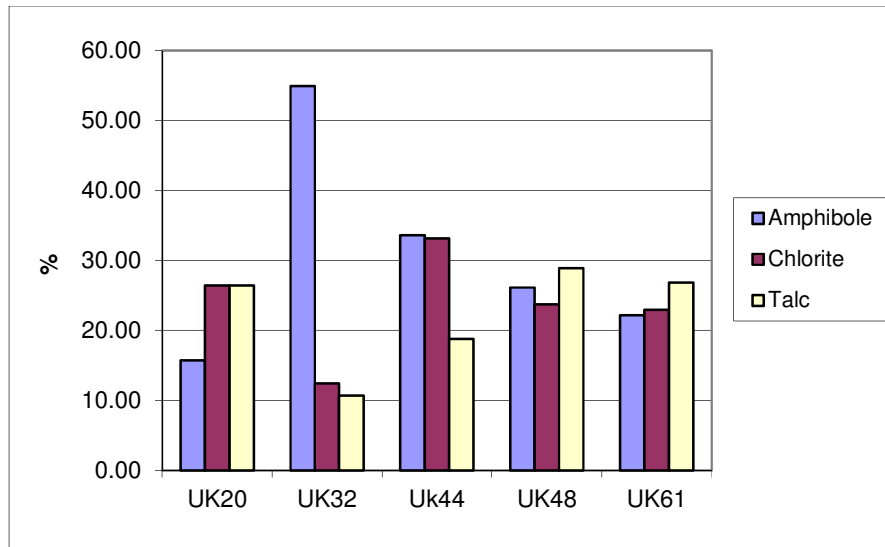
Figure 7.13. The average alteration mineral, expressed in percent, in a partial longitudinal section through the Uitkomst Complex in the PCR Unit. From UK20 (NW) to UK61 (SE).

From Figure 7.13 it may be inferred that the amphibole content decreases from the NW to the SE in the broader part of the study area. The chlorite content first decreases then increase and then decrease again in the NW to the SE in the broader part of the study area. Lastly, the talc contents increase from the NW to the SE in the study area. In Figure 7.14 a transverse section is given through the Uitkomst Complex in the PCR Unit.
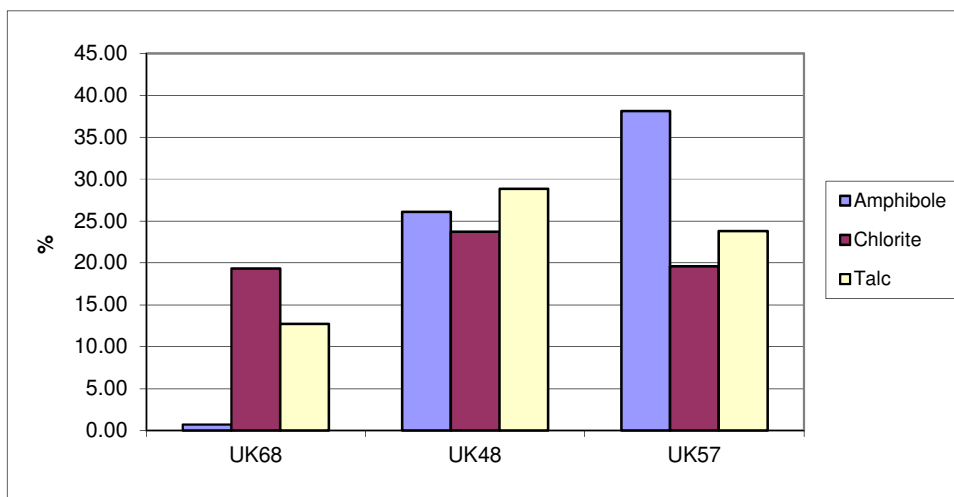
Figure 7.14. The average alteration mineral, expressed in percent, in a partial longitudinal section through the Uitkomst Complex in the PCR Unit. From UK68 (N) to UK57 (S).

From Figure 7.14 it may be inferred that the amphibole content increases from the N to the S in the study area. The chlorite and talc content seem to be lower closer to the inferred margins of the Uitkomst Complex in the PCR Unit.

7.5 Discussion of the distribution of amphibole, chlorite and talc

Decarbonization of dolomite in the presence of a mafic magma should lead to the co-existence of talc and amphibole in the resultant rock (Deer et al., 1992). However, in the profiles of the boreholes through Pit 3, the distribution of talc and amphibole with height indicates no systematic vertical relationship. There also appears to be no consistent increase or decrease of either talc or amphibole with height in any of the lithological units over the spatial distribution of the boreholes sections analysed. The highest occurrence of amphibole is located in the LHZBG Unit either at the top of the unit or near the bottom. The highest occurrence of talc and chlorite is found in the PCR Unit, but not at a consistent stratigraphic height. There appears to be no consistent decrease or increase of chlorite with height in any of the lithological units over the spatial distribution of the borehole sections analysed. There does not appear to be any consistent sympathetic variation between either amphiboles nor talc nor chlorite.

Spatially the vertical distribution of the amphiboles appears to follow a weakly defined mode of occurrence in the LHZBG Unit. Where the highest occurrence of amphibole is near the bottom of the LHZBG Unit, the borehole is positioned further away from the inferred margin of the Uitkomst Complex (UK 20, 32, 44). Where the highest occurrence of the amphiboles in the LHZBG Unit is towards the top of the unit, the borehole is positioned closer to the inferred margin of the Uitkomst Complex (UK12, 48, 57, 61 and 68). There is no apparent vertical spatial distribution pattern for the occurrence of amphiboles in the PCR Unit. The lateral distribution of amphibole in the BGAB Unit and LHZBG Units do not follow a specific trend along the longitudinal section. However, the lateral distribution of amphibole in the PCR Unit is indicated to decrease in a SE-direction. The distribution of

amphibole in the LHZBG Unit can not be considered conclusive, but appears to decrease from the S to the N in the PCR along the transverse section.

XRD data from Pit 1 (Singh and de Nooy, 2003) for amphiboles indicates that the presence of amphibole is higher in the upper part of the borehole, where samples were collected further away from the inferred margins of the Uitkomst Complex. In Pit 1 the amphibole content is the highest in the bottom of the borehole, close to the inferred margin of the Complex. In Pit 2 the observed trend is similar to the trend observed in the study area in Pit 3, where the highest occurrence of amphibole is found in the lower part of the borehole, further away from the inferred contact of the Complex. In Pit 2 the highest occurrence of amphibole in the upper part of the borehole, is from samples located closer to the inferred margin of the Complex. The lateral distribution of amphibole in Pit 1 seems highly variable, but the lateral distributions in Pit 2 appear to decrease towards the SE.

It thus appears that conditions favourable for the formation of amphibole prevailed in the NW-part of the exposed Complex, but changed toward the SE. It is also significant to note that the PCR Unit in the form of the PCMZ is not found further towards the SE in association with Pit 1 and Pit 2.

Talc is only weakly tied to spatial location in both the LHZBG and PCR Units. Talc has the highest occurrence in the lower part of the LHZBG Unit where the borehole is located in the wider area to the SE of the intrusion. This is in the part of the study area indicated to have a relative proportion of talc more than 15% (as indicated by Figure 10.1 ; UK48, 68, 57, 61). The highest occurrence of talc in the upper part of the LHZBG Unit is found in the boreholes that fall outside the study area indicated to have a relative proportion of more than 15% talc, in the narrower part of the intrusion in the north-western portion of the study area (UK12 and 20). Talc has the highest occurrence in the central part of the LHZBG Unit between the previously described two areas (UK32 and 44). Talc has the highest occurrence in the upper part of the PCR Unit in the north-western part of the study area (UK12, 20, 32 and 44) and the highest occurrence in the central part of the PCR Unit in the south-eastern

part of the study area (UK48, 57 and 61). Talc is found to decrease laterally from the NW to the SE in the LHZBG Unit, but to increase from the NW to the SE in the PCR Unit. Talc does appear to decrease closer to the inferred margin of the Uitkomst Complex relative the central part, in transverse section, in both the LHZBG and PCR Units.

In Pit 1 and Pit 2 the distribution of talc, both vertically and laterally, has been found to be highly variable (Singh and de Nooy, 2003). It was indicated that Pit 1 and Pit 2 has higher talc contents than Pit 3 (Singh and de Nooy, 2003). The highest occurrences of talc in Pit 1 appear near the inferred margins of the Complex and have no discernable lateral distribution pattern. In Pit 2 the talc occurrence increases from the N to the S, with the highest occurrence of talc being found in the boreholes located close to the inferred southern margin of the Complex

Chlorite has a weakly defined mode of occurrence in the PCR Unit where the highest occurrence in the lower part of the unit is found in the boreholes that fall outside the study area indicated to have more than 15% talc (UK12 and 20) in the narrower part of the intrusion. The highest occurrence of chlorite is found in the upper part of the PCR Unit. In the boreholes that falls in the part of the study area indicated to have more than 15% talc, in the wider part of the intrusion (UK32, 44, 48, 61 and 68), with the exception of UK57, where the highest occurrence of chlorite is found in the central part of the PCR Unit. The lateral distribution of chlorite in the BGAB, LHZBG and PCR Units, all seem to indicate a general decrease in abundance from the NW to the SE along the longitudinal section. The lateral distribution of chlorite in the LHZBG Unit seems to decrease from the N to the S in the transverse section, and the distribution in the PCR Unit may not be considered conclusive.

XRD data for Pit 1 (Singh and de Nooy, 2003) indicate the boreholes closer to the inferred margin of the Complex to have the highest occurrence of chlorite in their lower parts. The chlorite content seem to have the highest occurrence in the upper part of the borehole in the samples located furthest from the inferred contact of the Complex. Here the highest

occurrence of chlorite is found in the central part of the Complex. In Pit 2 the highest occurrence of chlorite is found in the central part of the Complex. The abundance of chlorite seems to decrease from the NW to the SE. This is the same general trend observed in the study area in Pit 3. As with the amphibole distribution, the process responsible for the formation of the chlorite and distribution pattern, seem to have differed slightly from the NW to the SE in the exposed part of the Complex.

The volatile content, as demonstrated by the Loss On Ignition (LOI) values show cycles of increase and decrease with height. In the NW of the intrusion the LOI values show a correlation with the distribution of talc, but this correlation diminishes progressively toward the SE of the intrusion. The cyclical nature of the LOI values may indicate that the volatiles are linked to a specific fluid migration regime that may have existed in the conduit. It is however not clear whether this reflects a fluid migration that is syn- or post-intrusive or perhaps a combination of both.

7.6 Relationship between mineral content, abundance of xenoliths and the nature of the underlying country rocks

In this section semi-quantitative mineral assemblages as determined by XRD will be considered. The levels of these minerals are above five percent cumulatively, thus having the capability of influencing the froth floatation recovery negatively. A histogram is used in an attempt to determine the relationship between the total abundance of primary magmatic precursor minerals (olivine and pyroxene) and the total alteration minerals (amphibole, chlorite, serpentine and talc), encountered in the LHZBG and the PCR Units. It is placed alongside the percentage of xenoliths in the LHZBG Unit as well as the thickness in meters of the underlying Malmani dolomite and quartzite. The thickness of the MCR Unit is also given. The comparison is presented in Figure 7.15 and 7.16.

It appears that there is a weakly defined similar trend variation between the percentage xenoliths and the percentage of alteration minerals in the PCR Unit, and the thickness of the MCR Unit layer, with the exception of borehole UK48.
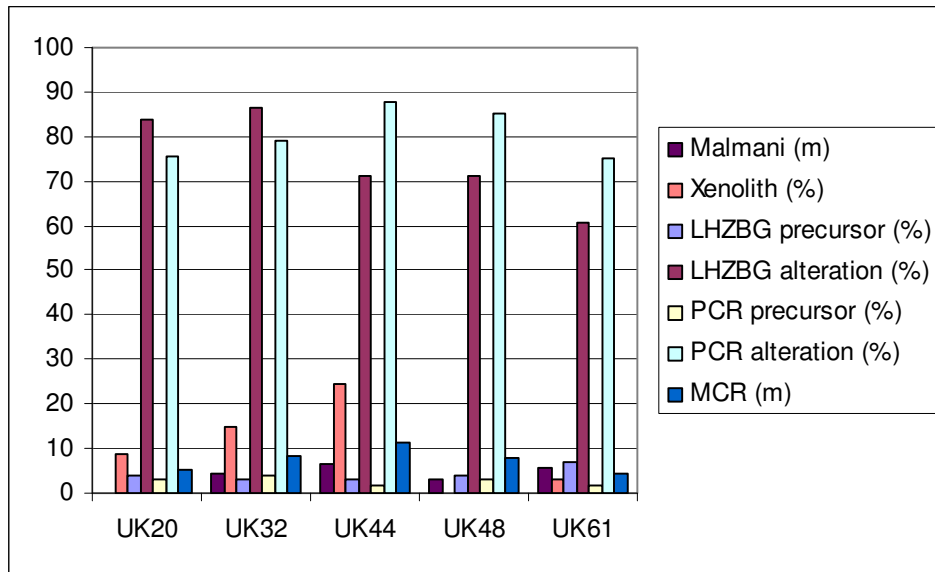
Figure 7.15. A histogram comparison (of a partial longitudinal section) between the percentage primary and alteration minerals in the LHZBG and PCR Units. The percentage xenoliths that forms part of the LHZBG Unit is also presented. The thickness of unassimilated Malmani dolomite and quartzite is also given. The thickness of MCR Unit is also included.
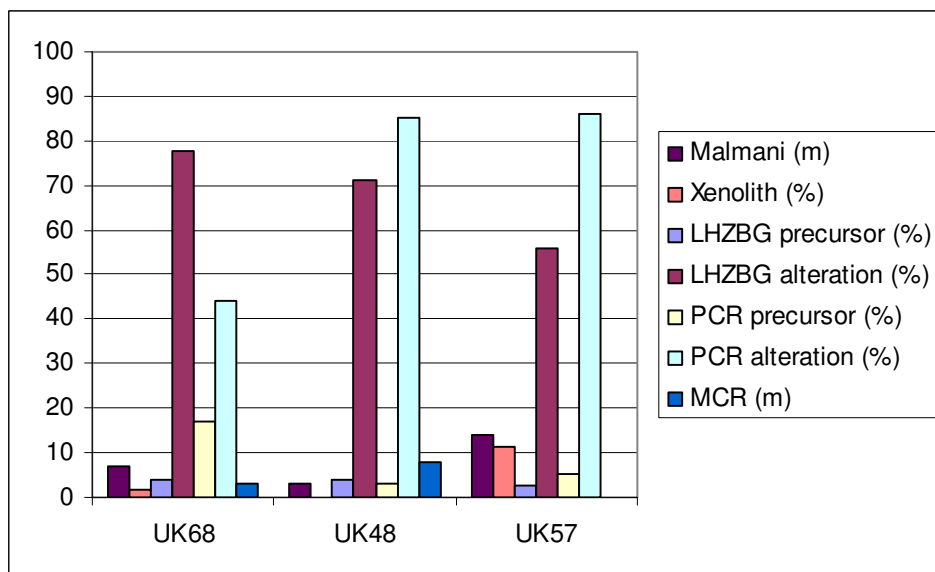
Figure 7.16. A histogram comparison (of a partial transverse section) between the percentage primary and alteration minerals in the LHZBG and PCR Units. The percentage xenoliths that forms part of the LHZBG Unit is also presented. The thickness of unassimilated Malmani dolomite and quartzite is also given. The thickness of MCR Unit is also included.

This comparison indicates that the samples taken from boreholes in the narrower part of the intrusion, and boreholes close to the edge of the Uitkomst Complex, especially in the PCR Unit, suffered less alteration, and therefore a greater preservation of the magmatic precursor minerals, relative to samples taken from boreholes further away from the edge of the Uitkomst Complex and in the broader part of the intrusion.

In general the total amount of alteration minerals in the LHZBG Unit appears to decrease in the broader part of the Uitkomst Complex in the study area, but in contrast appear to increase in the PCR Unit.

7.7 Significant implications of distribution of secondary minerals

The distribution of the secondary minerals may give an indication of the composition of the deuteric fluid(s) that influenced the intrusion. It was shown in the chapter dealing with secondary minerals that some minerals may only exist under certain temperature conditions with a specific X_{CO2}-content in the fluid. Amphibole, the most common secondary mineral in the intrusion, is not useful for delineating the fluid composition as it occurs in over too great a range. Minerals such as serpentine and chlorite will only develop under conditions with low X_{CO2}-content (Winkler, 1974). On the other hand, talc will only develop if the CO_2-partial pressure is high enough to stabilize the formation of it.

The cyclical nature of the LOI values, which is taken to represent the volatile content at the specific location, may give an indication as to the migration pattern of the deuteric fluid. The correlation between the LOI values and talc in the NE of the complex would suggest that it reflects the migration pattern of the CO_2-rich fluid. This fluid would have stabilized the formation of talc a height. The cyclical increase-decrease pattern, not correlating with a specific alteration mineral is noted in the SE of the complex. This may suggest that it represents the last deuteric regime, possibly of a later fluid, to affect that portion of the complex.

CHAPTER 8: CONSTRAINING THE EFFECT OF HYDROTHERMAL ALTERATION

In order to understand the effect that the alteration events had on the ultramafic to mafic rocks of the Uitkomst Complex, a geochemical approach was followed. Due to the fact that certain elements are mobilized more readily than others, and mobilization of some elements occurred in pairs, the composition of the altered rock differs from that of the original rock type. The aim of this chapter is to determine the extent of alteration in each of the units and determine if there is any detectable preferential distribution of elements during alteration. The degree of hydrothermal alteration is demonstrated with the use of the isocon diagram discussed in the next paragraph. Pseudo-sections were also modeled in an effort to constrain the fluid composition in terms of XCO_2 and XH_2O with temperature (T).

8.1 Isocon Diagram

The isocon diagram was developed by Grant (1986) to provide a simple graphical solution to Gresens' (1967) equations. The isocon method rearranges Gresens' equations into a linear relationship between the concentrations of components in the altered rock, relative to the concentration of components in the original rock. A simultaneous solution of these equations for all components, that show no relative gain or loss of mass, is defined as an "isocon". An isocon is represented by the straight line through the origin on a plot of concentrations in the altered rock against the concentrations in the original rock. The position of different elements plotted relative to the isocon gives an indication of the mobility of the elements. The slope of the isocon defines the mass change in the altered rock, whereas the deviation of a data point from the isocon defines the concentration change for that component.

In this study, the sample used as the "original" rock in the isocon for each mineralogical unit was the sample from the specific lithological unit exhibiting the most primitive mineral assemblages and displaying the least visible petrographic alteration. The samples with the least amount of alteration for the different units are the following: for the BGAB Unit, sample UK32N, for the LHZBG Unit, sample UK12J, for the xenoliths from the LHZBG

Unit, sample SH176, for the PCR Unit, sample UK12D and for the LrPRD Sub-unit, sample UK48C.

The x-axis marked"C_o" indicates the elemental concentration in the "original" rock and "C_a" on the y-axis indicates the concentration of elements in the "altered" rock.

One diagram for each of the lithological units is given (figures 8.1 to 8.3), along with a table indicating the immobile elements and the increase or decrease in elements relative to the isocon line. The least mobilized elements (< 10 %) are highlighted in the table in an effort to determine sympathetic variation of elements with Zr. Zr was selected as the isocon line of choice as Zr has been shown to be common and very stable in metamorphosed siliceous dolomite (Ferry, 2000). Zr is also not expected to be irregularly concentrated in mafic rocks, in contrast to felsic rocks in which a greater variance in the abundance of Zr may be possible, owing to the presence of zircon (Ferry, 2000).

The tables in which the isocon results are reported have been divided according to the mobility of the elements (Brownlow, 1979; Levinson, 1974). The mobile elements (section A of given table) are given as: Cl and S. The elements of high mobility (section B of given table) are given as: Mg, Ca, Na, Mo, Sr, U, Zn, F and V. The elements considered to be of medium mobility (section C of given table) are: As, Cu, Ni and Co. Elements considered having a low mobility (section D of given table) are: Si, K, P, Pb, Rb, Cs and Ba. Finally, the immobile elements (section E of given table) are: Ti, Al, Fe, Mn, Ga, Nb, Th, W, Y, Cr, Sc, La and Ce. The term "variable" in these tables refers to random enrichment and depletion of the samples relative to the "original" sample composition assumed.

8.2 Isocon analyses of the Lower Harzburgite Unit

Sample UK12J, a peridotite, is used as the original composition as it showed the least amount of alteration products. Sample UK12J contains, according to XRD analyses, 51 % diopside, which under the petrographic microscope appears unaltered and, after EMP analysis, was found to be diopside typical of the LHZBG Unit. Sample UK12J also contains chromite grains and minor olivine. Sample UK12J also contain very little sulphides. The diopside grains were replaced by some actinolite grains and contain pockets of chlorite. However, sample UK12J to appear to be the least altered of the sections encounted in the Uitkomst section. Some serpentine after olivine is also found in sample UK12J.

Most of the samples from the LHZBG Unit in this study show the effect of assimilation of dolomitic country rock and late stage hydrothermal alteration. Both may affect the composition or mobilization effects represented by the delta values obtained from the isocon analyses from this unit.

An example of an isocon from the LHZBG Unit is shown by Figure 9.2 and a summary of the increase and decrease in certain elements (delta value) relative to the Zr-isocon line is presented in Table 8.1.A to E. The elements that suffered less than 10% increase or decrease has been highlighted in the table.
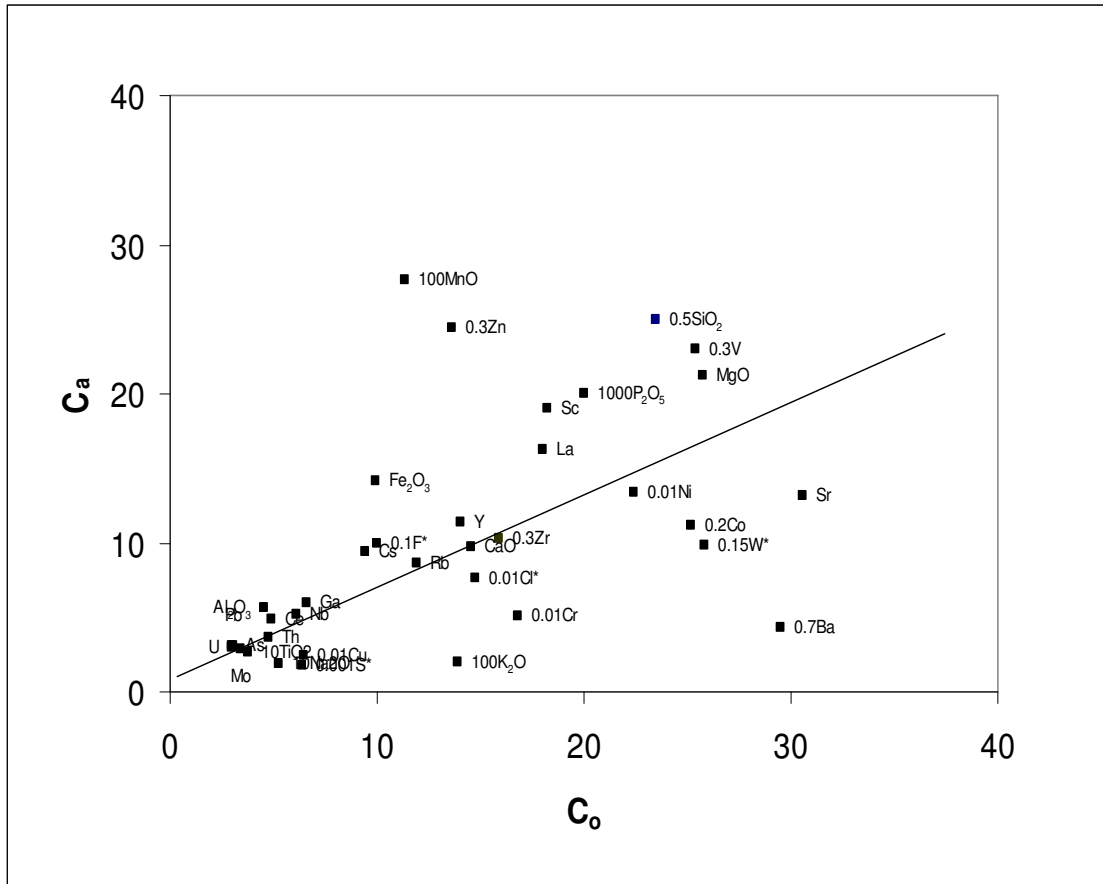
Figure 8.1. Isocon diagram for the LHZBG Unit using sample UK68G as C_a and based on sample UK12J, as unaltered composition C_o. The solid line indicates the Zr-isocon line. All elements marked with an asterix are to be considered semi-quantitative.

The elements in the area above the isocon line (Figure 8.1) indicate that those elements suffered a significant addition (positive delta values) in the sample and the elements in the area below the isocon suffered a significant loss (negative delta values) in the sample.

Table 8.1.A. The increase and decrease of mobile elements, relative to the Zr-isocon (expressed as delta values) for the LHZBG Unit. Sample UK12J is used as C_o (the least mobilized elements are highlighted).

Element	UK12H	UK12L	UK20G	UK20I	UK32G	UK32J	UK32L	UK44D	UK44G	UK44I	UK48L
Cl*	-48.38	90.03	15.75	-58.49	3.93	-80.33	-79.66	-49.10	-76.75	-68.34	-78.06
S*	-79.44	134.02	-71.55	68.98	229.89	-92.75	-93.76	-83.86	348.90	80.79	689.06
Element	UK48N	UK48O	UK48Q	UK57I	UK57K	UK61E	UK61F	UK68C	UK68E	UK68G	UK68I
Cl*	-72.46	-98.94	-96.45	-46.27	-82.13	-84.88	-77.77	-60.75	-87.27	-19.78	-97.29
S*	509.46	818.17	232.69	-16.23	717.57	583.46	475.34	16.11	416.69	-58.26	552.29

Element	Trend
Cl	Variably **depleted** in all samples, enriched in 12L, 20G and 32G.
S	**Enriched** in most samples, massively in UK48, 57, 61 and 68, but depleted in UK12H, 20G, 32J and L, 44D and 68G

Table 8.1.B. The increase and decrease of elements with high mobility, relative to the Zr-isocon (expressed as delta values) for the LHZBG Unit. Sample UK12J is used as C_o (the least mobilized elements are highlighted).

Element	UK12H	UK12L	UK20G	UK20I	UK32G	UK32J	UK32L	UK44D	UK44G	UK44I	UK48L
MgO	49.09	-45.10	93.17	154.65	158.22	-17.10	-9.58	76.06	52.18	-5.81	39.30
CaO	-38.98	-0.54	-70.02	-16.15	-19.40	-79.06	-50.88	-41.89	-42.97	-24.71	-55.11
Na$_2$O	-46.28	-21.50	-7.26	-39.19	24.15	-75.83	-72.22	-15.57	-71.41	-77.14	-41.08
Mo	-65.73	65.84	-64.53	26.46	17.70	-71.42	-41.99	-64.72	87.01	22.19	389.10
Sr	-64.24	197.78	-37.16	6.67	333.38	-65.77	-31.60	24.36	0.20	126.79	14.81
U	16.50	246.49	20.58	94.61	88.58	-33.61	-5.60	19.92	245.87	158.47	832.93
Zn	139.56	2.22	-31.50	65.46	109.54	-8.79	49.49	-16.36	25.49	70.23	63.58
F*	16.50	250.65	20.58	94.61	88.58	-33.61	-5.60	19.92	650.72	-7.83	467.43
V	72.11	38.48	-29.51	-18.17	23.98	-32.84	-7.44	-5.11	-76.43	-45.38	-45.33
Element	UK48N	UK48O	UK48Q	UK57I	UK57K	UK61E	UK61F	UK68C	UK68E	UK68G	UK68I
MgO	-21.97	166.44	47.57	69.27	-55.54	21.38	174.62	-6.74	24.39	27.23	-2.43
CaO	-22.91	-60.48	-65.01	14.49	87.63	57.37	64.02	-37.86	-42.23	3.94	-71.71
Na$_2$O	-27.99	-52.57	-82.86	-51.13	-75.55	-35.24	-53.92	-52.36	-88.14	-45.69	-72.49
Mo	343.81	316.07	97.27	-26.38	529.13	408.07	282.96	30.48	213.46	28.77	320.17
Sr	48.04	-9.12	-33.29	-51.71	1108.19	517.50	927.00	-56.40	8.92	-33.63	67.50
U	836.65	670.98	197.88	59.94	1520.63	1092.99	906.92	1.57	764.92	54.48	847.25
Zn	91.07	163.16	255.67	51.20	75.68	161.52	417.06	23.85	132.29	176.71	224.98
F*	24.13	105.56	18.73	59.94	913.44	632.15	151.50	1.57	23.90	54.48	214.16
V	75.90	-29.68	5.58	37.14	149.34	93.49	40.03	66.60	62.93	40.10	-7.65

Table 8.1.B. Continued.

Element	Trend
MgO	Variably **enriched**, but depleted in some samples
CaO	Variably **depleted** in all samples, excluding UK57 and 61 and 68G that is enriched. This may again be due the presence of micro-xenoliths or greater assimilation products in these samples
Na₂O	Variably **depleted** in all samples, but slightly enriched in UK32G.
Mo	Variably **enriched** in all samples, massively in UK48, 57 and 61, but depleted in UK12H, 20G, 32J and L, 44D and 57I.
Sr	Variably **depleted** and enriched in all samples. Most enriched in UK57 and 61
U	Variably **enriched** in all samples, but massively in UK48, 57, 61 and 68.
Zn	Variably **enriched** in all samples, increased enrichment with increase in depth in UK48 and 68. Depleted in UK20G, 32J and 44D.
F	Variably **enriched** in all samples, but depleted in UK32J and L and 44I.
V	**Variably** depleted and enriched, notably enriched in UK57, 61 and 68 depletingly enriched with depth.

Table 8.1.C. The increase and decrease of elements with medium mobility, relative to the Zr-isocon, (expressed as delta values) for the LHZBG Unit. Sample UK12J is used as C_o (the least mobilized elements are highlighted).

Element	UK12H	UK12L	UK20G	UK20I	UK32G	UK32J	UK32L	UK44D	UK44G	UK44I	UK48L
As	16.50	252.94	389.42	94.61	128.82	-33.61	-5.60	176.01	176.62	-7.83	23.56
Cu	-93.38	100.50	-42.73	77.03	-64.76	-69.87	-97.01	-25.45	364.88	119.15	343.60
Ni	-67.80	95.70	-44.84	116.45	170.05	-54.52	-62.22	-78.22	232.02	42.31	812.77
Co	-55.60	58.91	-22.84	108.45	356.13	-50.34	-24.41	-75.97	99.77	38.75	449.65
Element	UK48N	UK48O	UK48Q	UK57I	UK57K	UK61E	UK61F	UK68C	UK68E	UK68G	UK68I
As	24.13	307.85	34.19	111.49	29593.02	65.12	204.10	1.57	733.79	60.27	-9.69
Cu	456.60	135.08	1185.98	-63.53	918.94	398.49	47.06	9.05	1479.50	-42.26	1582.98
Ni	891.17	1283.23	92.24	66.83	699.46	740.90	643.68	7.14	148.27	-7.98	595.09
Co	52.72	186.12	45.53	31.43	399.21	449.50	358.50	6.48	602.48	-31.38	249.54

Table 8.1.C. Continued.

Element	Trend
As	Variably **enriched** in all samples, but massively enriched UK57K.
Cu	Variably **enriched** in all samples, massively in UK48, 57 and 68, but depleted in UK12H, 32, 57I and 68G.
Ni	Variably **enriched** in all samples, massively in UK48, 57 and 61 but depleted in UK12H, 20G, 32J and L and 44D
Co	Variably **enriched** in all samples, but depleted in UK12H, 20G, 32J and L, 44D and 68G.

Table 8.1.D. The increase and decrease of elements with low mobility, relative to the Zr-isocon, (expressed as delta values) for the LHZBG Unit. Sample UK12J is used as C_o (the least mobilized elements are highlighted).

Element	UK12H	UK12L	UK20G	UK20I	UK32G	UK32J	UK32L	UK44D	UK44G	UK44I	UK48L
SiO_2	29.70	-16.84	17.33	132.54	92.68	-20.59	-5.77	16.36	5.66	-5.22	-14.85
K_2O	-83.24	-86.79	-82.65	45.79	4.16	-90.45	-86.42	-82.74	-82.93	-86.74	-82.22
P_2O_5	16.50	23.54	20.58	94.61	88.58	114.62	-5.60	19.92	18.63	-7.83	23.56
Pb	266.41	171.16	81.00	481.60	266.24	179.55	151.00	390.89	16.24	11.63	524.75
Rb	-18.97	-15.83	-20.44	87.79	93.64	-49.15	-53.73	-44.26	42.19	-39.82	51.19
Cs	16.50	-8.18	20.58	94.61	88.58	-33.61	-5.60	19.92	18.63	-7.83	23.56
Ba	-34.34	-40.09	-76.13	-34.98	58.78	-66.36	-61.72	-76.51	-41.84	-78.98	-82.16

Element	UK48N	UK48O	UK48Q	UK57I	UK57K	UK61E	UK61F	UK68C	UK68E	UK68G	UK68I
SiO_2	4.93	81.22	22.44	82.22	-0.44	28.79	145.26	5.10	11.64	64.22	-29.32
K_2O	-82.14	-70.42	-82.92	-76.99	-76.68	-76.24	-63.81	-85.39	-82.17	-77.77	-87.00
P_2O_5	24.13	105.56	18.73	59.94	62.08	65.12	151.50	1.57	23.90	54.48	-9.69
Pb	193.84	955.40	225.03	56.72	58.82	1033.80	1071.90	132.13	79.17	56.41	514.38
Rb	48.47	93.17	-1.46	-44.57	86.59	74.14	193.38	-53.19	10.31	11.01	68.48
Cs	24.13	105.56	18.73	59.94	62.08	65.12	151.50	1.57	23.90	54.48	-9.69
Ba	-86.80	-78.14	-79.97	-46.59	-80.60	-67.62	-69.44	-77.75	-86.82	-77.57	-86.48

Table 8.1.D. Continued.

Element	Trend
SiO_2	Variably **enriched** and depleted. No vertical or lateral distribution pattern discernable.
K_2O	Variably **depleted** in all samples, but slightly enriched in UK20I and 32G.
P_2O_5	Variably **enriched** in all samples, but depleted in UK32L, 44I and 68I.
Pb	Variably **enriched** in all samples, mostly in UK48 and 61.
Rb	Variably **depleted** and enriched in all samples.
Cs	Variably **enriched** in most samples, but depleted in UK12L, 32J and L, 44I and 68I.

| Ba | Variably **depleted** in all samples, notably UK48 and 68, but enriched in UK32G. |

Table 8.1.E. The increase and decrease of immobile elements, relative to the Zr-isocon, (expressed as delta values) for the LHZBG Unit. Sample UK12J is used as C_o (the least mobilized elements are highlighted).

Element	UK12H	UK12L	UK20G	UK20I	UK32G	UK32J	UK32L	UK44D	UK44G	UK44I	UK48L
TiO$_2$	1.49	32.37	-36.43	-16.40	13.03	-4.36	2.74	2.75	-77.52	-45.85	-40.15
Al$_2$O$_3$	-19.46	-29.77	-77.93	-83.05	7.80	-24.68	91.33	-32.08	-99.74	-55.50	-99.73
Fe$_2$O$_3$	-15.73	12.52	57.14	131.06	132.08	-15.88	25.94	49.52	66.07	32.13	210.83
MnO	14.82	39.50	47.96	112.93	155.54	-40.48	57.33	78.89	52.78	52.37	48.97
Ga	16.52	0.33	-21.66	63.02	30.47	-11.69	16.61	6.83	-8.52	-33.20	-52.15
Nb	-34.74	32.17	-20.89	15.17	47.56	-24.81	-3.23	8.72	61.36	6.16	154.51
Th	-26.52	150.48	-23.94	22.76	18.96	-58.12	-40.45	-24.36	255.40	8.11	603.90
W*	-63.76	-31.38	-77.87	-60.69	-58.38	-97.68	-89.06	-74.96	-79.56	-90.71	-95.69
Y	-20.24	34.31	25.72	29.70	34.56	-27.34	-25.88	-16.93	14.48	-6.07	44.38
Cr	873.97	-46.70	-50.48	-66.27	-35.23	-91.97	-80.50	-85.38	-94.04	-91.87	-73.24
Sc	51.91	56.18	-27.81	26.58	83.17	-51.25	-16.85	17.27	-95.76	-77.46	-47.47
La	-8.14	6.39	11.21	55.15	78.42	-46.33	-1.35	6.22	35.48	-9.71	12.27
Ce	16.50	-8.18	20.58	94.61	88.58	120.23	131.53	45.34	18.63	-7.83	23.56
Element	UK48N	UK48O	UK48Q	UK57I	UK57K	UK61E	UK61F	UK68C	UK68E	UK68G	UK68I
TiO$_2$	15.24	-43.11	24.11	18.25	93.76	13.50	7.34	-5.99	-4.06	9.35	1.95
Al$_2$O$_3$	-67.82	-80.92	11.33	-13.31	-5.33	-99.64	75.56	23.27	52.80	92.38	-99.80
Fe$_2$O$_3$	193.48	271.52	94.09	19.04	283.25	217.58	350.55	44.10	100.95	119.81	146.88
MnO	87.76	67.50	33.18	113.98	237.21	169.38	335.94	57.46	72.28	276.98	-30.06
Ga	12.95	34.82	58.91	37.63	-8.65	-29.03	132.23	31.43	24.56	40.27	-23.67
Nb	137.62	192.76	59.99	-7.29	289.86	209.58	240.59	24.98	113.49	31.12	129.07
Th	590.31	607.01	165.03	0.89	839.71	754.92	542.88	8.65	337.52	20.21	552.65
W*	-95.67	-92.83	-95.86	-33.67	-69.15	-30.25	-91.23	-80.72	-69.83	-41.28	-96.85
Y	85.15	58.53	12.72	4.66	114.84	102.41	83.90	18.35	70.96	24.97	26.15
Cr	4.32	-85.39	-73.53	-15.10	-24.11	-11.62	-57.89	37.64	-16.75	-53.70	-92.29
Sc	106.92	-26.47	-14.68	38.87	128.82	59.74	68.94	78.06	114.62	60.93	-68.25
La	20.02	76.20	-14.93	49.62	87.13	88.35	121.83	-7.49	-2.57	39.44	-33.90
Ce	24.13	105.56	18.73	59.94	62.08	65.12	151.50	1.57	23.90	54.48	-9.69

Table 8.1.E. Continued.

Element	Trend
TiO_2	Variably enriched and **depleted**, UK57K notably enriched and 44G depleted.
Al_2O_3	Variable but mostly **depleted**. Enriched in UK32L, 48Q, 61F, 68C 68E and 68G. This may be due to the presence of micro-xenoliths or greater assimilation products in these samples.
Fe_2O_3	**Enriched** in most samples. Enriched with depth in UK68. Depleted in UK12H and 32J.
MnO	**Enriched** in all samples and increasingly with depth in UK12 and 20, except UK32G and 68I that is depleted
Ga	**Variably** enriched and depleted. Enriching with depth in UK48 and depleting in UK44**.**
Nb	**Variably** enriched in all samples, massively in UK48, 57 and 61 but depleted in UK12H, 20G, 32J and L and 57I**.**
Th	**Variably depleted** in samples UK12, 20, 32 and 44, but enriched in UK48, 57,61 and 68
W	**Variably depleted** in all samples and notably UK48.
Y	**Variably enriched** in all samples, but depleted in UK12H, 32J and L, 44D and I.
Cr	**Variably depleted** in all samples, notably UK32 and 44, but highly enriched in UK12H
Sc	**Variably** depleted and enriched, notably enriched in UK57, 61 and 68**.**
La	**Variably enriched** in all samples, but depleted in UK32J and L, 44I, 48Q, 68 C, E and I.
Ce	**Variably enriched** in all samples, but depleted in UK12L, 44I and 68I

No element appears to vary sympathetically with Zr. UK32L, UK44I and UK68C suffered the most mobilization of elements. UK32 and UK44 are samples that differ most often from the trend of enrichment or depletion relative to the other samples. UK32 and 44 are located in the NW central part of the broad part of the intrusion in the study area. The samples fall in the "talc rich zone" of the study area. UK48, 57 and 61, in the SE part of the broad part

of the complex, appear to have gained the most elements. Mo, Nb, Ni, Y, Th,, U, Y, Zn, S, and V seem to increase from the NW to the SE in the study area (Figure 10.0). The massive enrichment in especially U and Th towards the SE may be due to the fact that U, and for that matter Th if a U-Th coherence is assumed, forms highly mobile carbonate complexes (Dawood et al., 2004), which would precipitate once the hydrothermal fluid had cooled.

8.3 Isocon analyses of the calc-silicate xenoliths from the Lower Harzburgite Unit

Sample SH176 is used as the original composition as it showed the least amount of alteration products. The mineralogical composition of Sample SH176 has been found, by means of XRD analyses to be composed of 60 % diopside. EMP analyses revealed these diopside grains to be of fassaite composition. This sample also contains some epidote and grossular. Sample SH176 was chosen as representative of the original composition as it contains no visible sulphides and it was indicated by Hulley (2005) that the sulphides intruded the xenoliths as a late stage fluid, which may have affected the original composition. Dolomite values are not used as C_o value as it would demonstrate the recrystallization and formation of skarn minerals rather than the effects of alteration due to late stage fluids, the aspect this investigation is interested in.

An example of an isocon from the xenoliths from the LHZBG Unit is shown by Figure 8.2 and a summary of the increase and decrease in certain elements (delta value) relative to the Zr-isocon line is presented in Table 9.3.A to E. The elements that suffered less than 10% increase or decrease has been highlighted in the table.

Table 8.2.A to E. has been arranged in such a manner that the isocon results are listed, from right to left, according to a decrease in the total amount of alteration minerals, as determined by XRD analyses.
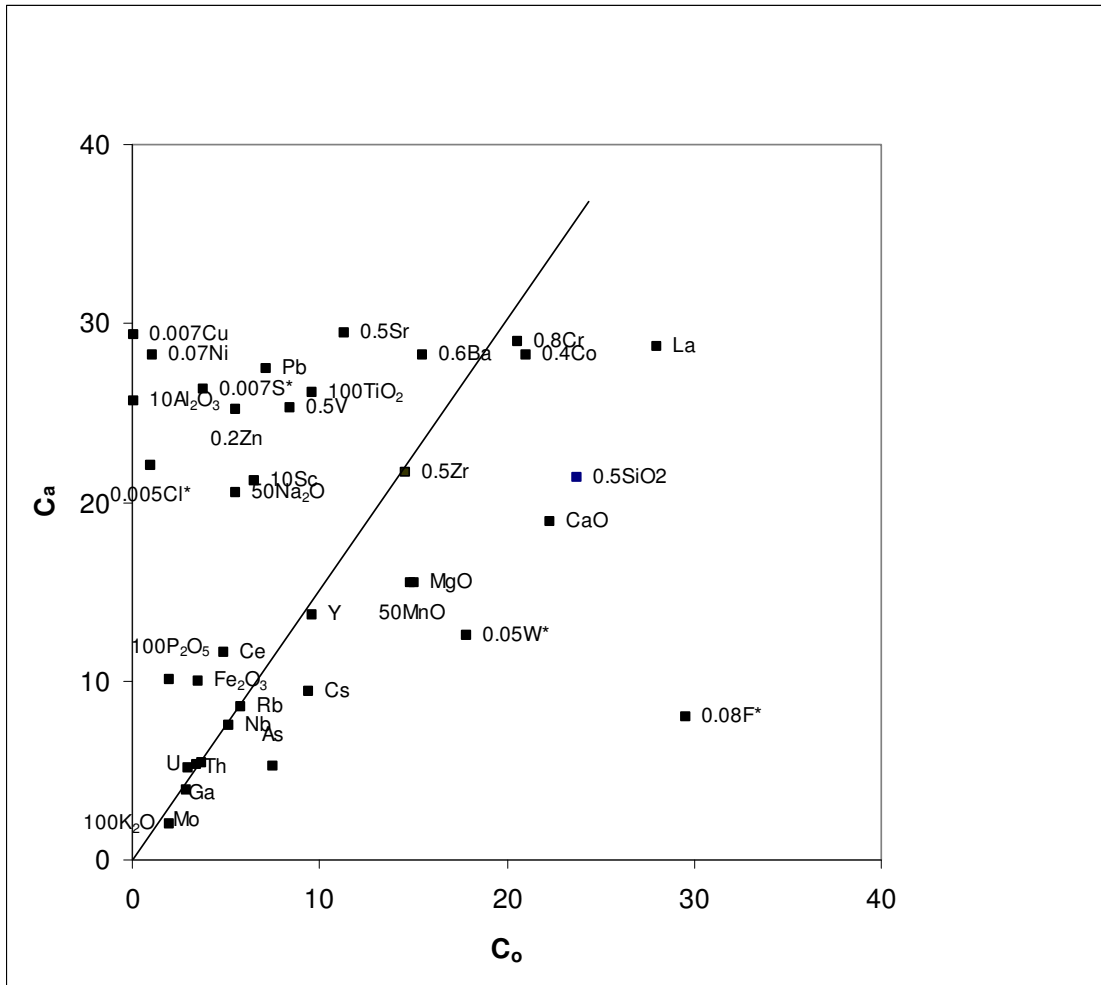
Figure 8.2. Isocon diagram for the xenoliths from the LHZBG Unit using sample UK3O as C_a and based on sample SH176, as unaltered composition C_o. The solid line indicates the Zr-isocon line. All elements marked with an asterix are to be considered semi-quantitative.

The elements in the area above the isocon line (Figure 8.2) indicate that those elements suffered a significant addition (positive delta values) in the sample and the elements in the area below the isocon suffered a significant loss (negative delta values) in the sample.

Table 8.2.A. The increase and decrease of mobile elements, relative to the Zr-isocon (expressed as delta values) for the xenoliths in the LHZBG Unit. Sample SH176 is used as C_o (the least mobilized elements are highlighted).

Element	UK12I	UK3O	UK48G	UK3U	UK3N	Trend
Cl*	-11.54	-93.17	132.27	-17.31	-91.76	Variable **depleted**, enriched in UK48G
S*	158.12	-78.55	-74.69	-82.92	-95.50	Variable **depleted**, enriched in UK12I

Table 8.2.B. The increase and decrease of elements with high mobility, relative to the Zr-isocon (expressed as delta values) for the xenoliths LHZBG Unit. Sample SH176 is used as C_o (the least mobilized elements are highlighted).

Element	UK12I	UK3O	UK48G	UK3U	UK3N	Trend
MgO	2037.11	44.51	450.62	44.97	25.63	**Enriched**, highly in UK12I
CaO	2001.68	75.65	548.83	37.78	-21.94	Variable **enriched**, highly in UK12I
Na$_2$O	-83.51	-59.84	251.04	-26.03	-42.14	Variable **depleted**, but enriched in UK48G
Mo	2097.80	11.06	121.16	-12.56	-60.16	**Variable**
Sr	-68.56	-42.62	-83.15	-70.21	-94.89	**Depleted**
U	767.82	-4.46	36.12	-29.30	-75.82	Variable **enriched** with alteration
Zn	676.18	-67.17	111.58	-38.48	-67.26	**Variable**
F*	425.00	449.72	1644.87	330.18	-24.52	Variable **enriched**, depleted in UK3N
V	43.46	-50.59	372.38	-6.91	-28.49	**Variable**, highly enriched in UK48G

Table 8.2.C. The increase and decrease of elements with medium mobility, relative to the Zr-isocon, (expressed as delta values) for the xenoliths from the LHZBG Unit. Sample SH176 is used as C_o (the least mobilized elements are highlighted).

Element	UK12I	UK3O	UK48G	UK3U	UK3N	Trend
As	1792.90	113.99	233.83	220.31	110.76	**Enriched**, highly in UK12I
Cu	-76.66	-99.56	-97.40	-99.51	-99.86	**Depleted**
Ni	-79.22	-94.36	-97.91	-95.44	-99.22	**Depleted**
Co	507.53	11.38	157.27	-4.07	-62.88	**Variable**

Table 8.2.D. The increase and decrease of elements with low mobility, relative to the Zr-isocon, (expressed as delta values) for the xenoliths from the LHZBG Unit. Sample SH176 is used as C_o (the least mobilized elements are highlighted).

Element	UK12I	UK3O	UK48G	UK3U	UK3N	Trend
SiO$_2$	505.65	65.61	386.50	34.57	17.34	**Enriched**
K$_2$O	-94.59	48.82	-78.07	28.29	-15.59	**Variable**
P$_2$O$_5$	-64.84	-70.48	372.38	28.29	-59.32	**Variable,** highly enriched in UK48G
Pb	407.54	-60.97	130.34	207.90	102.59	Variable **enriched**, depleted in UK3O
Rb	-14.59	-0.29	-17.69	7.64	-43.07	Variable **depleted**
Cs	658.14	48.82	372.38	28.29	-15.59	Variable **enriched**, depleted in UK3N
Ba	-87.41	-18.41	360.00	57.34	9.39	**Variable**, highly enriched in UK48G

Table 8.2.E. The increase and decrease of immobile elements, relative to the Zr-isocon, (expressed as delta values) for the xenoliths from the LHZBG Unit. Sample SH176 is used as C_o (the least mobilized elements are highlighted).

Element	UK12I	UK3O	UK48G	UK3U	UK3N	Trend
TiO$_2$	-7.41	-45.02	87.66	-14.37	3.72	Variable **depleted**, highly enriched in UK30
Al$_2$O$_3$	-99.60	-99.42	-99.21	28.29	-15.59	Variable mostly **depleted**
Fe$_2$O$_3$	553.77	-47.57	45.89	-38.83	-68.21	**Variable**, highly enriched in UK12I
MnO	2525.31	43.55	407.81	51.98	-32.54	Variable **enriched**, highly in UK12I
Ga	73.95	0.68	46.87	106.04	6.24	Variable **enriched**
Nb	221.14	2.38	151.50	-15.36	-47.69	**Variable**
Th	289.59	-12.74	-9.39	-33.88	-75.23	Variable **depleted** with alteration
W*	897.76	112.03	418.59	66.06	55.18	Variable **enriched**
Y	272.42	4.91	82.24	8.56	-50.91	Variable **enriched**, depleted in UK3N
Cr	-55.94	5.95	-37.60	41.81	84.49	Variable **depleted** with alteration
Sc	-42.68	-54.21	372.38	28.29	-15.59	**Variable**, highly enriched in UK48G
La	820.09	45.42	410.71	26.26	-28.65	Variable **enriched**, depleted in UK3N
Ce	-22.71	-37.09	61.83	28.29	-15.59	**Variable**

No element appears to vary sympathetically with Zr. UK3 O and U appear to have suffered the least mobilization of elements.

8.4 Isocon analyses of the Chromitiferous Harzburgite Unit

Sample UK12D is used as the original composition as it showed the least amount of alteration products and is located outside of the talc-rich area. Investigation under a petrographic microscope revealed sample UK12D to be composed of mainly fairly unaltered precursor mafic minerals. XRD analyses indicated that sample UK12D is composed of 12 % olivine, 21 % diopside, 20 % hornblende as well as 8 % chromite. EMP analyses revealed the olivine to be magmatic fosterite and the diopside as also being derived from a magmatic source. The main alteration minerals present is talc (10 %) and chlorite (14 %) after diopside.

Most of the samples from the PCR in this study show the effect of late stage deuteric hydrothermal alteration. All of the samples taken from the talc-rich area have been almost completely replaced by secondary minerals.

An example of an isocon from the PCR is shown by figure 8.3 and a summary of the increase and decrease in certain elements (delta value) relative to the Zr-isocon line is presented in Table 8.3.A to E. The elements that suffered less than 10% increase or decrease has been highlighted in the table.
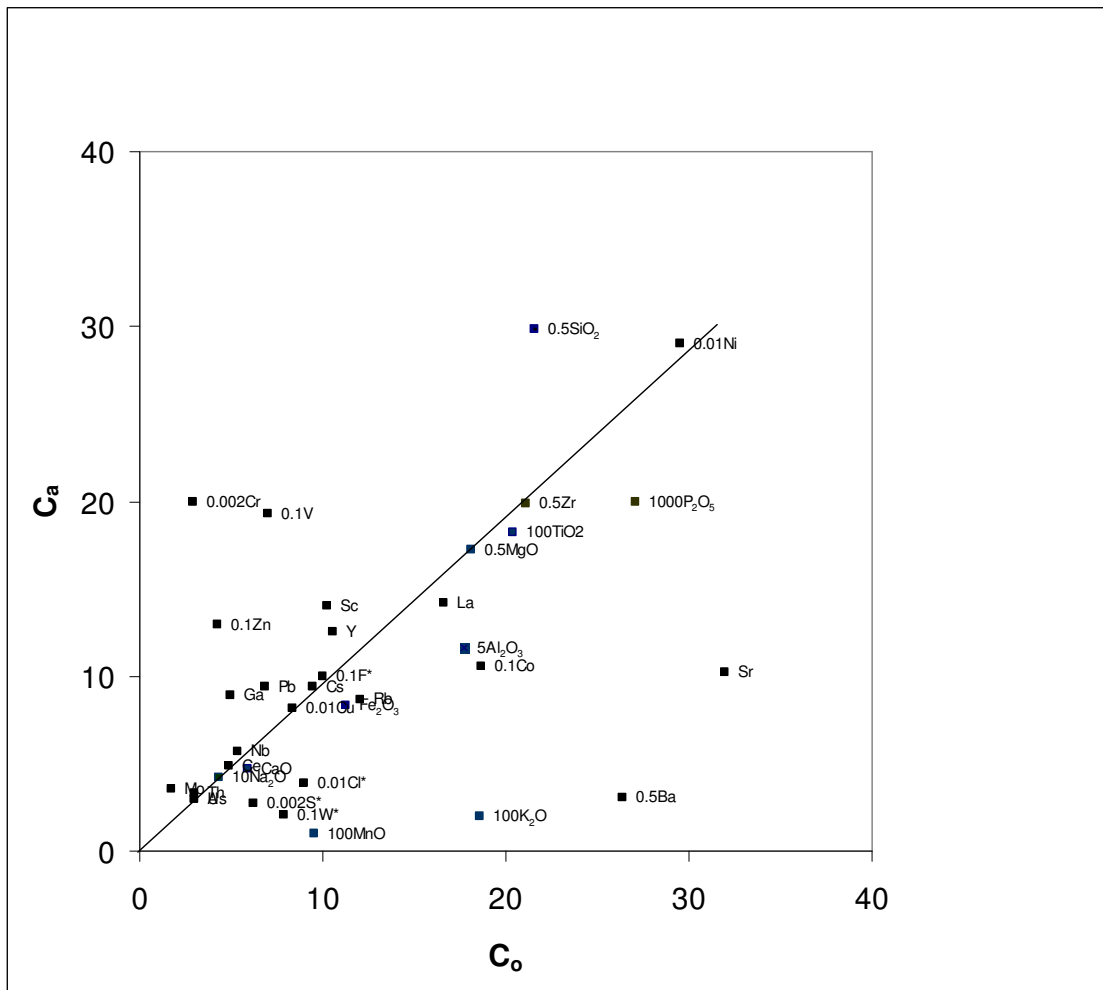

Figure 8.3. Isocon diagram for the PCR using sample UK32B as C_a and based on sample UK12D, as unaltered composition C_o. The solid line indicates the Zr-isocon line. All elements marked with an asterix are to be considered semi-quantitative.

The elements in the area above the isocon line (Figure 8.3) indicate that those elements suffered a significant addition (positive delta values) in the sample and the elements in the area below the isocon suffered a significant loss (negative delta values) in the sample.

Table 8.3.A. The increase and decrease of mobile elements, relative to the Zr-isocon (expressed as delta values) for the PCR Unit. Sample UK12D is used as C_o (the least mobilized elements are highlighted).

Element	UK12A	UK12G	UK20B	UK20D	UK32B	UK32D	UK44A	UK44C	UK48E	UK48G
Cl*	-6.37	18.81	-40.13	31.54	-26.78	-0.52	118.65	-6.52	-68.61	-10.08
S*	194.43	221.11	38.32	369.29	105.55	214.90	370.63	329.56	309.89	133.92
Element	UK48J	UK57A	UK57D	UK57F	UK57H	UK61A	UK61B	UK61C	UK61D	UK68A
Cl*	3.03	15.74	-15.59	-7.96	-21.75	3.70	9.88	2.06	-3.78	20.91
S*	706.57	136.73	-3.89	60.01	1150.24	423.31	94.08	46.80	7.29	873.18

Element	Trend
Cl	**Variably** depleted and enriched, notably enriched in UK48E.
S	Variably **enriched** in all samples.

Table 8.3.B. The increase and decrease of elements with high mobility, relative to the Zr-isocon (expressed as delta values) for the PCR Unit. Sample UK12D is used as C_o (the least mobilized elements are highlighted).

Element	UK12A	UK12G	UK20B	UK20D	UK32B	UK32D	UK44A	UK44C	UK48E	UK48G
MgO	-1.15	11.07	-0.37	63.77	0.65	-58.48	91.45	8.00	-8.66	12.74
CaO	-84.68	-43.84	-76.87	10.97	-15.84	38.04	-17.37	-10.41	-78.40	-66.44
Na$_2$O	-73.27	-10.46	-28.44	11.95	1.47	-39.66	-42.60	23.17	-56.81	-35.09
Mo	280.36	241.53	390.63	-9.43	114.88	15.38	2.09	-5.86	-53.24	24.91
Sr	-67.53	-38.48	-57.49	-31.36	-66.24	-34.64	-27.67	13.31	-84.70	-55.27
U	230.59	136.30	339.48	57.03	5.84	-25.21	77.01	4.93	-18.93	-1.18
Zn	-6.39	317.96	274.02	57.03	28.42	-25.21	77.01	141.52	-18.93	-1.18
F*	-74.12	131.75	-57.85	74.65	51.57	-48.77	-29.15	-80.94	498.86	689.07
V	-71.26	252.63	-51.98	-13.93	143.23	-61.44	28.25	8.83	-24.68	17.86
Element	UK48J	UK57A	UK57D	UK57F	UK57H	UK61A	UK61B	UK61C	UK61D	UK68A
MgO	51.40	-14.93	-0.22	38.48	74.97	14.69	-32.86	-7.60	-1.18	38.30
CaO	-7.43	-49.49	-93.34	73.60	80.18	-58.45	7.60	23.69	69.68	-71.94
Na$_2$O	-24.77	-36.31	-63.29	-42.94	-15.92	-49.12	-38.96	-79.71	-67.97	-70.35
Mo	-9.39	173.14	-43.43	-5.82	71.16	365.65	109.92	-41.45	-38.88	767.02
Sr	-56.18	-70.44	-87.89	-52.78	-55.62	-48.36	-59.49	153.12	209.51	-19.26
U	57.09	146.90	-1.91	63.29	82.08	336.51	37.38	1.52	5.97	849.90
Zn	211.69	-2.27	29.70	29815.89	82.08	35.80	-15.09	583.16	9.94	43.06
F*	957.10	40.02	2.31	705.46	827.26	232.09	-10.42	103.42	-36.88	1001.02
V	-30.54	-51.42	-70.38	1117.25	580.92	358.61	-63.55	-10.75	-54.48	165.32

Table 8.3.B. Continued.

Elements	Trend
MgO	Depleted in UK32D, 48E, 57A and **enrich**ing with increasing depth in UK12, 20, 57 and 61.
CaO	Decreasingly **depleted** with increasing depth in UK12, 20, 32, 48 and significantly depleted in UK57D.
Na$_2$O	Decreasingly **depleted** with increasing depth in UK 12, 20, 32, 44 and 48. UK61C significantly depleted.
Mo	**Variably** enriched and depleted.
Sr	Variably **depleted** in all samples, but enriched in UK44C and 61C and D.
U	Variably **enriched** in all samples, but depleted in UK32D, 48E and G and 57D.
Zn	Variably **enriched** in most samples. Massively in UK57H
F	**Variably** enriched and depleted. Most notably in the central part.
V	**Variably** enriched and depleted. UK57 massively enriched.

Table 8.3.C. The increase and decrease of elements with low mobility, relative to the Zr-isocon, (expressed as delta values) for the PCR Unit. Sample UK12D is used as C$_o$ (the least mobilized elements are highlighted).

Element	UK12A	UK12G	UK20B	UK20D	UK32B	UK32D	UK44A	UK44C	UK48E	UK48G
As	403.39	54.09	-7.85	167.78	5.84	-25.21	77.01	195.10	-11.96	180.87
Cu	11.60	219.42	-40.38	-32.62	-40.28	-85.79	-59.56	-44.76	-12.83	5.84
Ni	-3.60	25.27	21.35	82.35	44.81	181.34	129.20	16.49	-24.25	-18.80
Co	-72.46	96.39	-72.89	2.04	-33.94	-67.81	8.77	-69.13	220.89	253.32
Element	UK48J	UK57A	UK57D	UK57F	UK57H	UK61A	UK61B	UK61C	UK61D	UK68A
As	84.39	-13.52	10.08	63.29	96.66	461.56	-15.09	202.47	669.91	618.36
Cu	-37.75	-52.94	-40.17	-25.25	58.19	-38.86	-44.22	-77.76	-49.08	450.07
Ni	199.96	39.95	-4.59	107.40	117.76	116.04	73.51	32.56	-9.82	-55.35
Co	217.97	43.68	-54.85	533.86	460.25	71.01	9.08	156.83	-11.67	565.54

Table 8.3.C. Continued.

Element	Trend
As	**Enriched** in most samples.
Cu	**Depleted** in most samples, but decreasing depletion with depth in UK12, 20, 44, 57. Significantly enriched in UK68A.
Ni	**Enriched** in most samples. Depleting with depth in UK61
Co	**Variably** enriched and depleted. More enriched towards the SE.

Table 8.3.D. The increase and decrease of elements with low mobility, relative to the Zr-isocon, (expressed as delta values) for the PCR Unit. Sample UK12D is used as C_o (the least mobilized elements are highlighted).

Element	UK12A	UK12G	UK20B	UK20D	UK32B	UK32D	UK44A	UK44C	UK48E	UK48G
SiO_2	23.86	-4.10	-8.67	75.74	46.46	-12.06	94.84	20.16	-18.92	7.13
K_2O	-89.91	-88.28	-16.16	-83.07	-88.59	691.62	-47.38	13.02	-9.78	62.80
P_2O_5	-30.94	-19.79	-28.49	15.85	-21.92	-44.83	30.58	-3.74	-40.19	-27.10
Pb	51.94	8.67	-19.18	-31.40	44.71	0.74	-14.56	66.36	14.52	-43.12
Rb	-33.08	-8.77	36.64	-52.04	-23.73	432.45	21.40	27.43	1.39	60.75
Cs	-6.39	8.73	-7.85	57.03	5.84	-25.21	77.01	4.93	-18.93	-1.18
Ba	-92.04	-78.92	-77.25	-43.68	-87.76	-39.68	-19.86	-51.45	-65.19	-37.72

Element	UK48J	UK57A	UK57D	UK57F	UK57H	UK61A	UK61B	UK61C	UK61D	UK68A
SiO_2	107.64	16.16	45.94	116.49	113.58	4.40	-2.50	25.29	22.69	8.55
K_2O	-45.87	-90.68	-89.42	-82.39	-80.37	102.94	-90.84	-89.05	-88.58	-84.58
P_2O_5	15.89	-36.20	-27.64	20.47	34.33	-17.15	-37.36	-25.11	-21.82	5.54
Pb	86.99	11.92	-57.15	-28.67	-20.46	9.58	-62.91	-30.34	-53.71	440.50
Rb	40.53	-27.64	-81.31	-65.80	-31.09	83.22	-39.61	-76.94	-46.44	51.53
Cs	57.09	-13.52	-1.91	63.29	82.08	12.31	-15.09	1.52	5.97	43.06
Ba	-29.89	-92.65	-87.47	-71.78	-62.16	-26.35	-82.27	-76.30	-75.59	-87.84

Table 8.3.D. Continued.

Element	Trends
SiO_2	Variably **enriched** in most samples, but depleted in UK12G, 20B, 32D, 48E and 61B
K_2O	**Depleted** in most samples, but largely enriched in UK32D.
P_2O_5	**Depleted** in most samples, but with decreasing depletion with increasing depth in UK12, 20, 48, 57 and part of 61.
Pb	**Variably** enriched and depleted. Massively enriched in UK68A**.**
Rb	**Variably** enriched and depleted**.**
Cs	**Variable.** Enriching with depth in UK12, 20, 48, 57 and lower 61. Depleting with depth in UK32, 44 and top 61.
Ba	**Depleted** in all samples, but decreasingly depleted with depth in UK12, 20, 32 and 57**.**

Table 8.3.E. The increase and decrease of immobile elements, relative to the Zr-isocon, (expressed as delta values) for the PCR Unit. Sample UK12D is used as C_o (the least mobilized elements are highlighted).

Element	UK12A	UK12G	UK20B	UK20D	UK32B	UK32D	UK44A	UK44C	UK48E	UK48G
TiO_2	-17.66	-28.51	52.87	-8.67	-5.56	34.89	50.60	3.66	-25.43	-7.63
Al_2O_3	-42.97	-8.90	37.01	-73.37	-30.49	22.28	117.82	-4.25	-37.55	-76.71
Fe_2O_3	-12.48	59.62	7.60	13.44	-21.83	-17.29	34.54	14.89	-17.05	-7.82
MnO	-90.18	11.06	-90.33	64.71	-88.90	98.08	123.51	28.57	-58.99	-89.63
Ga	156.62	-18.14	255.80	-1.93	91.49	7.24	147.64	16.68	0.95	13.33
Nb	50.06	49.39	75.78	-41.67	12.49	-24.53	-34.25	0.05	-47.22	7.36
Th	274.51	304.90	377.23	57.03	17.24	-25.21	77.01	4.93	-18.93	-1.18
W*	128.72	-91.71	53.53	-47.37	-72.47	-65.35	-67.46	-63.97	-93.82	-38.36
Y	-2.31	35.47	21.09	-15.71	26.01	-31.14	24.11	-2.96	-18.49	-26.18
Cr	-47.56	56.51	-39.54	-7.07	-17.18	-15.31	81.44	-4.86	66.98	89.17
Sc	-3.60	25.27	21.35	82.35	44.81	181.34	129.20	16.49	-24.25	-18.80
La	-36.50	-0.60	-20.19	62.11	-9.59	3.31	137.52	3.58	-17.88	-12.20
Ce	-6.39	8.73	-7.85	57.03	5.84	36.87	291.45	4.93	-18.93	-1.18
Element	UK48J	UK57A	UK57D	UK57F	UK57H	UK61A	UK61B	UK61C	UK61D	UK68A
TiO_2	45.89	-17.31	-36.64	8.96	49.82	132.91	52.78	-3.45	54.57	-57.97
Al_2O_3	-0.81	-25.87	-99.72	0.12	9.28	342.87	65.35	-49.75	-94.86	-99.60
Fe_2O_3	43.66	-33.93	-42.80	20.14	84.90	29.12	-12.72	-24.40	-15.18	166.13
MnO	107.63	-90.93	-71.60	152.51	206.94	-88.22	-38.13	61.41	121.35	-25.00
Ga	98.68	91.47	-26.76	88.45	44.32	490.38	82.83	-20.19	0.99	-42.06
Nb	-9.26	32.73	-48.41	-6.51	26.05	92.31	-2.89	-52.70	-45.50	186.05
Th	57.09	215.20	-1.91	63.29	82.08	380.24	37.91	1.52	5.97	978.62
W*	-32.26	-26.50	-92.53	-25.89	99.92	29.36	83.06	-79.45	-81.94	-89.10
Y	17.37	15.09	-59.53	20.14	33.56	21.39	8.14	-12.97	-13.76	70.19
Cr	123.73	16.52	-43.14	292.79	241.38	52.09	4.49	74.92	-10.06	262.84
Sc	199.96	39.95	-4.59	107.40	117.76	116.04	73.51	32.56	-9.82	-55.35
La	35.03	-23.66	-1.44	73.12	94.24	-10.53	-3.55	10.43	20.92	36.10

| Ce | 57.09 | -13.52 | 212.90 | 63.29 | 82.08 | 12.31 | -10.50 | 8.01 | 19.76 | 43.06 |

Table 8.3.E. Continued.

TiO$_2$	Variably depleted and **enriched**, notably enriched UK61A.
Al$_2$O$_3$	Variably **depleted** and enriched, notably enriched 61A.
Fe$_2$O$_3$	Variably **enriched** and depleted.
MnO	Most samples variably highly **enriched** and slightly depleted.
Ga	**Enriched** in most samples, but depleted with depth in UK12, 20 and 32. Enriching with depth in UK48.
Nb	**Variably** enriched and depleted.
Th	Variably **enriched** in all samples, but depleted in UK32D, 48E, G and 57D. Massively in UK68A
W	Variably **depleted** in most samples. Less depleted with depth in UK48, 57.
Y	**Variably** enriched and depleted. Depleted with depth in UK20, 32, 44 and 61
Cr	**Variably** depleted and enriched. Most notably in the central part.
Sc	Variably **enriched** in all samples, but depleted in UK12A, 48E and G, 57D, 61D and 68A. Enriched with depth in UK12, 20, 32 and depleted with depth in UK44 and 61.
La	**Variable**. Enriching with depth in UK12, 20, 32, 48, 57 and 61.
Ce	**Enriched**. Enriching with depth in UK12, 20, 32, 48 and lower 61.

No element appears to vary sympathetically with Zr. It would appear that UK44C, UK48G and UK57D suffered the least mobilization of elements. It would appear that a significant number of elements are either depleted or enriched with depth. This may indicate mobilization of elements by a deuteric system.

8.5 Discussion of isocon results for the units

It was suggested by van Zyl (1996) that the Uitkomst Complex was affected by a deuteric late-stage fluid. The isocon method was employed to test this hypothesis and determine the

amount of elemental mobilization in such a system. It is conceivable that flow regimes may have developed in the fluid-enriched environment of the Uitkomst Complex's basal units, which would have contributed to redistribution of the compatible and incompatible trace elements.

The LHZBG Unit shows some spatial variation in element enrichment or depletion that may be related to a difference in conditions in the narrow relative to the broad part of the intrusion in the study area. It has been indicated that Mo, Nb, Ni, Y, Th, U, Y, Zn, S, and V increase in content from the NW to the SE. This may indicate mobilization of some elements that was then transported in the direction of indicated magma flow, and deposited in the broadening area of the intrusion. It has been shown that the massive increase in the U content towards the SE may due to the formation of a carbonate complex which would be able to transport it away from the source area to where it could precipitate due to cooling of the fluid (Dawood et al., 2004). With the exception of Fe_2O_3, MnO and Zn, no other major or trace elements show a spatial variation either increasing or decreasing with height. This may indicate that the final distribution of major and trace elements may be a function of the degree of assimilation of country rock by the intruding ultramafic magma or slight variations in the composition of the intruding magma. Here the selection of the C_o sample was again problematic, due to the high alteration mineral content in most samples from this unit. In this unit the most pristine sample was again selected with the same assumption as noted previously.

The xenoliths located in the LHZBG Unit was also variably enriched and depleted in both major and trace elements. This may be due to the compositional variation in the fluids that was expelled by the xenolith during the period it was subjected to partial assimilation or the composition of the fluid that infiltrated the xenolith at a late stage. As with the previous units, the selection of the C_o sample was problematic due to the presence of alteration minerals in all samples, again the most pristine samples was selected and assumed to represent the composition most akin to the original, unaltered composition.

The PCR Unit show a weakly defined spatial distribution of some major and trace elements that indicate a vertically moving themo-chemical agent may be responsible for the final distribution of the elements with height. Most of the elements show a vertical variation that changed with depth. This variation may indicate that the thermochemical agent suffered a loss in ability to transport the mobilized elements as it migrated upwards. However not all of the major and trace elements where mobilized in all of the sampled boreholes show the same variation. The irregular variation may indicate that the thermochemical conditions varied with position in the intrusion. The major and trace elements do not indicate a spatial variation in the horizontal distribution of elements. It should be noted again that the selection of the C_o sample was problematic, but was selected using the same criteria as noted before.

8.6 Compositional pseudo-sections

In order to constrain the temperature and CO_2-partial pressure that prevailed in the LHZBG and PCR units, during formation of the observed mineral assemblages, pseudo-sections were generated. The pseudo-sections were generated by means of the *Perple_X* (Connelly, 2005) modelling software version 7. The dataset used was the 2004 unpublished version of the Holland and Powell (1998) thermo dataset.

Two samples were selected for the LZHBG and PCR each. The bulk chemistry of the sample, as determined by XRF analyses, were used to generate the pseudo-sections. The T-X_{CO_2} for these samples are calculated and reported for the specific bulk composition, with a-x models that are appropriately complex to be representative of the observed mineralogy. The T-M_{H_2O} pseudo-sections represent adding progressively higher amounts of water to an anhydrous bulk composition. All the pseudo-sections are constructed at 3 Kbar

8.7 Limitations of pseudo-sections

The modelling of alteration processes performed using Perple_X is limited to low temperature environments, such as the observed talc-bearing assemblages. Higher temperature alteration processes resulting in e.g. pure fassaitic-diopside is not amenable to

such modelling as too few associated minerals developed to constrain the T-X conditions. Cr-bearing minerals cannot be modelled and a Cr-free system involving a spinel solid solution is assumed. Particular protolith rock types are assumed for the LHZBG and PCR. The LHZBG is assumed to be a harzburgite, but is skewed to favour diopside. The PCR is assumed to be a harzburgite-peridotite. The precursor mineralogy is used to check the corresponding alteration assemblages observed and calculated. The absence of K-bearing primary minerals precludes considering mica minerals in the retrograde assemblages, owing to the retrograde assemblages not having isochemical equivalents of the magmatic rocks. This particular approach does not allow discrimination between areas that were subject to the metasomatic effects of near similar fluids. This would require additional data on fluid fluxes that is not supported by the current spatial information available.

8.8 Modelling Results

The abbreviations used in the pseudo-sections are given in Table 8.4.

Table 8.4. Definitions of abbreviations used in pseudo-section models.

Abbreviation	Definition
Feldspar	Na-Ca plagioclase
Ol(HP)	Olivine solid solution
Opx (HP)	Orthopyroxene solid solution
Cpx (HP)	Clinopyroxene solid solution
cAmph(DP)	Ca-Na-Fe-Mg amphibole solid solution, which will be either hornblende or tremolite-actinolite depending on grade
Atg	Antigorite solid solution
T	Talc solid solution
Dol(HP)	Dolomite-magnesite solids solution
oCcM(HP)	Calcite-magnesite solid solution
Chl	Chlorite solid solution
q	Quartz
sid	Siderite
ky	Kyanite
ab	Pure albite

(Abbreviations after: http://www.perplex.ethz.ch/PerpleX_solution_model_glossary.html)

8.8.1 Lower Harzburgite Unit

Two samples were selected and modelled to be representative of the LHZBG unit, namely UK20G and UK48Q. The preserved primary magmatic mineral in these samples is olivine. Calcite has been texturally interpreted to represent relict country rock or xenolith inclusion, but may also represent secondary mineralogy. The secondary minerals for both samples are: amphibole (actinolite-tremolite), chlorite, dolomite, serpentine and talc. Based on the petrography, the formation of chlorite and serpentine is indicated to have formed last owing to the pocketed occurrence of these two minerals.

In Figure 8.4 (UK20G) and Figure 8.6 (UK48Q) it is indicated that the $T-X(CO_2)$ conditions that satisfy the mineral assemblages observed in both these samples are not present in the range of calculated conditions. The presence of either feldspar, albite or orthoproxene excludes these assemblages of being representative of the conditions that prevailed in the LHZBG at the time of formation.

The assemblages observed in the samples from UK20G are reflected by assemblage numbers 35, 39, 40, 49 and 51 in Figure 8.5. This would indicate the $T-X(CO_2)$ conditions to in the in this part of the LHZBG to have been between 300 and 480 °C (573 and > 753 K) and the CO_2-content of the fluid to have been $< 0.3^{E-1}$ bar.

In UK48Q the mineral assemblages observed in the samples (Figure 8.7) are represented by assemblages number 4, 10, 11, 16, 22, 24, 25, 32, 35 and 36. This would suggest that a broad range of $T-X(CO_2)$ conditions prevailed in the LHZBG unit during the formation of the observed mineral assemblages. The upper range is 660 °C (> 933 K) and the $X(CO_2)$ range is up to 0.1. This would indicate a cooling and buffering towards progressively lower $X(CO_2)$ conditions with decreasing temperature (T).

uk20gxco2a

P(bar) =0.300E+04

T(K)

1173 — 1053 — 933 — 813 — 693 — 573

0.200   0.400   0.600   0.800   1.00

Y(CO2)

1 - feldspar O(HP) Opx(HP) Cpx(HP)
2 - cAmph(DP) feldspar O(HP) Opx(HP) Cpx(HP)
3 - cAmph(DP) feldspar O(HP) Opx(HP) Cpx(HP)
4 - cAmph(DP) feldspar O(HP) Cpx(HP) ab
5 - cAmph(DP) O(HP) Cpx(HP) ab
6 - cAmph(DP) O(HP) Do(HP) Cpx(HP) ab
11 - cAmph(DP) feldspar O(HP) Opx(HP) Cpx(HP) ab
12 - cAmph(DP) O(HP) Opx(HP) Cpx(HP) ab
13 - feldspar O(HP) Do(HP) Opx(HP) Cpx(HP)
14 - cAmph(DP) O(HP) Do(HP) Cpx(HP) ab
15 - cAmph(DP) feldspar O(HP) Do(HP) Opx(HP) ab
16 - feldspar O(HP) Do(HP) Opx(HP)
17 - cAmph(DP) feldspar O(HP) Do(HP) Opx(HP)
18 - cAmph(DP) O(HP) Do(HP) Opx(HP) ab
19 - feldspar O(HP) Do(HP) Opx(HP) ab
20 - feldspar O(HP) Do(HP) oCcM(HP) Opx(HP)
21 - cAmph(DP) feldspar O(HP) Do(HP) oCcM(HP) Opx(HP)
22 - cAmph(DP) feldspar O(HP) Do(HP) oCcM(HP) Opx(HP) ab
23 - O(HP) Do(HP) oCcM(HP) Opx(HP) ab
24 - feldspar Do(HP) oCcM(HP) Opx(HP)
25 - cAmph(DP) O(HP) Do(HP) oCcM(HP) Opx(HP) ab
26 - O(HP) Do(HP) oCcM(HP) Opx(HP) ab
27 - cAmph(DP) O(HP) oCcM(HP) Opx(HP) ab
28 - cAmph(DP) cAmph(DP) O(HP) Do(HP) oCcM(HP) ab
29 - feldspar Do(HP) oCcM(HP) Opx(HP)
30 - cAmph(DP) Do(HP) oCcM(HP) Opx(HP) ab
31 - cAmph(DP) O(HP) oCcM(HP) ab
32 - cAmph(DP) O(HP) Do(HP) ab
33 - cAmph(DP) cAmph(DP) O(HP) oCcM(HP) ab
34 - cAmph(DP) O(HP) Do(HP) oCcM(HP) ab
35 - Do(HP) oCcM(HP) Opx(HP) ab
36 - feldspar Do(HP) oCcM(HP) Opx(HP) ab

37 - cAmph(DP) feldspar Do(HP) oCcM(HP) Opx(HP) ab
38 - cAmph(DP) T O(HP) oCcM(HP) ab
39 - cAmph(DP) Do(HP) oCcM(HP) ab
40 - cAmph(DP) feldspar Do(HP) oCcM(HP) Opx(HP)
41 - cAmph(DP) feldspar Do(HP) oCcM(HP) ab
42 - feldspar Do(HP) oCcM(HP) Opx(HP) q
43 - cAmph(DP) feldspar Do(HP) oCcM(HP)
44 - cAmph(DP) feldspar Do(HP) oCcM(HP) Opx(HP) q
45 - feldspar Do(HP) oCcM(HP) Opx(HP) ab q
46 - Do(HP) oCcM(HP) Opx(HP) ab q
47 - cAmph(DP) T feldspar Do(HP) oCcM(HP) ab
48 - cAmph(DP) T Do(HP) oCcM(HP) ab
49 - cAmph(DP) feldspar Do(HP) oCcM(HP) q
50 - feldspar Do(HP) oCcM(HP) q sid
51 - cAmph(DP) feldspar Do(HP) oCcM(HP) ab q
52 - cAmph(DP) T Do(HP) oCcM(HP) ab sid
53 - cAmph(DP) T Do(HP) oCcM(HP) ab q
54 - cAmph(DP) Do(HP) oCcM(HP) ab q
55 - T Do(HP) oCcM(HP) ab q sid
56 - oCcM(HP) feldspar Do(HP) ab q sid
57 - oCcM(HP) T Do(HP) ab sid
58 - T Do(HP) oCcM(HP) ab q sid
59 - oCcM(HP) Do(HP) and ab q sid
60 - oCcM(HP) Chl(HP) Do(HP) ab q sid
61 - oCcM(HP) Do(HP) ky ab q sid
62 - oCcM(HP) Do(HP) prl ab q sid
63 - Cpx(HP) Chl(HP) Do(HP) Atg ab sid
64 - cAmph(DP) O(HP) Atg Cpx(HP) Cpx(HP) br
65 - Cpx(HP) Chl(HP) Do(HP) Atg sid
66 - cAmph(DP) O(HP) Atg Cpx(HP) br
67 - Cpx(HP) oCcM(HP) Chl(HP) Do(HP) Atg sid
68 - oCcM(HP) Chl(HP) Do(HP) Atg ab sid

69 - Cpx(HP) Chl(HP) O(HP) Do(HP) Atg oCcM(HP)
70 - oCcM(HP) Chl(HP) T Do(HP) ab sid
71 - cAmph(DP) O(HP) Atg Cpx(HP)
72 - oCcM(HP) Chl(HP) O(HP) Atg Cpx(HP)
73 - Cpx(HP) Chl(HP) O(HP) Do(HP) Atg
74 - oCcM(HP) cAmph(DP) Chl(HP) O(HP) Atg Cpx(HP)
75 - Chl(HP) O(HP) Do(HP) Atg Cpx(HP) ab
76 - cAmph(DP) Chl(HP) O(HP) Do(HP) Atg Cpx(HP)
77 - oCcM(HP) Chl(HP) O(HP) Do(HP) Atg ab
78 - oCcM(HP) cAmph(DP) O(HP) Do(HP) Atg Cpx(HP)
79 - cAmph(DP) O(HP) Do(HP) Atg Cpx(HP)
80 - oCcM(HP) cAmph(DP) O(HP) Atg Cpx(HP) Cpx(HP)
81 - oCcM(HP) cAmph(DP) O(HP) Atg Cpx(HP)
82 - oCcM(HP) cAmph(DP) O(HP) Do(HP) Atg ab
83 - oCcM(HP) cAmph(DP) O(HP) Atg ab
84 - Chl(HP) O(HP) Do(HP) Atg ab
85 - oCcM(HP) cAmph(DP) O(HP) Atg Cpx(HP) ab
86 - cAmph(DP) O(HP) Do(HP) Atg Cpx(HP) ab
87 - cAmph(DP) O(HP) Do(HP) Atg Cpx(HP)
88 - cAmph(DP) O(HP) Do(HP) Atg ab
89 - cAmph(DP) Chl(HP) T Do(HP) oCcM(HP) ab
90 - cAmph(DP) O(HP) Atg Cpx(HP) ab
91 - Chl(HP) T O(HP) Do(HP) Atg ab
92 - Chl(HP) T O(HP) Do(HP) ab
93 - cAmph(DP) O(HP) Do(HP) Cpx(HP) ab
94 - cAmph(DP) T O(HP) Do(HP) ab
95 - cAmph(DP) Chl(HP) Do(HP) oCcM(HP) ab
96 - cAmph(DP) T O(HP) Do(HP) oCcM(HP) ab
97 - cAmph(DP) O(HP) Do(HP) Cpx(HP) ab

Figure 8.4: Pseudo-section for UK20G T-X(CO$_2$).

185

Figure 8.5: Pseudo-section for UK20G T-X(CO$_2$).

uk48q no1

Figure 8.6: Pseudo-section for UK48Q T-M(H$_2$O).

Figure 8.7:Pseudo-section for UK48Q T-X(CO_2).

8.8.2. Chromitiferous Harzburgite Unit

Two samples were selected and modelled to be representative of the PCR unit, namely UK44C and UK61B. XRD analyses indicated the preserved primary magmatic mineral in these samples are olivine in UK44C and diopside in UK61B. The secondary minerals in both are: calcite, amphibole (actinolite-tremolite), chlorite, dolomite, serpentine and talc. Based on the petrography, the formation of chlorite and serpentine is indicated to have formed during the last preserved alteration event, owing to the pocketed occurrence of these two minerals.

In the full water environment (Figure 8.8) no observed assemblages are present as all the reactions contain either feldspar or albite or orthopyroxene.

In UK44C the T-X(CO_2) conditions that are required for the mineral assemblages observed, numbers 87,88 and 89 (Figure 8.9) give a broad range of conditions. The temperature is above 540 up to 660 °C (> 813 to > 933 K) with the X(CO_2) condition range up to 0.8. In Figure 12.7 the range of observed assemblages occurs over a broad range of conditions. The observed assemblages are numbers 17, 20, 26, 28, 29, 30, 34, 35 and 36. This constrains the formation conditions to a temperature up to 660 °C (993 K). The range of the assemblages and conditions would suggest a decrease in X(CO_2) with a decrease in T.

In the broadest part of the intrusion, where sample UK61 B was collected, no observed assemblage is present in the full water condition diagram (Figure 8.11). All the assemblage present in this diagram either contains feldspar, albite or orthopyroxene that is not observed in the sample.

The T-X(CO_2) conditions are again over a very broad range. The observed assemblages, present in Figure 12.9, are present in numbers 7, 15, 17, 18, 20, 24, 25, 27, 28 ,29, 53, 54, 62, 67, 73, 77, 78 and 81. This places the X(CO_2) conditions up to 1.0. The temperature is constrained up to around 600 °C (> 873 K). The conditions represented in Figure 8.13 have the observed assemblages over the entire range of X(CO_2) conditions. The assemblages are

given by numbers 6 to 10, 34, 41 and 44. This constrains the upper temperature to 660 °C (< 993 K).

Figure 8.8: Pseudo-section for UK44C T-M(H_2O).

uk44cxco2a

P(bar) =0.300E+04

Y(CO2)

1 - cAmph(DP) O(HP) Do(HP) Opx(HP) Cpx(HP)
2 - feldspar O(HP) Do(HP) Opx(HP) Cpx(HP)
3 - feldspar O(HP) Do(HP) Opx(HP)

13 - cAmph(DP) cAmph(DP) Chl(HP) O(HP) oCcM(HP)
14 - cAmph(DP) cAmph(DP) Chl(HP) O(HP) Do(HP) oCcM(HP)
15 - cAmph(DP) cAmph(DP) Chl(HP) Do(HP) oCcM(HP)
16 - cAmph(DP) cAmph(DP) Do(HP) oCcM(HP) Opx(HP)
17 - cAmph(DP) feldspar Do(HP) oCcM(HP) Opx(HP)
18 - feldspar Do(HP) oCcM(HP) Opx(HP)
19 - cAmph(DP) cAmph(DP) Do(HP) oCcM(HP)
20 - cAmph(DP) oCcM(HP) Opx(HP)
21 - cAmph(DP) cAmph(DP) Chl(HP) T Do(HP) oCcM(HP)
22 - cAmph(DP) cAmph(DP) feldspar oCcM(HP) Opx(HP)
23 - cAmph(DP) T Do(HP) oCcM(HP)
24 - cAmph(DP) cAmph(DP) cAmph(DP) Do(HP) oCcM(HP)
25 - cAmph(DP) cAmph(DP) feldspar Do(HP) oCcM(HP)
26 - cAmph(DP) feldspar Do(HP) oCcM(HP)
27 - cAmph(DP) feldspar Do(HP) oCcM(HP) q
28 - cAmph(DP) feldspar feldspar Do(HP) oCcM(HP)
29 - feldspar Do(HP) oCcM(HP) Opx(HP) q
30 - cAmph(DP) cAmph(DP) T feldspar Do(HP) oCcM(HP)
31 - cAmph(DP) T feldspar Do(HP) oCcM(HP) q

32 - cAmph(DP) T feldspar feldspar Do(HP) oCcM(HP)
33 - cAmph(DP) feldspar feldspar Do(HP) oCcM(HP) q
34 - cAmph(DP) T feldspar Do(HP) oCcM(HP)
44 - oCcM(HP) Do(HP) and ab q sid
45 - oCcM(HP) Do(HP) ky ab q sid
46 - oCcM(HP) Do(HP) prl ab q sid
47 - oCcM(HP) Chl(HP) Do(HP) ab q sid
48 - cAmph(DP) Chl(HP) O(HP) Atg Cpx(HP) br
49 - oCcM(HP) cAmph(DP) Chl(HP) Do(HP) Atg ab
50 - Chl(HP) T Do(HP) Atg ab
51 - cAmph(DP) cAmph(DP) Chl(HP) O(HP) Atg ab
52 - Chl(HP) T Do(HP) Atg ab sid
53 - oCcM(HP) cAmph(DP) Chl(HP) Do(HP) Atg ab
54 - cAmph(DP) T Do(HP) Atg ab
55 - cAmph(DP) Chl(HP) O(HP) Atg Cpx(HP)
56 - oCcM(HP) cAmph(DP) Chl(HP) O(HP) Atg ab
59 - cAmph(DP) Chl(HP) T Do(HP) Atg ab
58 - oCcM(HP) Chl(HP) T Do(HP) ab sid
60 - oCcM(HP) cAmph(DP) Chl(HP) O(HP) Atg Cpx(HP)
61 - oCcM(HP) cAmph(DP) Chl(HP) O(HP) Atg
62 - cAmph(DP) cAmph(DP) Chl(HP) Do(HP) Atg ab

63 - oCcM(HP) cAmph(DP) cAmph(DP) Chl(HP) O(HP) Atg
64 - cAmph(DP) cAmph(DP) Chl(HP) O(HP) Do(HP) Atg
65 - cAmph(DP) Chl(HP) O(HP) Do(HP) Atg ab
75 - Chl(HP) T O(HP) Do(HP) ab
76 - cAmph(DP) Chl(HP) O(HP) ab
77 - cAmph(DP) Chl(HP) O(HP) Do(HP) oCcM(HP) ab
78 - cAmph(DP) Chl(HP) T O(HP) Do(HP) ab
79 - cAmph(DP) Chl(HP) O(HP) oCcM(HP) ab
81 - cAmph(DP) Chl(HP) T O(HP) oCcM(HP) ab
82 - cAmph(DP) cAmph(DP) Chl(HP) O(HP) oCcM(HP) ab
83 - cAmph(DP) Chl(HP) T O(HP) Do(HP) oCcM(HP)
84 - cAmph(DP) cAmph(DP) Chl(HP) Do(HP) oCcM(HP) ab
85 - cAmph(DP) Chl(HP) T O(HP) oCcM(HP)
86 - cAmph(DP) Chl(HP) T O(HP) ab
87 - cAmph(DP) Chl(HP) T O(HP)
88 - cAmph(DP) cAmph(DP) Chl(HP) O(HP)
89 - cAmph(DP) cAmph(DP) O(HP)
90 - cAmph(DP) O(HP) Opx(HP)
91 - cAmph(DP) O(HP) Opx(HP) Cpx(HP)
92 - feldspar O(HP) Opx(HP) Cpx(HP)
93 - cAmph(DP) feldspar O(HP) Opx(HP) Cpx(HP)

Figure 8.9: Pseudo-section for UK44C T-X(CO$_2$).

191

uk44cxco2b

P(bar) =0.300E+04

Figure 8.10: Pseudo-section for UK44C T-X(CO$_2$)
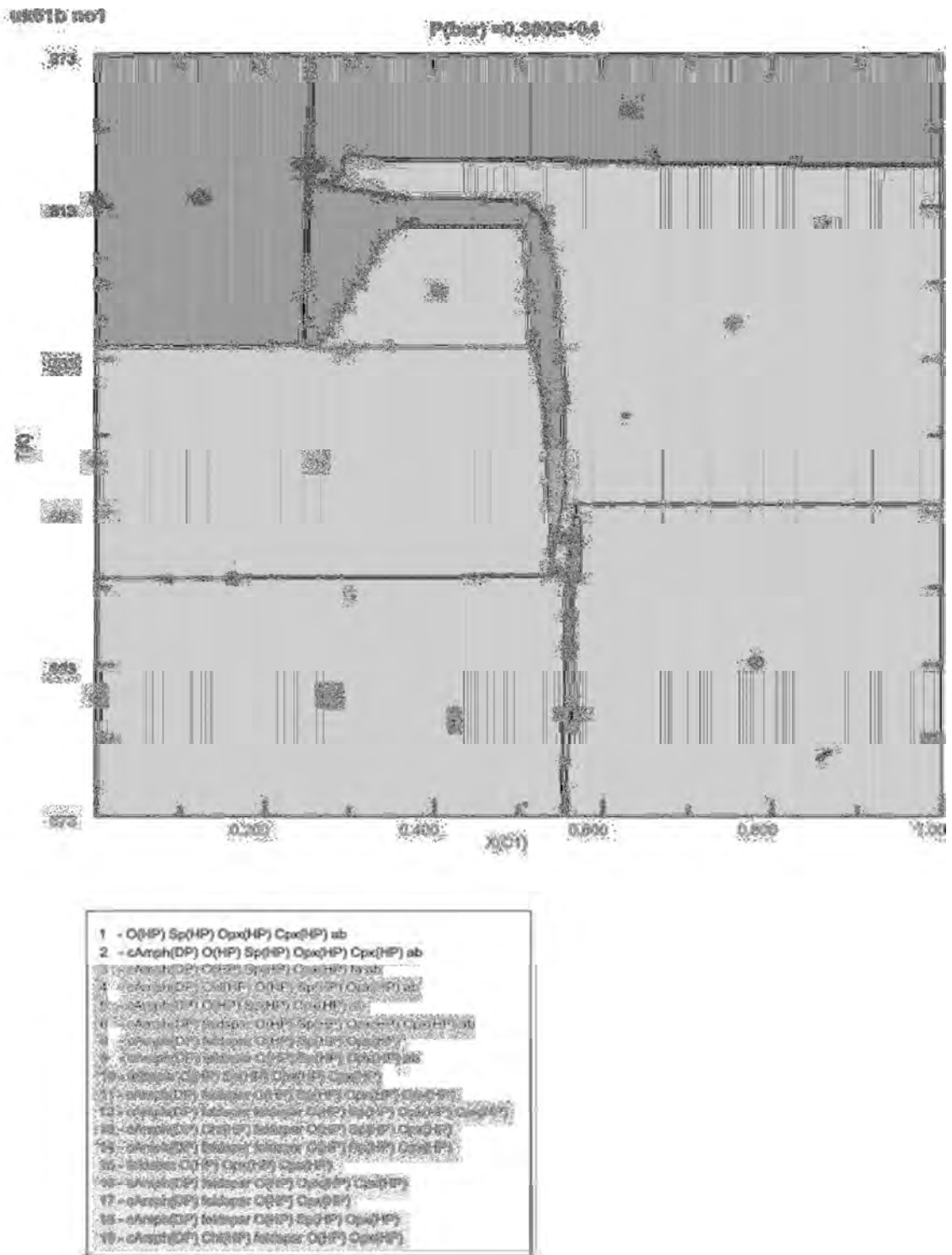
Figure 8.11: Pseudo-section for UK61B T-M(H$_2$O).
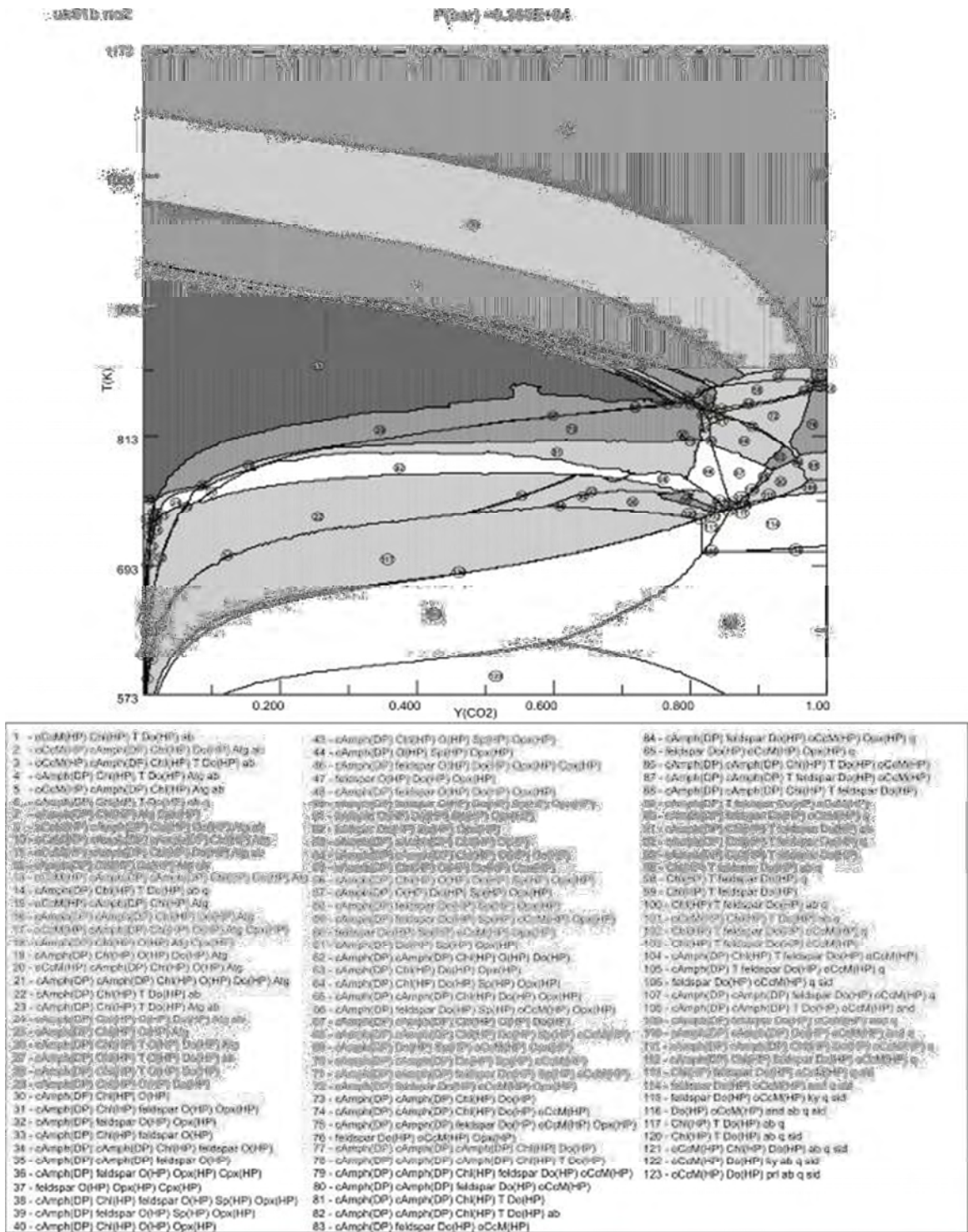
Figure 8.12: Pseudo-section for UK61B T-X(CO$_2$).

Figure 8.13: Pseudo-section for UK61B T-X(CO$_2$).

8.9 Deuteric Fluid Compositions

The lateral distribution of elements, due to the effect of the hydrothermal alteration, based on borehole averages, does not seem to indicate a discernable distribution over the entire complex, for the boreholes analysed. There is little to no consistency in the hydrothermal alteration signature, as determined by the isocon method, both within and between units. This would suggest that the hydrothermal fluid responsible for the alteration was not derived from a magmatically generated fluid. A late-stage magmatic fluid would concentrate incompatible elements and it is expected that such an enrichment trend would be obvious in the isocon diagrams.

In the light of both the inconsistent enrichment and depletion trends shown by the isocon method and the apparent mobilization of Th and U it is suggested that the fluid was mixture of magmatic and meteoric fluids. The mobilization of Th and U in a carbonate-rich fluid environment was indicated earlier. Assimilation of dolomite country rock is the most obvious source of such a carbonate-rich fluid, releasing meteoric water into the system. The isotope study of Sakar et al. (2005) supports this hypothesis of assimilation of a crustal component. However, in a later study by Sakar et al., (2008) assimilation of country rock is indicated not to have taken place in the Uitkomst Complex, but field evidence to the contrary, in especially the LHZBG, is neglected.

The CO_2-rich fluids are capable of transporting certain elements more effectively e.g. Th and U (Dawood et al., 2004) and Ti and Al (Hynes, 1980) relative to an H_2O-rich fluid. It is suggested here that the deuteric fluid was very variable in composition and possibly pH and Eh (no work was done to establish this proposition). The mineralogy suggest variable X_{CO2} conditions such as high X_{CO2} conditions for the formation of talc and low X_{CO2} conditions for the formation of serpentine. This non-homogeneous fluid composition led the variable enrichment and depletion of elements observed in this study.

It is not possible to constrain the exact T-X(CO_2) conditions that prevailed in the two units investigated. It is however evident that a broad range of CO_2-partial pressures and temperature ranges would be able to achieve the assemblages observed in these units. It is suggested that only the effect, of the last set of conditions that prevailed in the system is reflected by the observed mineral assemblages. Earlier assemblages that were amenable to later over-printing would not be preserved in the current samples.

It is suggested that the X(CO_2) conditions in the LHZBG were more hydrous with a lower CO_2 content during the final retrograde event that affected this unit. In contrast the last retrograde event that affected the PCR had a higher X(CO_2), resulting in the stabilization of a larger amount of talc-carbonate-chlorite assemblage. It is suggested that the assemblages indicate cooling and buffering towards progressively lower X(CO_2) conditions in the system.

The lack of correlating assemblages in the M(H_2O) pseudo-section, due to the presence of albite, feldspar and orthopyroxene, would suggest that either: a) the system was disrupted not to produce the expected assemblages or b) that the system was not hydrated by the addition of external water to the system during formation. The presence of retrograde metamorphic assemblages eliminates the last option.

CHAPTER 9 SUMMARY AND RELATING PROCESSES

9.1 Related processes

In this chapter processes that had an influence on the petrogenesis and mineralization of the Uitkomst Complex will be discussed, both in comparison with examples from other similar intrusions and in relation to the observations made in the preceding chapters. The effects of assimilation of country rock and the resulting products on the magmatic evolution of the complex are discussed first. This is followed by a discussion of mineralization and formation models. An overview of assimilation- and external addition process is then discussed and reviewed in terms of the Uitkomst Complex. The fluid flow in a conduit system is investigated and related to observations in the study area, and finally, the development of solidification fronts and the effects these had on the physical development of the Uitkomst Complex is considered.

9.2 Magma interaction with dolomitic country rock

9.2.1 Contact mineralization

As could be expected, the dolomitic country rock to an intrusion such as the Uitkomst Complex suffers contact metamorphism resulting in the formation of skarn mineral assemblages and petrographic textures. The effects of this are well documented for the Ioko-Dovyren intrusion in Russia. The Ioko-Dovyren Intrusion is divided into (1) plagiolherzolite, (2) dunite, (3) troctolite and (4) gabbro-gabbronorite zones. Investigations here found that the dominant mineral in the skarns is brucite in pseudomorph form after periclase (Wenzel et al, 2001b). The skarn was also found to contain fosterite and Cr-poor spinels (Wenzel et al, 2001b). Fine grained fosterite-spinel skarns occur with the brucite skarns or as isolated schlieren in the magmatic host rock (Wenzel et al, 2001a).

Wenzel et al., (2001b) suggest that rapid heating of quartz-poor dolomite leads to the formation of minor olivine within the skarn, followed by the breakdown of such olivine to calcite and periclase. In the magma the partial melting of xenoliths results in the formation of a calcite melt with a low viscosity and low density, which can be easily squeezed out of the xenolith, leaving periclase and olivine behind (Wenzel et al, 2001b). This calcite melts

reacts with the mafic magma to form a new olivine with an elevated CaO content of up to 1.67 wt % (Wenzel et al, 2001a, Wenzel et al, 2001b). The calcite melt is then assimilated into the mafic magma and this leads to the crystallization of Ca-Tschermak-rich interstitial clinopyroxene instead of plagioclase (Wenzel et al, 2001b).

It was found in the Uitkomst Complex that plagioclase is found exclusively, mostly as relict grains, in the wehrlite layers of the LHZBG unit with clinopyroxene (diopside) dominating in this unit. Plagioclase is absent from the PCR and even relict grains are absent. Olivine is also relatively rare in even the pristine parts of the LHZBG and completely absent from the xenoliths in this unit. Olivine is slightly more abundant in the pristine parts of the PCR unit, otherwise only "ghost" pseudomorphs of talc-chlorite are preserved. This is sufficient to propose that the effect of assimilation of dolomite in the PCR was not as pronounced as in the LHZBG. Olivine was able to develop, without their composition being driven towards clinopyroxene composition.

Wollastonite, andradite, grossular, spurrite, rankinite, merwinite and melilite have been found to be the most common minerals to crystallize at the interface between the dolomitic xenoliths and the magma, while no melting of calcite was observed (Wenzel et al, 2001a). Owens (2000) suggests that a metastable phase of stable state pyroxene, olivine and oxides may nucleate under conditions of local cooling in the area immediatedly surrounding the xenoliths. The incorporation of the various inclusions into the magma results in the preferential nucleation of mafic phases at the xenolith-magma contact.

The intermittent development of pegmatite phases around calc-silicate xenoliths in the LHZBG would suggest that the effect of localized cooling may have been too short-lived for continuous development of pegmatite phases around the xenoliths. The development of large diopside and calcite grains at the contacts along with semi-massive pyrrhotite does however suggest that nucleation of mafic phases was able to occur preferentially around the xenoliths.

At the very high temperatures which existed in the Uitkomst Complex conduit, akermanite should have formed as a product in the xenoliths. It has been found to be stable at temperatures between 1385 and 500 °C at 4.8 to 6.7 kbar (Deer et al., 1992). The formation of akermanite is given in the following reaction (after: Fulignati, Marianelli, Santcroce and Sbaran, 2004):

$$CaMgSi_2O_6 + CaCO_3 = Ca_2MgSi_2O_7 + CO_2$$

Diopside + calcite akermanite
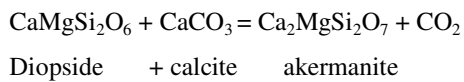
Another means of forming akermanite, by the reaction of impure dolomite suffering contact metamorphism and metasomatic exchange with magma, is proposed by Owens (2000):

Diopside + fosterite + monticellite = akermanite
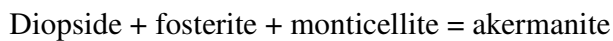
However, the lack of akermanite in samples from the Uitkomst Complex provides evidence that the temperature in the magma chamber did not attain temperatures high enough to lead to the formation of such minerals. This may be because the magma conduit was cooler than the required temperature, owing to the loss of heat during serpentinization of xenoliths and retrograde metamorphism.

9.2.2 Clinopyroxene formation due to the assimilation of dolomites

During the initial stages of limestone/dolomite assimilation into a mafic magma, wollastonite may precipitate due to the resorption of plagioclase (Baker and Black, 1980). The $CaAl_2Si_2O_8$ component is incorporated in pyroxene rather than in the crystallization of an anorthite-rich plagioclase. This process involves a desilicification of the primary igneous phases, without requiring the precipitation of nepheline (Baker and Black, 1980).

$$CaAl_2Si_2O_8 + 2CaFeMgSi_2O_6 + 2CaO = 2CaFe^{II,III}MgAlSi_5O_6 + 3CaSiO_3 + \tfrac{1}{2}O_2$$

An-component + component of px = aluminous px wollastonite
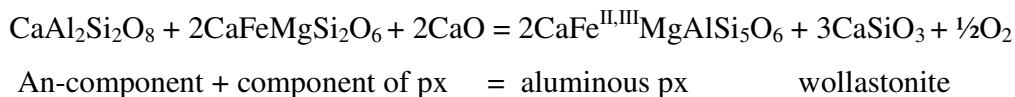
When Al substitutes in the tetrahedral sites of pyroxene, at the expense of Si, it effectively enriches the coexisting liquid in silica (Baker and Black, 1980).

The lack of wollastonite in especially the LHZBG unit would suggest that plagioclase was only developed in the wehrlite layer and did not develop in the main LHZBG magma. The preservation of relict plagioclase grains in an otherwise completely altered matrix suggest the plagioclase grains to be less susceptible to resorption. It was suggested in Chapter 4 that this may due to the presence of Al in the crystalline structure of the plagioclase.

Basic magmas are able to process the addition of Ca into the system by producing clinopyroxene and Ca-amphiboles (Barnes et al., 2005), owing to the high content of Fe and Mg in the primary magmas (Barnes et al., 2005). The conversion of olivine and orthopyroxene to clinopyroxene leads to the enrichment of the Mg content in clinopyroxene relative to Fe (Tilley and Harwood, 1931). High temperature phases of clinopyroxene, such as esseneite, indicate crystallisation in high fO_2 conditions, whereas at low fO_2 conditions iron-bearing calcic pyroxenes would be of a hedenbergite composition (Povoden et al., 2002). The early crystallization of clinopyroxene as observed in the Uitkomst Complex may be demonstrated to have taken place during the early stages of assimilation. This seems to confirm Bowen's suggestion that the mineralogy of the crystallising assemblage will not change during assimilation if the chemical imbalances could be accommodated within a solid solution series (Baker and Black, 1980). The point at which these imbalances can no longer be incorporated into the solid solution series will be marked by the crystallization of other phases such as wollastonite and garnet (Baker and Black, 1980), but the stability of these minerals depends on the CO_2-content of the system.

The presence of the minerals discussed above, demonstrates the assimilation of carbonate rocks. It also provides an indication of the amount of dolomite that may be assimilated, as demonstrated by the inability to further accommodate the imbalances of additional component during assimilation. The degree to which these different product minerals are

present or absent, also gives an indication of the conditions prevailing in the conduit at the time of their formation.

The dominance of diopside development in the LHZBG unit and lack of development of wollastonite and garnet suggest that the magma was able to accommodate the imbalances. It is suggested here that this is due to the continual influx of fresh magma capable of accommodating the additional Ca and Mg from the assimilated dolomite country rock.

Baker and Black (1980) also suggest that to produce a hybrid rock containing as much as 30% decarbonised limestone, most of the calcium would be incorporated into the hybrid melt before it intrudes as a calcite phase into a fracture system. Baker and Black (1980) speculated that if the depth of magma emplacement is shallow enough, the development of a circulating hydrothermal system and the formation of a late-stage hydrous mineral assemblage may occur.

The development of quartz-carbonate veins in both the LHZBG and PCR units suggest that a Ca-rich phase hybrid melt may have been present in the magma. The Ca-rich phase may have mixed with the additional Si in the magma, due to the substitution of Al in the clinopyroxene, to create these features during cooling of the system. The presence of a hydrous phase at this time may also have begun circulating leading to retrograde metamorphism of the primary magmatic mineral phases.

9.2.3. The significance of triple junction points in the LHBZG unit

Triple junction points observed between diopside grains in the studied rocks indicate that the present mineral assemblage in the LHZBG Unit formed due to metamorphic recrystallization of the precursor material. During a previous reconnaissance investigation of the LHZBG Unit (Steenkamp, 2004), it was found that some of the clinopyroxene-rich pyroxenites, could be classified as calc-silicate rocks and these rocks display classical metamorphic triple junction textures. The xenoliths also consist of calc-silicate rocks.

Triple junctions between clinopyroxene grains have been described for the parapyroxenite unit in the Platreef (Harris and Chaumba, 2001). In the Ioko-Dovyren Intrusion triple junction textures are also present, but with the difference that brucite replaces the precursor periclase associated with the triple junction intersections and some of the remaining grain boundries are lined with Fo-rich olivine and Mg-rich Cr-free spinel (Wenzel et al, 2001b). The occurrence of Fo-rich olivine in the junction points of clinopyroxene grains can also observed in samples of the LHZBG Unit (Figure 3.2).

These textural observations support the hypothesis that the interaction between the dolomite county rock and the intruding ultramafic magma, lead to the formation of the skarn and hybrid rocks. The olivine may be relict mineralization that segregated from the magmatic melt prior to sufficient assimilation of dolomite country rock, inhibiting the further development of olivine from the melt. The melt now effectively moved away from purely magmatic to a hybrid melt. The addition of Ca to the melt, and possibly hydrous fluids, would lead to the preferential development of diopside. This triple junction diopside would seem to indicate that the LHZBG unit suffered the effects of metamorphism shortly after of during development of the unit.

9.3 Models for the formation of sulphide deposits

9.3.1 General models

Several models have been proposed to explain the genesis of dunite-peridotite class Ni-S deposits (Edwards and Atkinson, 1986). The general consensus is that these deposits were formed by the segregation of immiscible sulphide liquid from an ultrabasic magma (Edwards and Atkinson, 1986). The "billiard ball"-model has been proposed to explain the close spatial association of massive, net-textured and disseminated sulphides, in which the formation of the textures is ascribed to gravitational settling of the sulphides within the cooling flow (Edwards and Atkinson, 1986). Another model is the "dynamic model" which assumes the segregation of sulfide and silicate components occurred during vertical flow, owing to a viscosity contrast (Edwards and Atkinson, 1986). Later modification of this model emphasizes the separation of sulfide liquid, silicate liquid and olivine crystals during

horizontal flow (Edwards and Atkinson, 1986). The lower viscosity sulphide phase tends to precede the silicate magma during flow, with partial crystallization having already occurred before the sulphide crystal mush is overwhelmed by the slower, more viscous silicate magma, effectively implying separate magma flows for sulphide and silicate melt (Edwards and Atkinson, 1986).

The development of net-texture sulphides in the wehrlite layer and the massive sulphide body suggest that such a segregation of sulphide liquid occurred from the melt. The development of these deposits in a conduit environment is considered in the following sections. It interesting to note that most other conduit deposits (Kabanga, Voisey's Bay etc.) exhibit the same relationship of net-textured sulphides in the lower units of the intrusion and a massive sulphide body near the bottom or in the floor underlying the intrusion.

9.3.2 Conduit model

It has been noted that a common trigger for the formation of sulphide deposits in conduit settings is the interaction between the intruding magma and the wall rock (Arndt, 2005; Arndt et al., 2005). Various physical properties influence the way in which magma will interact with crustal rocks, and these may be summarized as:

a) Density (the less dense the magma the further it can ascend),

b) Viscosity (magma with a low viscosity can thermally erode and assimilate wall rock faster),

c) Temperature (high temperatures enhance the extent of interaction)

d) Volatile content (Arndt et al., 2005)

e) High magma flux coupled with a turbulent flow regime

Staging chambers and conduits will usually develop at junctures where the crustal density drops, such as at an Archean granite – sedimentary basin contact (Ernest and Buchan, 1997; Arndt, 2005; Arndt et al., 2005). The upward migration of the magma will be influenced and guided by structures and the stresses present in the affected crust (Arndt, 2005). The

intersection between the magma and horizontally layered sedimentary strata may lead to the formation of either horizontal intrusions or sills (Arndt, 2005). In layer-parallel sills, magma flow may be rapid and even turbulent (Arndt, 2005). This type of flow will result in thermo-mechanical erosion and increased assimilation of wall rock. Arndt et al. (2005) stated that the best sulphide ore deposits forms when a highly S-undersaturated magma assimilates S-bearing wall rocks in the upper part of a volcano-sedimentary basin.

In sedimentary sequences, at shallow levels, the magma and wall temperature levels will be lower. If the magma flows through an easily fusible, S-rich rock stratum, the amount of assimilation may increase and a magmatic sulphide deposit may form (Arndt, 2005). In thicker parts of the sill, the flow rate will decrease, possibly leading to the sedimentation of the transported sulphides (Arndt, 2005).

The precipitation of sulphides in dynamic conduit systems owing to crustal contamination are suggested for Noril'sk and Talnakh (Li et al., 2003; Arndt et al., 2003; Arndt, 2005) and Voisey's Bay (Li et al., 2001).. In general, it is suggested that sulphide segregation in this deposit occurred in an open system where sulphur was introduced via circulating fluids that transported sulphur from the underlying evaporate-bearing sedimentary sequence or from the gneissic basement. The heat of the intrusion initiated fluid-flow in the crust, and the interaction of hydrothermal fluids and sediments may have led to the formation of sulphur-bearing brines. The sulphates were leached by the hydrothermal fluids and diffusive transfer of such S-rich material to the magma via the hydrothermal fluid occurred. The resulting immiscible sulphide liquid, which segregated due to the contamination, settled down in the wider parts of the conduit, while the magma continued to flow through the conduit. Successive pulses of new chalcophile- undepleted magma entered the conduit, which reacted with the sulphides already present and upgrading the sulphides with chalcophile elements as well as displacing much of the earlier magma in the conduit. In an open system the magma may leave the early sulphides in the conduit as it continues to travel to higher levels. Pulsed flow of magma may also result in the remobilization and redeposition of sulphide-crystal mixtures.

205

Disseminated sulphides will form if simultaneous cotectic crystallization of silicate and liquidation of sulphide takes place in the system (Naldrett, 1981). It is suggested (d'Ars et al., 2001) that the sulphide droplets grow during transport. This occurs due to cooling of the magma, which decreases sulphide solubility and crystallization, and reduces the volume of the silicate liquid. The assimilation of wall rock and the large interfacial tension of sulfide droplets have the effect of making coalescence unlikely during transport. The sulphides which segregate later in the magmatic process are likely to nucleate on pre-existing sulphide droplets, which will continue to grow until they become too large to transport (d'Ars et al., 2001). In a conduit, these disseminated sulphide droplets may become trapped upstream of irregularities or concentrated in the widening part of the conduit (Maier et al., 2001; d'Ars et al., 2001) or in depressions or riffles in the floor of the flow (d'Ars et al., 2001). The droplets of proto-ore will be remobilized and interact with the intruding surges of fertile magma, upgrading their metal content (Maier et al., 2001, Arndt et al., 2005). Droplets of non-coalesced sulphide have a large surface area/volume ratio and will effectively scavenge the chalcophile elements (Ni and PGE) from the flowing magma (d'Ars et al., 2001; Arndt et al., 2005).

9.3.3 Petrogenetic implications for the Uitkomst Complex

The formation of a massive sulphide deposit may result when the immiscible sulphide liquid has segregated and the sulphide droplets, initially dispersed throughout the magma, coalesce (Naldrett, 1981). In order to form a massive sulphide deposit, the sulphide droplets has to be locally concentrated without significant dilution due to silicate crystallization (Naldrett, 1981). This means that the segregation process has to occur extensively and quickly, during a period where little to no crystallization of silicate minerals is taking place (Naldrett, 1981). It is also reported by Arndt et al. (2005) that massive ores or ore-breccia locally transgresses their host rocks in a position near the base of the host intrusion. It is suggested that in this situation, the ore was injected as separate pulses of massive liquid sulphide or as a breccia rich in sulphide. In a conduit, the low viscosity of the host magma may allow the rapid

transformation of accumulated sulphide droplets into a massive sulphide layer, following deposition (d'Ars et al., 2001).

The process for the formation of a massive deposit is not clear, but it is suggested that either deformation along a fault or possibly the collapse by the roof of a magmatic body may expel the accumulated sulphide and a mixture of silicate liquid and cumulus mineral along with wall rock fragments from depth (Arndt et al, 2005). Alternatively the transgressive relationship may be due to mobilization of molted sulphide melts during a period of structural adjustment around the host intrusion (Arndt et al., 2005). The process envisaged by Hornsey (1999) for the Uitkomst Complex is discussed in section 2.2.1., but can be briefly summarised as being the result of a dense cloud of sulphide droplets that were able to penetrate into the basement rock underlying the main intrusion.

The Main Mineralized Zone (MMZ), hosted in the LHZBG Unit, is by far the most significant ore body in the Uitkomst Complex. Mineralization in this ore body includes net-textured mineralization located in the wehrlite layers. Similar mineralization has also been observed in the Kabanga intrusion (Evans et al., 1999), where the net-textured sulphides are seen to be representative of the accumulation of olivine and pyroxene together with immiscible sulphide liquid in a magma chamber or conduit (Evans et al., 1999). Evans et al., (1999) proposed that the accumulation was influenced by gravity and that the strata-bound sulphide bodies represent stratigraphically stacked units. Net-textured sulphides are also developed in the Jinchaun deposit, suggested to represent a deformed magmatic conduit (Lehmann et al. (2007). Barnes et al. (2001) suggested that sulphide droplets may settle out of the magma along with olivine crystals. The result would be an accumulation of olivine crystals with interstitial sulphide liquid.

It is suggested here that the hybrid rocks within the LHZBG Unit of the Uitkomst Complex represent the assimilation product after the reaction between the initial magma and the dolomite country rock. This is confirmed by the presence of less primitive diopside (depleted in Cr-content relative to diopside from the wehrlite layers) and metamorphic

textures. The wehrlite layers in the same unit with more primitive diopside (richer in Cr-content relative to the main LHZBG) and olivine represents fresh magma pulses that escaped the assimilation reaction. The presence of plagioclase in the wehrlite layers also suggests that the magma responsible for the development of these layers were of a slightly different composition that the surrounding host rock. The net-textured sulphides would also have only been able to form if it segregated from a melt. It is suggested here that olivine segregated from the melt first. Assimilation of dolomite triggered significant sulphide segregation from the melt to create the net-textures. Continued assimilation of dolomite led to the formation of a hybrid melt that led to the formation of the diopside rich mush that settled on top of the wehrlite layers. The transition of the composition from a magmatic phase to a hybrid phase may have been rapid as the contact between the wehrlite layers and the host rock is always sharp and no scouring of the top of the wehrlite layers is observed.

9.4. Assimilation

9.4.1 Assimilation models

An investigation of the effect the assimilation of the dolomitic country rock had on the Platreef led Gain and Mostert (1982) to propose a model for assimilation. In this model, dolomite rafts assimilated into the Platreef initially suffered prograde metamorphism, releasing CO_2, H_2O and probably S into the surrounding magma. The CO_2 was absorbed more readily than H_2O because the P_{H2O} of the Bushveld magma prevented large-scale addition. As a result, H_2O remained confined in the aureole around the xenoliths, changing the physiochemical parameters to favour precipitation of sulphides. Serpentinization and other retrograde metamorphic processes occurring in the xenoliths lowered the temperature within the xenoliths and immediate surroundings. Contributions of sedimentary sulphur to the cooling magma are derived by dissolution of evaporitic layers of anhydrite and disseminated iron-sulphides in the dolomite xenoliths. Some of the xenoliths are enclosed in an alteration halo of up to 20 m in width, while others are broken up. The sulphides were also affected by the retro-metamorphic processes, with magnetite replacing some of the grains. Erratic variations in PGE content at different localities in the serpentine zone may be due to post-consolidation processes that led to the redistribution of the PGE's. The

feldspathic pyroxenites at the bottom of the Platreef might have extracted sufficient PGE's, even if there is modally less sulphur than higher up in the stratigraphy.

This model provides a good analogue to what is seen in the Uitkomst Complex, where development of economic sulphide deposits are limited to the units hosted by dolomite country rock and the development of semi-massive sulphides around xenoliths. The entire economically important units were affected by late-stage retrograde metamorphism in both locations. The distribution of PGE does in both also appear to be the result of low temperature, post-consolidation, metamorphic processes.

Wallmach et al (1989), regarding the occurrence of extreme phase xenoliths in the Eastern Bushveld Complex, proposed the second model discussed here. Extreme phase xenoliths form in environments with a temperature around 1200 ℃. An influx of water into the xenoliths during decarbonation reactions ensured that the partial pressures of the fluid phase within the xenolith was equal to total pressure and the partial pressure of the fluid phase within the surrounding magma was much lower. In this case the H_2O was much more soluble in magma than CO_2. Since the xenoliths were completely enclosed in magma during metamorphism, any H_2O present in the fluid will tend to diffuse out of the xenoliths into the magma, leaving behind a fluid phase enriched in CO_2. Relatively fast heating and concomitant degassing during decarbonation not only result in loss of volume, but also prohibit magmatic fluids from invading the xenoliths. Fluid inclusions in high-grade metamorphic rocks thus contain high concentrations of CO_2 or almost pure CO_2.

The second model may not be applicable to the xenoliths of the Uitkomst Complex. Indications are that the H_2O did not diffuse into the magma, but may have remained in proximity with the xenoliths leading to the observed serpentinization in the LHZBG Unit. Assimilation of carbonate xenoliths have been recorded in the eastern lobe of the Bushveld Complex, e.g. Willemse and Bensch (1964) and Wallmach et al. (1995). However the vast difference in mineralogy and geological setting makes comparison with the Uitkomst Complex impossible.

The third model and most compatible with the inferred conditions in the Uitkomst Complex, is that of the Jinchaun intrusion, China. Lehmann et al., (2007) suggest that during the emplacement of the Jinchuan magmatic deposit, magma was emplaced along a thrust contact between a series of marbles forming the footwall and gneisses and minor marble form the hanging wall. This magma had earlier assimilated a high proportion of granitic material from the lower crust. The northern lowermost contact with marbles is sharp, but undulating and appears to be magmatic in origin. In places the crystal-laden magma invaded the floor rocks, and xenoliths of marble, transformed into diopside-rich rocks, were incorporated into the lowermost part of the intrusion. The chemical data presented by Lehmann et al. (2007), especially the major element and oxygen isotope compositions, provided evidence that the lowermost border of the intrusion assimilated marble. Xenoliths within the intrusion and some marginal rocks along the lower contact are partially to completely decarbonated, with the original mineralogy of the marbles being replaced by diopside and other silicates. This led Lehmann et al. to suggest that during its emplacement, the lowermost part of the intrusion interacted with the floor rocks and that this part of the intrusion was invaded by CO_2-rich fluids released by decarbonatization of the uppermost marbles and of marble xenoliths. These fluids would have percolated up into the crystal mush of the intruding magma.

It is further suggested by Lehmann et al. (2007) that heat from the magma may have partially melted the marble wall rocks or xenoliths, causing blobs of low-density and low-viscosity calcite-rich liquid to rise up through the olivine cumulate mush in the lower part of the intrusion. It is alternatively suggested by Lehmann et al. (2007) that the CO_2-rich fluids released by decarbonatization of the floor rocks and / or by the xenoliths could have percolated up through the cumulate mush. Upon reaching the cumulate-liquid interface, these fluids reacted with the magmatic liquid, thereby increasing its oxygen fugacity and causing sulphide liquid to segregate. If the magma were moving through the intrusion, the carbonate would oxidize and cause sulphide droplets to segregate from a constantly flowing magma stream. This would result in a large volume of sulphide that accumulated at the site

of this interaction. The denser sulphide liquid, relative to the silicate liquid, would percolate down through the crystal mush that formed the upper part of the cumulate pile, to just above the level where the rock was completely solid. The sulphide droplets accumulated at this level to form the net-textured ores that characterize the Jinchuan deposits.

This model has several common points with what is observed in the Uitkomst Complex. Both intrusions are hosted by carbonate country rock that developed a diopside selvage at the bottom of the intrusion. It is also suggested that increased oxygen fugacity, due to the addition of CO_2, led to the development of the economic sulphide deposits. The proposed mechanism of net-texture development may also be applicable to the wehrlite layers of the Uitkomst Complex. The major difference is that the Uitkomst Complex was not subject to severe structural deformation like the Jinchaun intrusion.

9.5. Assimilation characteristics

The assimilation of sedimentary rocks by magma has been described by McBirney (1993). If magma was contaminated by e.g. a shale or dolomite, the added components would be the same as those that would normally enter a crystallizing mineral at the same stage of cooling. Under these conditions the effect of assimilation may be concealed in the way in which the magma responds to the addition of large amounts of these components. As long as the crystal-liquid relationship control the course of differentiation, the major compositional elements of the evolving liquids are constrained to follow a liquid-line of descent that would not deviate from that defined by crystal fractionation.

The principal effect of assimilation of crustal material added to a crystallizing magma would be to change the proportions of the end-members of any crystals forming. The major-element composition of the liquid on the other hand would remain essentially unchanged. For example: if a basaltic magma was contaminated by shale, it would react with the xenolithic material and form more of the already present minerals, such as augite and anorthite. When equilibrium is approached during the process, the effect of country rock addition is absorbed by increased crystallization of minerals that remove the added

211

components. The liquid would evolve along a path that differs little from the one it would have followed, had assimilation not taken place. Although the proportion of the liquid and crystalline residue will be altered, the magma that erupts at surface would be consistent with normal fractionation. Thus evidence of assimilation would be reflected in the relative volumes of differentiated rocks.

9.5.1 Addition of carbonate rock

The assimilation of limestone or dolomite leads to the reduction of the stability field of olivine in favour of that of clinopyroxene (diopsidic) and orthopyroxene (Tilley and Harwood, 1931). The addition of lime and silica and the removal of oxides results in selective diffusion and enrichment of clinopyroxene in Mg relative to Fe, while the liquid becomes Fe-enriched (Tilley and Harwood, 1931). The addition of CO_2 during assimilation of carbonate rocks results in the decrease of viscosity of the melt and allows free growth of comparatively large crystals (Tilley and Harwood, 1931). Larger, uralized diopside grains have been observed near the contact of xenoliths and in the surrounding hybrid rock within the LHZBG Unit. This may be due to the addition of CO_2, during the assimilation of the country rock dolomite, which causes a decrease in viscosity around the xenolith, which also results in larger growth of diopside grains.

According to Barnes et al. (2005), the main features indicative of carbonate rock assimilation by magma are:

a. The abundance of Ca-rich minerals, such as clinopyroxene. In the Uitkomst Complex clinopyroxene (diopside) is present in the LHZBG and the PCR Units. The amphiboles are also dominated by calcic-amphiboles, suggesting that the diopside grains may have been the precursor mineral that resulted in the actinolite-tremolite after retrograde metamorphism of these units.
b. The evolution of the complex to alkaline compositions. Alkali enrichment is a function of Ca-depletion of melt due to clinopyroxene formation. It is suggested here that this may not be necessarily preserved in a dynamic system such as a magma conduit. Continued influx of fresh magma and assimilation of dolomite country rock would ensure that the melt never became Ca-depleted, even with continued crystallization of diopside.

c. The presence of interstitial calcite in apparent textural equilibrium with igneous silicates. Van Zyl (1996) found in her study that calcite is more prominent in the LHZBG Unit and to a lesser extent in the PCR Unit. She also found that there is a crude correlation between the mineralization and the occurrence of calcite and amphibole. The current investigation also confirms this weak correlation. The presence of calcite in apparent equilibrium with tremolite grains is demonstrated in Figure 3.48.

Barnes et al. (2005) suggest that the effect of assimilation would be pervasive because a calc-silicate contaminant would probably contain hydrous silicates. This would lead to the production of a hydrous, carbonate-rich partial melt. Such a melt would have a low viscosity and would be able to percolate as intergranular melt through the crystallizing mush of mafic magma. This may be demonstrated in the Uitkomst Complex by the actinolite-tremolite mineralization, especially where it has intergrown the interstitial sulphide minerals. The development of quartz-carbonate veins has been discussed earlier in this chapter.

The addition of calcium to the magma will initially be compensated for by the solid-solution of the crystallizing mineral phases (Baker and Black, 1980). Accompanying any solution of country rock (an endothermic reaction) there must be a corresponding crystallization within the magma of, for example, pyroxene. This reaction has the implication that the addition of sedimentary inclusions will add nothing in terms of mineralogy to the primary magma that is not already present in the primary magma (Baker and Black, 1980). The best example of this in the Uitkomst Complex may be the different ranges of diopside mineralization observed in the hybrid rock of the LHZBG Unit and the fassaite-diopside that is associated with xenoliths.

The order of metamorphic transformation of dolomite has been determined by Winkler (1974) to be firstly talc, followed by tremolite and then diopside. This progession is mainly heat driven as CO_2 concentration; fluid pressure and temperature increase simultaneously (Cui et al., 2003). Since tremolite and diopside forming reactions span a wide fluid composition range, these minerals can not be used to constrain the CO_2 concentration in the

system at the time of their formation (Cui et al., 2003). Initially talc has a higher growth rate than tremolite, but futher growth of tremolite eventually consumes the early produced talc. The LHZBG is dominated by tremolite, even though this unit is hosted by dolomite. The presence of dolomite would have led to an increase in the partial pressure of CO_2, leading to the stability of talc and other carbonate minerals. The lack of talc in the LHZBG unit suggests that it was consumed by tremolite. Talc is dominantly developed in the PCR unit, suggesting that conditions of higher CO_2 partial pressures did exist in the intrusion.

It has also been determined that dolomite is only an important reactant if quartz is also present in the original rock (Winkler, 1974). If dolomite is present in excess to the amount required for various reactions, it will persist to exist into higher grades (Winkler, 1974). Thus the mineralogy and the distribution of especially the alteration minerals may be influence by the proximity to the inferred margins of the intrusion (Section 4.5). Dolomite is found mostly in association talc-chlorite and appears to be secondary, but it may represent unconsumed dolomite.

The presence of calcite in siliceous dolomitic sediments is not necessary for thermal metamorphic reactions; the calcite taking part in these reactions has been produced by previous reactions starting with dolomite and quartz only (Winkler, 1974). Any calcite present in excess over the amount necessary for various reactions will also persist into higher metamorphic grades (Winkler, 1974). Calcite in the LHZBG Unit is only observed associated with minerals indicative of low metamorphic grades (section 3.7). Magnesite in siliceous dolomite is completely consumed in metamorphic reactions (Winkler, 1974). No magnesite was found in the Uitkomst rocks during the current investigation.

9.5.2 Addition of carbon dioxide

During thermal metamorphism of dolomites, it dissociates into periclase (MgO), carbon dioxide gas and calcite ($CaCO_3$) at the high temperature, low pressure conditions of contact metamorphism (Winkler, 1974). Together with water released the CO_2 will be able to leave the system when the overpressure created by the formation of gases within the rocks causes

cracks to form, allowing part of the gas mixture to escape, the fluid pressure is thereby approximately equalized with the load-pressure (Winkler, 1974). The metamorphism of carbonate rocks will release CO_2, but the composition of the fluid phase is not constant as the molecular ratio of H_2O to CO_2 will vary (Winkler, 1974). The presence of H_2O and CO_2 has the effect of reducing the density of the magma (Arndt et al., 2005).

Experimental investigations have shown that the fluid phase must have had a high CO_2 mole fraction at the time of metamorphic reactions. No noticeable dilution of the CO_2-rich fluid took place even though water is liberated in the surrounding rocks. The view was thus advanced by Winkler (1974) that during the relatively short time required for reactions to proceed, the fluid phase remains essentially unchanged.

It is suggested that in very high temperature volcanic-magmatic fluids, with temperatures exceeding 400°C, that Cl is present as HCl and partitions together with CO_2 into vapour phase (Giggenbach, 1989). The relative proportions of CO_2 lost through either (a) boiling or (b) conversion to calcite, depends on the order these processes occur (Giggenbach, 1989). Neutralization of acid fluids through interaction with county rock, causes some of the CO_2 to be deposited as calcite (Giggenbach, 1989). During further rising, or decrease in pressure, the fluids start to boil, leading to the loss of variable, but generally a minor (<2%) fraction of vapour (Giggenbach, 1989). Up to half the CO_2 in a system may be lost in this way (Giggenbach, 1989). It is important to note that CO_2 dissolves solely as carbonate (CO_3^{2-}) groups in basaltic melts, in contrast with the solely molecular form of CO_2 in rhyolites while intermediate melts like andesite will contain both species (Lowenstern, 2001).

An investigation into the reactive flow of a mixed CO_2–H_2O fluid and the progress of calc-silicate reactions in contact metamorphic aureoles by Cui et al. (2003) gives insight into the flow pattern of a CO_2-H_2O fluid in a conduit system with significant calc-silicate xenoliths. It is suggested that CO_2-rich fluids are driven upward thermally in the inner aureole and a CO_2-poor dense fluid flows downward in the outer aureole. The progression of devolatization reactions causes local fluid expulsion what is termed reacting fronts. The

progress of decarbonation reactions may be strongly influenced by the dynamics of the CO_2 transport away from the reaction fronts (Cui et al., 2003).

A water-rich fluid could be derived form either the crystallizing magma or sedimentary rock-pore fluids or as metamorphic water derived from dehydration reactions (Cui et al., 2003). The thermodynamics of each specific fluid may have different impacts on mineral reactions, consequently resulting in differing characteristic distributions of mineral assemblages as demonstrated here in section 4.5 (Cui et al., 2003). The CO_2 may be advected away by the flow of these fluids.

The assimilation of carbonates in a closed system is limited by the solubility of CO_2 (Barnes et al., 2005). The solubility of CO_2 increases with pressure and magma alkalinity (Lowenstern, 2001). This author found experimentally that the solubility of CO_2 increases with pressure at a near linear rate, while the temperature effect on solubility is very small compared to composition and pressure. In comparison, the solubility of CO_2 in natural melt is about an order of magnitude less than that of H_2O and the addition of H_2O to a melt-CO_2 system will decrease the solubility of CO_2 further (Lowenstern, 2001). Solubility of CO_2 depends further on the nature and abundance of various cations, in particular Ca, K, and Na where the effect of Ca^{2+} is most pronounced, followed by K^+, Na^+, Mg^{2+} and Fe^{2+} (Lowenstern, 2001). Carbonate is therefore more soluble in alkaline basalts than tholeiites (Lowenstern, 2001).In contrast CO_2 does not react with a felsic melt as it dissolves in molecular form, resulting in little variation of CO_2 solubility in felsic magmas (Lowenstern, 2001).

Carbonate assimilation reactions will proceed only when heat for assimilation is available in a system where the CO_2-rich fluids are lost as soon as they evolve (Barnes et al., 2005). Cui et al., (2003) suggests that the release of metamorphic fluids is controlled by the progress of mineral reactions. The progress of each reaction is a kinetic process defined by the rates of heat input and the rate of flow of chemically disequilibrium fluid. Other rate-limiting

processes identified include dissolution and growth of minerals and mass transfer into or out of the reacting sites.

The mechanisms suggested for the removal of CO_2 from a system, by Barnes et al. (2005) can be either:

a. CO_2 is removed upward from the complex in a mixed H_2O-CO_2 fluid entrained in, or steaming through the magma.

b. CO_2-rich fluids caused formation of an immiscible carbonate melt, which may be removed by upward migration. Evidence for such a process is found in the fact that it only operates at high temperatures, and that it is not a late stage phenomenon. No calcite veins or carbonatite dikes will be present in such a situation. In the Uitkomst Complex quartz-carbonate veins are present in both the LHZBG and PCR Units and the Units above (pers. comm. H.F.J. Theart, 2008). The siliceous nature of these veins suggests that a late stage siliceous fluid was enriched in carbonate products.

Cui et al. (2003) propose that the CO_2-rich fluid will only prevail in the early stage. Due to the greater buoyancy of the CO_2-rich fluid, upward flow is enhanced and the CO_2 is transported away from the reaction fronts and displaced by H_2O-rich fluid, diluting the CO_2 concentrations further.

If $P_f = P_{CO2} + P_{H2O}$ the equilibrium temperature is not uniquely determined. The greater the mole fraction of CO_2 in the fluid phase, the lower the equilibrium temperature. As a result the equilibrium becomes bivariant in nature (Winkler, 1974). Even if P_f could be estimated on the basis of depth, nothing is known about the probable composition of the fluid phase (Winkler, 1974).

Low grade metamorphic rocks are predicted to record the presence of CO_2-rich fluids where as high grade metamorphic rocks record the presence of CO_2-poor fluids (Cui et al., 2003). The interaction of the magma with the carbonate country rock may lead to high CO_2 partial pressure and Ti mobility (de Waal and Gauert, 1997). The presence of CO_2 and H_2O in

217

magma is indicated by the presence of phlogopite and magmatic amphibole in the groundmass (Arndt et al., 2005).

Gomwe (2000) concluded that the release of CO_2 caused the increase in oxygen fugacity along with a decrease in FeO resulted in sulfur-supersaturation (due to decreased S-carry capacity) and sulfur-segregation followed by chromite crystallization. Waal (1977) suggested that carbon dioxide and water from metamorphic reactions may serve as agents for the precipitation of sulphide and spinel in mafic magma.

The effect of the CO_2-rich deuteric fluid, as well as the possible direction of fluid flow in the Uitkomst Complex is discussed in section 5.4.

The main influence on the Uitkomst Complex, where sulphide mineralization took place, was the assimilation of Malmani dolomites. Gomwe (2002) found that the sulphides of the mineralized units have δ^{34} S values between -8 and -2 similar to the isotopic signature of the pyrite-bearing shaly intervals in the Malmani dolomites in the Fochville area. In turn the sulphides of the sulphide-poor units have a mantle signature. Gomwe (2002) therefore discards the possibility of the sulphide-rich units being derived from the Timeball Hill shales, which has a δ^{34} S values of between -12 and -18, that is too divergent from the Uitkomst Complex sulphides. In turn the sulphides in the BGAB Unit are compositionally more heterogeneous, with δ^{34} S values between -20 and +2 (Gauert et al., 1996: In Maier et al., 2004) and +0.2 and +2.7 (Li et al., 2002: In Maier et al., 2004). This might be because the rapid cooling of this unit prevented isotopic mixing (Gauert et al., 1996). The sulfur isotope (δ^{34}S) for country rocks around the Uitkomst Intrusion is presented in Table 9.1.

Table 9.1. Sulfur isotope (δ^{34}S) for country rocks around the Uitkomst Intrusion (Li et al., 2002).

Group	Timeball Hill	Penge Iron Formation	Upper ¾ Malmani *	Lower ¼ Malmani*	Black Reef Quartzites
δ^{34}S (°/$_{oo}$)	-12 to -18	-3 to -6	0 to -8	+3 to +10	Near +3

*For Malmani, all samples from pyrite-bearing shaley intervals, no chert analyses

It has been found that using mass balance calculations and assuming that mixing took place between B1-type magma and dolomite, that only about 10% mass assimilation of dolomite is required to obtain the observed isotope ratio (Gauert et al., 1996; Li et al., 2002). Isotope analyses of oxygen and hydrogen by Sakar et al., (2005) indicate the ranges of δ^{18}O in pyroxene to be 5.3 to 6.3‰ and 5.9 to 6.5‰ for plagioclase in what they term as the "harzburgite unit". A simple two component mixing calculation involving a crustal component (assumed δ^{18}O = 18‰) and magmatic component (δ^{18}O = 6‰) done by them, suggests that 10 to 20% assimilation is required to produce a magma with δ^{18}O values between 7 and 10‰.

In turn Harris et al., (2001) calculated, from oxygen isotope data, that the Platreef assimilated approximately 18% dolomitic material.

Both the sulphide-rich and sulphide-poor units have similar incompatible trace element values, suggesting that the assimilation of external sulfur was not accompanied by significant silicate assimilation, which in turn suggests the assimilation of sulfur took place by means of devolitization that may be associated with the decarbonation of the dolomite country rock (Gomwe, 2002). All of this supports the concept that a degree of carbonate assimilation may have served as a source for the sulphur.

Contamination of the mafic magma with either siliceous crustal -rocks or –sulphides can result in sulphide over-saturation (Maier et al, 2003). The assimilation of S-bearing country rocks or the transfer of S from sulphide mineral-bearing country rock into the magma by

volatiles in response to contact metamorphism may raise the S-content of the mafic magma and lead to S-supersaturation (Maier et al, 2003).

The contrasting S isotopic composition found by Maier et al. (2004) in the sulphides of the ultramafic and mafic rocks of the Uikomst Complex, is interpreted as a result of assimilation of S from different country rocks. The implication is that the BGAB Unit assimilated S from the basal parts of the Malmani dolomites and the Black Reef Quarzites as it has positive δ^{34} S values (Maier et al., 2004). Whereas the overlying ultramafic units could have derived S from the upper portions of the Malmani dolomites preserved in this area and/or Timeball Hill shales that has negative δ^{34} S values (Maier et al., 2004). It was also conceded by Maier, Li and de Waal (2001) that the source of the sulphides was unclear as the Complex is hosted by S-rich and S-poor rocks. This is considered a more likely scenario than isotopic heterogeneity in the original magma source, considering the scale of the Uitkomst Complex (Gauert et al., 1996). It is also considered unlikely that the sulfide isotopes may have been altered by redox reactions and/or concomitant degassing (Gauert et al., 1996), as effective sulphur fractionation is only feasible at very low temperature conditions.

The current investigation supports a scenario where the magmas that formed the Basal Units of the Uitkomst Complex were only able to interact with the dolomite country rock for a limited time, due to the formation of solidification fronts asdiscussed in section 5.5. It is thus suggested that the Malmani dolomites were the principal source of assimilated sulphur, forming the proto-ore.

9.6. Direction of hydrous hydrothermal fluid flow

Baker and Black (1980) suggested that a shallow intrusion may lead to the formation of a circulating hydrothermal system and the formation of hydrous late stage mineral assemblages. Ferry et al. (2002) investigated the direction of fluid flow during contact metamorphism of siliceous carbonate rocks by various intrusions, and came to the following general conclusions. The peak pressures were between 500 and 3 500 bar (2 to 13 km) and

had peak temperatures of between 400 and 750 ˚C. The reactive flow in the systems was found to have a large vertical upward component with a significant horizontal component, directed away from the aureole. This is based in part on the occurrence of reactants and products of decarbonation reactions occurring together in the contact aureole. The occurrence studied indicates arrested retrograde carbonation reactions rather than prograde metamorphism.

Ferry (2000) also suggests that partial equilibrium during retrograde metamorphism (as has been established for the basal units of the Uitkomst Complex) with the preservation of reactants and products may alternatively be interpreted as arrested retrograde reactions. In this case fluid flow must have been in the direction of decreasing temperature as the aureole cooled. The co-existence of reactants and products of a retrograde mineral-fluid reaction is explained by Ferry et al. (2002) as being the result of continues fluid flow as the aureole cools in the same direction as during prograde metamorphism. Fluid flow will thus be in the direction of decreasing temperature, either vertical or horizontal.

The reactive flow of mixed CO_2–H_2O fluids and the progress of calc-silicate reactions in the contact metamorphic aureoles are described by Cui et al. (2003). The CO_2-rich fluids are indicated to be driven upward thermally in the inner aureole and the CO_2-poor dense fluid flows are driven downward in the outer aureole.

An idealized fluid flow regime that operated in the Uitkomst Complex is presented in the final interpretation. Here all the factors that influenced the flow regime are taken into consideration, as well as the effect that this deuteric fluid has on the host rock it moved through.

Ferry et al. (2002) also suggest that the infiltration of meteoric water is controlled by the mechanical properties of the rock. Meteoric-hydrothermal systems will develop in highly fractured competent rocks (e.g. volcanic) where the fracture system will assume hydrostatic pressure and surface water may be drawn downward towards the thermal anomaly created

by the cooling pluton. Carbonate rocks in contrast are more ductile during the period of metamorphism with the result that the fluid flow will be closer to lithostatic pressure. Flow systems near or at lithostatic pressure will not have a significant downward component. However, as the aureole cool, it will pass through the brittle-ductile transition. This may cause the rock to fracture and assume hydrostatic pressure, allowing meteoric water to flow toward the pluton. Channeled fluid flow may take place along bedding, but likely along permeable structures, including dykes, faults, fold hinges and fracture zones.

The mentioned paper does not discuss the mechanical properties of thermally metamorphosed shale. It may however be assumed the fissility of the unaffected shale may allow the infiltration of meteoric water to the contact with the hornfels which forms as a result of thermal metamorphism of shale. This may lead to the entire outer hornfels contact area being subjected to the effects of hydro-chemical processes. The breakdown of the hornfels or increase in permeability of the hornfels may depend on the thickness of the hornfels zone and the physio-chemical properties of the hornfels.

The effect of ground water is also considered. A de-watering study for Pit 3 was undertaken and reported on by Smith and Kotze (2010). It was found that the only potential de-watering problems for Pit 3 are:

- The northwest-southeast trending Pit 3 shear zone
- The north-eastern contact zone with the Transvaal rocks
- Adit Stream fault

As part of the study the depth of the water table to extent from 10 meters to a maximum depth of 60 meters. The confined to semi-confined aquifers that occur in the area are associated with the weathered and fractured rocks. There is also little to no evidence that the upper purely inter-granular aquifer, associated with weathering 20 to 30m deep, yield high volumes of water. The average depth to rest groundwater level is 23m. The majority (73%) of test boreholes indicate a depth to groundwater of between 10 and 30m (Smith and Kotze, 2010). It is therefore suggested here that ground water could not be responsible for the alteration products observed at depth in the study area. It is also suggested here that the coincidence of the higher ground water flow rate, at the north-eastern contact of the

intrusion and the "high talc" is due to the rock types developed prior to weathering to the current level and not as a result of the ground water movement.

Channeled fluid flow along the diabase sill intrusions in the Uitkomst Complex is considered unlikely. The sills show a chill zone along their contacts (Strauss, 1995) and fresh, unaltered mineralogy towards the center of the sill (Theart, Personal communication, 2007).

It is also suggested here that the irregular distribution of both CO_2- and H_2O-rich fluid in the melt may be responsible for the irregular development of secondary minerals such as amphibole, chlorite, serpentine and talc. In locations of higher CO_2-fluids, the partial pressure increase would stabilize the development of talc, replacing the precursor primary magmatic minerals. It is suggested that the CO_2-rich fluid may have been more acidic, aiding the dissolution of the precursor magmatic minerals. The locations where the fluid was dominated by a H_2O-rich fluid the precursor magmatic minerals would suffer retrograde metamorphism.

The fluid composition would also influence the bulk composition of the rock through which it migrated. The inconsistent effect of mobilization of elements was demonstrated with the isocon diagrams. No specific circulation regime could be established. The only elements that clearly show the effect of being transported and deposited by a CO_2-rich fluid is U and Th that is depleted in the narrow part of the intrusion and enriched in the broader part of the intrusion

It is suggested here that upward migration of the CO_2-rich fluid was constrained by the development of a skarn selvage along the contact of the intrusion and later emplacement of the MCR unit. This resulted in the situation where the CO_2-partial pressure in the PCR unit would have been higher than in the underlying LHZBG unit. Still, no specific lateral or vertical fluid component regime existed. Later cooling of the system led to a H_2O-

dominated fluid regime. This resulted in preferential development of chlorite along the center of the intrusion. These ideas are further expanded on in the following section.

9.7 Solidification fronts

Following an investigation to determine the type of magmatism and the type of host-rock interaction taking place in the magma chambers of Vesuvius, it was inferred that different solidification fronts may exist in a magma chamber (Fulignati et al, 2004). A solidification front may be described a feature that develop due to the assimilation of carbonate wall rocks by the magma and consequent exsolution of CO_2-rich vapour and complex melts from the contaminated magma that reacted with the carbonate wall rocks to form skarns (Gilg et al., 2001). At the reaction front the reactants and products will coexist along the flow path only at a sharp interface, provided the hydrodynamic dispersion is negligible and that reaction kinetics are not excessively sluggish (Ferry, 2002). It should be noted that the Vesuvian volcanism is rhyolitic, thus lower temperatures and higher viscosity than anticipated in a mafic to ultramafic magma.

Three types of skarns may form due to reaction between dolomitic host-rock and magma, as considered by Fulignati et al (2004), magmatic-, endo- and exoskarn.

Magmatic Skarn: this is the main type of solidification front that may form in a magma chamber (Fulignati et al, 2004). The strong crystallization occurring in this zone supplies energy for endothermic decarbonation reactions that destroy wall rocks, increasing the porosity and enhancing infiltration of melts (Fulignati et al, 2004). Addition of CaO and MgO to differentiated melt has the effect of lowering viscosity to about 30 and even 7 Pa.s and thus enhancing the mobility and infiltration of melts into the host-rocks (Fulignati et al, 2004).

Hulley (2005) found that the major and trace elements show two distinct patterns, during the calc-silicate xenoliths' interaction with magma in the Uitkomst Complex. It was found that the elements: Al, Fe, Cr, Ti, Si, As, Co, Cu, S, Ni, Ba, Zn, V showed increasing

concentrations near the contact of the xenolith relative to the centre. This would seem to indicate the infiltration of these elements into the xenolith from the magma. It was found that the elements: Ca, K, Mg, Na_2O, P, C, Sr and Mn show a decrease in concentration from the contact with the xenolith to the ultramafic rock. This would seem to suggest that these elements were lost from the xenolith to the magma.

The viscosity of magma is influenced by the addition or removal of certain elements in magma (Hall, 1996). Addition of Si, Al and K contribute to a high viscosity, while Na, Ca, Fe and Mg contribute to a low viscosity (Hall, 1996). The normal viscosity of basalt melt at 1200ºC is $10\text{-}10^2$ Pa.s (Hall, 1996). The viscosity of basalt on eruption is $10^2\text{-}10^4$ Pa.s (Hall, 1996).

During the formation of Endo- and Exoskarn, the circulation of a hypersaline fluid phase in the peripheral upper parts of the more evolved magma chamber induces carbonate melting through sintectic reactions (Fulignati et al, 2004). This complex fluid (Na-K-Ca-carbonate-chloride-rich hydrosaline melt) metasomatizes the rigid crust (Fulignati et al, 2004).

The expected reactions are:

$FeCl_2(aq) + CaCO_3 + SiO_2(aq) + H2O = CaFeSi_2O_6 + CO_2 + 2HCl(aq)$

$\qquad\qquad$ Calcite $\qquad\qquad\qquad\qquad$ hedenbergite
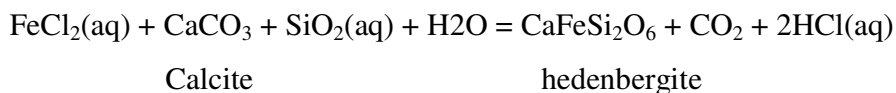
The HCl(aq) further reacts with the remaining calcite as follow:

$2HCl(aq) + CaCO_3 = CaCl_2(aq) + CO_2 + H_2O + porosity$
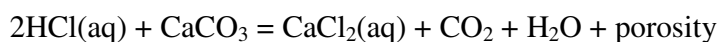
All of the above evidence seems to indicate that the interaction between the magma and the xenoliths, along with the exchange of elements, lead to the formation of solidification fronts in the magma conduit, lowering of viscosity, increasing the efficiency of mixing.

Del More (2001) suggests that the endoskarn, the solidification front and skarn shell in the Vesuvius chamber effectively isolate the interior from new inputs of contaminants, as mass

exchange occurs at the boundary between the crystallizing magma and the wall rocks. It is reported by Cui et al. (2003) that during the process of devolitization, local fluid expulsion takes place at the reaction fronts. The presence of reaction rims (pegmatoidal veins) at the contact between calc-silicate xenoliths and the magma, consisting of retrograde metamorphic minerals, may indicate the remobilization of fluids towards the margins of the xenolith (Hulley, 2005).

Hulley (2005) states that hydrothermal alteration and fluid flux in the calc-silicate xenoliths are proven by the disequilibrium of S-isotopes in sulphide minerals and the in the oxygen and carbon isotopic fractionation. Owens (2000) also suggested that the clinopyroxene reaction zones, observed in his study, once formed, would have served as an effective barrier to diffusion. Thus, any contamination effects (isotopic contamination of magma) would have been achieved prior to reaction zone formation. This may have the implication that in the area upstream from the reaction front the decarbonation reactions would have gone to completion and downstream from the reaction front no further reaction/interaction may take place (Ferry et al., 2002).

In the Uitkomst Complex the initial interaction between the intruding mafic magma and the dolomitic country rock would have led to the release of a CO_2-rich fluid and a hydrous fluid enriched in elements, such as Ca, Mg, Fe and Al. The CO_2-rich fluid may have brought about the physio-chemical conditions (increased oxygen fugacity, etc.) needed to segregate sulphide from the magmatic melt. At the same time however, the dolomitic rocks would be affected by thermal alteration leading to the formation of skarn minerals. The extensive development of diopside, a more refractory mineral, would start to decrease the amount of interaction taking place between the remaining xenolith and the intruding mafic magma. After the collapse of the xenolith, with resultant expulsion of calcite melt, the contamination effect of the xenolith would be significantly decreased. If the development of a skarn consisting of refractory minerals is extensive enough, it may stop the influx of more magma into that specific stratigraphic position.

This decrease in interaction between the xenoliths and intruding magma may lead to a decrease in the amount of CO_2-rich fluids being released into the lower parts of the conduit. As the CO_2-rich fluids are migrated upward, the hydrous fluid may remain in the lower parts of the conduit, and become dominant. The addition of the CO_2-rich fluid, enriched in elements that favour an increase in viscosity, would also affect the magmatic melt, probably increasing the ability to transport xenoliths out of the system, in the upper parts of the conduit.

The hydrous fluid, which remains in the system, may now start affecting the precursor minerals. The hydrous fluid led to the serpentinization of the remaining xenoliths and the adjacent hybrid rock. This caused wide-spread retrograde metamorphism and late-stage hydrothermal alteration products being formed. Late-stage fluids may also have intruded the xenoliths, affecting the original skarn minerals. As the system cooled further, the fluid system operating in the system, may have become completely hydrous dominated. This cooler hydrothermal fluid may have led to the amphibole-chlorite assemblages forming. The hydrothermal alteration system may have been strongest in the central parts of the Complex, away from the margins, as the occurrence of chlorite is dominant in the central parts of the Complex. This may have been due to a longer retention of heat, required for driving the system, and not suffering the moderating effect of the cooling margins or being able to escape from the system.

The skarnification of the country rocks along the margins of the Complex would also have resulted in the formation of a solidification front along the edges of the Complex. This may have served a containment mechanism, inhibiting interaction between the fluids in the conduit and infiltration of meteoric water, especially after cooling of the Complex. It would also contain the fluids in the conduit, possibly aiding in the intense alteration of the Basal Units.

The effect of the solidification fronts along with the fluid flow regime and the effect this had on the development of the Uitkomst Complex are further discussed in the interpretation section.

9.8 Effect of county rock on the shape of the Complex

The Uitkomst Complex is interpreted as being a conduit feeding into an unexposed or eroded layered intrusion (Gauert et al., 1995; Maier et al., 2004). This is based on the tabular shape, the large proportions of sulfide and chromite relative to silicate, and the absence of fractionation trends in the conduit part of the ultramafic units (Gauert et al., 1995; Li et al., 2002; Maier et al., 2004). Apart from indications that the Uitkomst Complex represents a magma conduit, the nature of the surrounding country rock undoubtedly also had an effect on the shape of the intrusion. As noted in the section on the country rock, the main lithologies intruded by the Complex are the Malmani dolomites, with interstitial layers of sulphidic shale and chert, and Timeball Hill graphitic shales with minor iron stones and quartzites.

The "anvil-shape" geometry of the Uitkomst Complex has been noted before (van Zyl, 1996; Gauert et al., 1996; de Waal and Gauert., 1997; de Waal et al., 2001; Li et al., 2002; Maier et al., 2004). The "foot" of the anvil is formed by the central trough, the sides of the central trough have been found to be formed by a very irregular contact, where sedimentary sidewall rocks protrude into the complex (Theart, 2000). The transition of the "foot" to the "head" of the anvil is controlled by a bench that is formed by the Bevets Conglomerate Member of the Rooihoogte Formation (Theart, 2000). The "head" of the anvil is formed where the Uitkomst Complex stoped out large volumes of the Timeball Hill shales above the central trough feature (Theart, 2000).

Gauert et al., (1996) suggested that the shape of the intrusion was controlled by a major fracture and fault system which strikes in a northwesternly direction. de Waal et al., (2001) postulated that the tabular shape is the result of the intersection of a near-horizontal bedding fault-plane with an existing vertical fracture zone under tension conditions.

Due to the thermal metamorphism of dolomites and limestones to skarns during intrusion of mafic bodies, the composition of the carbonate rocks change. It has been found that the intrusion of siliceous fluid into limestone ordinarily result in the formation of Ca-rich minerals such as wollastonite and idocrase (Park and MacDiarmid, 1975). The intrusion of the same fluids in dolomites results in Mg-rich minerals such as serpentine and diopside (Park and MacDiarmid, 1975). Gauert (1998) suggested that the tabular shape of the lower part of the intrusion might be due to the dolomites being more resistive due to its massive nature. During the present investigation it was found that the "clean" xenoliths, consisting of pyroxenes, amphibole, chlorite and carbonate, appear to be more resistive to further assimilation. Owens (2000) also suggests that the formation of a clinopyroxene reaction zone effectively inhibit any further reaction of the carbonate rock with the intruding magma.

It is suggested that the intrusion of the mafic magma reacted with the dolomitic country rock until a sufficiently thick pyroxenite solidification front is formed that would prevent any further interaction and assimilation of the dolomite by the magma. This feature is best explained as a combination of the structural controls, determining the orientation of the intrusion, along with the properties of the skarn preventing large scale thermo-chemical erosion of the country rock. Due to the more evolved nature of the basal gabbroic magma, there was not enough Mg and Fe present in the magma to accommodate the addition of Ca, and resulting formation of Ca-rich minerals. Thus no solidification front was formed, causing the greater lateral intrusion of the BGAB Unit into the dolomites than seen in the overlying LHZBG Unit.

The Uitkomst Complex has been found to be broader, forming the head of the "anvil", where it intersects the Timeball Hill shales. This part of the Uitkomst Complex might be compared to the Kabanga conduit that also intruded into shales. Evans et al., (2000) interpret the internal layering of the Kabanga intrusion to be broadly conformable with the sedimentary bedding structure due to utilization by the intrusion of earlier layer-parallel structures within the basin as the planes of intrusion. Alternatively, since the body has been

emplaced predominantly within shales, adjacent to quartzite units, the layering may be due to the more fissile nature of the shales.

The fact that the MHZBG Unit is laterally more extensive than the underlying LHZBG and PCR Units, led Li et al., (2002) to suggest that the Timeball Hillshale and minor Rooihoogte sediments were more amenable to thermal-mechanical-chemical erosion than the underlying dolomites. Alternatively it is suggested that the fissile nature of the shales might enhance the emplacement and expansion of the magma conduit relative to the dolomite-skarn and quartzite, leading to the "anvil-head" of the intrusion.

The main elements found in shale are Si and Al. Partial or total melting of shale may occur and the Al-content of the magma would increase. The addition of these elements (Si and Al) may not be as easily accommodated by the mafic magma as Mg and Ca. It is also suggested that the skarn products that forms due to thermal metamorphism of shale is not as resistant to thermal erosion and will continue to be broken down and may be completely assimilated by the intruding magma. This may prevent the formation of a reaction front and continual thermal-mechanical-chemical erosion will continue to advance into the side walls of the shale country rock. The lack of xenoliths in the upper part of the conduit stage, as reflected in the upper parts of the LHZBG and the PCR Units, may also indicate that all xenoliths was flushed out of the conduit system by the magma pulses, removing evidence of interaction between the magma and shale country rock.

It was suggested by Chandrasekharam et al., (2000) that magma of gabbroic-basaltic composition would on contamination with shaley sediments form a norite containing anorthite-rich plagioclase. Maier et al., 2004 proposes that the UGN Unit rocks represent roof crystallization from the initial magma pulses. Further investigation is needed to confirm this interpretation.

Wallmach (1988) suggested that the quartzite and calc-silicate xenoliths in the Eastern Bushveld Complex, only survived due to the more refractory nature of these rock. It is

suggested that the pelitic and greywacke rocks were melted and assimilated due to the minerals and mineral assemblages of these rocks having much lower melting points.

It is suggested here that the LHZBG Unit formed a solidification front at the end of its intrusion, from which only late stage CO_2-rich acidic hydrothermal fluids may escape upwards resulting in a secondary alteration assemblages in the PCR Unit, under the MCR Unit layer. The formation of which effectively sealed the lower part of the conduit and forced the new influx of magma to intrude and run through a larger conduit stoped out of the Timeball Hill shale.

Chapter 10 Discussion and interpretation

10.1 Influence of the MCR layer on the distribution of alteration features

The investigation demonstrated that alteration mineral assemblages are predominantly developed in the area selected for the current investigation. These assemblages resulted from amphibolization, serpentinization, saussuritization, uralitization and talc-carbonate alteration of primary and secondary minerals. The occurrence of a talc-carbonate assemblage in the LHZBG Unit and especially the PCR Unit suggests the development of a deuteric CO_2-rich environment, and confirms the conclusions of van Zyl (1996).

It has been established by various authors that the lithological units below the MCR layer suffered the most severe alteration. In the Bushveld Complex the presence of the so-called mixed layer and UG2 pegmatoid below the UG2 chromitite has been suggested to have formed due to metasomatism and partial melting of the pyroxenite protolith (Mathez and Mey, 2005). In the model suggested by Mathez and Mey (2005) the UG2 pegmatoid formed due to a hydrous interstitial melt that percolated up through the partially molten crystal pile below the UG2. The hydrous melt accumulated beneath the pre-existing, compacted UG2 chromitite layer, which then led to the metasomatism and partial melting of the pyroxenite protolith. This material, upon cooling crystallizes, to form coarse-grained pegmatoid. The hydrous melt was however not able to cause partial melting of the UG2 chromitite, and this unit remained relatively impermeable. The model require the permeability of the chromitite to have been less than that of the underlying rocks, which may be possible if the chromite grain size are smaller than the grain sizes of the minerals constituting the underlying rocks. Another reason for the low permeability has been suggested to be due to the presence of interstitial plagioclase in the UG2 chromitite.

It is also suggested by Butcher and Merkle (1991) that the development of *in situ* cumulus plagioclase would have led to the complete elimination of porosity in the anorthosite that underlies the lower most magnetite layer found in the Upper Zone of the Bushveld Complex.

It has been reported by Theart (1997; 2000) that MCR layer has on average a thickness ranging from 0 up to six meters in areas without structural duplication. In this rock type, chromite represent as much as 85 mass % of the rock. The chromitite layers are internally laminated due to variation in abundance of chromite and interstitial silicate minerals. The interstitial silicates now consist of secondary chlorite, talc, and amphibole with minor serpentine, plagioclase, biotite and phlogopite (Theart, 1997; 2000). The chromite grain has an average size of about 100 micron (Theart, 1997; 2000).

It is suggested here that the MCR layer served as an effective barrier to the CO_2-rich hydrothermal fluids, confining these hydrothermal fluids to the basal units and concentrating the fluids in the PCR Unit. Thus, in effect, the MCR layer shielded the units above from the effects of the hydrothermal alteration and metasomatic processes that affecting the basal units.

In a similar vein Mathez and Mey (2005) noted that the Merensky Reef and UG2 chromitite layer are the only extensive layers that exhibit intense magmatic metasomatism in the entire Bushveld Complex. These two layers are also the economic sources of platinum group minerals. Mathez and Mey (2005) remarks that the possibility that metasomatism and metallogenesis were somehow related, but that the process remains enigmatic.

10.2 Association of sulphide mineralization with alteration mineral assemblages

Other ultramafic intrusions with associated nickeliferous sulphides, also host the economic sulphide deposits in rocks that have suffered alteration of the primary host rock. In the Platreef the economic mineralization has been found to occur in areas of the intrusion that has calc-silicate xenoliths present, that has been serpentinized, the highest concentrations of PGE, nickel and copper are found rimming the xenoliths (Gain and Mostert, 1982; Hammerbeck and Schurmann, 1998; Harris and Chaumba, 2001; Manyeruke, 2003; MacDonald et al., 2005; Kinnard et al., 2005). The economic sulphide mineralization at Selebe-Phikwe is associated with an amphibolite, although in this instance the regional metamorphic grade is also of the upper amphibolite facies (Snyman,

1996). The deposit in Shangani, Zimbabwe, is found in a serpentine-talc schist within a greenschist fragment (Snyman, 1996). The sulphide mineralization of the Pechenga deposits, in the Kola Peninsula, north-western Russia, is associated with serpentinized peridotite (Barnes et al., 2001).

The nickeliferous sulphides show a tendency to be associated with hydrothermal metamorphosed host rocks. This may be due, firstly, to extensive assimilation of country rock that release volatiles (CO_2, H_2O, etc.) into the intruding magma. This will, secondly, result in an increase in the oxygen fugacity, with the effect being sulphur super saturation. Thirdly, a skarn and magma mix could have acted as a trap for sulphide droplets. Fourthly, under such magmatic conditions, the crystallization of typical magmatic sulphide mineral assemblages including: pyrrhotite, chalcopyrite, pentlandite and Platinum Group Minerals will occur. Lastly, retrograde metamorphic mineralization of magnetite and pyrite will modify and react with the magmatic mineralization. During this time there appears to be a bottom-up escape of hydrothermal fluid, and top-down introduction of immiscible sulphide fluids.

The relationship between metasomatism and metallogenesis may be explained by the following model: the assimilation of country rock, which contains hydrous minerals or has been hydrated due to prior metasomatism, by the intruding magma leads to an increase in the oxygen fugacity. Fluids may also be introduced into the system by a hydrous interstitial melt. The role of addition of H_2O and CO_2 to magma and the resultant precipitation of sulphides and spinels has been noted before (de Waal, 1977). This may result in the formation of e.g. sulphide or chromite deposist as was the case suggested for the Uitkomst Complex and Bushveld Complex. In the event of the formation of an impermeable layer higher up in the succession, the fluid will now become trapped beneath that layer. The overlying layer may be impermeable due to smaller grain size of the new mineralization regime, e.g. chromite grains of the UG2 layer in the Bushveld Complex or MCR layer of the Uitkomst Complex. It may also be due to the formation of adcumulus minerals or the presence of interstitial minerals that is either in equilibrium with the fluid or slow dissolution of the mineral in the fluid e.g.

primary plagioclase in the case of LHZBG Unit in the Uitkomst and the UG2 layer of the Bushveld Complex.

The fluid responsible for the precipitation sulphide or spinel from the magma would now be effectively trapped beneath this impermeable layer. This may lead to metasomatism (in the case of the Uitkomst Complex and Bushveld Complex) and if temperatures remain high enough, partial melting of the protolith (suggested in the Bushveld Complex). Upon cooling this fluid might lead to the formation of retrograde metamorphic alteration of the precursor minerals. This model would also suggest that the most intense alteration of precursor minerals will occur beneath the impermeable layer.

10.3 Discussion of the features in the lower parts of the Uitkomst Complex

In brief the possible sequence of alteration in the Uitkomst Complex may be summarised as:

1. The main mafic magma of the PCR and MHZBG Units on or near the contract Bevets conglomerates and the overlying shales and underlying Malmani Dolomite. The original extent of the conduit is represented by the lateral extent of the PCR Unit. Chromite grains segregated from the melt and formed the stringers and schlieren observed in the PCR Unit and the lower parts of the MHZBG.

2. The shale was more susceptible to magmatic erosion and developed into the broader dimensions observed in the current body. Due to the rapid broadening of the conduit upward less chromite grains could remain in suspension. This led to the development of the MCR Unit near the upper contact of the dolomite host rock. The broadening of the conduit also resulted in the decreased ability of the magma to suspend chromite grains. This resulted in preferential deposition of the MCR to form the three chromitite hills. The signature of the shale country rock is evident in the isotopic signature observed in the lower units.

3. The magma of the PCR did probably not suffer as much assimilation and hybridisation due to interaction with dolomite country rock, as xenoliths are

absent in this unit. This would also indicate a more rapid emplacement of this magma. Primary sulphides formed in the form of disseminated mineralization. Here the presence of both hexagonal and monoclinic pyrrhotite may support the hypothesis of less assimilation of country rock. Olivine preserved in this unit also indicates its magmatic source. Diopside composition points to a mixed source of magmatic and transitional material. This unit completely lacks skarn diopside.

4. The PCR Unit may have been emplaced by continual pulses of chromite-bearing magma source magma, as indicated by the chromite lenses layers and schlieren. The magma emplacing the PCR Unit would have started stoping into the Rooihoogte sediments, changing the range of elements contaminating the magma. The magma would now be contaminated by a Si and Al country rock component. The edges of the Complex in the PCR Unit may now be bound by a combination of skarn and hornfels at different stratigraphic heights.

5. The next phase of magmatic activity, that formed the LHZBG Unit, followed without a significant hiatus. The magma that formed the LHZBG Unit may have mixed with some of the residual peridotic/harzburgitic magma present in the conduit system.

6. The initial pulses of intruding magma intruded in a passive style. This led to a gradual downward development of the conduit and resulted in the formation of the skarn aureole in the lower third of the LHZBG Unit. The passive style of intrusion is demonstrated by the preservation of horizontal layering in the calc-silicate xenoliths. The siliceous dolomite rafts between the layers of intruded magma were thermally metamorphosed and formed diopside-rich calc-silicate xenoliths. Skarn rocks that formed prior to the intrusion of the lower LHZBG magma influenced the intrusion pattern of the LHZBG magma. The passive nature of the intrusion led to assimilation of dolomitic skarn xenoliths and the hybridisation of the magma. The collapse of xenoliths may have released a calcite-rich fluid into the hybrid magma. This is demonstrated by the presence of calcite that appears to be in equilibrium

with the surrounding magmatic minerals. The release of this fluid may also have contributed elements such as Ca, Fe and Mg that led to a decrease in viscosity of the hybrid magma. This decrease in viscosity may also have contributed to the preservation of xenoliths in the lower parts of the LHZBG Unit, as the less viscous hybrid magma may not have been able to suspend the xenolith blocks. This phenomenon may also be responsible for the formation of relatively large diopside crystals at the contact between the xenolith and the surrounding hybrid pyroxenite. The pegmatoidal rocks surrounding some of the xenoliths may therefore have developed at this time. The original magma responsible for the formation of the LHZBG Unit was more primitive in nature, and able to accommodate the addition of Ca. The addition of Ca led to the crystallization of Ca-rich minerals from the hybrid magma. The Ca-rich minerals that formed include: transitional range clinopyroxene (diopside) and Ca-amphiboles forming part of the solidification fronts that developed. The formation of these solidification fronts may have prevented the conduit in which the magma of the LHZBG was transported, from attaining the same lateral extent as the underlying BGAB Unit. Intrusion of magma during this stage formed the "foot" of the anvil-shape of the intrusion.

7. Magmatic fluids released during the intrusion would not be in chemical equilibrium with the siliceous dolomite rock and the elevated temperature would drive the decarbonation reactions. The decarbonation reactions may also have led to the release of CO_2 and H_2O and other volitiles that were taken up in fluids that migrated in or were removed form the conduit system. This may have resulted in the enrichments of elements such as: Mo, Nb, Ni, Y, Th, U, Y, Zn, S, and V towards the SE of the Complex, as determined by the isocon method. Evidence has been provided that the magma flow in the conduit was from the NW to the SE.

8. The magma may have become sulphur supersaturated due to the partial assimilation of dolomitic country rock and accompanying devolitization. The assimilation of dolomitic country rock led to an increase in oxygen fugacity,

lowering the FeO content and thus the sulphur carrying capacity of the magma. The magma may also have suffered contamination by Si, especially during the period the Rooihoogte sediments formed the roof. The system may also have been enriched with Si, as Al substituted for Si in the hybrid diopside, possibly leading to a slight increase in the Si content of the melt. The magma may also have been contaminated by sulphides derived from the dolomite country rock.

9. The initial pulses of magma forming the LHZBG Unit had a higher oxidation potential, which led to the formation of minor primary magnetite. The oxidation potential however lowered, which favoured the formation of nickeliferous sulphides. The preserved magnetite suffered silicification and where the grains came into contact with pyrrhotite, an exsolution rim of ilmenite and a Ti-rich phase formed.

10. The top-down infiltration of a sulphide fluid with a low viscosity resulted in the formation of the net-textured wehrlite layers. Here the sulphide fluid infiltrated between the magmatic derived olivine grains that had segregated from the melt. Hydrous acidic fluids associated with the sulphide fluids may have led to the partial or complete serpentinization of these olivine grains.

11. The initial contamination of the magma by volatiles may have led to the formation of high grade amphiboles like pargasite and hornblende, referred to here as the "first generation" amphiboles. These amphiboles, along with precursor mafic minerals such as olivine and clinopyroxene, and skarn minerals served as traps for the sulphide fluid. Evidence for this is found in the sharp contacts between the precursor minerals and hornblende grains and the interstitial sulphide grains.

12. The dynamic nature of the deuteric system may have led to the formation of the alteration assemblages observed throughout the LHZBG Unit. As the CO_2-rich fluids were removed from the system, the hydrous fluids would dominate the system. This would lead to the retrograde metamorphism observed in this unit. The hydrous fluids may have led to the further serpentinization of the preserved olivine grains, especially along cracks. This

resulted in the formation of serpentine and secondary magnetite assemblages. It would also lead to the formation of actinolite-tremolite pseudomorphs after diopside, referred to here as "second generation" amphiboles. These actinolite-tremolite grains are then intergrown with the interstitial sulphide grains, effectively reducing the size of the nickeliferous sulphide grains. The actinolite-tremolite grains are preferentially intergrown with the nickeliferous sulphides, in between the coarse grained pentlandite and the chalcopyrite rims around the main pyrrhotite grain. The migration of the fluids would also influence the distribution of the alteration minerals. These fluids may also have been responsible for the formation of late stage alteration derived magnetite and euhedral pyrite associated with the pyrrhotite grains.

13. The alteration assemblages observed in the LHZBG Unit vary greatly in distribution, both with spatial and height distribution. The most common silicate alteration assemblages observed in the LHZBG are: talc-dolomite (carbonate)-chlorite, talc-chlorite-tremolite, chlorite-serpentinte-carbonate, chlorite-serpentine-tremolite, hornblende-chlorite and hornblende-tremolite.

14. Amphibole has its highest abundance in the upper part of the LHZBG Unit close to the top of the unit, close to the margins of the trough and in the lower part of the unit in the broader part of the Complex. The amphibole content also seems to decrease from the north to the south in the study area. The talc content is highest in the upper part of the LHZBG Unit in the narrow part of the Complex and then again highest in the lower part of the unit in the broader area. The talc content decreases towards the southeast. The serpentine content increases towards the northwest. The chlorite content decreases from the north to the south in the study area. The hydrothermal metamorphism and metasomatism may already have commenced during the emplacement of the LHZBG Unit.

15. The MCR layer may have served as an effective barrier, preventing further upward circulation of fluids from the underlying units and concentrating the fluids in the PCR Unit.

16. The CO_2-rich deuteric fluid, being trapped under the MCR layer and bound by the skarn margins of the complex, affected the entire PCR Unit. The precursor minerals were metasomatically altered by the hot, acidic CO_2-rich fluid, to yield the observed completely altered matrix minerals observed in the PCR Unit. The extensive alteration of the PCR Unit may also have led to a substantial increase in the volume of the unit. The main alteration assemblages found in the PCR Unit are: talc-chlorite-amphibole, talc-carbonate-chlorite-amphibole, serpentine-amphibole, tremolite-hornblende and talc-phlogopite.

17. The amphibole content shows no vertical preference of occurrence but decrease towards the southeast. Talc has the highest occurrence in the upper part of the unit in the northwest of the study area and decrease in content towards the margins of the Complex. The talc content increases towards the southeast in the study area. Chlorite has its highest occurrence in the bottom part of the narrower part of the Complex and highest in the central part, decreasing in content towards the southeast of the study area. Serpentine is found to increase in content towards the southeast in the study area. This may indicate the hydrothermal fluids to have been more hydrous towards the margins and southeast of the Complex, in this unit, in the study area.

18. The deuteric fluid was able to mobilize certain elements to different extents. This led to the observed either enrichment or depletion of certain elements (Mg, Ca, K, Cu, Ga, Ni Sc, Cs and Ba) with depth, as determined by means of the isocon method. This may indicate a hydrothermal system operating vertically in the PCR.

19. Where the MCR layer was not developed, the CO_2-rich fluid was able to escape into the lower part of MHZBG Unit and affect it. This led to the formation of the LrPRD Sub-unit that was hydrothermally metamorphosed, though less so than the PCR Unit, but more than the rest of the MHZBG Unit. It may also have led to an increase in the oxygen fugacity that was enough to cause sulphide over saturation in the LrPRD Sub-unit and in some areas of the MHZBG Unit. Using the isocon method it was also established that

certain elements (Mg, Na, Zn, Co and Sc) were enriched or depleted with depth in the LrPRD. This indicates that the hydrothermal system operated vertically out of the PCR Unit into the LrPRD Sub-unit before entering the MHZBG Unit.

20. Preceding the "closed" phase of the conduit, the noritic magma was emplaced above the MHZBG unit and below the lower contact of the LHZBG Units. Work by previous workers indicated the composition of the BGAB and GN to not differ significantly.

21. The less mafic nature of the BGAB magma did not allow for the formation of Ca-rich minerals to form effective reaction fronts. The intrusion was such that little mixing and hybridisation with the dolomite host rock took place. Due to the lack of significant solidification fronts, a system of hydrous fluids may have developed and started to interact with the magmatic precursor minerals (hornblende, quartz and plagioclase) of the gabbroic rocks. This may have resulted in the observed secondary mineralogy in the BGAB Unit, consisting of actinolite, chlorite, muscovite and lizardite. The assimilation of country rocks and interaction with hydrous fluids, may have led to the general enrichment of elements (such as As, Ga, Mo, Nb, etc.) in the BGAB Units as determined by the isocon method.

22. Emplacement of the Marginal Gabbro may have been contemporary with the BGAB and GN Units. This unit was never as fully developed due to the limiting effects of the surrounding skarn.

23. The characteristics of the skarn aureole around the lower units (BGAB, LHZBG and PCR Units) may have prevented the infiltration of meteoric water during the initial stages of metamorphism. Thus, it may be assumed that the fluids responsible for the metasomatic alteration of these units were derived from the breakdown of dolomitic derived skarn and to a lesser extent magmatic fluids.

24. After most of the CO_2-rich fluids were removed from the system, the hydrothermal system may have become hydrous dominated. In the central part of the Complex, the preserved heat may have driven this hydrous system

that led to the late-stage chlorite alteration. This is demonstrated by the chlorite pockets on the amphibole grains. Since the chlorite alteration is most prominent in the central part of the Complex, it may indicate that the margins of the Complex may have had a moderating effect on the circulation system operating in the Complex at this time.

25. The BGAG, LHZBG and PCR Units were affected by tectonic events post-dating the cooling of the Uitkomst Complex that also had an effect on the alteration assemblages. Tectonic events that affected the Uitkomst Complex are discussed by Hornsey (1999). These include sub-vertical strike-slip faulting and thrusting. Thrusting is evident from the duplication of lithological units. Two main events are postulated; the first is related to the deformation of the contact between the PCR and the MHZBG Units, likely due to the increase of volume in this unit as the precursor minerals were altered. The second is related to regional deformation, with the most prominent feature being Basal Shear Zone. Related thrust zones within the Complex are represented by talc-chlorite schist zones. These shear zones may have provided pathways for minor fluids to infiltrate the Complex, leading to further alteration processes, possibly affecting mineralogy and leading to further volume changes.

26. The Uitkomst Complex may also have suffered minor alteration due to the intrusion of sills and dykes. The intrusion of the sills and dykes may have led to alteration of the host rock mineralogy in direct contact with the dyke and also affected the total volume of the Uitkomst Complex by dilation. The effect may be most profound in the PCR Unit where diabase intrusions exploited the weakened area of deformation between the MCR layer and the MHZBG Unit. It is conceivable that the intrusive event may have released some of the volatiles associated with the alteration minerals found in the shear zones.

27. Later processes responsible for the formation of the present escarpment exposed, weathered and eroded the Uitkomst Complex. Where the lower units (BGAB, LHZBG and PCR Units) are exposed on the farms Slaaihoek

and Vaalkop the units suffered weathering due to meteoric water infiltration. This changed the mineralogy, and resulted in the oxidation of silicate and sulphide minerals and the formation of hydroxide and clay minerals. The present overburden derived mainly from the Timeball Hill shale, Klapperkop quartzite and diabase, is variable in depth.

14.4 Conclusion

It is suggested that the presence and presevation of calc-silicate xenoliths in the Lower Harzburgite Unit, due to the formation of solidification fronts, may have been an important factor in limiting the hydrothermal alteration of the precursor mafic minerals in this unit. The second important factor may have been the up- and outward removal of the CO_2-rich fluids by the hydrothermal circulation system operating in a rapidly flowing conduit system emplaced at depth. The third factor, that may have limited the alteration in the LHZBG Unit, may be the physical properties of the skarn margin surrounding the intrusion, preventing the inflow of meteoric water.

It is suggested that the almost complete hydrothermal alteration of the precursor mafic minerals in the PCR Unit may be due the entrapment of CO_2-rich fluids in a deuteric system operating in this unit by the overlying MCR layer and ineffective removal of the CO_2-rich fluid through the skarn and reaction front surrounding the Uitkomst Complex. The hydrothermal fluid would be in effect "trapped" in the PCR Unit. The heat of the system will drive the CO_2-rich fluid upward and outward, but would be prevented from leaving the PCR Unit by the overlying MCR layer and the surrounding skarn solidification fronts. It is also considered unlikely that the fluid may cool and percolate back down into the, by now mostly solidified, LHZBG Unit. The fluid may then only have been able to be removed by escaping the system where the MCR layer is not well developed, into the LrPRD Sub-unit and MHZBG Unit, as long as the conduit system was still operational.

The proposed processes discussed in this section are illustrated by Figures 10.2 to 10.7. It should be noted that the processes discussed here is most likely to have been

continuous, leading to successive alteration events and alteration assemblages. Later events, such as the intrusion of the dykes and tectonic remobilization may have led to a partial over print of the earlier recorded events.
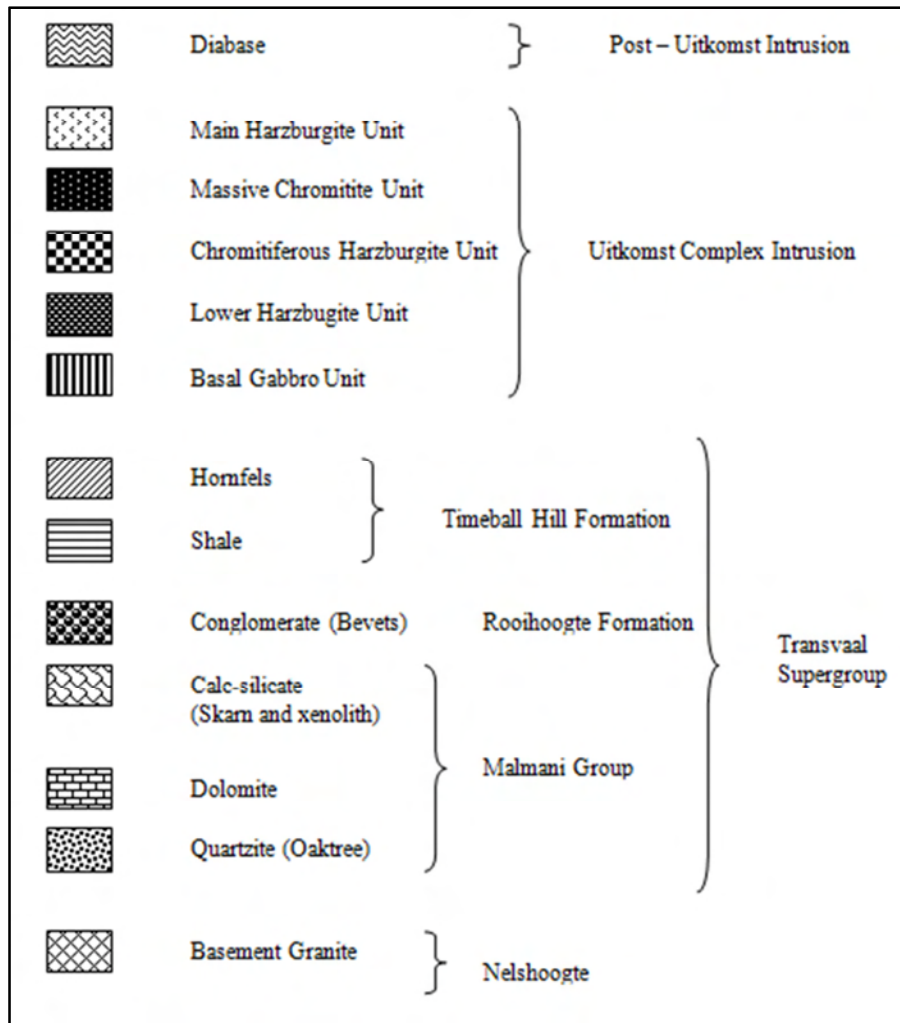
Figure 10.1. Legend to all diagrams in this section.
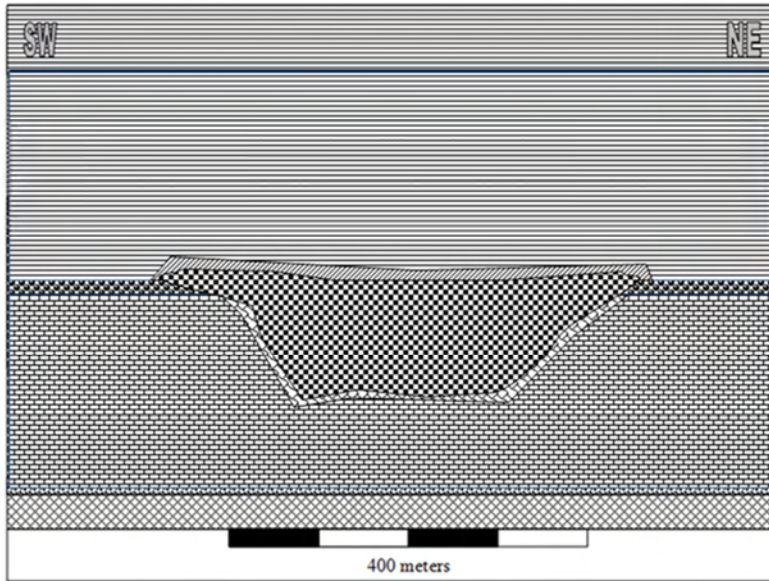
Figure 10.2. Initial intrusion of the PCR and MHZBG magma, between the Bevets Conglomerate and Oaktree Formations. This led to the formation of the first skarn and hornfels aureoles. Figure is looking down the conduit in a northwesternly direction.
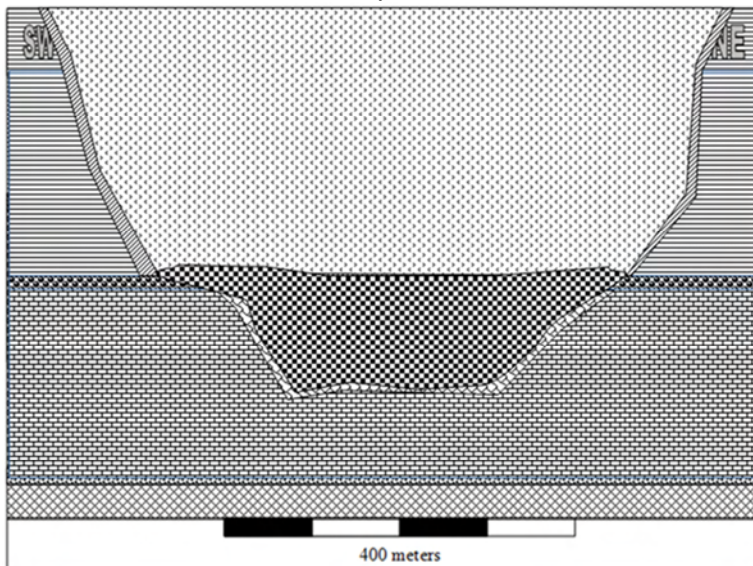
Figure 10.3.   Intrusion of the initial pulses of the magma that formed the PCR and MHZBG Unit. Deposition of the chromitite layers and schlieren in the PCR. Rapid expansion of the MHZBG into the overlying shale roof rocks continue and minor hornfels development. Devolitization of the underlying Malmani Formation start and the fluid generated is expelled by the movement of magma in the conduit.
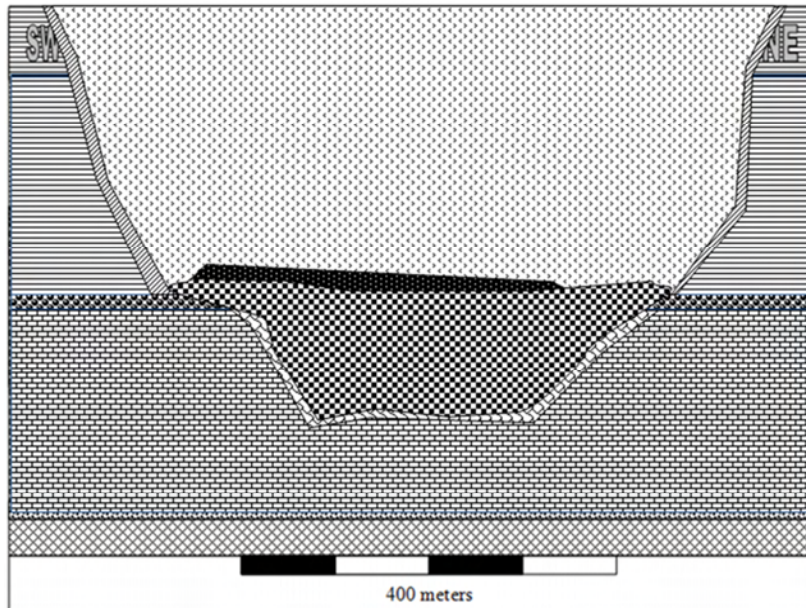
Figure 10.4. The upward expansion of the MHZBG Unit and localized broadening of the conduit resulted in the deposition of the MCR Unit. Further development of the thin hornfels aureole continue. Sulphide saturation is reached and droplets accumulate in a disseminated manner in the PCR Unit. Sulphide saturation is not attained in the MHZBG and only minor sulphide segregation takes place.
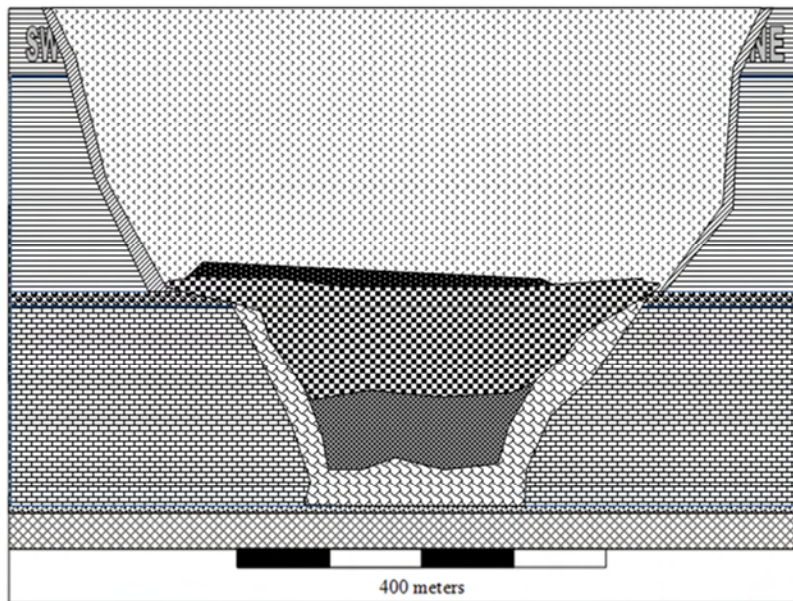
Figure 10.5. Intrusion of the LHZB G magma. Intrusion of the LHZBG magma scoured the bottom of the PCR Unit. The formation of extensive skarn along the margin and specifically in the lower third of the Unit take place. Sulphide saturation of the magma is reached. Devolitization of the country rock and included xenoliths take place. The fluid migrates upward and outward. The fluid migrates up to the PCR unit were it leaves the system less efficiently. Talc and secondary dolomite is stabilized.
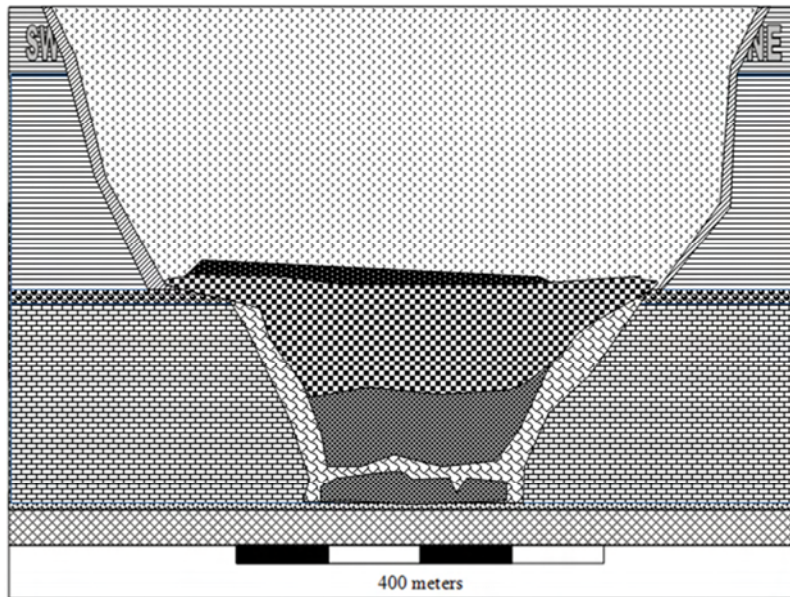
Figure 10.6. The passive emplacement of the LHZBG results in the preservation of the undisturbed calc-silicate xenoliths in the lower third of the intrusion. Devolitization of the country rock and included xenoliths continue. The resulting fluid migrates from the LHZBG, leaving the residual fluid more hydrous. This results in retrograde metasomatism of the overlying mafic minerals.
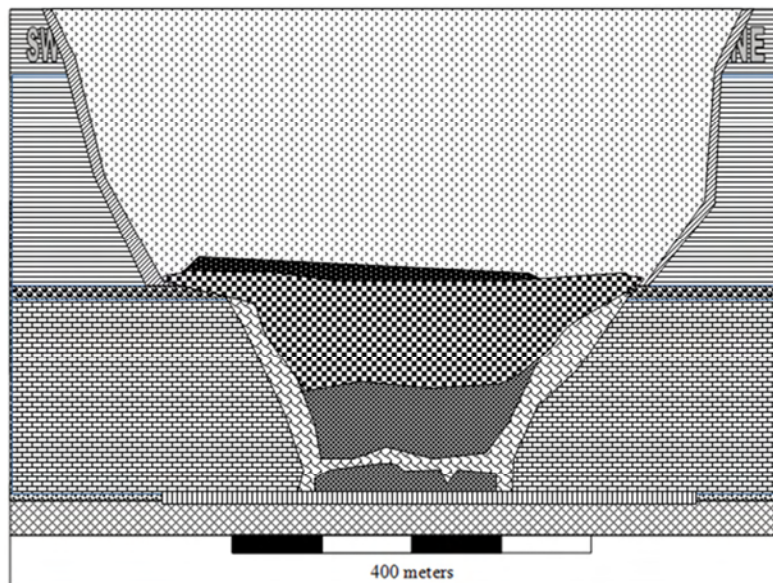
Figure 10.7. The BGAG Unit is emplaced. This unit is less mafic and interacts to a far lesser extent with the country rock. Devolitization of the country rock results in the alteration mineral assemblages observed in this unit. The fluid in the LHZBG is more hydrous, whereas the fluid in the PCR is more CO_2-rich

247
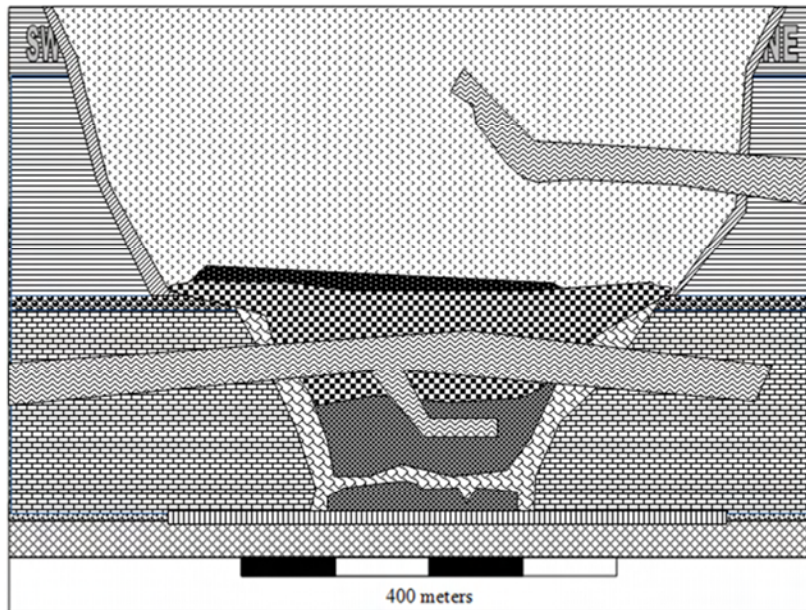
Figure 10.8. The Uitkomst Complex is intruded by diabase dykes and sills. The Complex suffers tectonic deformation. The Complex is weathered down to be exposed in its current form

An idealized section through the Uitkomst Complex is given in Figure 10.9. It is inferred that the main source of fluids was the assimilation of the dolomites. The meteoric water derived from the assimilated dolomite country rock would have migrated in the conduit. This would lead to the serpentinization of the xenoliths and the formation of the pyroxenite and amphibolite associated with the xenoliths. The lower part of the LHZBG will be affected by retrograde metamorphism. It has been determined that the migration of CO2-rich fluid would be up and outward, so the lower part of the unit will be dominated by a hydrous fluid. After the formation of the solidification fronts, no further fluids are expected to be expelled from the xenoliths into the magma. The fluids may now be driven upward, and not affect the precursor minerals in the lower part of the LHZBG Unit any further.

The CO_2-rich fluids would migrate up into the PCR Unit, and lead to the CO_2-rich deuteric system which results in the initial alteration of the PCR Unit. This may have resulted in the almost complete talc-carbonate alteration observed in this unit. Some fluid may, however, have been able to escape the system along the flow of the conduit. The fluid may also have been able to escape into the MHZBG Unit where the MCR layer is not developed, and led to the formation of the LrPRD Sub-unit. Some of the fluids,

especially the CO_2-rich fluid may also have been able to leave the system along the margins, where the hornfels margins was not well developed. The resultant increase in volume of the PCR Unit due to the formation of the alteration assemblages is inferred to have led to the formation of the shear zone between the PCR Unit and MCR layer. Fluids may have migrated more effectively along the shear zone.

The system may eventually have become hydrous dominated. The occurrence of a late-stage cooler circulation system, only operating in the central part of the Complex, is proposed to have developed, with the margins having a moderating effect on the system. Meteoric water is not expected to have entered the Complex, influencing the hydrothermal system.
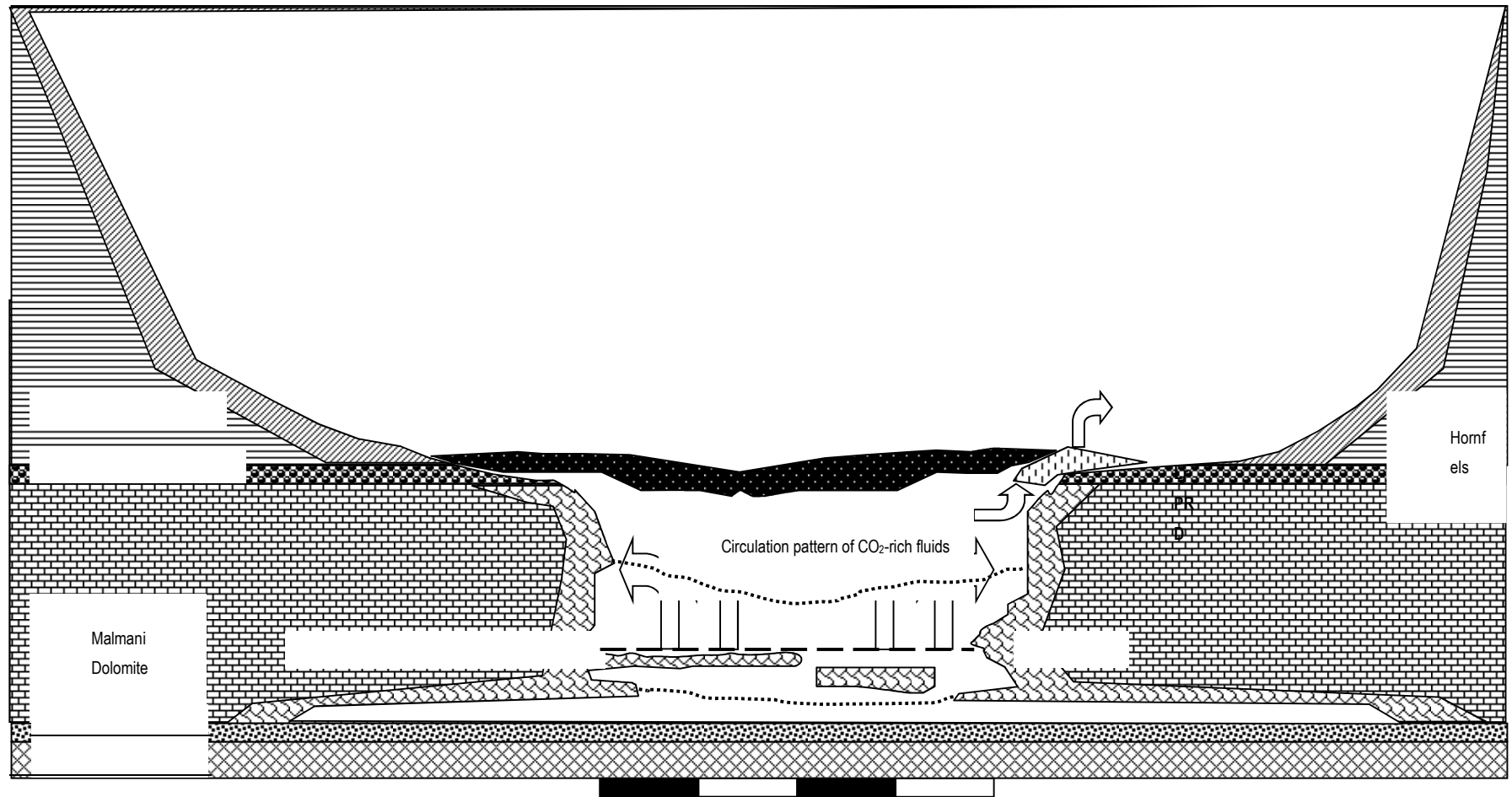
Figure 10.9. An idealized representation of the hydrothermal circulation system operating in the Uitkomst Complex.

CHAPTER 11: CONCLUSIONS

Based on the current research results and combining it with previous research on the petrogenesis of the Uitkomst Complex, the following conclusions can be made:

The Uitkomst Complex represents a satellite body related to the larger adjacent Bushveld Igneous Complex (BIC), but was the magma was derived from a separate staging chamber. This resulted in the composition of the Uitkomst magma differing from the BIC magmas. The Uitkomst Complex was emplaced as a conduit, where a significant portion of the complex had been eroded away during the development of the Great Escarpment.

The Uitkomst Complex was emplaced on or near the contact between the Malmani dolomite and the Timeball Hill shale. The first pulse of magma is represented by the Chromatiferous Harzburgite unit, the most mafic of the units in the layered complex. This is indicated by the abundance of chromitite lenses and schlieren in this unit and the more primitive composition of the olivine and clinopyroxene grains. This was followed by the emplacement of the Lower Harzburgite and Main Harzburgite units. The Lower Harzburgite unit is indicated to have stoped downward into the dolomite country rock and the Main Harzburgite upward into the overlying shale. The slight difference in mineralogy between these two units is ascribed to the limited assimilation of dolomite country rock by the Lower Harzburgite. The downward emplacement of the Lower Harzburgite unit in a "passive" pulse-like manner resulted in the formation of the xenolith horizon in the lower third of this unit. Devolitization of the xenoliths and dolomite country rock is suggested to have taken place during emplacement of this magma. It has been suggested that the addition of CO_2 to the system resulted in the super saturation of sulphide in the magma, resulting in the observed mineralization in the Chromatiferous Harzburgite and Lower Harzburgite units.

The fluid derived from the devolitization of the xenoliths and country rock migrated upward from the emplacing Lower Harzburgite into the overlying Chromatiferous Harzburgite unit. This deuteric fluid was initially very CO_2-rich, but as the supply of

additional fluids from devolization decreased and was expelled from the system it became more H_2O-rich. The fluid that did not migrate out of the Lower Harzburgite unit was more H_2O-rich and resulted in the retrograde metamorphic assemblages, dominated by amphibolite, observed in this unit.

The fluid that migrated upward was trapped in the overlying Chromatiferous Harzburgite unt. The fluid remained CO_2-rich for a sufficiently long time to stabilize the formation of talc-carbonate assemblages that completely pseudomorphically replaced the precursor mafic minerals in this unit. As the system cooled, the CO_2-content of the fluid(s) migrating in the Basal Unit decreased. This resulted in minor overprinting of the previous alteration events. This last alteration event is reflected by the serpentinization and secondary magnetite replacement in otherwise pristine olivine grains and pockets of chlorite associated with amphibolite. The deuteric fluid was constrained to the Basal Unit, with the Main Unit remaining largely unaffected.

REFERENCES

Abu El-Enen, M.M., Okrusch M. and Will, T.M. (2004). Contact metamorphism and metasomatism at a dolerite-limestone contact in the Gebel Yelleq area, Northern Sinai, Egipt. *Mineralogy and Petrology* **81**, 135-164.

Akima, H. (1978). A Method of Bivariate Interpolation and Smooth Surface Fitting for Irregularly Distributed Data Point. *ACM Transactions on Mathematical Software*, **4**, p. 148-159.

Alva-Valdivia, L.M., Goguitchaichvili, A., Unutia-Fucugauchi, J., Caballere-Miranda, C., Vivillo, W. (2001). Rock-magnetism and Ore Microscopy of the Magnetite-apatite Ore Deposit from Cerro de Mercado, Mexico. *Earth Planets Space,* **53,** 181-192.

Anhaeusser, C.R. (2001). The Anatomy of an Extrusive-Intrusive Archaean Mafic-ultramafic Sequence: the Nelshoogte Schist Belt and Stolzberg Layered Ultramafic Complex, Barberton Greenstone Belt, South Africa. *South African Journal of Geology.* **104**, nr. 2, 167-204.

Anonymous (2007). African Rainbow Minerals: 2006 Annual Report. 188p.

Anonymous (2010). African Rainbow Minerals: 2010 Mineral Resources and Reserves. 33 p.

Armitage, P.E.B., MacDonald, I., Edwards, S.J. and Manby, G.M. (2002). Platinum-Group Element Mineralization in the Platreef and Calc-silicate Footwall at Sandsloot, Potgietersrus District, South Africa. *Transactions of the Institute of Mining and Metallurgy* **III** (Reprinted from Applied Earth Science, January-April 2002). B36-45.

Arndt, N.T. (2005). The Conduits of Magmatic Ore Deposits. In Mungall, J. (ed). Exploration for Platinum-group Element Deposits. Mineralogical Association of Canada. Special Volume. 181-201.

Arndt, N.T., Lesher, C.M., Czamanske, G.K. (2005). Mantle-derived Magmas and Magmatic Ni-Cu (PGE) Deposits. *Economic Geology,100th Anniversary Volume.*.5-24.

Arndt, N.T., Czamnske, G.K., Walker, R.J., Chauvel, C. and Fedorenko, V.A. (2003). Geochemistry and Orogin of the Intrusive Hosts of the Noril'sk-Talnakh Cu-Ni-PGe Sulphide Deposits. *Economic Geology,* **95,** 495-515.

Baker C.K. and Black P.M. (1982). Assimilation and Metamorphism at a Basalt-Limestone contact, Tokatoka, New Zealand. *Mineralogical Magazine.* **43**, 797-807.

Barnes, C.G., Prestvik, T., Sundvoll, B and Surratt, D. (2005). Pervasive assimilation of carbonate and silicate rocks in the Horavaer igneous complex, north-central Norway. *Lithos* .**80**, 179-199.

Barnes, S-J, Melezhik, V.A., Sokolov, S.V. (2001). The Composition and mode of Formation of the Pechenga Nickel Deposits, Kola Peninsula, Northwestern Russia. *The Canadian Mineralogist* **39,** 447-471.

Becker M., de Villiers, J. and Bradshaw, D. (2010). The Mineralogy and Crystallography of Pyrrhotite from Selected Nickel and PGE Ore Deposits. Economic Geology; **105**; p. 1025-1037.

Blom, M.P. (1988). Selected Magnetic and Gravity Anomalies in the Eastern Transvaal and Their Possible Relationship to the Rustenburg Layered Suite. Unpublished MSc. University of Pretoria, 53p.

Bottinga, Y and Javoy, M. (1990). The Degassing of Hawaian Tholleiite. *Bulletin of Volcanology,* **53**, 73-85.

Boudreau, A.E. and McCallum, I.S. (1992). Concentrations of Platinum-Group Elements by Magmatic Fluids in Layered Intrusions. *Economic Geology* **87**, 1830-1848.

Bowen, N.L. (1940). Progressive Metamorphism of Siliceous Limestone and Dolomite. *Journal of Geology,* **48**, 225-274.

Brownlow, A.H. (1979). Geochemisty. Prentice-Hall Inc. Eaglewood Cliffs, New York. 30-31.

Bucher-Nurminen, K. (1982). On the Mechanism of Contact Aureole Formation in Dolomitic Country Rock by the Adamello Intrusion (Norhtern Italy). *American Mineralogist,* **67,** 1101-1117.

Butcher, A.R., Merkle, R.K.W. (1991). Unusual Textures and Structures associated with a Magnetite Layer in the Bushveld Complex: a Contribution to the Adcumulus Debate. *Mineralogical Magazine,* **55,** 465-477.

Chandraharam D., Vaselli O., Sheth H.C. and Keshav S. (2000). Petrogenetic Significance of Ferro-enstatite Orhtopyroxene in Basaltic Dikes from the Tapi Rift, Deccan Flood Basalt Province, India. *Earth and Planetary Letters* **179,** 469-476.

Craig J.R and Vaughn D.J. (1990). Composition and Textural Variations of the Major Iron and Base-metal Minerals. In: *Sulphide Deposits - Their Origin and Processing.* (Ed) Gray P.M.J., Bowyer G.J., Castle J.F., Vaughn D.J. and Warner N.A. The Institution of Mining and Metallugy, 1 – 16.

Cui, X., Nabelek, P.I. and Liu, M. (2003). Reactive Flow of Mixed CO_2–H_2O Fluid and Progress of Calc-silicate Reactions in Contact Metamorphic Aureoles: Insights from

Two-dimensional Numerical Modelling. *Journal of Metamorphic Geology.* **21,** Issue 7, 663-684.

d'Ars, J de B., Arndt, N.T., Hallot, E. (2001). Analog Experimental Insights into the Formation of Magmatic Sulphide Deposits. *Earth and Planetary Science Letters,* **186,** 371-381.

Dawood, Y.H., Abd El-Naby, H.H. and Sharafelden, A.A. (2004). Influence of the Alteration Process on the Origin of Uranium and Europium Anomalies in Trachyte, Central Eastern Desert, Egipt. *Journal of Geochemical Exploration*, **88,** 15-27.

Deblond, A., Tack, L. (1999). Main characteristics and review of mineral resources of the Kabanga-Musongati mafic-ultramafic alignment in Burundi. *Journal of African Earth Sciences.* **29**, No 2, 313-328.

Deer, W.A., Howie, R.A., Zussman, J. (1997). The Rock-forming Minerals Vol 2B, Double-chain Silicates, 2nd Edition. Longman, 764p.

Deer, W.A., Howie, R.A., Zussman, J. (1992). An Introduction to the Rock-forming Minerals 2nd Edition. Longman.696p.

De Nooy D. (2003). Mineralogy of the Base Metal Sulphide Mineralization of the Uitkomst Complex. *Mineralogy and Geochemistry of Base Metal Deposits in Southern Africa – Implications for Exploration and Benefication.* Proceedings Volume. 11-13.

De Waal S.A., (1977). Carbon Dioxide and Water from Metamorphic Reactions as Agents for Sulphide and Spinel Precipitation in Mafic Magmas. *Transactions of the Geological Society of South Africa,* **80,** 193-196.

De Waal S.A., Gauert C.D.K. (1997). The Basal Gabbro Unit and the Identity of the Parental Magma of the Uitkomst Complex, South Africa. *South African Journal of Geology*, **100(4)**, 349-361.

De Waal, S.A., Graham, I.T. and Armstrong R.A. (2006). The Lindques Drift and Heidelberg Intrusions and the Roodekraal Complex, Vredefort, South Africa: Comagmatic Plutonic and Volcanic Products of a 2055 Ma Ferrobasaltic Magma. *South African Journal of Geology* **109** nr. 3, 279-300.

De Waal, S.A., Maier, W.D., Armstrong, R.A. and Gauert, C.D.K. (2001). Parental Magma and Emplacement of the Stratiform Uitkomst Complex, South Africa. *The Canadian Mineralogist* **39**, 557-571.

Dipple, G.M. and Ferry, J.M. (1996). The Effect of Thermal History on the Development of Mineral Assemblages During Infiltration-Driven Contact Metamorphism. *Contributions to Mineralogy,* **124,** 334-345.

Dodd D.C. (2004). Exploration Strategies for Nickle Sulphide Deposits. Unpublished MSc. Dissertation. University of Pretoria. 134p.

Dokuchaeva, V.S. and Yakovlev, Y.N. (1994). Monchegorsk Pluton. *Geological Institute KSC RAS. 7th International Platinum Symposium. Kola Belt of Layered Intrusions. Guide to the Pre-symposium field trip July 27-31, 1994.* Edited by: Mitrofanov, F. and Torokhov, M. 71-108

Ebel, D.S. and Naldrett, A.J. (1996). Fractional Crystallisation of Sulphide Ore Liquids at High Temperature. *Economic Geology* **91**, 607-621.

Edwards, R. and Atkinson, K. (1986). Ore Deposit Geology and its Influence on Mineral Exploration. Chapman and Hall ltd, New York. p. 47.

Ernst R.E. and Buchan K.L. (1997). Layered Mafic Intrusions: a Model for Their Feeder Systems and Relationship with Giant Dyke Swarms and Mantle Plume Centres. *South African Journal of Geology,* **100(4)**, 319-334.

Evans, D.M., Byemelwa, L and Gilligan, J. (1999). Variability of magmatic sulphide compositions at the Kabanga nickel prospect, Tanzania. *Journal of African Earth Sciences* **29**, No 2, 329-351.

Evans, D.M, Boadi, I, Byemelwa, L., Gilligan, J., Kabete, J. and Marcet, P. (2000). Kabanga magmatic nickel sulphide deposits, Tanzania: morphology and geochemisty of associated intrusions. *Journal of African Earth Sciences* **30**, No 3, 651-674.

Ferry, J.M. (2000). Patterns of Mineral Occurance in Metamorphic Rocks. *American Mineralogist.* **85**, 1573-1588.

Ferry, J.M., Wing, A.B., Penniston, S.C. and Runble, D.III (2002). The Direction of Fluid Flow During Contact Metamorphism of Siliceous Carbonate Rocks: New Data for the Monzoni and Predazzo Aureoles, Northern Italy and a Global Review. *Contributions to Mineralogy and Petrology,* **142,** 679-699.

Fulignati, P., Marianelli, P., Santacroce, R. and Sbaran, A. (2004). Probing the Vesuvius magma chamber-host rock interface through xenoliths. *Geological Magazine* **141** (4), 417-428.

Gain S.B. and Mostert A.B. (1981). The Geological Setting of the Platinoid and Base Metal Sulfide Mineralization in the Platreef of the Bushveld Complex in Drenthe, North of Potgietersrus. *Institute for Geological Research on the Bushveld Complex, Research Report nr.* **28**. University of Pretoria. 22p.

Gain S.B. and Mostert A.B. (1982). The Geological Setting of the Platinoid and Base Metal Sulfide Mineralization in the Platreef of the Bushveld Complex in Drenthe, North of Potgietersrus. *Economic Geology* **77,** 1395-1404.

Ganino, C, Arndt, N.T., Mei-Fu Zhou and Chauvel C. (2008). Interaction of magma with sedimentary wall rock and magnetite ore genesis in the Panzhihua mafic intrusion, SW China.. *Mineralium Deposita*, **43,** 677-694.

Gauert, C.D.K. (1998). The petrogenesis of the Uitkomst Complex, Mpumalanga Province, South Africa, PhD thesis, University of Pretoria, 315 p.

Gauert, C.D.K. (2001). Sulphide and Oxide Mineralization in the Uitkomst Complex, South Africa: Origin in a Magma Conduit. *Journal of African Earth Sciences.* **32,** nr. 2, 149-161.

Gauert C.D.K, de Waal S.A. and Wallmach T. (1995). Geology of the Ultrabasic to Basic Uikomst Complex: Eastern Transvaal, South Africa: an Overview. *Journal of African Earth Sciences*, **21**, 553-570.

Gauert C.D.K., Jordaan L.J., de Waal S.A. and Wallmach T. (1996) Isotopic Constrains on the Source of Sulphur for the Base Metal Sulphides of the Uitkomst Complex, Badplaas, South Africa. *South African Journal of Geology,* **99**, 41-50.

Giggenbach, W.F. (1989) Processes Controlling CO_2- and Cl-Content of Thermal Discharges from the Taupo-Rotorua volcanic-magmatic-hydrothermal system, New Zealand. In: Water-Rock Interaction WRI6. Proceedings of the 6th international symposium, Malvern, U.K. Edited by Miles, D.L. A.A.Bakema/Rotterdam/Brookfield. 259-262

Gilg, H.A., Lima, A., Somma, R., Belkin, H.E., de Vio, B. and Ayuso, R.A. (2001). Isotope Geochemistry and Fluid Inclusion Study of Skarns from Vesuvius. *Mineralogy and Petrology*, **73**, 145-176.

Glazner, A.F. (2007). Thermal Limitation on Incorporation of Wall Rock into Magma. *Geology*, **35**, 319-322.

Gomwe, T., (2002). A Geochemical Profile Through the Uitkomst Complex on the Farm Slaaihoek, with Special Reference to the Platinum-group Elements and Sm-Nd isotopes. Unpublished MSc. Dissertation, University of Pretoria, 107p.

Grant, J.A. (1986). The Isocon Diagram – A Simple Solution to Gresen's Equation for Metasomatic Alteration. *Economic Geology* **81**, 1976-1982.

Gresens, R.L. (1967). Composition-volume Relationships of Metasomatism. *Chemical Geology,* **2,** 47-55.

Hall, A. (1996). Igneous Petology 2nd Edition. Longman. Malaysia. p.26-28

Hammerbeck, E.C.I. and Schürmann (1998). Nickel *in:* The Mineral Resources of South Africa (M.G.C. Wilson and C.R. Anhaeusser, eds): Handbook, Council for Geoscience, **16**, 471-482.

Hanley, J.J and Mungull, J.E. (2003). Chlorine Enrichment and Hydrous Alteration of the Sudbury Breccia Hosting Footwall Cu-Ni-PGE Mineralization at the Frasier Mine, Sudbury, Ontario, Canada. *Canadian Mineralogist*, **41,** 857-881.

Harris,C. and Chaumba, J.B. (2001). Contamination and Fluid-Rock Interaction During the Formation of the Platreef, Northern Limb of the Bushveld Complex, South Africa. *Journal of Petrology* **42,** issue 7, 1321-1346.

Hattingh P.J. (1980). The Structure of the Bushveld Complex in the Groblersdal-Lyndenburg-Belfast Area of the Eastern Transvaal as Interpreted from a Regional Gravity Survey. *Transactions of the Geological Survey of South Africa*, **83**, p. 125 – 133.

Hawley, J.E. (1965). Upside-down Zoning at Frood, Sudbury, Ontario. *Economic Geology,* **60,** 529-575.

Hornsey R.A. (1999). The Genesis and Evolution of the Nkomati Mine Ni-Sulphide Deposit. Mpumalanga Province, South Africa. Unpublished MSc. Dissertation. University of Natal. 155p.

Hui W.Y., Tenailleau C., Pring A. and Brugger J. (2004). Experimental Study of the Transformation of Pentlandite/Pyrrhotite to Violarite. *Regolith,* 146-150.

Hulley, V. (2005). Reactions Between Country Rock Xenoliths and the Magma of Uitkomst Complex, with Implications for the Origin of the Sulphide Mineralization. Unpublished MSc. Dissertation. University of Pretoria. 117p.

Irvine, T.N. (1977). Origin of Chromitite Layers in the Muskox Intrusion and Other Stratiform Intrusions: A New Interpretation. *Geology,* **5,** 273-277.

Kacandes G.H., Ulmer G.C. and Grandstaff D.E. (1989). Monitoring the evolution of alteration minerals and fluids during a hydrothermal experiment. In Water-Rock Interaction WRI6. Proceedings of the 6th international symposium, Malvern, U.K. Edited by Miles, D.L. A.A.Bakema/Rotterdam/Brookfield. 353-356.

Kenyon A.K., Attridge R.L., Coetzee G.L. (1986). The Uitkomst Nickel-Copper Deposit, Eastern Transvaal.1009-1017. In: Anhaeusser C.R. and Maske S. (Eds) *Mineral Deposits of Southern Africa* I. Geological Society of South Africa. 1020p.

Kinnard, J.A., Hitchinson, D., Schurmann, L., Nox, P.A.M. and de Lange, R. (2005). Petrology and Mineralization of the Southern Platreef, Northern Limb of the Bushveld Complex, South Africa. *MIneralium Deposita*, **40,** 576-597.

Kruger, F.J. (2004). Filling the Bushveld Complex Magma Chamber: Lateral Expansion, Floor Interaction, Magmatic Unconformities and Chromite and PGE Deposits. Information Circular no. 377. Economic Geology Reasearch Institute. Hugh Allsopp Laboratory. University of the Witwatersrand. Johannesburg. 28p.

Kruger, F.J. (2005). Filling the Bushveld Complex magma chamber: lateral expansion, roof and floor interaction, magmatic unconformities, and the formation of giant chromitite, PGe and Ti-V-magnetite deposits. *Mineralium Deposita*, **40(5),** 451-472.

Lehmann, J., Arndt, N.T., Windley, B., Zhou, M.F., Wang, C., Harris, C. (2007). Geology, Geochemistry and Origin of the Jinchuan Ni-Cu-PGE sulfide deposit. *Economic Geology*, **102**, 75-94.

Levinson, A.A. (1974). Introduction to exploration geochemistry. Applied publishing Ltd., Illinois, U.S.A., 924 pp

Li C., Ripley, E.M., Maier W.D., Gomwe T.E.S. (2002). Olivine and Sulfur Isotopic Composition of the Uitkomst Ni-Cu Sulfide Ore-bearing Complex, South Africa: Evidence for Sulfur Contamination and Multiple Magma Emplacements. *Chemical Geology* **188**, 149-159.

Li, C., Naldrett, A.J., Coats, C.J.A. and Jonhannessen, P. (1992). Platinum, Palladium, Gold and Copper-rich Stringers at the Strathcona Mine, Sudbury: Their Enrichment by Fractionation of a Sulphide Liquid. *Economic Geology*, **87,** 1584-1598.

Li, C., Ripley, E.M. and Naldrett, A.J. (2001). Critical Factors for the Formation of a Nickel-copper Deposit in an Evolved Magma System: Lessons from a Comparison of the

Pants Lake and Voisey's Bay Sulfide Occurance in Labrador, Canada. *Mineralium Deposita* **36,** 85-92.

Li, C., Ripley, E.M. and Naldrett A.J. (2003). Compostional Variations of Olivine and Sulfur Isotopes in the Noril'sk and Talnakh Intrustions, Siberia: Implications for Ore-Forming Processes in Dynamic Magma Conduits. *Economic Geology* **85**, 69-86.

Liebenberg L. (1968). The Sulphides in the Layered Sequence of the Bushveld Igneous Complex. Unpublished PhD Thesis. University of Pretoria. 260p.

Lipin, B.R. (1993). Pressure Increases, the Formation of Chromite Seams and the Development of the Ultramafic Zones in the Stillwater Complex, Montana. *Journal of Petrology,* **34**, 995-976.

Loubser, M and Verryn S. (2008). Combining XRF and XRD analyses and sample preparation to solve mineralogical problems. South African Journal of Geology, **111**, 229 - 238.

Lowenstern J.B. (2001). Carbon Dioxide in Magmas and Implications for Hydrothermal Systems. *Mineralium Deposita* **36**, 490-502.

MacDonald, I., Holwell, D.A., Armitage, P.E.B. (2005). Geochemistry and Mineralogy of the Platreef and "Critical Zone" of the Northern Lobe of the Bushveld Complex, South Africa: Implications for Bushveld Stratigraphy and the Development of PGE Mineralization. *Mineralium Deposita,* **40,** 526-549.

Maier W.D. and Barnes S-J (2003). Magmatic Ni-Cu-PGE Sulphide Deposits: Genesis and Exploration. *Short course on Magmatic Cu-Ni-PGE Sulphide Deposits.* Department of Geology, University of Pretoria. 1-61.

Maier W.D., Gomwe T., Barnes S-J, Li C., Theart H.F.J. (2004). Platinum Group Elements in the Uikomst Complex, South Africa. *Economic Geology* **99**, 499-516.

Maier, W.D., Li, C. and de Waal, S.A. (2001). Why are there no Major Ni-Cu Sulphide Deposits in Large Layered Mafic Ultramafic Intrusions? *The Canadian Mineralogist. 39,* 547-556.

Maier, W.D., Sliep, J., Barnes, S-J, de Waal, S.A. and Li, C. (2001). PGE-bearing Mafic-ultramafic Sills in the Floor of the Eastern Bushveld Complex on the Farms Blaawboschkraal, Swartkopje and Waterval. *South African Journal of Geology*, **104,** 343-354.

Manyeruke T.D. (2003). The Petrography and Geochemistry of the Platreef of the Farm Townlands, near Potgietersrus, Northern Bushveld Complex. Unpublished MSc. Dissertation. University of Pretoria. 99p.

Marsh, J.S. (2003). Review of South African Research on Volcanic and Related Rocks and Mantle Derived Materials: 1999-2002. *South African Journal of Science* **99**, 381-388.

Mathez E.A. and Mey J.L. (2005). Character of the UG2 Chromitite and Host Rocks and Petrogenesis of its Pegmatiodal Footwall, Northeastern Bushveld Complex. *Economic Geology* **100,** 1617-1630.

McBirney, A.R. (1993). Igneous Petrology. Jones & Bartlett Publishers. p.342.

McLeod P., Stephen R., Sparks J. (1998). The Dynamics of Xenolith Assimilation. *Contributions to Mineralogy and Petrology* Issue **132**, 21-33.

Morimoto N. (1989). Nomenclature of pyroxenes. *Canadian Mineralogist* **27,** 143-156.

Morse S.A., Owens B.E., Butcher A.R. (1987). Origin of Finger Structures in the Rhum Complex: Phase Equilibrium and Heat Effects. *Geological Magazine* **124**, 205-210.

Mostert A.B. (1982). A Mineralogical and Petrographical Investigation of the Platreef on Dente 778LR, NW of Potgietersrus. Unpublished MSc. Dissertasion. University of Pretoria. 82p.

Murck, B.W. and Campbell, I.H. (1986). The Effects of Temperature, Oxygen Fugacity and Melt Composition on the Behaviour of Chromium in Basic and Ultrabasic Melts. *Geochimica et Cosmochimica Acta,* **50,** 1871-1887.

Naldrett, A.J., Ebel, D.S., Asif, M., Morrison, G. and Moore, C.M. (1997). Fractional Crystallisation of Sulphide Melts as Illustrated at Noril'sk and Sudbury. *European Journal of Mineralogy,* **9,** 365-377.

Naldrett, A.J. (1981). Nickel Sulphide Deposits: Classification, Composition and Genesis. *Economic Geology*, **75,** 628-685.

Naldrett, A.J. (1999). World Class Ni-Cu-PGE Deposits: Key Factors in their Genesis. *Mineralium Deposita,* **34,** 227-240

Neradovsky, Y.N., Borisova, V.V., Sholokhnev, V.V. (1997?). The Monchegorsk Layered Complex and Related Mineralization. *4th Biennial SGA Meeting. August 11-13, 1997, Turku, Finland. Excursion Guidebook B4 Ore Deposits in the Kola Peninsula, Northwestern Russia.* Edited by Mirtofanov, F., Torokhov, M. and Iljina, M. pp27-31

Owens, B.E. (2000). High-temperature contact metasomatism of calc-silicate xenoliths in the Kiglapait Intrusion, Labrador. *American Mineralogist* **85**, 1595-1605.

Park, C.F. and MacDiarmid, R.A. (1975). *Ore Deposits 3rd Edition*. W.H. Freeman and Company. San Francisco. 141-142.

Perritt, S. and Roberts M. (2007) Flexural-slip structures in the Bushveld Complex, South Africa? *Journal of Structural Geology*, **29**, p. 1422 – 1429.

Polovina, J.S. Hudson, D.M. and Jones, R.E. (2004). Petrographic and Geochemical Characteristics of Postmagmatic Hydrothermal Alteration and Mineralization in the J-M Reef, Stillwater Complex, Montana. *Canadian Mineralogist,* **42,** 261-277.

Povoden E., Horacek M. and Abart R. (2002). Contact Metamorphism of Siliceous Dolomite and Impure Limestones from the Werfen Formation in the Eastern Monzoni Contact Aureole. *Mineralogy and Petrology*, **76**, 99-120.

Robb, L. (2005). Introduction to Ore-forming Processes. Blackwell publishing. Australia. 48-53.

SACS (South African Committee for Statigraphy) (1980). Stratigraphy of South Africa. Part 1 (Kent, L.E. comp.), Lithostratigraphy of the Republic of South Africa, South West Africa/Namibia and the Republics of Bophuthatswana, Transkei and Venda. *Handbook fo the Geological Survey of South Africa*, **8**, 690 p.

Sakar, A., Ripley, E.M. and Li, C. (2005). Oxygen and Hydrogen Isotopic Studies of the Uitkomst Ni-Cu Sulfide Deposit, South Africa: Evidence of Selective Crustal Contamination, Multiple Magma Injection, and Hydrothermal Alteration. Geological Society of America *Abstracts with Programs*, **37**, No. 7, 451.

Sakar, A., Ripley, E.M., Li, C. and Maier, W.D. (2008). Stable isotope, fluid inclusion, and mineral chemistry constraints on contamination and hydrothermal alteration in the Uitkomst Complex, South Africa. *Chemical Geology*, **257**, p. 129-138.

Schürmann, L.W., Grabe, P-J and Steenkamp, C.J. (1998). Chromium *in* The Mineral Resources of South Africa: Handbook, Council for Geoscience, **16**, 90-105.

Shannon, K (1981). Assessment Report Geological and Geochemical survey Barb claims 1-3. Atlin Mining Division. 22 p.

Sharp , M.R. and Chadwick, B. (1981). The Geometry and Origin of Structures in Certain Transvaal Sequence Rocks within and Adjacent to the Eastern Compartment of the Bushveld Complex. Institute for Geological Research on the the Bushveld Complex, University of Pretoria, Report No. 27, 19 p.

Shoji, T. (1975). Role of Temperature and CO2 Pressure in the Formation of Skarn and Its Bearing on Mineralization. *Economic Geology,* **70,** 739-749.

Singh, V and de Nooy, C.D. (2003). Mineral Investigation of Eighty-six Borehole Core Samples Derived from the Pit1 and 2 Areas of the Nkomati Mine. Minlab Project P1176, Moruo Mineralogical Services, Florida, South Africa, 48 p.

Smith, L and Kotze J. (2010). Challenges of Open Pit Dewatering for an Intrusive Ore Body. "Mine Water and Innovative Thinking", IMWA 2010 Abstracts, p. 59- 62.

Snyman, C.P. (1996). Geologie vir Suid-Afrika (in Twee Volumes). Departement van Geologie. University of Pretoria. 534-536.

Snyman, J.E.W. (1998). Gemstones *in* The Mineral Resources of South Africa (M.G.C. Wilson and C.R. Anhaeusser, eds): Handbook, Council for Geoscience, **16**, 284.

Spandler C., Mavrogenes J. and Arculus R. (2005). Origin of Chromitites in Layered Intrusions: Evidence form Chromite-hosted Melt Inclusions from the Silverwater Complex. *Geology,* **33**, nr. 11, 893-896.

Stanton, R.L. (1972). Ore Petrology. McGraw Hill, Johannesburg, South Africa. 713 p.

Steenkamp, N.C. (2004). The Origin of the Wehrlite Layers hosted in the Lower Harzburgite (Lower Pyroxenite) Unit of the Uitkomst Complex. Unpublished Hons. Dissertation, University of Pretoria. 47p.

Steenkamp, N.C. (2009). In-house guide: XRF and XRD Sample Preparation and - Instrument Operation. University of Pretoria. Unpublished in-house guide. 18p.

Strauss, T.A.L. (1995). Petrology and Geochemistry of the Basal Gabbro Unit, Uitkomst Complex. MSc. Dissertation, Rhodes University. 103p.

Taber, S. (1917). Pressure Phenomena Accompanying the Growth of Crystals. *Proceedings of the National Academy of Sciences of the United States of America,* **3**, 297-302.

Theart, H.F.J. (1997). The Geology of the Shallow Chromite Resource within the Uitkomst Complex. Unpublished Report. 9p.

Theart, H.F.J. (2000). The Geology of the Uitkomst Complex. Unpublished Report. 57p.

Theart H.F.J and de Nooy C.D. (2001) The Platinum Group Minerals in Two Parts of the Massive Sulphide Body of the Uitkomst Complex, Mpumalanga, South Africa. *South African Journal of Geology* .**104,** 287-300.

Theriault, R.D., Barnes, S-J and Severson, M.J. (1997). The Influence of Country-rock Assimilation and Silicate to Sulfide Ratio (R factor) on the genesis of the Dunka Road Cu- Ni-Platinum-Group element deposit, Duluth Complex, Minnesota. *Canadian Journal of Earth Science* **34**, 375-389.

Tilley, C.E. and Harwood, H.F. (1931). The Dolerite-Chalk Contact of Scawt Hill Co. Antrim. The Production of Basic Alkali-rocks by the Assimilation of Limestone by Basaltic Magma. *The Mineralogical Magazine,* **22**, 439-468.

Ulmer, G.C. (1969). Experimental Investigation on Chromite Spinel. *Monographs in Economic Geology,* **4**, 114-131.

Uytenbogaart W. and Burke E.A.J. (1985). Tables for Microscopic Identification of Ore Minerals. Elsevier Publishing Company, Amsterdam. 430p.

Van Zyl A.M. (1996). The Sulphides of the Uitkomst Complex, Badplaas, South Africa. Unpublished MSc. Disseration. University of Pretoria. 121p.

Ward, J.H.W. and Wilson, M.G.C. (1998). Gold Outside the Witwatersrand Basin *in* The Mineral Resources of South Africa (M.G.C. Wilson and C.R. Anhaeusser, eds): Handbook, Council for Geoscience, **16**, 361-363.

Wallmach, T.W. (1988). The Petrogenesis of High Grade Contact Metamorphic Mineral Assemblages in Calc-silicate Xenoliths, Eastern Bushveld Complex, South Africa. Unpublished PhD thesis, University of Pretoria. 201p.

Wallmach, T.W., Hatton, C.J., de Waal, S.A. and Gibson, R.L. (1995). Retrogressive Hydration of Calc-silicate Xenoliths in the Eastern Bushveld Complex: Evidence for Late Magmatic Fluid Movement. *Journal of African Earth Sciences.* **21 (4),** 633-646.

Wallmach T.W., Hatton C.J., Droop G.T.R. (1989). Extreme Facies of Contact Metamorphism Development in Calc-Silicate Xenoliths in the Eastern Bushveld Complex. *Canadian Mineralogist* **27,** 509-523.

Watson, J.S. (1996). Fast, Simple Method of Powder Pellet Preparation for X-Ray Fluorescence Analysis. *X-Ray Spectrometry*, **25**, 173-174

Wenzel, T. Baumgartner, L.P. Brugmann, G.E. Konnikov, E.G. Kislov, E.V. and Orsoev, D.A. (2001). Contamination of Mafic Magma by Partial Melting of Dolomitic Xenoliths. *Terra Nova,* **13,** issue 3, 197-202.

Wenzel, T. Baumgartner, L.P. Brugmann, G.E. Konnikov, E.G. and Kislov, E. (2002). Partial Melting and Assimilation of Dolomitic Xenoliths by Mafic Magma: the Ioko-Dovyren Intrusion (North Baikal Region, Russia) *Journal of Petrology,* **13** number 11, 2049-2074.

Willemse, J. and Bensch, J.J. (1964). Inclusion of Original Carbonate Rocks in Gabbro and Norite of the Eastern Part of the Bushveld Complex. *Transactions Procedures Geological Society of South Africa.* **67,** 1-87.

Winkler, H.G.F. (1974). Petrogenesis of Metamorphic Rocks. Springer-Verlag. New York Inc. 348p.

Woolfe, J.A.S. (1996). The Nkomati Joint Venture – a Nickel Mine in the Making. *Geobulletin* **39 (1),** 5-7

Website visited:

http://www.arm.co.za (accessed bimonthly from January 2005 – April 2008).